İSTANBUL TECHNICAL UNIVERSITY ★ INSTITUTE OF SCIENCE AND TECHNOLOGY

ELECTROPOLYMERIZATION AND CHARACTERIZATION OF SYNTHESIZED THIOPHENE AND NONYLBITHIAZOLE BASED COMONOMERS

Ph.D. Thesis by

Fevzi Çakmak CEBECİ, M. Sc.

Department : Polymer Science and Technology

Programme: Polymer Science and Technology

NOVEMBER 2006

İSTANBUL TECHNICAL UNIVERSITY ★ INSTITUTE OF SCIENCE AND TECHNOLOGY

ELECTROPOLYMERIZATION AND CHARACTERIZATION OF SYNTHESIZED THIOPHENE AND NONYLBITHIAZOLE BASED COMONOMERS

Ph.D. Thesis by
Fevzi Çakmak CEBECİ, M.Sc.

(515992001)

Date of submission : 15 September 2006

Date of defence examination: 17 November 2006

Supervisor (Chairman): Prof. Dr. A. Sezai SARAÇ

Members of the Examining Committee: Prof. Dr. Candan ERBİL

Prof. Dr. Tuncer ERCİYES

Prof. Dr. H. Yıldırım ERBİL (GYTE)

Prof. Dr. Atilla GÜNGÖR (MÜ)

NOVEMBER 2006

İSTANBUL TEKNİK ÜNİVERSİTESİ ★ FEN BİLİMLERİ ENSTİTÜSÜ

SENTEZLENEN TİYOFEN VE NONİLBİTİYAZOL TABANLI KOMONOMERLERIN ELEKTROPOLİMERİZASYONLARI VE KARAKTERİZASYONLARI

DOKTORA TEZİ
Y. Kimyager. Fevzi Çakmak CEBECİ
(515992001)

Tezin Enstitüye Verildiği Tarih : 15 Eylül 2006
Tezin Savunulduğu Tarih : 17 Kasım 2006

Tez Danışmanı: **Prof. Dr. A. Sezai SARAÇ**

Diğer Jüri Üyeleri: **Prof. Dr. Candan ERBİL**

Prof. Dr. Tuncer ERCİYES

Prof. Dr. H. Yıldırım ERBİL (GYTE)

Prof. Dr. Atilla GÜNGÖR (MÜ)

KASIM 2006

ACKNOWLEDGEMENT

I would like to thank my advisor, Professor Dr. A. Sezai SARAC, for his guidance, continuous encouragement throughout this work, and discussions during my Ph.D. studies.

I am grateful to Associate Prof. Dr. Esma SEZER for her invaluable help, good suggestions, and supports.

I would like to express my appreciation to Prof. Dr. Candan Erbil and Prof. Tuncer Erciyes for their guidance and support throughout this thesis.

My special thanks go to my friend Gürsel Sönmez, I learned a lot from him and he still gives me inspiration.

I like to thank to Assoc. Prof. Dr. Belkıs Ustamethmetoğlu, Mehmet Erginer, Orhan Güney, Yener Rakıcıoğlu, Şerife Özkara, Yusuf Bardavit, Elif Parlak, Nermin Gündoğan, Asli Gençturk, Ece Ayaz, Koray Yılmaz, and Gamze Bakkalcı for their support and friendship.

I would love to thank to Hülya Geyik for her ambitious encouragement.

I would like to thank my little brother Durmuş Cebeci for his special helps during preparation of my thesis. Finally, I would like to offer the most gratitude to my parents for their patience, understanding, moral support and encouragement during all stages in the preparation of this PhD study.

November, 2006 Fevzi Çakmak CEBECİ

TABLE OF CONTENTS

ABBREVIATIONS

AFM	**:**	Atomic Force Microscopy
AC	**:**	Alternating Current
ATR-FTIR	**:**	Attenuated Total Reflectance Fourier Transform Infrared
ACN	**:**	Acetonitrile
BLA	**:**	Band Length Alteration
CP	**:**	Conducting Polymer
CA	**:**	Chronoamperometry
CV	**:**	Cyclic Voltammetry
CF	**:**	Carbon Fibre
CFME	**:**	Carbon Fibre Microelectrode
CPE	**:**	Constant Phase Element
DC	**:**	Direct Current
DCM	:	Dichloromethane
DPV	:	Differential Pulse Voltammetry
EIS	:	Electrochemical Impedance Spectroscopy
EPR	:	Electronic Paramagnetic Resonance
ECD	:	Electrochromic Device
EDOT	**:**	Ethylenedioxythiophene
ENBTE	:	Edot-Nonylbithiazole-Edot
FE-SEM	**:**	Field Emmision Scannin Electron Microscopy
HM	**:**	High Modulus
HT	**:**	High Tensile
HOMO	:	Highly Oriented Molecular Orbitals
IHP	:	Inner Helmholtz Plane
IRE	:	Internal Reflectance Element
ILSS	:	Interlaminar Shear Strength
ITO	:	Indium Tin Oxide
IM	:	Intermediate Modulus
MO	:	Molecular Orbital
MIR	:	Multiple Internal Reflectance

NBT	:	Nonylbithiazole
OHP	:	Outer Helmholtz Plane
PA	:	Polyacetylene
PPV	**:**	Poly(p-phenylene vinylene)
PPS	**:**	Poly(phenylenesulfide)
PEDOT	**:**	Poly(3,4-ethylenedioxythiophene)
PpPV	**:**	Poly(p-phenylenevinylene)
PpP	**:**	Poly(p-phenyelene)
PAN	:	Polyacrylonitrile
PANI	:	Polyaniline
PBTh	:	Poly(2,2'-Bithiophene)
PENBTE	:	Poly(edot-nonylbithiazole-edot)
PEDOT	:	Poly(3,4-ethylene-dioxthiophene)
PTNBTT	:	Poly(thiophene-nonylbithiazole-thiophene)
PTh	:	Polythiophene
SCE	:	Saturated Calomel Electrode
SEM	**:**	Scanning Electron Microscope
TNBTT	:	Thiophene-Nonylbithiazole-Thiophene
XRAY	:	X-Ray Electron Microscopy

LIST OF TABLES

LIST OF FIGURES

LIST OF SYMBOLS

B	**:**	Susceptance
CP	**:**	Conducting Polymer
C_1	**:**	Capacitance
C_{dl}	**:**	Double Layer Capacitance
E_g	:	Band Gap
E_{eq}	**:**	Equivalant Potential
$E_{1/2}$	**:**	Half wave potential
F	**:**	Faraday Constant
G	**:**	Conductance
L	:	Inductance
Q_{dep}	:	Deposition Charge
R	:	Resistance
R_p	:	Polarization Resistor
Y	:	Admittance

ELECTROPOLYMERIZATION AND CHARACTERIZATION OF SYNTHESIZED THIOPHENE AND NONYLBITHIAZOLE BASED COMONOMERS

SUMMARY

During previous ten years few other areas in polymer research can have generated interest among a wide variety of disciplines as that of so called conducting polymers. These materials, whilst being organic polymers, have unusual property of possessing high electrical conductivity, and can exhibit a range of properties from semi-conducting to near-metallic behavior. Electrical conductivity is achieved in the film of conducting polymer by oxidation (p-doping) or reduction (n-doping), followed respectively by the insertion of anionic or cationic species. Due to the double bond alternation in the conjugated polymer backbone, the charged species formed upon doping are able to move along the carbon chain (delocalization) allowing electron transport and thus giving an electronically conductive material.

The current interest in such materials began in the 1970's, many researchers have been focused on the conducting polymers to commercialize them with applications such as thin film transistors, polymer light-emitting diodes (PLEDs), and electrochromic devices. Conducting polymers can be prepared via chemical or electrochemical polymerization. Films of electronically conducting polymers are generally obtained onto a support electrode surface by anodic oxidation (electropolymerization) of the corresponding monomer in the presence of an electrolyte solution.

The most general use of carbon fibers is to reinforce composite materials due to its unique properties such as high strength, high modulus and low density. It is important to increase surface characteristics of the reinforcing carbon fibers and polymer matrix for demanding high technological applications. In order to achieve this, the surface properties of high strength and high modulus carbon fibers were studied recently and modification of carbon fiber surfaces by electropolymerizing 3-methyl thiophene, ter-thiophene, pyrrole, 3,4-ethylene dioxythiophene (EDOT) and their copolymers and by electrocopolymerizing acrylamide, carbazole, thiophene, carbazole, pyrrole, carbazole, indole onto the fibers have investigated in detail. Also carbon based materials are popular materials for the electrochemical applications, as an active electrode material, carbon has offer advantages compared to others, i.e. well polarization of the electrode, high surface area, processability, low cost, accessibility, thermal and chemical stability. Porous carbon is the most frequently selected electrode materials which offer large surface area and very well polarization due to porosity which makes porous carbon is the one of the most promising electrode material for supercapacitors applications.

Conducting polymers, such as polypyrrole, polyaniline, polythiophene, and their derivatives, were reported as electrode materials for supercapacitors. Supercapacitors can be classified into two types the double-layer which store the energy within the electrochemical double-layer at the electrode-electrolyte interface and the redox

supercapacitors. For redox supercapacitors, among several types of electrode materials employing of conducting polymers has received much attention due to their use in both aqueous and organic electrolytes and their wide potential working range. The electrochemical impedance spectroscopy (EIS) is one of the most effective and the reliable method to extract information about electrochemical characteristics of the electrochemical system for instance double-layer capacitance, diffusion impedance, determination of the rate of the charge transfer and charge transport processes, solution resistance etc. EIS was used to explain behavior of the polymer coated electrodes by established theories employing two models which are known as uniform and porous medium.

Among the conducting polymers 3,4-ethylenedioxythiophene (EDOT) has appeared as a new thiophene derivative combining high conductivity, low band gap, good electrochemical properties and unusual thermal stability in the oxidized state of its polymer. Its conductivity and stability make PEDOT applicable for a conducting electrode in light emitting diodes, electrochromic windows and electrochemical supercapacitors. Besides its exceptional properties the processability of EDOT based polymers improved by incorporating solubilising segment such as N-alkylcarbazole in the PEDOT main chain.

The poly(alkylbithiazoles) has received considerable attention because of its n-doping capability and usage in light emitting diode construction, this new class of conjugated polymer exhibit interesting thermochromic and electrochemical behavior especially nonyl derivative shows unusual optical properties as a result of its crystallinity and π-π stacking behavior. Curtis et al. showed that they are n-dopable contrast to the most studied polymers in LEDs which are reported to be hole carriers. Previously very low optical band gap bis-heterocycle-substituted arylene monomers have been reported. These monomers easily polymerize to form stable electroactive polymers potentially useful for electrochromic devices.

In this study, synthesis of copolymers containing nonylbithiazol groups and their characterizations with cyclic voltammetry, spectroelectrochemistry and electrochemical impedance spectroscopy were investigated. The 2,2'-bithiophene 5,5'-Bis-(4-methyl-thiazole)-[2,2']bithiophenyl; 4-Methyl-2-thiophene-2-yl-thiazole; thiophene-nonylbithiazole-thiophene (TNBTT) comonomer; EDOT-nonylbithiazol-EDOT (ENBTE) comonomer were synthesized as will be explained in the following chapters. The electropolymerization of 2,2'-bithiophene, TNBTT, ENBTE were succeeded but other two of them could not manage to electropolymerize due to the thiazoles at the end caps that block electropolymerization.

PBTh(poly(2,2'-Bithiophene) was first grown by cyclic voltammetry from Et_4NBF_4/dichloromethane electrolyte solution containing 0.005 M of BTh onto CFME between -0.3 V and 1.4V with a scan rate of 50mV s^{-1}. A regular growth of polymer was observed. EIS measurements were performed at different applied potentials in the range of -0.2 to 1.2 V with a potential step of 0.1V in parallel to cyclic voltammogram of the PBTh in monomer free electrolyte solution. And the obtained results show us PBTh is not a very good polymer because of its very narrow electroactivity range and lower capacitance values compared to other conducting polymers.

Thiophene-nonylbithiazol-thiophene (TNBTT) comonomer was synthesized and then electropolymerized on CFME containing 0.005 M of TNBTT in 0.1 M Et_4NBF_4/DCM solution. The electrodeposition of the comonomer was performed at

scan rate of 20 mV s^{-1} between 0.0 V and 1.4V. The monomer oxidation onto bare electrode starts at (E_{onset} of the TNBTT) 1.096 mV vs. Ag/AgCl. Scanning range from the 0.0V to 1.4V generates a broad cathodic peak at around 0.96V on the return scan. The increase in the size of this peak indicates that it is due to the electroactive film formed on the surface of the CFME. A regular growth is not observed. Current densities of the consecutive cycles do not increase linearly. This might be due to the possibility of the more than one polymerizable site on the thiophene. The morphology of the films electrodeposited at different deposition charges were monitored using FE-SEM.

Conducting polymers are known to be highly sensitive to over-oxidation due to the degradation of the conducting polymer's backbone at high potentials. A PTNBTT film has been exposed to a series of potentials above the half wave potential of the polymer by multiple cycling between its neutral (0.0 V) and oxidized forms at different upper potential limits (from +1.0 to +1.6 V). After cycling twice in each potential values, the second cyclic voltammogram was recorded. The results, see Figure 1, show the stability of PTNBTT to overoxidation without any electroactivity loss up to +1.6 V vs Ag/AgCl. This result shows that the PTNBTT film exhibits electroactivity between 0.9V to 1.5V without any significant deformation in shape of the anodic and cathodic peaks above the half wave potential of the polymer.

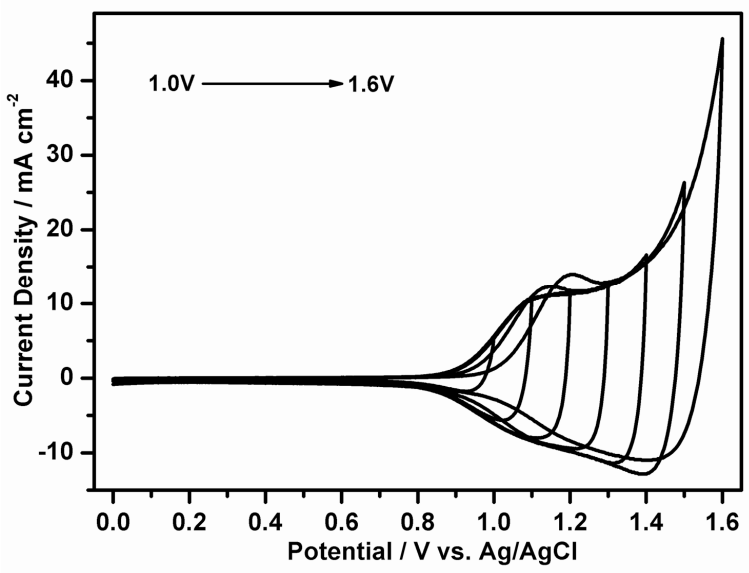

Figure 1: Stability test of PTNBTT films to over oxidation by cyclic voltammetry from 0.0V to a) 1.0V, b) 1.1V, c) 1.2V, d) 1.3V, e) 1.4V, f) 1.5V, and g) 1.6V.

Moreover, the polymer films have very large capacitive currents at potentials above $E_{1/2}$. Note that these capacitive currents are very stable and can be an advantage for this polymer's in supercapacitor applications.

The synthesis and characterization of a novel donor acceptor donor type bis(3,4-ethylenedioxythiophene)-(4,4'-dinonyl-2,2'-bithiazole) comonomer and its electrochemically prepared polymer on carbon fiber, Pt button and ITO plate is also reported in this study. Cyclic voltammetry of the polymer in 0.1 M Et_4NBF_4/DCM exhibits a very well defined and reversible redox processes and this co-monomer can be either p-doped or n-doped. The halfwave oxidation potentials of the polymer ($E_{1/2}$) were observed at 0.303 V and 0.814 V versus Ag/AgCl.

Spectroelectrochemistry of PENBTE films were studied on the potentiodynamically deposited ITO-coated glass slides. The polymer is electrochromic; the onset for the π to π* transition (*E*g) of 1.75 eV with a λmax at 2.15 eV and the homogeneous and high quality film of the polymer is stable of its optical properties offering fast switching time which is less than 0.25s. The experiments, carried out by spectroelectrochemical methods, have demonstrated the ability of PENBTE to switch between its neutral and doped states (i.e. coloring/bleaching process of the PENBTE) with a significant change in transmittance at 555 nm. The polymer were switched for 5 second step time between the absorbing, neutral state and the transmissive, oxidized state as shown in Figure 2.

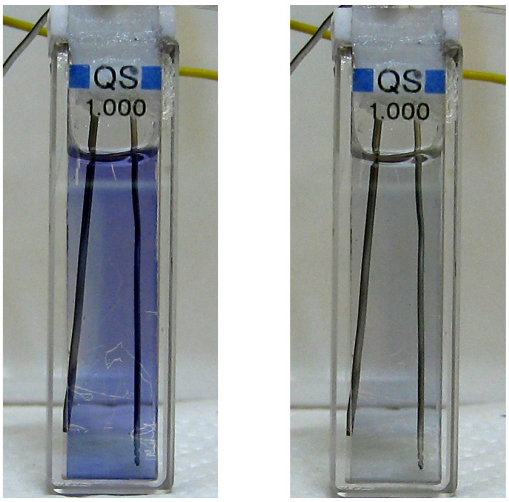

Figure 2: A PENBTE film on an ITO coated glass slide electrode reduced at -0.4 V (colored), and oxidized at 0.8 V (bleached) vs. Ag/AgCl.

The morphological studies reveal that the polymer was deposited as a continuous and very well adhering film to surface of the carbon fiber microelectrode. All these properties make this polymer favorable for use in electronic devices. Electrochemical impedance studies at different applied potentials in the range of -0.5 to 1.2 V with a potential step of 0.1V to cover entire polymerization range of the ENBTE comonomer of the prepared electrode is also reported in this paper, too. Capacitive behavior of the CFME/PENBTE film was firstly noticed from CV experiments which exhibit a rectangular shape, for a galvanostatically prepared polymer film with a charge of 5 C cm^{-2} which specific capacitance value was obtained about ~340 mF cm^{-2}

The following figure illustrates the variation in the specific capacitance values of galvanostatically deposited (Q_{dep}=5 C cm^{-2}) at 0.01 Hz and 1.170 Hz at DC potentials between -0.5V and 1.2V. PENBTE on film the shape of the plot has a very good agreement with the corresponding CV of the polymer film in monomer free solution. Capacitance values have two peaks at 0.4V and 0.8V. These two maximum points converge very well those of two oxidation peaks observed in CV of the PENBTE film at 0.4V and 0.9V for 100 mV s^{-1}

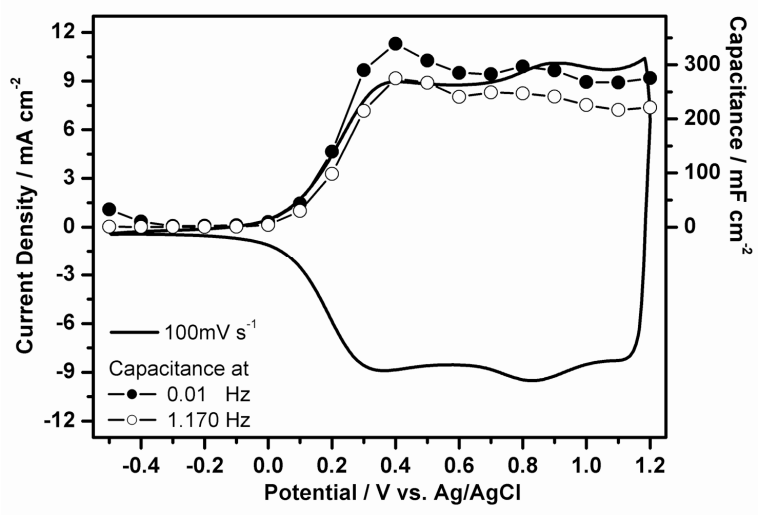

Figure 3: Variation of the specific capacitance values of galvanostatically deposited (Q_{dep}=5 C cm^{-2}) PENBTE onto CFME and CV of a PENBTE film at 100mV s^{-1}.

The electrochemical parameters of the CFME and the polymers prepared with ENBTE were evaluated by employing the ZSimpWin software. The electrochemical impedance data were fitted to several equivalent circuit models to find out numerical values of the proposed components and the following model, Figure 4, generated for best calculation results.

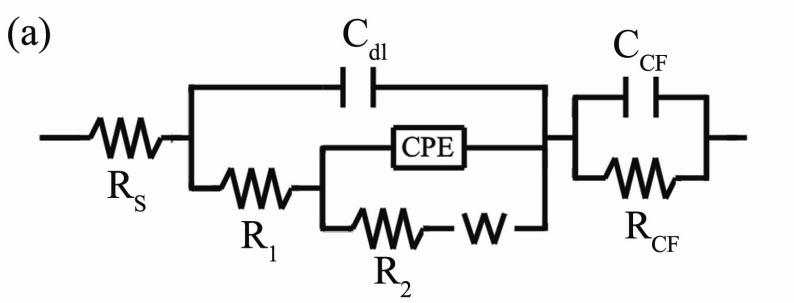

Figure 4: Electrical equivalent circuit used for simulating the experimental impedance data from 0.2 V to 1.2V.

Effect of the solvent and the deposition charge on the capacitive behavior of the film was investigated. The galvanostatic charge/discharge characteristic of a film was investigated and the morphology of the films electrodeposited at different deposition charges were monitored using FE-SEM.

Initial device properties based on PENBTE were checked with switching properties and results shows that 0.25 s is short enough to use as electrochromic applications. From the obtained results, we can conclude that use of synthesized novel comonomers in polymer electrode shows very good capacitive behavior on carbon fiber microelectrode. The measured capacitance values are quite promising for supercapacitor constructions with a good engineering.

SENTEZLENEN TİYOFEN VE NONİLBİTİYAZOL TABANLI KOMONOMERLERIN ELEKTROPOLİMERİZASYONLARI VE KARAKTERİZASYONLARI

ÖZET

Geçtiğimiz son otuz yılda farklı disiplinlerdeki polimer araştırmalardan pek azı iletken polimerlerin gördüğü ilgiye erişebilmiştir. Bu malzemeler, organik polimer olmasına karşın yarı iletkenden neredeyse metal kadar yüksek iletkenlik değerlerine sahiptirler. İletken polimer filmlerde, elektrik iletkenliği, yükseltgenmeyi (p-katkılandırma) veya indirgenmeyi (n-katkılandırma) takip eden anyonik veya katyonik türlerin yüklenmiş olarak yapıya girmesi yolu ile gerçekleşmektedir. Konjüge polimer omurgasında çift bağların değişmesiyle katkılandırmadan meydana gelen yüklenmiş türler vasıtasıyla karbon zinciri boyunca elektronun taşınmasına müsaade eder ve malzemeye elektronik iletkenlik kazandırır.

Bu malzemelere ilgi 1970'li yıllarda başlamıştır. Pek çok araştırmacı iletken polimerleri, ince film transistorü, polimer ışık yayıcı diyotlar (LEDs), elektrokromik cihazların yapımında kullanarak ticarileştirmeye çalışmışlardır. İletken polimerler, kimyasal veya elektrokimyasal olarak hazırlanabilmektedirler. Elektrolit çözelti içerisindeki monomer anodik polimerizasyon ile çalışma elektrotu üzerine elektropolimerizasyon yapılarak iletken polimer filmler elde edilmektedir.

Karbon fiberler sahip oldukları yüksek mukavemet ve düşük yoğunluk gibi üstün özellikleri ile genellikle kompozit malzemelerin güçlendirilmesinde kullanılmaktadır. Yüksek teknoloji uygulamalarında daha iyi sonuçlar alabilmek için güçlendirici karbon fiber ile polimerin yüzey özelliklerinin geliştirilmesi gerekmektedir. Bu amaçla karbon fiber yüzeyi 3-metil tiyofen, tertiyofen, pirol, 3,4-etilen dioksitiyofen (EDOT) ve bunların kopolimerleri ile ayrıca akrilamid, tiyofen, karbazol ve indol gibi monomerlerin elektropolimerizasyonu ile değiştirilmesi için detaylı olarak çalışılmıştır. Ayrıca karbon temelli malzemeler elektrot malzemesi gibi elektrokimyasal uygulamalarda da kullanılan popüler malzemelerdir. Karbon diğer malzemelerle kıyaslanınca elektrotunun iyi polarize olması, yüzey alanının büyüklüğü, işlenebilirlik, düşük maliyet, erişilebilirlik, termal ve kimyasal kararlılık gibi özellikleri ile öne çıkmaktadır. Gözenekli yapıdaki karbon, geniş yüzey alanı ve iyi polarize olması sebebi ile süperkapasitör uygulamalarında en çok umut vaat eden elektrot malzemelerindendir.

Poliasetilen, polipirol, polianilin, politiyofen ve türevleri literatürde süperkapasitörlerde elektrot malzemesi olarak kullanıldığı rapor edilmiştir. Elektrokimyasal çift tabaka ile elektrot-elektrolit ara yüzeyinde enerjiyi depolayan süperkapasitörler; çift yüzey ve redoks olmak üzere ikiye ayrılmaktadırlar. Redoks süperkapasitörleri için, pek çok elektrot malzemesi arasından iletken polimerler hem sulu ortamda hem de organik elektrolitlerde kullanılması ve geniş potansiyel aralığında çalışılabilmesi sebebi ile daha çok dikkat çekmektedirler.

Elektrokimyasal empedans spektroskopisi (EIS), elektrokimyasal sistemlerin, çift yüzey kapasitansı, difüzyon empedansı, yük taşınması ve iletmesi, çözelti direnci gibi elektrokimyasal incelenmesi hakkında bilgi veren en etkili metotlardandır. EIS, polimer kaplı elektrotların davranışını açıklamak için düzenli ve gözenekli ortam olarak adlandırılan iki teoriyi kullanmaktadır.

İletken polimerler arasında 3,4-etilendioksitiyofen (EDOT) yüksek iletkenliği, düşük bant aralığı, iyi elektrokimyasal özellikleri ve yükseltgenmiş halinin nadir olarak görülen termal kararlılığı ile yeni bir tiyofen türevi olarak öne çıkmaktadır. İletkenliği ve kararlılığı PEDOT'ı ışık yayıcı diyotlarda, elektrokromik camlarda ve elektrokimyasal süperkapasitörler de iletken elektrot olarak kullanılmasına olanak sağlamaktadırlar.

Polialkilbitiyazoller, n-katkılandırılabilme özellikleri ve ışık yayıcı diyotların yapısında kullanımı nedeniyle ile dikkat çekmektedirler. Bu yeni konjüge polimer sınıfı ilginç termokromik ve elektrokimyasal özellikler göstermektedir. Özellikle de nonil türevi kristal yapısı ve π-π yığınlarının davranışı sebebi ile nadir görülen optik özelliklere sahiptirler. Curtis, LED'lerde çalışılmış özellikle bu türevlerin pek çok polimerin tersine bunların n-katkılandırılabilir olduğunu göstermiştir. Daha önce yapılan çalışmalarda düşük optik bant aralığına sahip özellikle elektrokromik cihazlarda faydalı çift halkalı alkil zincirli monomerleri kolaylıkla polimerleşebileceğini ve karakterli elektro aktif polimerler oluşturduğunu bildirmiştir.

Bu çalışmada, nonilbitiyazol grupları içeren kopolimerler ve bunların döngülü voltametri, spektroelektrokimyasal ve elektrokimyasal empedans spektroskopisi ile incelenmesi yapılmıştır. 2,2'-bitiyofen, 5,5'-Bis-(4-metil-tiyazol)-[2,2']bitiyofenil, tiyofen-nonilbitiyazol-tiyofen (TNBTT) komonomer, EDOT-nonilbitiyazol-EDOT (ENBTE) komonomerlerinin sentezi daha sonraki bölümlerde anlatılacaktır. 2,2'-bitiyofen, TNBTT ve ENBTE kopolimerlerinin elektropolimerizasyonları başarı ile yapılmıştır. Fakat diğer iki tanesi sonlardaki uçlardaki tiyazol halkaları sebebi ile elektropolimerizasyonu gerçekleştirilememiştir.

Polimerizasyonu başarılan BTh (2,2'-Bitiyofen), 0.005M lik çözeltisinden 0.1 M Et_4NBF_4/diklormetan elektrolit çözeltisi içerisinde -0.3V ile 1.4V aralığında 50mV s^{-1}'lik tarama hızı ile döngülü voltametriyle karbon fiber mikroelektrot (KFME) üzerine elektropolimerizasyonla yapılmıştır. Polimer normal bir gelişim göstermiştir. EIS ölçümleri ise -0.2V ile 1.2V aralığında 0.1V'luk adımlarla döngülü voltametri ile paralellik gösterecek şekilde gerçekleştirilmiştir. Elde edilen sonuçlar göstermiştir ki PBTh diğer iletken polimerlerle karşılaştırıldığında dar çalışma aralığı ve düşük kapasitans değerleri ile iyi bir polimer değildir.

Tiyofen-nonilbitiyazol-tiyofen (TNBTT) komonomeri sentezlenmiş ve KFME üzerine 0.005M TNBTT'nin 0.1 M Et_4NBF_4/DCM elektrolit çözeltisinde elektropolimerizasyonu başarıyla yapılmıştır. Komonomerin biriktirilmesi 0 V ile 1.4V arasında 20 mV s^{-1} tarama hızı ile gerçekleştirilmiştir. Monomerin kaplanmamış elektrot üzerine oksidasyonu Ag/AgCl'ye karşı 1.096mV'ta başlamaktadır. 0.0V ile 1.4V tarama aralığında 0.96V civarında dönüş taramasında geniş bir katodik pik ortaya çıkmaktadır. Pikin genişliğindeki artış KFME yüzeyinde oluşan elektroaktif film sebebi ile meydana gelir. Ardışık döngülerdeki akım yoğunluğu lineer olarak artmamaktadır. Bunun sebebi de tiyofen üzerindeki birden fazla polimerizasyona müsait yer olması yüzünden kaynaklanabilir. Farklı yük

miktarlarında biriktirilmiş filmlerin yüzey görüntüleri FE-SEM kullanılarak görüntülenmiştir.

İletken polimerler yüksek potansiyellerde iletken polimerlerin omurgasının bozunması sonucu meydana gelen aşırı oksitlenmeye karşı son derece hassas davranış göstermektedirler. PTNBTT filmi polimerin yarı dalga potansiyelinden daha yüksek potansiyellere (+1.0 ile +1.6V arasında) maruz bırakılmıştır. Her potansiyel değeri için iki seferlik yapılan döngüden ikinci döngü alınarak kaydedilmiştir. Sonuçlar aşağıda Şekil 1'de gösterilmiştir ve Ag/AgCl'ye karşı +1.6V'a kadar herhangi bir elektroaktivite kaybetmeksizin aşırı oksitlenmeye karşı kararlılık göstermektedir. Bu sonuçlar PTNBTT filminin 0.9V ile 1.5V arasında polimerin yarı dalga potansiyelinden daha yüksekte anodik ve katodik piklerinde herhangi bir şekil bozukluğu göstermeksizin kararlı davranmaktadır.

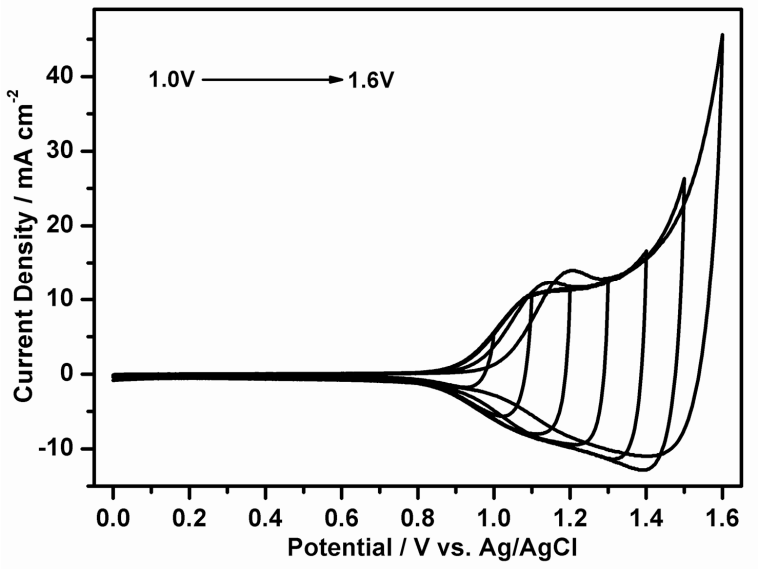

Şekil 1: PTNBTT filmlerinin aşırı oksitlenemeye karşı CV ile 0 V dan 1.6V'a kadar stabilitesinin test edilmesi.

Bunun yanı sıra polimer filmi $E_{1/2}$ değerlerinden yüksek değerlerde daha büyük kapasitif akımlar göstermektedir. Bu kapasitif akımlar son derece kararlı ve polimerin süperkapasitör uygulamaları için avantajı olarak değerlendirilebilir.

Yeni elektron alıcı verici alıcı türündeki bis(3,4-etilen-dioksitiyofen)-(4,4'-dinonil-2,2'-bitiyazol) komonomerinin sentezi, incelenmesi ile karbon fiber, Pt elektrotlar ve İndiyum Kalay Oksit (İTO) kaplı cam üzerine elektrokimyasal polimerizasyonu da bu çalışmada gerçekleştirilmiştir. Polimerin 0,1 M Et_4NBF_4/DCM konsantrasyonlu elektrolit çözelti içerisindeki döngülü voltamogramı çok iyi ve tersinir redoks davranışı göstermektedir. Ayrıca bu komonomer hem p-katkılandırma hem de n-katkılandırma özelliklerine sahiptir. Polimerin yarı dalga potansiyeli Ag/AgCl elektrota karşı 0.303 V ve 0.814 V değerlerinde gözlemlenmiştir.

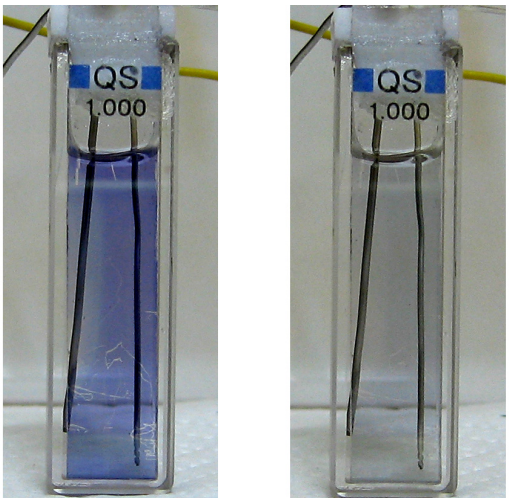

Şekil 2: İTO kaplı cam üzerine kaplanan PENBTE filminin Ag/AgCl referansına karşı -0.4 V da indirgenmiş (renkli) ve 0.8 V'da yükseltgenmesi (renksiz).

PENBTE filminin spektroelektrokimyası değişen potansiyelde ITO kaplı cam üzerinde çalışılmıştır ve alınan sonuçlara göre polimer elektrokromiktir. π-π^* geçişleri için başlangıç değerinden yola çıkılarak band aralığı E_g 1.75 eV olarak hesaplanmıştır, λ_{max} değerinin 2.15 eV olduğu gözlemlenmiştir. Polimerin homojen ve kaliteli filmi 0.25 s den daha az zamanda anahtarlama özelliği ile kararlı optik özellikler sunmaktadır. Spektroelektrokimyasal yöntemlerle gerçekleştirilen deneylerde yüksüz ve katkılandırılmış hallerinde 555 nm de renklenme ve geçirgenlik değişikliği ile anahtarlama kabiliyetini göstermektedir, Şekil 2. Polimer 5 saniyelik zaman dilimlerinde yüksüz durumdan yükseltgenmiş duruma yukarıdaki şekilde gösterildiği gibi geçiş yapmıştır.

Morfolojik çalışmalar ise polimerin karbon fiber mikro elektrot yüzeyine homojen ve sürekli film şekilde biriktirildiğini göstermektedir. Bütün bu özellikler polimerin elektronik cihazlarda kullanıma elverişli olduğunun bir göstergesidir. Karbon fiber mikro elektrot /PENBTE'nin kapasitif davranışı ilk defa sabit akımda 5C cm^{-2} yükle biriktirilmiş filminin incelenmesi ile polimer filmin dikdörtgen şekil gösteren döngülü voltamogramı ve deneysel sonuçlardan filmin spesifik kapasitansı yaklaşık olarak ~340 mF cm^{-2} hesaplanmıştır.

Aşağıdaki şekil sabit akımda depolanmış olan (Q_{dep}=5 C cm^{-2}) PENBTE filminin 0.01 Hz ve 1.170 Hz değerlerinde -0.5V ile 1.2V DC potansiyel aralığında spesifik kapasitans değerlerini göstermektedir. Grafik, polimer filmin monomersiz ortamda alınan döngülü voltamogrami ile son derece uyum içindedir. Kapasitans değerleri 0.4V ve 0.8V'da iki pike sahiptir. Bu iki maksimum nokta döngülü voltametride 100 mVs^{-1} hızı ile taranmış 0.4V ve 0.9V'taki yükseltgenme pikleri ile gayet iyi şekilde çakışmaktadır.

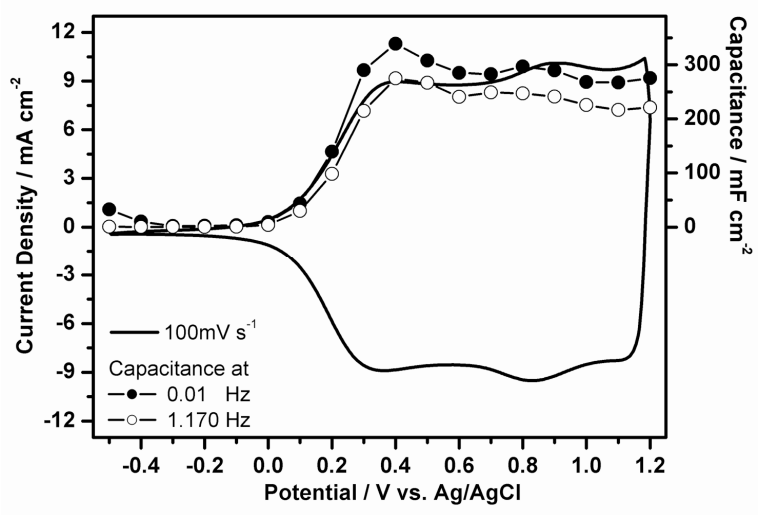

Şekil 3: Sabit akımla KFME üzerine biriktirilen PENBTE filminin spesifik kapasitans ve polimerin monmersiz ortandaki CV grafigi.

KFME/PENBTE/elektrolit sisteminin parametreleri ZSimpWin yazılımı ile hesaplanmıştır. Deneysel olarak elde edilen empedans verileri seçilmiş iki eşdeğer devrede kullanılarak filmin benzetimi yapılmıştır. Elektrokimyasal empedans verileri çeşitli eşdeğer elektriksel devrelere uygulanarak önerilen devre elemanların değerleri hesaplanmaya çalışılmış ve aşağıda verilen model, şekil 4, en uyumlu sonuçları vermiştir.

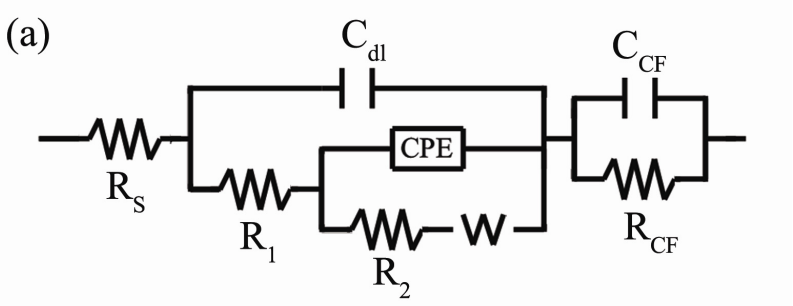

Şekil 4: Deneysel verilerin simulasyonunu PENBTE için 0.2V ile 1.2V arasında yapmak için kullanılan elektriksel eşdeger devre.

Filmin sabit akımda yükleme/boşaltma özelliği, çözücünün ve biriktirme yükünün filmin kapasitif davranışı üzerindeki etkisi de ayrıca incelenmiştir. Elektrokimyasal olarak farklı biriktirme yükleri ile hazırlanmış filmlerin morfolojisi FE-SEM ile görüntülenmiştir.

Elektrokromik cihazlara uygunluğu test edildiğinde PENBTE'nin homojen ve kaliteli filminin 0.25 s den daha az zamanda anahtarlama ve kararlı optik özellikler sunması sebebiyle basarîlidir. Elde edilen sonuçlardan sentezlenen yeni komonomerlerin polimer elektrot olarak KFME üzerinde kullanılmaları çok iyi derecede kapasitif davranış göstermiştir. Ölçülen kapasitans değerleri iyi mühendislik çalışmasıyla süperkapasitör uygularında oldukça umut vaat etmektedir.

1. INTRODUCTION

Since the first appearance of the conducting polymers in the late 70s, [1] many researchers have been focused on the conducting polymers [2] to commercialize them with applications such as thin film transistors [3], polymer light-emitting diodes (LEDs) [4], and electrochromic devices [5, 6]. Through the judicious choice of molecule combinations it is possible to prepare multifunctional molecules that provide possibility for desired applications.

3,4-ethylenedioxythiophene (EDOT) has appeared as a new thiophene derivative combining high conductivity, low band gap, good electrochemical properties and unusual thermal stability in the oxidized state of its polymer [7, 8]. Its conductivity and stability make PEDOT applicable for a conducting electrode in light emitting diodes [9], electrochromic windows [10, 11] and electrochemical supercapacitors [12]. Besides its exceptional properties the processability of EDOT based polymers improved by incorporating solubilising segment such as N-alkylcarbazole in the PEDOT main chain [13, 14].

The poly(alkylbithiazoles) has received considerable attention because of its n-doping capability and usage in light emitting diode construction, this new class of conjugated polymer exhibit interesting thermochromic and electrochemical behavior [15-22] especially nonyl- derivative shows unusual optical properties as a result of its crystallinity and π-π stacking behavior [16, 18, 19, 23, 24]. Curtis et al. showed that they are n-dopable contrast to the most studied polymers in LEDs are reported to be hole carriers [15, 23].

The most general use of carbon fibers is to reinforce composite materials due to its unique properties such as high strength, high modulus and low density. It is important to increase surface characteristics of the reinforcing carbon fibers and polymer matrix for demanding high technological applications. In order to achieve this, the surface properties of high strength and high modulus carbon fibers were studied recently and modification of carbon fiber surfaces by electropolymerizing 3-

methyl thiophene [25], ter-thiophene [26], pyrrole, 3,4-ethylene dioxythiophene (EDOT) and their copolymers [27] and by electrocopolymerizing acrylamide, carbazole [28], thiophene, carbazole, pyrrole [29], carbazole, indole [30] onto the fibers have investigated in detail. EDOT-Ethylcarbazole-EDOT was electrochemically coated onto carbon fiber microelectrodes and very stable films were obtained at high potentials [31].

Supercapacitors [32, 33] which store the energy within the electrochemical double-layer at the electrode-electrolyte interface can be classified into two types the double-layer and the redox supercapacitors. For redox supercapacitors, among several types of electrode materials employing of conducting polymers has received much attention due to their use in both aqueous and organic electrolytes and their wide potential working range [34-37].

The electrochemical impedance spectroscopy (EIS) is one of the most effective and the reliable method to extract information about electrochemical characteristics of the electrochemical system for instance double-layer capacitance, diffusion impedance, determination of the rate of the charge transfer and charge transport processes, solution resistance etc. [38, 39]. EIS was used to explain behavior of the polymer coated electrodes by established theories employing two models which are known as uniform [40-44] and porous medium [2, 45-47].

Previously very low optical band gap bis-heterocycle-substituted arylene monomers have been reported these monomers easily polymerize to form stable electroactive polymers [48-52] potentially useful for electrochromic devices.

In this thesis, we report the synthesis of five novel comonomers based on a thiophene and alkylbithiazole derivatives. Electrochemical polymerizations of 2,2'-bithiophene, thiophene-nonylbithiazole-thiophene (TNBTT) and EDOT-Nonylbithiazole-EDOT (ENBTE) comonomers and their characterization with electrochemical impedance, Field Emission Scanning Electron Microscopy (FE-SEM), Attenuated Total Reflectance (ATR-FTIR) were studied. Electropolymerizations of 2,2'-bithiophene, thiophene-nonylbithiazole-thiophene and ENBTE comonomers were also successfully performed. In order to further increase these properties of ENBTE, we have prepared and investigated copolymers of this comonomer with bithiophene and EDOT. All polymers were tested for their suitability for supercapacitor applications.

2. THEORETICAL PART

2.1. Conducting Polymers

Electrical conductivity in a conjugated polymer (polyacetylene) in 1977 were reported by Shirakawa, Heeger and MacDiarmird [1], the field of conducting polymer has attracted the interest of thousands of academic and industrial researchers for more than three decades. The possibility of combining in these new materials the properties of organic polymers and the electronic properties of semiconductors has been the driving force for various applications [53-55]. Conducting polymers can be prepared via chemical or electrochemical polymerization [56]. Films of electronically conducting polymers are generally obtained onto a support electrode surface by anodic oxidation (electropolymerization) of the corresponding monomer in the presence of an electrolyte solution. Different electrochemical techniques can be used including potentiostatic (constant potential), galvanostatic (constant current) and potentiodynamic (potential scanning *i.e.* cyclic voltammetry) methods [57]. Electrical conductivity is achieved in the film of conducting polymer by oxidation (p-doping) or reduction (n-doping), followed respectively by the insertion of anionic or cationic species [57], Due to the double bond alternation in the conjugated polymer backbone, the charged species formed upon doping are able to move along the carbon chain (delocalization) allowing electron transport and thus giving an electronically conductive material [49].

2.1.1. Theory of Band Gap and Electrical Conductivity

The polyacetylene (PA) produced by Shirakawa [1] in the late 1970s exhibited a 12 order of magnitude increase in electrical conductivity when exposed to oxidizing agents. Since that discovery, vast arrays of other conducting polymers (CP) have been synthesized. The most common of these, in addition to PA, are shown below in Figure 2.1.

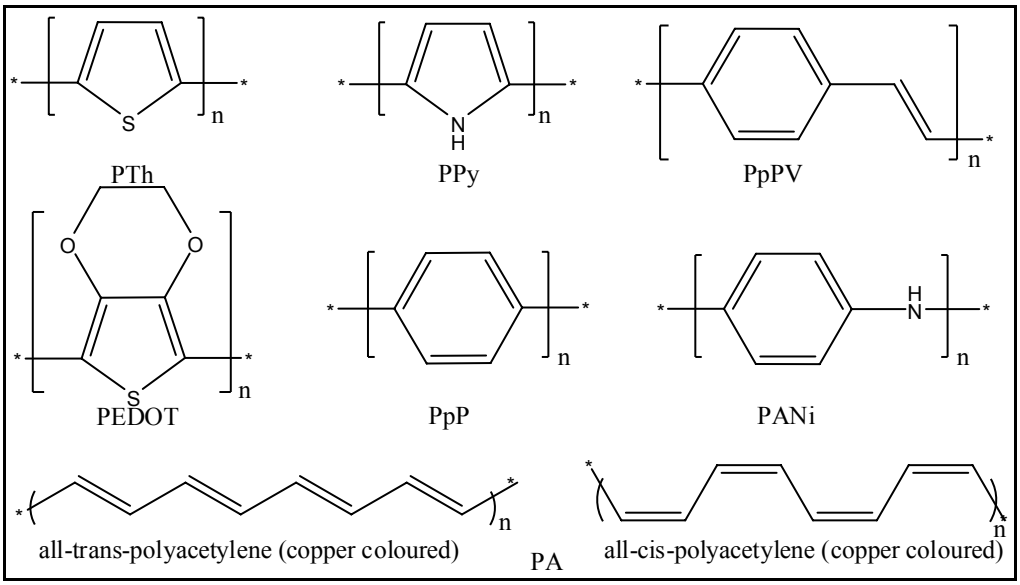

Figure 2.1: Some conducting polymers.

A large number of conjugated polymers have been synthesized and studied in the last two decades. Their structures, electronic structures, and numerous properties have been reviewed extensively [55]. A few representative structural formulas are shown in Figure 2.1. In addition to bond length alternation (BLA), defined as the difference between the long and short carbon-carbon bonds in a conjugated molecule, several other factors influence the band gaps of these complex systems. Most of the factors involved are normally interdependent; no general formula can be given. For instance, as in the case of poly(thiophene), PTh, and poly(pyrrole), PPy, heteroatoms affect the gap by both influencing the degree of BLA and mixing of the heteroatom orbital. The latter can be viewed as a direct heteroatomic effect. For purely interpretative purposes, based on the perturbation approach of qualitative molecular orbital theory, the following qualitative formula expresses the main contributions affecting the band gap [58]:

$$Eg \cong E_g^{topol} + E_g^{\Delta r} + E_g^{\theta} + E_g^{arom} + E_g^{sub} + E_g^{error} \qquad \textbf{(2.1)}$$

where E_g^{topol} is the topological band gap, $E_g^{\Delta r}$ is the contribution from BLA or geometry relaxation along the main chain (including a large exchange contribution), E_g^{θ} is a contribution arising from the effect of ring torsion (non-planarity), E_g^{arom} is owing to the presence of an aromatic ring along the chain, which limits π-electron

delocalization outside the ring, E_g^{sub} comes from substitution effects, and E_g^{error} normally includes geometry defects, disorder, and inter-chain interactions. Bond distances play a key role in those cases, when the topological band gap is zero, e.g., PA or polyacetylene. However, the strong coupling of the frontier orbital(s) remains important even if the topological band gap is not zero, as is the case for all polymers in Figure 2.1, except PA. Therefore, the geometry influences the band gap directly [59].

2.1.1.1. The Extended π-system

Since that discovery of conducting polymers, vast arrays of other (Conducting Polymers) CPs have been synthesized. Apart from polyaniline, all of these systems share one common structural feature, namely a rigid nature brought about by the sp^2 carbon-based backbone. The utilization of the conjugated construction affords polymer chains possessing extended π-systems, and it is this feature alone that separates CPs from their other polymeric counterparts.

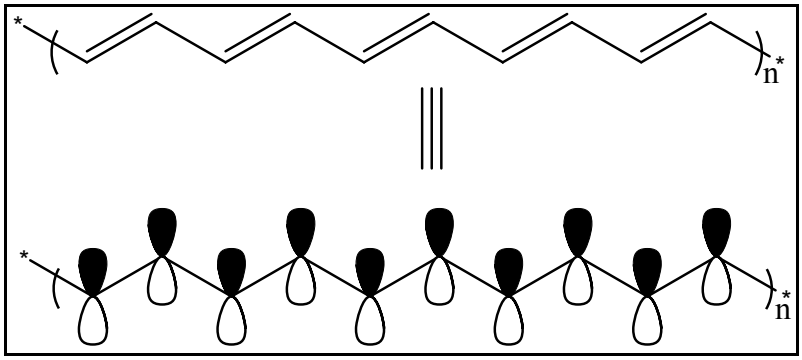

Figure 2.2: The π-system model.

Using this generic, lowest energy (fully bonding) molecular orbital (MO) representation as shown by the π-system model, the picture of primary concern that is generated by these networks consists of a number of π and π* levels (Figure 2.2).

The electrical properties of any material are a result of the material's electronic structure. The presumption that CP's form bands through extensive molecular orbital overlap leads to the assumption that their electronic properties can be explained by band theory. With such an approach, the bands and their electronic population are the chief determinants of whether or not a material is conductive. Here, materials are

classified as one of three types shown in Figure 2.4, being metals, semiconductors, or insulators.

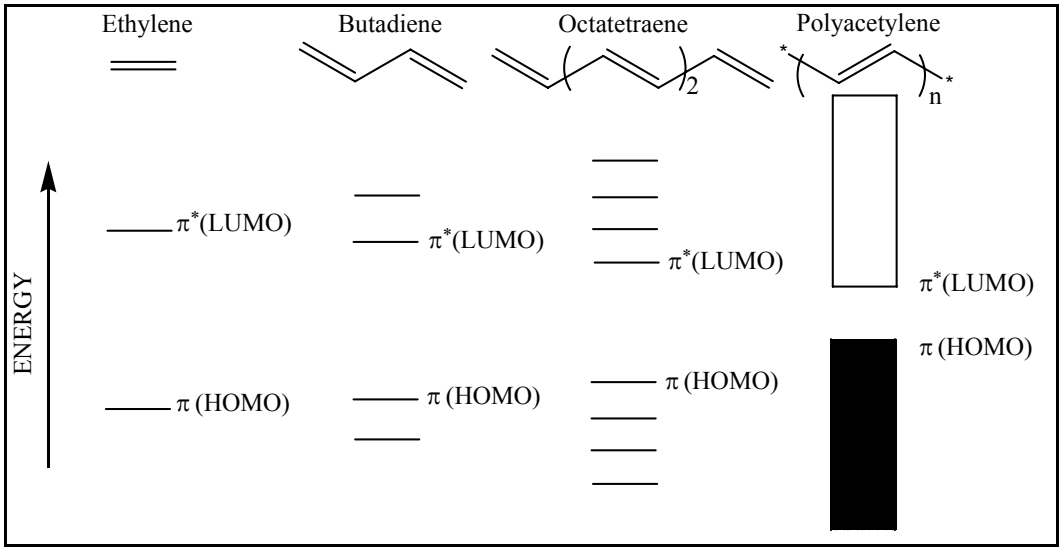

Figure 2.3: Molecular orbital (MO) diagram.

Metals are materials that possess partially filled bands, and this characteristic is the key factor leading to the conductive nature of this class of materials.

Semiconductors, on the other hand, have filled (valence bands) and unfilled (conduction bands) bands that are separated by a range of forbidden energies (known as the "band gap"). The conduction band can be populated, at the expense of the valence band, by exciting electrons (thermally and/or photochemically).

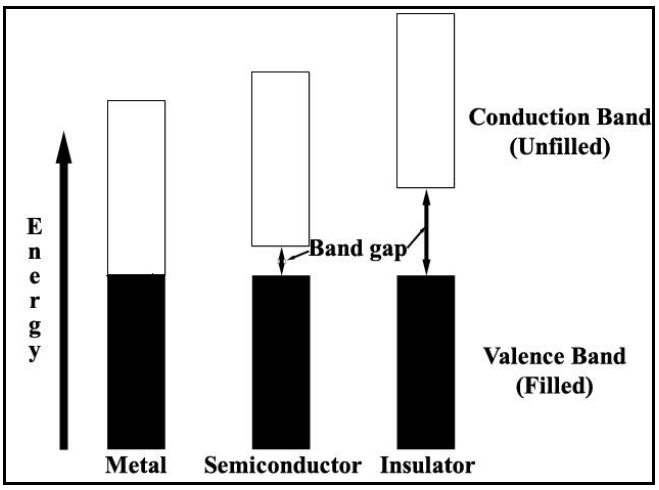

Figure 2.4: Classification of materials, and schematic of valence and conduction

Insulators possess a band structure similar to semiconductors except here the band gap is much larger and inaccessible under the environmental conditions employed.

At first glance one might necessarily expect that the p electrons of polyacetylene would produce a half-filled band and result in the polymer being metallic in nature. However, the one-dimensional nature of the polyacetylene chain leaves it susceptible to an instability that forces the polymer to retain its strict, alternating series of long and short bonds. This instability, analogous to a "Peierl's distortion", is very common among molecular solids and is the result of the coupling of electrons with phonons (lattice vibrations) [60]. Given the relatively soft nature of the lattice in such low dimensional solids, the total energy of the system can be decreased through a doubling of the unit cell, concomitantly opening a gap in the conduction band at the Brillouin zone boundary. In fact, structural studies of polyacetylene have shown the polymer to possess a localized backbone consisting of alternating long and short bonds [61]. This is in stark contrast to aromatic molecules, such as benzene, where the bonds are completely delocalized.

It is the Peierl's instability that is believed to be responsible for the fact that most CPs in their neutral state are insulators or, at best, weak semiconductors. Hence, there is enough of an energy separation between the conduction and valence bands that thermal energy alone is insufficient to excite electrons across the band gap. To explain the conductive properties of these polymers, several concepts from band theory and solid state physics have been adopted. For electrical conductivity to occur, an electron must have a vacant place (a hole) to move to and occupy. When bands are completely filled or empty, conduction can not occur. Metals are highly conductive because they possess unfilled bands. Semiconductors possess an energy gap small enough that thermal excitation of electrons from the valence to the conduction bands is sufficient for conductivity; however, the band gap in insulators is too large for thermal excitation of an electron across the band gap.

2.1.1.2. Doping and Electrical Conductivity

In the late 1970s Heeger and MacDiarmid found that polyacetylene produced by Shirikawa's method exhibited a 12 order of magnitude increase in electrical conductivity when exposed to oxidizing agents. So how does this 12 order of magnitude increase in electrical conductivity for polyacetylene occur? The diffuse nature of the extended π-system readily allows electron removal from, or injection, into the polymer. The term "doping" has been borrowed from semiconductor physics

with "p-doping" and "n-doping" being used to describe polymer oxidation and reduction, respectively. Doping in regards to semiconductors is quite different as it is a very distinct process carried out at low levels (< 1 %) as compared to CP doping (usually 20-40%). However, the manner by which doping transforms a neutral CP into a conductor remained a mystery for many years.

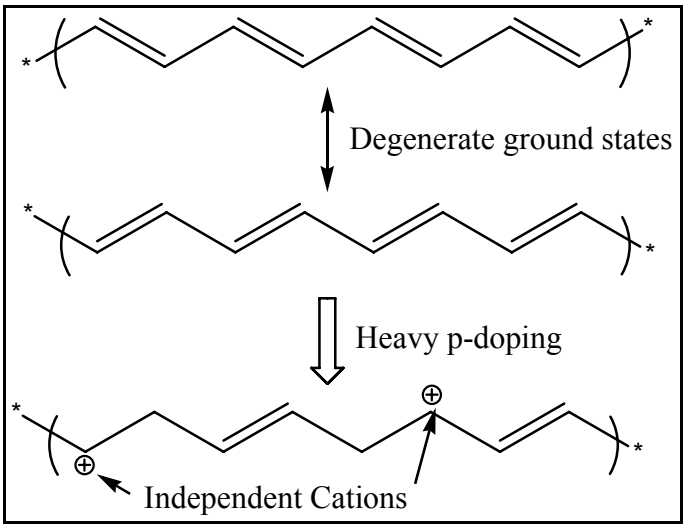

Figure 2.5: p-doping of polyacetylene.

Electron Paramagnetic Resonance (EPR) studies have shown that both the neutral and heavily doped CPs possess no net spin, interpreted as no unpaired electrons, while moderately doped materials were discovered to be paramagnetic in nature. Conductivity experiments showed that it was the "spin-less", heavily-doped form that is the most conductive for a given CP. Such behavior marks an abrupt departure from simple band theory, which centers around spin-containing charge carriers.

Polyacetylene turns out to be a special case when considering its neutral and doped forms. Comparison of the two neutral forms, shown in Figure 2.5, reveals them to be structurally identical, and thus, their ground states are degenerate in energy. Two successive oxidations on one chain could yield radical cations that, upon radical coupling, become non-associated charges termed positive "solitons".

In contrast to polyacetylene, the other CPs shown in Figure 2.1, have non-degenerate ground states (i.e. they do not possess two equivalent resonance forms), and thus, do not show evidence of soliton formation. In this instance, the oxidation of the CP is believed to result in the destabilization (rising of the energy) of the orbital from which the electron is removed. This orbital's energy is increased and can be found in the energy region of the band gap as shown in Figure 2.6a. Initially, if only one

electron per level is removed a radical cation is formed and is known as a "polaron" (Figure 2.6b). Further oxidation removes this unpaired electron yielding a dicationic species termed a "bipolaron" (Figure 2.6c). High dopant concentrations create bipolaron-"rich" materials and eventually lead to band formation of bipolaron levels. Such a theoretical treatment, thereby, explains the appearance, and subsequent disappearance, of the EPR signal of a CP with increased doping as the neutral polymer transitions to the polaronic form and subsequently to the spinless bipolaronic state.

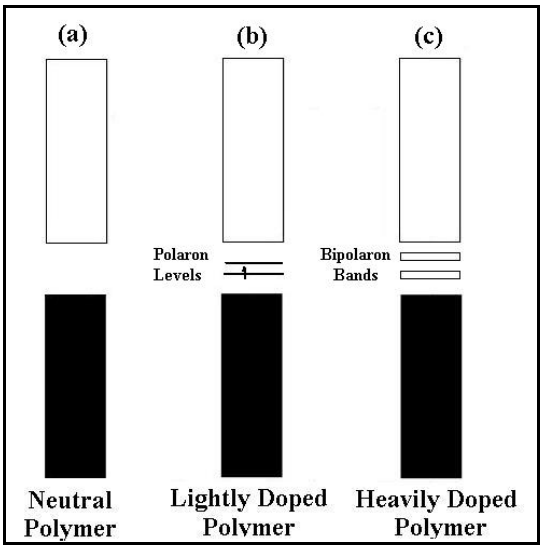

Figure 2.6: The energy region of the band gap.

Contrary to polyacetylene's independent charges, the bipolaron unit remains intact and the entire entity propagates along the polymer chain. Figure 2.7 shows this behavior using polythiophene as an example. In the case of unsubstituted polythiophene, the bipolaronic unit is believed to be spread over six to eight rings. This "bipolaron length" is by no means an absolute number as different polymer backbone and substituent types yield various lengths.

While this general model for charge carrier generation has developed over the years, it is not without conjecture. As one alternate possibility, the presence of diamagnetic π-dimers, resulting from the combination of cation radicals, has been proposed [62, 63]. Much of the basis for these theories comes from investigations into the structural and electronic properties of small conjugated molecules.

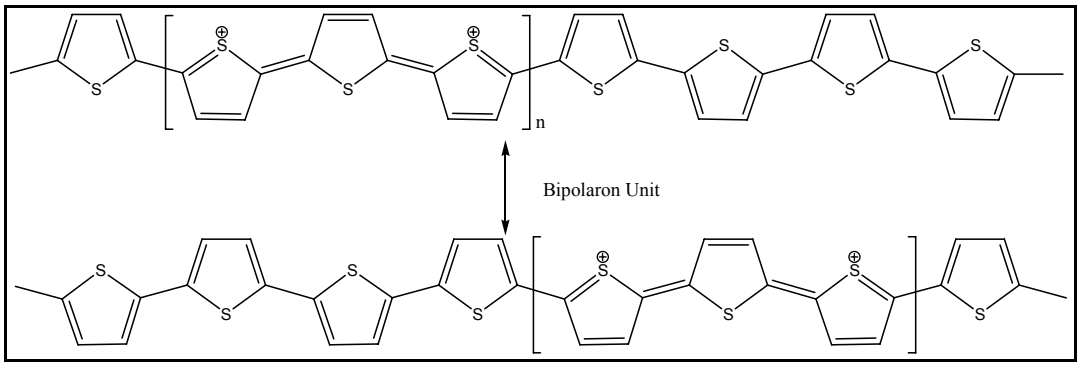

Figure 2.7: Bipolaron unit on polythiophene.

One early explanation of conducting polymers used band theory as a method of conduction. This said that a half filled valence band would be formed from a continuous delocalized π-system. This would be an ideal condition for conduction of electricity. However, it turns out that the polymer can more efficiently lower its energy by bond alteration (alternating short and long bonds), which, introduces a band width of 1.5 eV making it a high energy gap semiconductor. The polymer is transformed into a conductor by doping it with either an electron donator or an electron acceptor. This is reminiscent of doping of silicon based semiconductors where silicon is doped with either arsenic or boron. However, while the doping of silicon produces a donor energy level close to the conduction band or a acceptor level close to the valence band, this is not the case with conducting polymers. The evidence for this is that the resulting polymers do not have a high enough concentration of free spins, as determined by electron spin spectroscopy. Initially the free spins concentration increases with concentration of dopant. At larger concentrations, however, the concentration of free spins levels of at a maximum. To understand this it is necessary to examine the way in which charge is stored along the polymer chain and its effect.

The polymer may store charge in two ways. In an oxidation process it could either lose an electron from one of the bands or it could localize the charge over a small section of the chain. Localizing the charge causes a local distortion due a change in geometry, which costs the polymer some energy. However, the generation of this local geometry decreases the ionization energy of the polymer chain and increases its electron affinity making it more able to accommodate the newly formed charges. This method increases the energy of the polymer less than it would if the charge was delocalized and, hence, takes place in preference of charge delocalization. This is

consistent with an increase in disorder detected after doping by Raman spectroscopy. A similar scenario occurs for a reductive process.

Typical oxidizing dopants used include iodine, arsenic pentachloride, iron (III) and chloride. A typical reductive dopant is sodium naphthalide. The main criteria is its ability to oxidize or reduce the polymer without lowering its stability or whether or not they are capable of initiating side reactions that inhibit the polymers ability to conduct electricity. An example of the latter is the doping of a conjugated polymer with bromine. Bromine it too powerful an oxidant and adds across the double bonds to form sp^3 carbons.

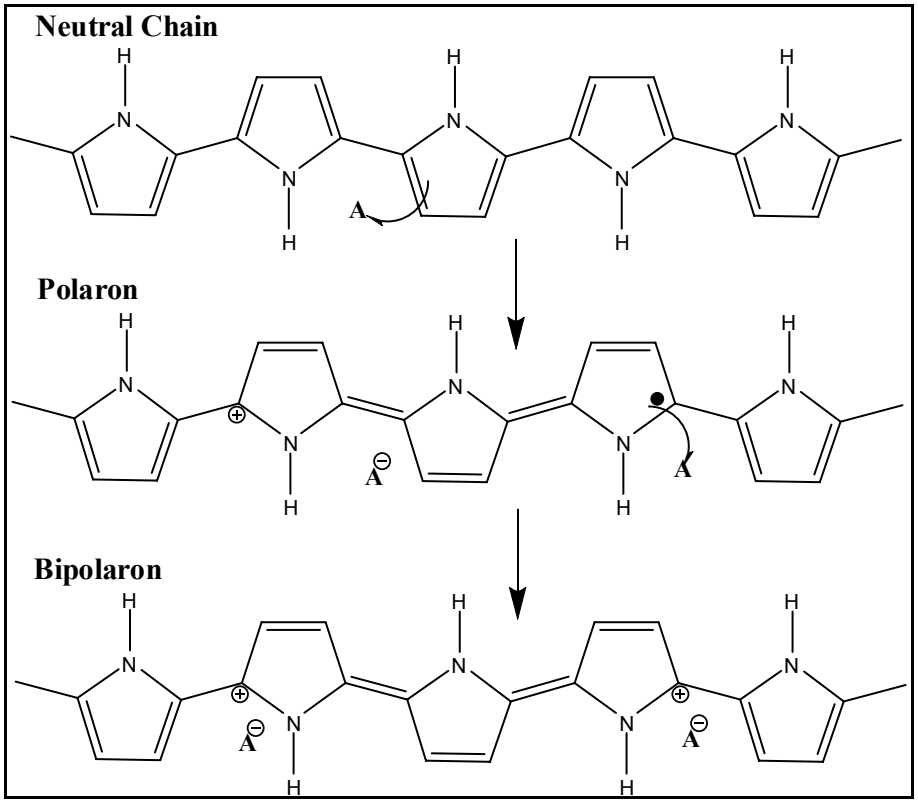

Figure 2.8: Oxidative doping of pyrrole. ($A^{\ominus}$: dopant).

The oxidative doping of polypyrrole proceeds in the following way (Figure 2.8). An electron is removed from the π-system of the backbone producing free radical and a spinless positive charge. The radical and cation are coupled to each other via local resonance of the charge and the radical. In this case, a sequence of quinoid-like rings is used. The distortion produced by this is of higher energy than the remaining portion of the chain. The creation and separation of these defects costs a considerable amount of energy. This limits the number of quinoid-like rings that can link these two bound species together. In the case of polypyrrole it is believed that the lattice

distortion extends over four pyrrole rings. This combination of a charge site and a radical is called a polaron. This could be either a radical cation or radical anion. This creates a new localized electronic state in the gap, with the lower energy states being occupied by a single unpaired electron. The polaron state of polypyrrole is symmetrically located about 0.5 eV from the band edges.

Upon further oxidation the free radical of the polaron is removed, creating a new spinless defect called a bipolaron. This is of lower energy than the creation of two distinct polarons. At higher doping levels it becomes possible that two polarons combine to form a bipolaron. Thus at higher doping levels the polarons are replaced with bipolarons. The bipolarons are located symmetrically with a band gap of 0.75 eV for polypyrrole. This eventually, with continued doping, forms into a continuous bipolaron bands. Their band gap also increases as newly formed bipolarons are made at the expense of the band edges. For a very heavily dope polymer it is conceivable that the upper and the lower bipolaron bands will merge with the conduction and the valence bands respectively to produce partially filled bands and metallic like conductivity.

2.1.1.3. Charge Transport

Although solitons and bipolarons are known to be the main source of charge carriers, the precise mechanism is not yet fully understood. The problem lies in attempting to trace the path of the charge carriers through the polymer. All of these polymers are highly disordered, containing a mixture of crystalline and amorphous regions. It is necessary to consider the transport along and between the polymer chains and also the complex boundaries established by the multiple numbers of phases. This has been studied by examining the effect of doping, of temperature, of magnetism and the frequency of the current used. These test show that a variety of conduction mechanisms are used. The main mechanism used is by movement of charge carriers between localized sites or between solitons, polaron or bipolaron states. Alternatively, where inhomogeneous doping produces metallic island dispersed in an insulating matrix, conduction is by movement of charge carriers between highly conducting domains. Charge transfer between these conducting domains also occurs by thermally activated hopping or tunneling. This is consistent with conductivity being proportional to temperature

2.1.2. Stability and Processability

There are two distinct types of stability. Extrinsic stability is related to vulnerability to external environmental agent such as oxygen, water, peroxides. This is determined by the polymers susceptibility of charged sites to attack by nucleophiles, electrophiles and free radicals. If a conducting polymer is Extrinsic unstable then it must be protected by a stable coating.

Many conducting polymers, however, degrade over time even in dry, oxygen free environment. This intrinsic instability is thermodynamic in origin. It is likely to be cause by irreversible chemical reaction between charged sites of polymer and either the dopant counter ion or the π-system of an adjacent neutral chain, which produces an sp^3 carbon, breaking the conjugation. Intrinsic instability can also come from a thermally driven mechanism which causes the polymer to lose its dopant. This happens when the charge sites become unstable due to conformational changes in the polymer backbone. This has been observed in alkyl substituted polythiophenes.

Conjugated polymers may be made by a variety of techniques, including cationic, anionic, radical chain growth, co-ordination polymerization, step growth polymerization or electrochemical polymerization. Electrochemical polymerization occurs by suitable monomers which are electrochemically oxidized to create an active monomeric and dimeric species which react to form a conjugated polymer backbone. The main problem with electrically conductive plastics stems from the very property that gives it its conductivity, namely the conjugated backbone. This causes many such polymers to be intractable, insoluble films or powders that cannot melt. There are two main strategies to overcoming these problems. There are to either modify the polymer so that it may be more easily processed, or to manufacture the polymer in its desired shape and form. There are, at this time, four main methods used to achieve these aims.

The first method is to manufacture a malleable polymer that can be easily converted into a conjugated polymer. This is done when the initial polymer is in the desired form and then, after conversion, is treated so that it becomes a conductor. The treatment used is most often thermal treatment. The precursor polymer used is often made to produce highly aligned polymer chain which is retained upon conversion.

These are used for highly orientated thin films and fibers. Such films and fibers are highly anisotropic, with maximum conductivity along the stretch direction.

The second method is the synthesis of copolymers or derivatives of a parent conjugated polymer with more desirable properties. This method is the more traditional one for making improvements to a polymer. What is done is to try to modify the structure of the polymer to increase its processability without compromising its conductivity or its optical properties. All attempts to do this on polyacetylene have failed as they always significantly reduced its conductivity. However, such attempts on polythiophenes and polypyrroles proved more fruitful. The hydrogen on carbon 3 on the thiophene or the pyrrole ring was replaced with an alkyl group with at least four carbon atoms in it. The resulting polymer, when doped, has a comparable conductivity to its parent polymer whilst be able to melt and it is soluble. A water soluble version of these polymers has been produced by placing carboxylic acid group or sulphonic acid group on the alkyl chains. If sulphonic acid groups are used along with built-in ionizable groups then such system can maintain charge neutrality in its oxidized state and so they effectively dope themselves. Such polymers are referred to as "self-doped" polymers. One of the most highly conductive derivatives of polythiophene is made by replacing the hydrogen on carbon three with a $-CH_2-O-CH_2CH_2-O-CH_2CH_2-O-CH_3$. This is soluble and reaches a conductivity of about 1000 S cm^{-1} upon doping.

The third method is to grow the polymer into its desired shape and form. An insulating polymer impregnated with a catalyst system is fabricated into its desired form. This is then exposed to the monomer, usually a gas or a vapor. The monomer then polymerizes on the surface of the insulating plastic producing a thin film or a fibre. This is then doped in the usual manner. A variation of this technique is electrochemical polymerization with the conducting polymer being deposited on an electrode either the polymerization stage or before the electrochemical polymerization. This cast may be used for further processing of the conducting polymer. For instance, by stretching aligned bends of polyacetylene/polybutadiene the conductivity increase 10 fold, due to the higher state of order produced by this deformation.

The final method is the use of Langmuir-Blodgett trough to manipulate the surface active molecules into a highly ordered thin films whose structure and thickness which are controllable at the molecular layer. Amphiphilic molecules with hydrophilic and hydrophobic groups produces monolayers at the air-water surface interface of a Langmuir-Blodgett trough. This is then transferred to a substrate creating a multilayer structure comprised of molecular stacks which are normal about 2.5 nm thick. This is a development from the creation of insulating films by the same technique. The main advantage of this technique is its unique ability to allow control over the molecular architecture of the conducting films produced. It can be used to create complex multilayer structures of functionally different molecular layers as determined by the chemist. By producing alternating layers of conductor and insulator it is possible to produce highly anisotropic film which is conducting within the plane of the film, but insulating across it

Table 2.1: Stability and Processing Attributes of Some Conducting Polymers.

POLYMER	Conductivity (Ω^{-1} cm^{-1})	Stability (doped state)	Processing Possibilities
Polyacetylene	10^3 - 10^5	poor	limited
Polyphenylene	1000	poor	limited
PPS	100	poor	excellent
PPV	1000	poor	limited
Polypyrroles	100	good	good
Polythiophenes	100	good	excellent
Polyaniline	10	good	good

2.1.3. Polythiophenes

Polythiophene and its derivatives are stable both in their doped and in their un-doped states. The most important aspect of this heterocycle is the ease of 3-substitution, which can be used to prepare new polymers with exciting properties. By substituting long flexible chains in the 3-position, one can decrease the inter-chain interaction and achieve high solubility (and processability) with some sacrifice in conductivity. Several organic solvent soluble and even water-soluble 3-substituted polythiophenes with high conductivities have been prepared. For example, poly(3-hexylthiophene) has a room temperature conductivity of 30 S cm^{-1}. Poly(3-methylthiophene) has much higher conductivity (a = 500 S cm^{-1}). It has been reported [64] that certain

substituted polythiophenes with conductivities above l000 S cm^{-1} can be prepared. The parent polythiophene has a room temperature conductivity of 50-100 S cm^{-1}. Molecular design concepts resulted in the modification of polythiophene; by benzannelation, a new polymer, poly(isothianaphthene), was synthesized with the smallest band gap among all conjugated conducting polymers. This polymer has a band gap of 1 eV compared with the parent polythiophene, which has a band gap of 2 eV.

2.1.4. 3,4-Ethylenedioxythiophene (EDOT)

During the second half of the 1980s, scientists at the Bayer AG research laboratories in Germany developed a new polythiophene derivative, poly(3,4-ethylenedioxythiophene), having the backbone structure shown in Figure 2.9.

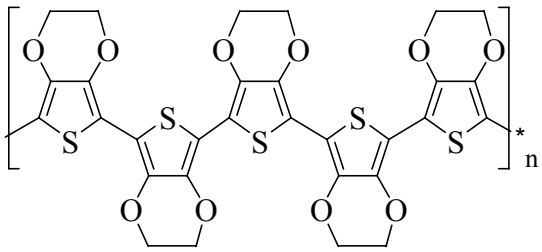

Figure 2.9: Poly(3,4-ethylenedioxythiophene).

This polymer, often abbreviated as PEDT or PEDOT, was initially developed to give a soluble conducting polymer that lacked the presence of undesired α,β- and β,β-couplings within the polymer backbone. Prepared using Standard oxidative chemical or electrochemical polymerization methods, PEDOT was initially found to be an insoluble polymer, yet exhibited some very interesting properties. In addition to a very high conductivity (ca. 300 S/cm), PEDOT was found to be almost transparent in thin, oxidized films and showed a very high stability in the oxidized state [7, 8, 65-67]. The solubility problem was subsequently circumvented by using a water-soluble polyelectrolyte, poly(styrene sulfonic acid) (PSS), as the charge-balancing dopant during polymerization to yield PEDOT/PSS. This combination resulted in a water-soluble polyelectrolyte system with good film-forming properties, high conductivity (ca. 10 S/cm), high visible light transmissivity, and excellent stability [68]. Films of PEDOT/PSS can be heated in air at 100°C for over 1000 h with only a minimal change in conductivity. With this new system, now known under its commercial name BAYTRON P (P stands for polymer), Bayer researchers have been able to

develop several applications. Although initially used as an antistatic coating in photographic films from AGFA, several new applications have been implemented over the past few years (e.g., electrode material in capacitors, material for through-hole plating of printed circuit boards), and more are expected [11,12]. Driven by the properties and utility of PEDOT/PSS, a number of research groups have entered the area of PEDOT chemistry over the past decade. The latter has resulted in an exponential increase in the number of patents and journal publications. This expanding interest is indicative of new materials, processes, devices, and in-place industrial applications.

Although several routes towards EDOT (5) are possible, Jonas et al. developed a synthetic strategy, shown in Figure 2.10, starting from thiodiglycolic acid, based on the synthesis of 3,4-ethylenedioxythiophene-2,5-dicarboxylic acid (4) reported by Gogte et al. [69] Subsequent decarboxylation using a copper salt led to EDOT in five steps. EDOT has a boiling point of 225 °C (1013 mbar) and slowly turns dark upon exposure to air and light due to partial oxidation.

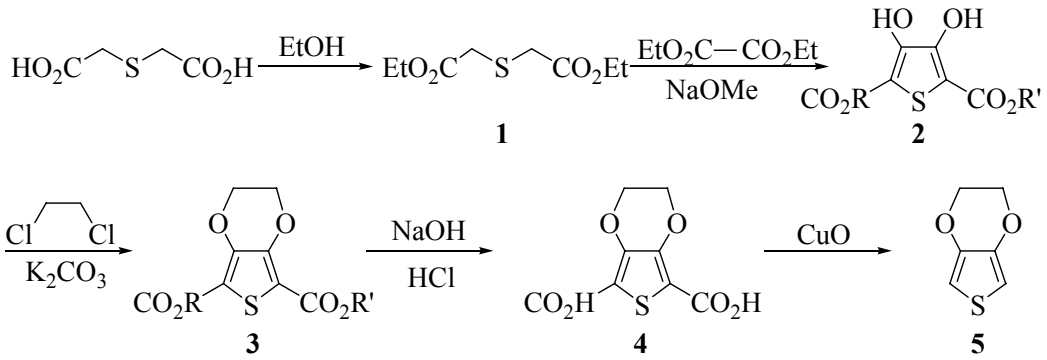

Figure 2.10: Synthesis of EDOT (R,R' = Methyl or Ethyl).

2.1.5. Thiazoles

There has been some interest recently in thiazole-based conjugated polymers. [70] Bredas and co-workers [71] have used valence effective Hamiltonian (VEH) calculations, a method known to give very good band structures for sulfur and nitrogen-containing polymers, [72] to investigate the effect of placing nitrogen atoms in the conduction pathway of a poly(a-thiophene) structure. They conclude that doped polythiazoles should be good conductors.

The electronic, optical, and electric properties of π-conjugated poly(arylene)s have been the subject of many papers [55]. Among the poly(arylene)s, those made up of

recurring five-membered rings (Figure 2.11) have received much attention because of their interesting chemical and physical properties. They are considered to take coplanar structures and to form highly extended π-conjugated systems owing to their less sterically hindered structures compared with those of poly(arylene)s constituted of six-membered rings [e.g., poly(*p*-phenylene), PPP].

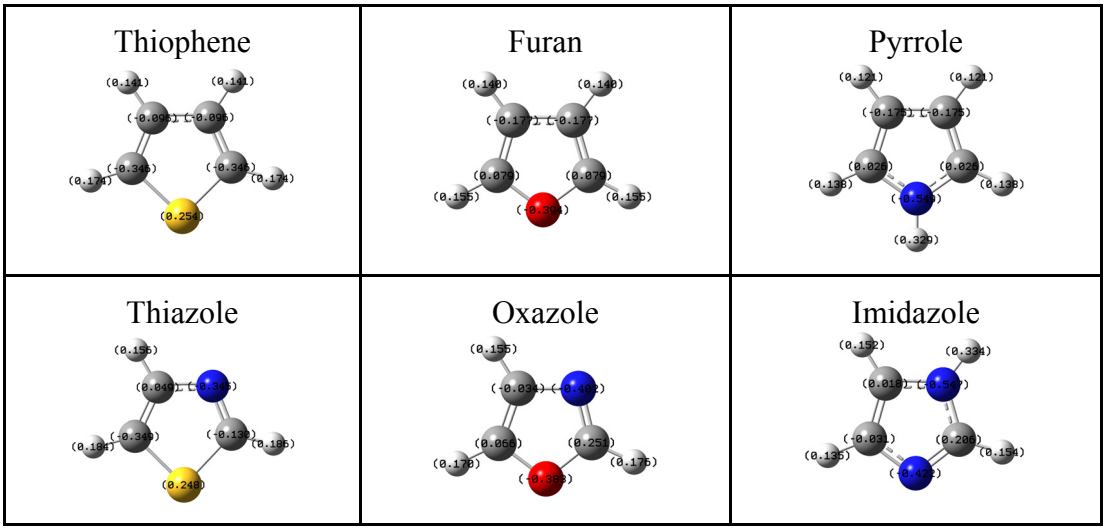

Figure 2.11: The most studied five-membered rings with Mulliken atomic charges.

Table 2.2: Mulliken atomic charges calculated using Gaussian 98 with Hartree Fock using the b3lyp/6-31g basis set.

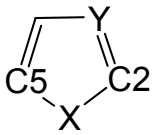

X	Y	ρ (C2)	ρ (C5)
S	CH	-0.346	-0.346
O	CH	0.079	0.079
NH	CH	0.026	0.026
S	N	-0.130	-0.349
O	N	0.251	0.066
NH	N	-0.031	0.206

PTh and PPy are made up of "electron-excessive" heterocyclic units and are susceptible to chemical and electrochemical oxidation (or p-doping). On the other hand, it has been recently reported that π-conjugated polyheterocycles containing electron-withdrawing imine nitrogen(s) (e.g., poly(pyridine-2,5-diyl) PPyb and poly-(quinoxaline-5,8-diyl) derivatives P[5,8-Qx(R1R2)]) show electron-accepting properties and are susceptible to reduction (or n-doping).

However, despite many examples of six-membered ring poly(arylene)s with imine nitrogen(s), analogous π-conjugated polymers composed of recurring five-membered heterocyclic units have received much less attention. Here we report the preparation

of new π-conjugated five-membered-ring poly(arylene)s containing the imine nitrogen and their redox and optical properties in comparison with those of other π-conjugated polyheterocycles described above.

2.1.6. Polypyrroles

Among the conducting polyheterocycles, the most intensively studied polymers are polypyrrole, polythiophene, and their derivatives as well as polyphenylene and polyphenylene chalcogenides. Polypyrrole was shown to be a conducting polymer in 1968. Dall'Olio et al [73] prepared it by oxidation of pyrrole in sulfuric acid as a black powder with room temperature conductivity of 8 S cm^{-1}. This work was then extended by workers at IBM who showed that films of this polymer can be obtained by electrochemical polymerization. These films could be cycled electrochemically between a conducting (doped) state and an insulating state, with conductivities varying from [74] 100 to 10^{-10} S cm^{-1}. Unlike the morphology of the Shirakawa's polyacetylene, which is fibrillar, polypyrrole films are dense. Thus, physically impermeable films of polypyrrole could be prepared.

A fairly long period elapsed before this organic π-system attracted general interest and was found to be electrically conductive. Conductive polypyrrole films are obtained directly by anodic polymerization of pyrrole in aqueous or organic electrolytes (acetonitrile) [74]. They are black and, under suitable reaction conditions, can be detached from the anode in the form of self-supporting films (minimum thickness ca. 30 μm). Some of the conducting salt used in the electrolyte solution is incorporated in the film as a counterion. In contrast to polyacetylene, polypyrrole has a high mechanical and chemical stability and can be produced continuously as flexible film (thickness 80 μm; trade name: Lutamer, BASF) by electrochemical techniques. The quality of the polymers is greatly influenced by many factors, e.g., impurities, electrode material, pressure, concentrations, temperature, and comonomers. The most decisive, however, are the current density and the electrolyte, particularly the conducting anion X^- [75] because it is incorporated into the polymer as a counterion. The properties of the counterion (e.g., its size, geometry, charge) influence the properties of the polymer. The amount of counterion (anion) incorporated depends on the reaction conditions. In general, one anion is incorporated for every three pyrrole units. Exceptions are pyrrole or

thiophenesulfonic acids where the counterion is coupled directly to the monomer (self doping) [76]. Some typical conducting anions are fluoroborate, perchlorate, aromatic sulphonic acids, penicillin, n-dodecyl sulfate [75], phthalocyanine sulphonic acid, poly(styrene sulphonic acid), camphor sulphonic acid, styrene sulphonic acid, and heparin.

By changing reaction conditions, polymers with different surface morphologies, (e.g., an open porous structure) can be obtained.

The anion X^- can also be released, e.g., by applying a negative potential. Release can be specifically controlled, offering interesting possibilities for active counterions of medical interest (e.g., heparin and monobactam) that are incorporated into polypyrrole. Variation of the monomers and their substituents yields polymers with conductivities between 10^2 and 10^{-4} S/cm. Alkyl substituents also increase the solubility of the polymers with the result that electrically conducting polymers can be applied as coatings from solutions. This also applies to polymers derived from bridged pyrroles. An interesting variant is the chemical oxidation of heterocycles (e.g., thiophene or pyrrole [77] dissolved in an organic solvent (e.g., ethanol) on the surface of various materials. Conductive coatings (thickness 0.01 μm) can be produced on films of poly(phenylene sulfone), block copolymers of butadiene and styrene (Ultrason, Styrolux), poly(vinyl chloride), or other polymer films to give transparent, antistatic films with conductivities of about 0.001 S/cm. Ceramics and glass can also be coated in this way. Porous material (e.g., wood, fabrics, and open celled foams) or fibers (e.g., polyamide, glass, or carbon fibers) can also be modified and rendered antistatic by this method. Conductive powders (e.g., polypyrrole) with particle sizes of about 0.1 μm and conductivities of up to 10 S/cm can also be produced by chemical oxidation and can be incorporated as fillers in thermoplastics. These materials can be used for chip carriers.

2.1.7. Application Areas of Conducting Polymers

The commercialization exemplified by the following list of materials illustrates the effects of Heeger's, McDiarmid's and Shirakawa's work on the later development of conductive polymers. The principal interest in the use of polymers is in low-cost manufacturing using solution-processing of film-forming polymers. Light displays and integrated circuits, for example, could theoretically be manufactured using

simple inkjet printer techniques [56, 78-80]. Doped polyaniline is used as a conductor and for electromagnetic shielding of electronic circuits. Polyaniline is also manufactured as a corrosion inhibitor.

Poly(3,4-ethylenedioxy-thiophene) (PEDOT) doped with polystyrenesulfonic acid is manufactured as an antistatic coating material to prevent electrical discharge exposure on photographic emulsions and also serves as a hole injecting electrode material in polymer light-emitting devices.

Poly(phenylene vinylidene) derivatives have been major candidates for the active layer in pilot production of electroluminescent displays (mobile telephone displays).

Polythiophenes have been studied extensively for use in light-emitting diodes, among other applications, due to the chemical variability offered by substitution at the 3- and 4- positions. The regularity of the side-chain incorporation strongly affects the electronic band gap of the conjugated main chain and is critical to device performance [81].

Polypyrrole has been tested as microwave-absorbing "stealth" (radar-invisible) screen coatings and also as the active thin layer of various sensing devices. The conductivity of polypyrrole film suggests applications such as flexible conductive paths in printed circuits, heating films, and film keyboards. Polypyrrole films show good electromagnetic shielding effects of about 40 dB over a wide range of frequencies (0 – 1500 MHz).

Other possible applications of conductive polymers include supercapacitors and electrolytic-type capacitors. Some conductive polymers such as polyaniline show a whole range of colors as a result of their many protonation and oxidation forms. Their electrochromic properties can be used to produce, e.g. "smart windows" that absorb sunlight in summer. An advantage over liquid crystals is that polymers can be fabricated in large sheets and unlimited visual angles. They do not generally respond as fast as in electron-gun displays, because the dopant needs time to migrate into or out from the polymer - but still fast enough for many applications.

2.1.7.1. Electrochemical Capacitors (ECs)

ECs are sometimes called supercapacitors, ultracapacitors, or hybrid capacitors. The term ultracapacitor or supercapacitor is usually used to describe an energy storage

device based on the charge storage in the electrical double layer (EDL) of a high-surface area carbon in aqueous electrolytes. The market for these devices used for memory protection in electronic circuitry is about $150-$200 million annually. New potential applications for ECs include the portable electronic device market, the power quality market, due particularly to distributed generation, and low-emission hybrid cars, buses, and trucks.

There is no commonly accepted nomenclature for ECs except that the definitions of anode, cathode, etc., carry over from battery and fuel cell usage, such as the anode as the negative terminal and cathode as the positive terminal. In general, ultracapacitors have referred to capacitors with two high-surface area carbon electrodes for the anode and cathode. This arrangement where both electrodes have the same configuration will be referred to as a symmetric capacitor. The term supercapacitor has also been used to refer to the symmetric combination of two carbon electrodes that are catalyzed with ruthenium dioxide (RuO_2). The RuO_2 introduces a redox couple between two valence states of ruthenium, to result in higher capacitance for the carbon electrodes, but with a penalty in slower time constant for reacting to a pulse demand. A second type of EC combines a battery or redox electrode with a carbon electrode, such as nickel hydroxide cathode with a carbon anode. These supercapacitor or hybrid capacitors will be referred to as an asymmetric EC.

When an electrode, that is, an electronic conductor, is immersed into an electrolyte solution, that is, an ionic conductor, there is a spontaneous organization of charges at the surface of the electrode and in the electrolyte facing the electrode. This EDL forms at the electrode-electrolyte interface with one layer at the surface inside the conductor and the other layer in the electrolyte. The two charged layers are considered to behave as a physical capacitor, with the charges in the solution and in the conductor separated by a distance of the order of molecular dimensions. The characteristics of the EDL depend on the electrode surface structure, the composition of the electrolyte, and the potential field between the charges at the interface. Depending on the surface charge of the electrode materials, positive or negative ions from the electrolyte form the solution part of the EDL at the interface between the electrode and the electrolyte. According to this simple Helmholtz model, the charges are concentrated on each side of the electrode surface. A more complex model of the EDL structure takes into account the different sizes of the ions and their reactivity

with the surface. The outer Helmholtz plane (OHP) refers to the distance of closest approach of nonspecifically adsorbed ions (generally cations) in solution. Cations that populate the OHP are usually solvated and thus are generally larger than the less solvated anions. The interactions of the ions of the OHP with the surface charge have the character of coulombic interactions. The inner Helmholtz plane (IHP) refers to the distance of closest approach of specifically adsorbed ions (generally anions) and/or adsorbed solvent molecules to the electrode surface. These adsorption processes are determined by chemical affinities of the ions to the electrode surface and the field strength in the EDL. In practice, the structure of the EDL is much more complex than the models discussed above.

The double layer at the electrode surface forms and relaxes almost instantaneously. It has a time constant, or time of formation, of 10^{-8} s. Therefore, the structure of the double layer has the capability to respond rapidly to potential changes in the same time frame. The process involves only a charge rearrangement, not a chemical reaction. This rapid response to change is in contrast to the situation with the redox electrode reactions in batteries and fuel cells. The time constant for the redox reactions is much slower and in the range of 10^{-2}-10^{-4} s related to the impedance of the reaction. The redox reactions contribute to "polarization capacitance" associated with the electrode reactions. The other main difference between supercapacitors and batteries and fuel cells is the reversibility (short time constant) of the EDL process compared to the longer time constant of the redox reactions and the stress from detrimental side reactions, which reduce the cycle life and long term stability of the device. Whereas cycle life and stability of the double layer electrochemical capacitor can easily exceed 1 million cycles, battery electrodes can reach this level only if charged and discharged at a low depth of discharge. When carbons are placed in an electrolyte, they generally assume a voltage near the zero point of charge of the EDL. In aqueous solutions, this is near 0 V versus hydrogen.

2.1.7.2. Electrochromic Devices [82]

There are three main types of electrochromic materials in terms of their electronically accessible optical states. The first type includes materials with at least one colored and one bleached state. These materials are especially useful for absorption/transmission-type device applications such as smart windows and optical

shutters. Typical examples of this area are metal oxides, viologens, and polymers such as poly(3,4-ethylenedioxythiophene) (PEDOT). A second class of materials consists of electrochromes with two distinctive colored states. These EC materials lack a transmissive state but are useful for display-type applications where different colors are desired in different redox states. Polythiophene is a good example of this type, where the thin films of this polymer switch from red to blue upon oxidation. A third class includes the growing interest in the electrochromic field, where more than two color states are accessible depending on the redox state of the material. This is the area where conjugated polymers have found the most interest due to their versatility for making blends, laminates, and copolymers.

Switching speed is often reported as the time required for the coloring/bleaching process of an EC material. It is important especially for applications such as dynamic displays and switchable mirrors. The switching speed of electrochromic materials is dependent on several factors such as the ionic conductivity of the electrolyte, accessibility of the ions to the electroactive sites (ion diffusion in thin films), magnitude of the applied potential, film thickness, and morphology of the thin film. Today sub second switching rates are easily attained using polymers and composites containing small organic electrochromes.

Electrochromic stability is usually associated with electrochemical stability since the degradation of the active redox couple results in the loss of electrochromic contrast and hence the performance of the EC material. Common degradation paths include irreversible oxidation or reduction at extreme potentials, iR loss of the electrode or the electrolyte, side reactions due to the presence of water or oxygen in the cell, and heat release due to the resistive parts in the system.

One of the benefits of using an electrochromic material in a display as opposed to a light-emitting material is its optical memory (also called open-circuit memory), which is defined as the time the material retains its absorption state after the electric field is removed. In solution-based electrochromic systems such as viologens, the colored state quickly bleaches upon termination of current due to the diffusion of soluble electrochromes away from the electrodes (a phenomenon called self-erasing). In solid-state ECDs, where the electrochromes are adhered to electrodes, the electrochromic memory can be as long as days or weeks with no further current

required. In reality, however, ECDs may require small refreshing charges to maintain the charge state because side reactions or short circuits change the desired color.

2.2. Electropolymerization and Characterization Techniques

In an electrochemical polymerization, the monomer, dissolved in an appropriate solvent containing the desired anionic doping salt, is oxidized at the surface of an electrode by application of an anodic potential (oxidation). The choice of the solvent and electrolyte is of particular importance in electrochemistry since both solvent and electrolyte should be stable at the oxidation potential of the monomer and provide an ionically conductive medium. Organic solvents like acetonitrile or propylene carbonate have very large potential windows [38], and a high dielectric constant which allows a good dissociation of the electrolyte and thus a good ionic conductivity. As a result of the initial oxidation, the radical cation of the monomer is formed and reacts with other monomers present in solution to form oligomeric products and then the polymer. The extended conjugation in the polymer results in a lowering of the oxidation potential compared to the monomer. Therefore, the synthesis and doping of the polymer are generally done simultaneously. The anion is incorporated into the polymer to ensure the electrical neutrality of the film and, at the end of the reaction, a polymeric film of controllable thickness is formed at the anode. The anode can be made of a variety of materials including platinum, carbon fiber, gold, glassy carbon, and tin or indium-tin oxide (ITO) coated glass [83]. The electropolymerization is generally achieved by potentiostatic (constant-potential) or galvanostatic (constant-current) methods. These techniques are easier to describe quantitatively and have been therefore commonly utilized to investigate the nucleation mechanism and the macroscopic growth. Potentiodynamic techniques such as cyclic voltammetry corresponds to a repetitive triangular potential waveform applied at the surface of the electrode. The latter method has been mainly used to obtain qualitative information about the redox processes involved in the early stages of the polymerization reaction, and to examine the electrochemical behavior of the polymer film after electrodeposition [83].

Cyclic voltammetry (CV) is very often used to characterize conducting polymer films. This is the method of choice for studying the reversibility of electron transfer because the oxidation and reduction can be monitored in the form of a

current-potential diagram [84]. Intermediate species of very short lifetimes can be observed with microelectrodes using high scanning speeds [85]. These intermediate species (radical cations) are extremely important for the understanding of the polymerization mechanism. Another electrochemical technique, coulometry, and measures the amount of electricity involved in the oxidation process. The knowledge of the initial charge used to polymerize the monomer, and the charge involved in the doping process allows the estimation of the doping level in the conducting polymer

Chronoamperometry, *i.e.* measuring the current as a function of time, is a method of choice to study the kinetic of polymerization and especially the first steps [83]. As a potential step is large enough to cause an electrochemical reaction is applied to an electrode, the current changes with time. The study of this current response as a function of time is called chronoamperometry (CA). CA is a useful tool for determining diffusion coefficients and for investigating kinetics and mechanisms. Unlike CV, CA can yield this information in a single experiment.

2.2.1. Factors Effecting Electropolymerization

2.2.1.1. Effect of Electrolyte

One important parameter affecting the physical characteristics and morphology of PPy is the nature and the concentration of the dopant that represents about 30% of the weight of the polymer film. The choice of an electrolyte is made by considering its solubility and its nucleophilicity. Moreover, the anion oxidation potential should be higher than the monomer. The dopant can be organic or inorganic and can be varying sizes (from chloride to polystyrenesulfonate). The size of the anion controls the microstructure and the porosity of the polymer. Indeed, this determines the ability of the polymer to undergo an easier diffusion of the dopants during the redox process [86]. The nature of the anion has an impact on the quality of the film produced which depends on the hydrophobic character of the anion, and the interactions between the polymer and the dopant. For instance, Kassim et al. [87] have shown that in aqueous solution, the utilization of a large aromatic sulfate anion (surfactant in nature) gives stable conducting polymers with better mechanical properties than when a perchlorate anion is used. Because of their hydrophobic interaction with water, one of the roles played by these organic anions is to orient the polymer chain parallel to

the electrode surface. This chain orientation increases the order in the polymer structure [88]. Kuwabata et al. [89] have shown by studying a series of carboxylate anions that the basicity of the anion plays a role in polymer growth. The higher the basicity of the anion yields the lower the conductivity of the polymer. This phenomenon is due to an increase in the interactions between the positive charges of the polymer and the anions. Inversely, anion acidity leads to an increase in the conductivity of PPy [88]. On another hand, anion nucleophilicity interferes with the reaction by increasing the formation of soluble products. The electrolyte concentration is also important although the effect is not entirely understood. The polymers of the highest conductivity are produced when elevated concentrations of electrolyte are used. For instance, the conductivity and tensile strength of the as-prepared nitrate doped PPy films increased by ca. 50-70% when the electrolyte concentration changed from 0.2 to 1 M. Above 1 M, no improvement was observed in the quality of the PPy films. Note that the influence of the cation associated with the anion is not negligible. In fact, the size of the cation (for example tetraalkylammonium) can equally have an influence on the polymer conductivity. It has been found that the larger cation, the higher conductivity of the polymer [90].

2.2.1.2. Effect of Monomer Concentration

In a classical electropolymerization, monomers are continually oxidized while the electroactive polymer film forms at the electrode surface. Since the oxidation of the monomer occurs at a higher potential than that of the redox processes of the polymer, side reactions including crosslinking and/or over-oxidation of the polymer could take place. One disadvantage of pyrrole is the presence of available sites for coupling in the beta positions. Waltman et al. has shown by using theoretical calculations that the ability to distinguish between the α and β positions decreases as the conjugation increases for pyrrole oligomers [91]. π-coupling leads to a conjugation break along the polymer backbone which results in an increase of the observed band gap and a decrease in conductivity. Cross et al [92] have shown that the α-disubstituted monomers yield only soluble products while the α-monosubstituted monomers can give a low molecular weight polymer where β-bonding is certainly present. However, substitution in β-position avoids the β couplings and causes an increase in crystallinity of the polymer. However, the steric effect of beta substitution cannot be ignored. For instance, 3,4-dimethylpyrrole produces polymers with lower

conductivities and lower mean conjugation length relative to pyrrole [93]. However, the substituents in position 3- or 4- of the pyrrole ring can also affect the electron density of the heterocycle. Merz et al. have studied the effect of substitution in the 3.4-dimethoxypyrrole and showed that the electron donating effect of the methoxy groups results in a 350 mV decrease of the monomer oxidation potential. Thus, polymerization occurs exclusively through the alpha-positions and is likely to proceed without crosslinking and over-oxidation of the deposited polymer because of the lower potential required for the electropolymerization [94]. In order to substitute both the 3, 4 positions while avoiding steric interactions between repeat units of the polymer, Reynolds et al. have studied the electropolymerization of 3,4-alkylenedioxypyrrole monomers [95, 96]. The resulting polymers exhibit a lower band gap (2.0 to 2.2 eV) and a lower half-wave oxidation potential (ca. -0.3 V vs. SCE) compared to polypyrrole. This low half-wave oxidation potential is of particular interest for biological applications since these new polymers, which are water compatible, are not reduced by strong biological reductants such as 1,4-dithiothreitol. Poly(3,4-alkylenedioxypyrrole)s have also demonstrated interesting properties as electrochromic materials switching rapidly from a red or orange neutral state to a light blue-gray doped state [96]. Substitution by halogen atoms in the 3,4 positions was found to result in a higher doping level compared to pyrrole [97]. This phenomenon is due to the greater charge delocalization in the polyhalopyrroles because of the mesomeric effect of the halogen atoms.

N-substituted pyrroles are known to exhibit a conductivity three orders of magnitude lower than that of PPy as demonstrated by Diaz and coworkers for poly(N-methylpyrrole) [93]. These results were further confirmed by monitoring the conductivity of poly(3,4-dimethoxy-/V-methylpyrrole) which was found to be three orders of magnitude lower than poly(3,4-dimethoxypyrrole) [94]. The larger the substituent on the nitrogen atom result in the greater the steric interaction between repeating units and subsequently causes the weaker the conductivity. This drop in conductivity is due to fact that the pyrrole units are not totally coplanar in the polymer, as demonstrated by the X-ray studies performed by Street on the alpha-alpha-substituted tetramer of N-methylpyrrole [55]. The influence of N-substitution on the electropolymerization characteristics was examined by Waltman et al, [98]. The polymer yield and the rate of oxidation were found to decrease as the size of the alkyl group increases. Bonding large substituents to the nitrogen atom or to the beta-

carbon stabilizes the cation radical without stopping the polymerization. If this intermediate is too stable it can diffuse into the solution and form soluble products. As a result, the yield and the molecular weight of the polymer will be low. It should also be noted that some specific N-substituent inhibit the polymerization because of their basicity, as observed for N-pyrrolidic pyrrole [92].

2.3. Characterization Techniques

2.3.1. Electrochemical Impedance Spectroscopy (EIS)

With impedance data a complete description of an electrochemical system is possible [99]. Representations of the electrified interface have gradually evolved from repeated modifications (see Figure 2.12.) of the model first proposed by Helmholtz [100]. In a simple case, the interface can be modeled by an equivalent circuit (see Figure 2.13.), also called a Randles circuit [101], made of a double-layer capacitor in parallel with a polarization resistor (also known as a charge transfer resistor with certain constraints) and a Warburg impedance, connected in series with a resistor that measures the resistance of the electrolyte solution. Depending on the types of electrochemical reactions involved at the interface, the equivalent circuit can be much more complicated.

The model given in the Figure 2.13 predicts that a faradic current, which is due to the redox reactions, is always coupled with a capacitive component. Capacitance is regarded as noise, and considerable efforts have been made to eliminate or minimize it, resulting in tast (sampling), normal pulse, and differential pulse voltammetry [38]. However, reducing or minimizing the effects of non-faradic currents is considered a passive way to solve the problem. A more active and direct approach would be to determine and separate the faradic currents from the non-faradic signals [102], which is possible with Electrochemical Impedance Spectroscopy (EIS) because it provides all the information about the interface and the electrolyte solution.

Impedance is a totally complex resistance encountered when a current flows through a circuit made of resistors, capacitors, or inductors, or any combination of these. Depending on how the electronic components are configured, both the magnitude and the phase shift of an ac can be determined. Because an inductive effect is not

usually encountered in electrochemistry, we consider only the simple equivalent circuit shown in Figure 2.13 in which no inductor is present.

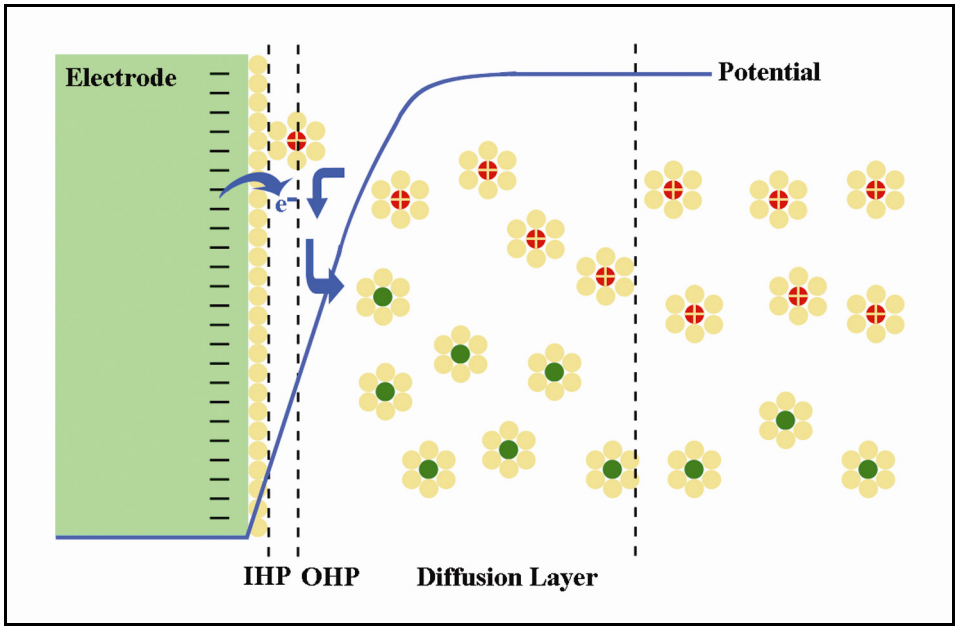

Figure 2.12: The oxidants (red) with a positive charge diffuse toward the negatively charged electrode, accept electrons from the electrode at the interface, become the reductants (green), and diffuse to the bulk of the solution. The oxidant is also a counterion to the electrode. No specific adsorption is considered at the interface. IHP and OHP are the inner and outer Helmholtz planes, respectively.

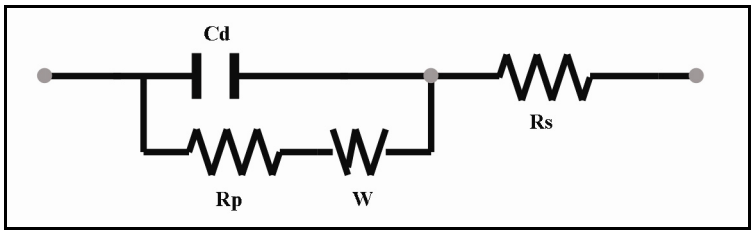

Figure 2.13: An equivalent circuit representing each component at the interface and in the solution during an electrochemical reaction is shown for comparison with the physical components. Cd, double layer capacitor; Rp, polarization resistor; W, Warburg resistor; Rs, solution resistor.

However, first consider an experiment in which a series of increasing dc potentials (a ramp) are applied to a working electrode in an electrochemical cell containing an electroactive species. A current–potential curve (Figure 2.14) is obtained, which is described by the Butler–Volmer equation (solid line)

$$i = i_0 \left[e^{\frac{-\alpha nF}{RT}\eta} - e^{\frac{(1-\alpha)nF}{RT}\eta} \right] \qquad \textbf{(2.2)}$$

in which η is the overpotential defined as $E - E_{eq}$, with E and E_{eq} representing the applied and equilibrium potentials, respectively; i_0 is the exchange current at $\eta = 0$; n is the number of electrons transferred; F is the Faraday constant; R is the gas constant; T is the absolute temperature; and α is the transfer coefficient for electron transfer. The faradic current i is limited by the mass transport (dashed line curving to the right) when the rate of electron transfer becomes large enough. At a given overpotential η_{bias}, the slope of the curves, $d_i/d\eta_{bias}$, is $1/R_p$, in which R_p is the polarization resistance. When a small ac voltage wave of frequency ω at η_{bias} (Figure 2.14.) is superimposed, the ac of the same frequency will be flowing on top of the dc. Because the interface has resistors and a capacitor (Figure 2.13), the flowing ac will experience a phase shift, expressed as i_{bias}, caused by the ac wave perturbation. For an equivalent circuit (Figure 2.13), a straightforward impedance expression can be derived by applying Ohm's law to two components connected in parallel. One of these is R_p, and the other is $1/(j\omega C_d)$, in which C_d is the double-layer capacitance.

$$Z(\omega) = R_s + \frac{R_p}{1 + j\omega R_p C_d} = R_s + \frac{R_p}{1 + \omega^2 R_p^2 C_d^2} - \frac{j\omega R_p^2 C_d}{1 + \omega^2 R_p^2 C_d^2} = Z' + jZ'' \qquad \textbf{(2.3)}$$

To make the derivation of the equation and its interpretation straightforward, we neglected the contribution of the Warburg component. Thus, the impedance of the interface consists of two parts, a real number Z' and an imaginary number Z'' with a complex representation, $Z(\omega) = Z'(\omega) + jZ''(\omega)$ with phase angle $\phi = \tan^{-1}[Z''(\omega) + Z'(\omega)]$. Although the capacitance is relatively constant over the potential at a given electrode, the R_p varies as a function of η_{bias} applied to the electrode.

At a given dc bias potential, a series of $Z(\omega)$ data are obtained in a range of frequencies, typically 100 kHz to 10^{-4} Hz. The impedance varies, depending on frequencies, and is often plotted in different ways as a function of frequency (making it a spectroscopic technique), hence, the name EIS [38, 39].

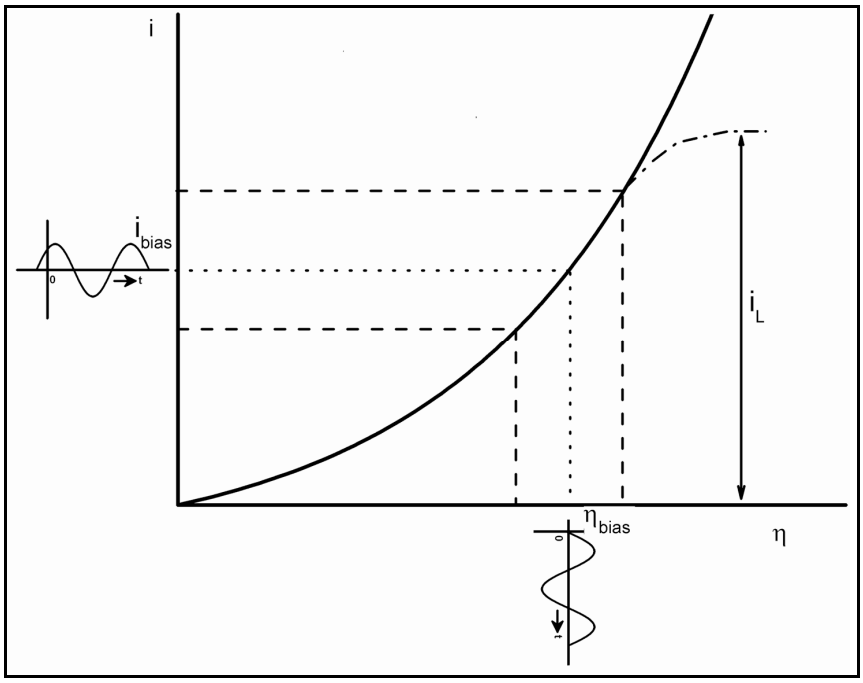

Figure 2.14: The dc plotted as a function of overpotential according to the Butler–Volmer equation (solid line), which is limited by mass transport at large overpotentials (dashed line curving to the right), an ac voltage (broken line) superimposed on the dc bias potential, η_{bias} (dot-dashed line), shown on the *i* axis $[\eta_{bias} + \Delta\eta \sin(\omega t)]$, and the resulting ac superimposed on the dc on the *i* axis $[i_{bias} + \Delta i \sin(\omega t + \phi)]$. R_p is obtained by taking $\Delta\eta/\Delta i$, in which *i* is obtained after applying the ac voltage wave at a given η.

By treating the impedance data in such a frequency range, system characteristics for an electrochemical reaction (i.e., R_s, R_p, and C_d) can be obtained. R_p is a function of potential; however, at $\eta = 0$, it becomes the charge-transfer resistance R_{CT}. Two convenient ways of treating the impedance data are the Nyquist plot, in which imaginary numbers $Z''(\omega)$ are plotted against real numbers $Z'(\omega)$, and the Bode plot, in which absolute values of impedance or phase angle are plotted against the frequency. Extraction of the system characteristics requires interpreting the Nyquist plot according to Equation 2.4. At high frequencies, the frequency dependent term of Equation 2.4 vanishes, resulting in $Z(\omega) = Z'(\omega) = R_s$, which is an intercept on the $Z'(\omega)$ axis on the high-frequency side ($\phi = 0$ or $Z''(\omega) = 0$). For $\omega \rightarrow 0$, Equation 2.3 becomes $Z(\omega) = R_s + R_p$, which is an intercept on the $Z'(\omega)$ axis on the low frequency side. At the frequency where a maximum $Z''(\omega)$ is observed, the straightforward relationship (Equation 2.4), which is the time constant of the electrochemical reaction, can be shown and indicates how fast the reaction takes place. Also, if

$R_p \bullet C_d$ is known, C_d can be obtained because R_p is already known from the low-frequency intercept on the $Z'(\omega)$ axis.

$$R_p \bullet C_d = 1/\omega_{\max} = 1/(2\pi f_{\max}) = \tau_{rxn} \qquad \textbf{(2.4)}$$

The Nyquist plot gives all the necessary information about the electrode–electrolyte interface and the reaction. Similar information is obtained by examining the Bode diagram using Equation 2.2. log R_s and log (R_p+R_s) are obtained straightforwardly from the $Z(\omega)$ versus log ω plot at high and low frequencies from the same argument as the Nyquist plot. In the intermediate frequency region, an almost straight line with a slope of ~ –1.0 can be seen. The equation for this line is obtained by ignoring the frequency-independent terms, R_s and 1 in the denominator, of Equation 2.3 to yield 2.5

$$Z(\omega) = R_s + \frac{R_p}{1 + j\omega R_p C_d} \qquad \textbf{(2.5)}$$

Taking the logarithm on both sides of the resulting equation yields $Z(\omega) = -\log\omega - \log C_d$, which says that $\log|Z(\omega)|$ vs. $\log\omega$ would have a slope of –1, and C_d can be obtained from the intercept of this line with the $Z(\omega)$ axis when $-\log\omega = 0$ at $\omega = 1$. Thus, the Bode plot provides the same information as the Nyquist plot. The ϕ vs. $\log\omega$ plot shows that the impedance responses are resistive primarily at high and low frequencies as indicated by practically no phase shifts, whereas at intermediate frequencies, they are mostly capacitive as their phase shifts get closer to 90°.

Contribution and the effect of the Warburg impedance can be important at low frequencies because the mass transport of the electroactive species may limit the electron-transfer process. The Warburg impedance is imparted by mass transfer and can be derived by

$$Z(\omega) = R_s + R_p\left[1 + \frac{\lambda}{\sqrt{2\omega}}\right] - R_p^2\lambda^2 C_d - \frac{jR_p\lambda}{\sqrt{2\omega}} \qquad \textbf{(2.6)}$$

in which $\lambda = k_f \Big/ \sqrt{D_O} + k_b \Big/ \sqrt{D_R}$, and k_f and k_b are the forward and backward electron-transfer rate constants, respectively, and D_O and D_R are the diffusion coefficients for the oxidant O and the reductant R, respectively, for the reaction $O + ne^- \leftrightarrow R$. Here the frequency-dependent terms $\lambda/\sqrt{2\omega}$, appearing in both the real and the imaginary terms in Equation 2.5, are called the Warburg impedance. When $Z''(\omega)$ is plotted against $Z'(\omega)$with the Warburg component included, the high- and low-frequency intercepts on the $Z'(\omega)$ axis are still R_s and $R_s + R_p$, as was the case without the Warburg impedance, and the plot of the Warburg components becomes a straight line with a slope of unity and an intercept of $R_s + R_p - R_p^2 \lambda^2 C_d$. Thus we can calculate λ, and thereby the diffusion coefficient from λ when k_f is known, and k_f can be obtained from $i_f = nFAk_f C_O$, in which C_O is the bulk concentration of oxidant and A is the area. In other words, we now have a complete description of the electrochemical system.

2.3.2. Attenuated Total Reflectance (ATR)-FTIR

Attenuated total reflectance (ATR) spectroscopy, also known as internal reflection spectroscopy or multiple internal reflectances (MIR), is a versatile, nondestructive technique for obtaining the infrared spectrum of the surface of a material or the spectrum of materials either too thick or too strongly absorbing to be analyzed by standard transmission spectroscopy. ATR spectroscopy has been developed since 1959, when it was reported that optical absorption spectra could conveniently be obtained by measuring the interaction of the evanescent wave with the external less dense medium [103]. In this technique, the sample is placed in contact with the internal reflection element (IRE), the light is totally reflected, generally several times, and the sample interacts with the evanescent wave (Figure 2.15) resulting in the absorption of radiation by the sample at each point of reflection. The internal reflection element is made from a material with a high refractive index; zinc selenide (ZnSe), thallium iodide – thallium bromide (KRS-5), and germanium (Ge) are the most commonly used. To obtain total internal reflection the angle of the incident radiation θ must exceed the critical angle θ_c. The critical angle is defined as:

$$\theta_c = \sin^{-1} \frac{n_2}{n_1} \qquad \textbf{(2.7)}$$

where n_1 is the refractive index of the internal reflection element and n_2 is the refractive index of the sample.

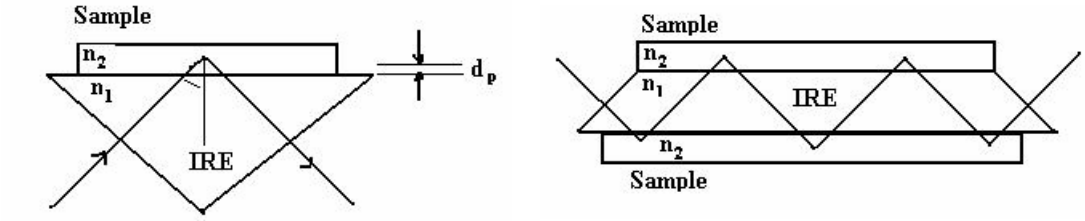

Figure 2.15: : Schematic representation of total internal reflection with: a) Single reflection; b) Multiple reflection IRE (internal reflection element) n_1=Refractive index of the internal reflection element; n_2=Refractive index of the sample with $n_2 < n_1$; θ = Angle of incidence; d_p=Depth of penetration.

What makes ATR a powerful technique is the fact that the intensity of the evanescent wave decays exponentially with the distance from the surface of the internal reflection element. As the effective penetration depth is usually a fraction of a wavelength, total internal reflectance is generally insensitive to sample thickness and so permits thick or strongly absorbing samples to be analyzed. The depth of penetration d_p, defined as the distance required for the electrical field amplitude to fall to e^{-1} of its value at the interface, is given by:

$$d_p = \frac{\lambda_1}{2\pi(\sin^2\theta - n_{21}^2)^{1/2}} \qquad \textbf{(2.8)}$$

where $\lambda_1 = \lambda/n_1$ is the wavelength in the denser medium, and $n_{21} = n_2 / n_1$ is the ratio of the refractive index of the less dense medium divided by that of the denser. Although ATR and transmission spectra of the same sample closely resemble each other, differences are observed because of the dependency of the penetration depth on wavelength: longer wavelength radiation penetrates further into the sample, so that in an ATR spectrum bands at longer wavelengths are more intense than those at shorter ones. The depth of penetration also depends on the angle of incidence; hence, an angle of 45°, which allows a large penetration depth, is generally used to analyze organic substances, rather than an angle of 60°, which results in a substantially

weaker spectrum due to the decreased depth of penetration. The degree of physical contact between sample and internal reflection element determines the sensitivity of an ATR spectrum. To achieve this, a horizontal ATR accessory such as FastIR, in which the top plate is the sampling surface, is used; reproducible contact is ensured by a special sample clamp or powder press. Good quality spectra are thus obtained for many materials that present problems of analysis with routine transmission methods, e.g., powders, pastes, adhesives, coatings, rubbers, fibers, thick films, textiles, papers, greases, foams, and viscous liquids. Liquid samples are also well suited to ATR analysis. Most liquids require a very short path length; aqueous samples, for instance, are measured at path lengths of no more than ca. 15 μm, which makes the design of transmission cells difficult because flow of liquids is hindered; they also exhibit interference fringes because of the small spacing between the high refractive index infrared windows. These problems are eliminated by using liquid ATR cells, a variant of solid ATR, in which the internal reflection element is surrounded by a vessel into which the liquid is poured.

2.4. Cross-Coupling Reactions

The cross-coupling reaction accessible via a variety of organometallic reagents may provide a fundamentally common synthetic methodology. In 1972, Kumada and Tamao [104, 105] and Corriu [106] reported independently that the reaction of organomagnesium reagents with alkenyl or aryl halides could be markedly catalyzed by Ni(II) complex. Kochi [107-109] found the efficiency of Fe(III) catalyst for the cross-coupling of Grignard reagents with 1-halo-l-alkenes and Li_2-$CuCl_4$ catalyst for haloalkanes. The palladium-catalyzed reaction of Grignard reagents was first reported by Murahashi, [110] the synthetic utility of which was then amply demonstrated by Negishi [111, 112] on the reactions of organoaluminum, zinc, and zirconium reagents. After those discoveries, many other organometallic reagents have proven to be highly useful as nucleophiles for the cross-coupling reaction, e.g., organolithiums by Murahashi, [113] organostannans by Migita [114, 115] and Stille, [22, 116] l-alkenylcopper(I) by Normant, [117] organosilicon compounds by Hiyama [118-120].

Palladium-catalyzed cross-coupling reactions of organohalides (or triflates) with organometallic reagents follow a general mechanistic cycle. The 14-electron Pd (0)

[the active catalyst PdL is 6 electron when P (*o*-Tol)$_3$ is used as the ligand] catalyst 4 is sometimes reduced from a Pd(II) species 1 by an organometallic reagent R_1M (2). The transmetalation product 3 from 1 and 2 undergoes a reductive elimination, giving rise to Pd (0) species 4, along with the homocoupling product R_1-R_1. This is one of the reasons why the organometallic coupling partners are often used in a slight excess relative to the electrophilic partners. When the Pd(0) catalyst 4 is generated, the catalytic cycle goes through a three-step sequence,

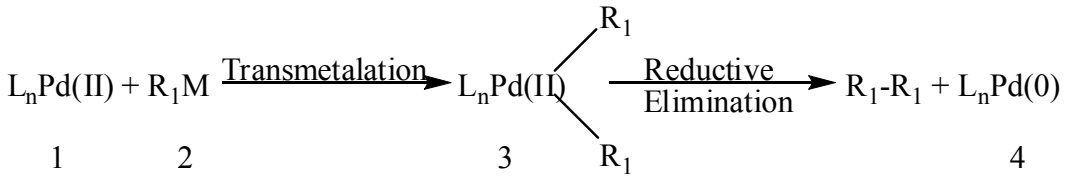

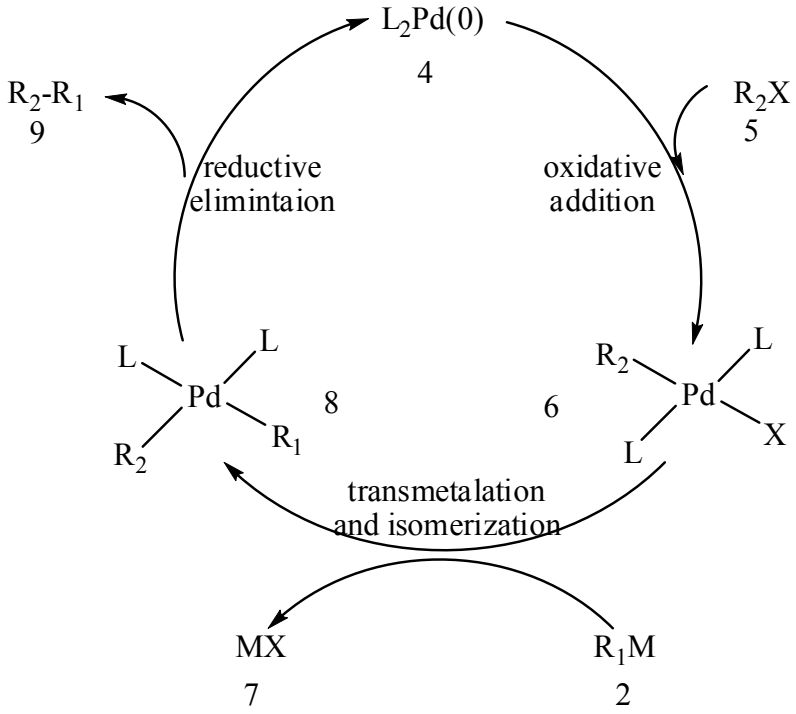

Figure 2.16: A general mechanistic cycle of palladium catalyzed cross-coupling reactions of organohalides with organometallic reagents.

a) Electrophile R_2-X (5) undergoes an oxidative addition to Pd(0) to afford a 16-electron Pd(II) intermediate 6;

b) Subsequently, 6 undergoes a transmetalation step with the organometallic reagent R_1M (2) to produce intermediate 8. When there is more than one group attached to metal M, the order of transmetalation for different substituents is:

alkynyl > vinyl > aryl> allyl ~ benzyl >> alkyl

The transmetalation step, often rate-limiting, is the step to which attention should be directed if the reaction goes awry;

c) Finally, with appropriate syn geometry, intermediate 8 undergoes a facile reductive elimination step to produce the coupling adduct R_2-R_1 (9), regenerating palladium (0) catalyst 4 to close the catalytic cycle.

2.4.1. Stille Coupling; Tin

The Stille Coupling is a versatile C-C bond forming reaction between stannanes and halides or pseudohalides, with very few limitations on the R-groups. Well-elaborated methods allow the preparation of different products from all of the combinations of halides and stannanes depicted below. The main drawback is the toxicity of the tin compounds used, and their low polarity, which makes them poorly soluble in water. Stannanes are stable, but boronic acids and their derivatives undergo much the same chemistry in what is known as the Suzuki Coupling. Improvements in the Suzuki Coupling may soon lead to the same versatility without the drawbacks of using tin compounds.

$$R'—X + RSnBu_3 \xrightarrow{\text{Pd-Cat}} R'—R + XSnBu_3 \qquad \textbf{(2.9)}$$

The palladium catalyzed coupling with organotin compounds is known as the Stille reaction and is probably the most widely studied of all of these reactions [22]. One reason for its popularity is the number of ways that tin reagents can be prepared [121]. A trialkyl tin group can be introduced as an electrophile or a nucleophile. Trialkyl tin groups can also be introduced by free radical methods and by palladium catalysed coupling reactions. The organotin compounds can be further elaborated before coupling, as the carbon-tin bond is stable to many reagents. In general it is not stable to butyl lithium, acids and strong electrophiles, such as halogens. Even silica gel can be sufficiently acidic to cause protiodestannylation, so column chromatography must be done quickly. This low reactivity of tin reagents makes the Stille reaction ideal for the preparation of highly functionalized molecules. Many functional groups will survive the Stille reaction intact.

An important limitation of the Stille reaction comes from the valency of tin (IV). Only one of the groups attached to tin will transfer during coupling. The other three are lost. This is not important if the group is readily available and reactive.

Tetramethyltin is one of the rare examples of this. Usually the group to be transferred is valuable and cannot be wasted. It must be transferred selectively over the other three groups on tin. The cyclopropyl group and certain substituted alkyl groups are transferred in preference to simple alkyl groups. Typically, therefore, derivatives of tributyltin or trimethyltin are used, the butyl or methyl groups acting as dummies. The butyl and methyl groups are not entirely 'dumb' and minor products resulting from butyl or methyl group transfer are sometimes obtained. Tributyltin derivatives are most commonly used because they are much cheaper than the corresponding trimethyltin compounds. Various tri-n-butyl tin compounds are manufactured on a large scale for addition to marine paint as antifouling agents. Trimethyl derivatives have some advantages. In some cases trimethyltin compounds are more reactive, especially where steric hindrance is a problem.

The trimethyltin halide byproducts are water soluble and easily removed from the reaction mixture by extraction. Tributyltin halides cannot be removed by aqueous extraction, and often have to be removed by chromatography. An alternative method is to add saturated potassium fluoride to the reaction mixture, which can convert tin halides to the insoluble, polymeric tin fluorides [122].

An important extension of the Stille reaction has been the use of vinyl and aryl triflates. This has opened up many possibilities; not only are triflates very reactive, they can also be readily prepared from phenols and from ketones, via enolates. In many cases the corresponding bromides and iodides are difficult to prepare. Triflates of phenols can be easily prepared by treatment with tri-flic anhydride and an amine base [123]. The reaction also works in heterocyclic cases. The coupling reaction with organotin compounds proceeds as would be expected, with one exception: it is almost always necessary to include one equivalent of lithium chloride.

2.4.2. The Negishi Coupling; Zinc

The Negishi Coupling, published in 1977 [124], was the first reaction that allowed the preparation of unsymmetrical biaryls in good yields. The versatile nickel- or palladium-catalyzed coupling of organozinc compounds with various halides (aryl, vinyl, benzyl, or allyl) has broad scope, and is not restricted to the formation of biaryls.

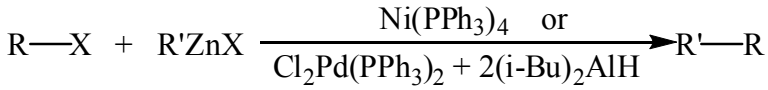

(2.10)

R ; alkenyl, aryl, allyl, benzyl, propargyl
R'; alkenyl, aryl, alkynyl, alkyl, benzyl, allyl

The Negishi reaction is the palladium-catalyzed cross-coupling between organozinc reagents and organohalides (or inflates) [111]. Zinc organometallics are less reactive and hence see greater use. For instance ketones, which would react with lithium or magnesium species, can be formed using zinc reagents by coupling with acid chlorides [125]. Organozinc reagents are usually generated and used in *situ* by transmetalation of Grignard or organolithium reagents with $ZnCl_2$. In addition, some halides may oxidatively add to Zn (0) to give the corresponding organozinc reagents. In one case, Knochel's group has developed a facile method to prepare organozinc reagents via direct oxidative addition of organohalides to Zn (0) dust. This approach is more advantageous than the usual transmetalation using organolithium or Grignard reagents because of better tolerance of functional groups [126, 127].

2.4.3. The Suzuki Coupling; Boron

The equation (2.11) shows the first published Suzuki Coupling, which is the palladium-catalysed cross coupling between organoboronic acid and organohalides(or inflates) [128, 129]. Recent catalyst and methods developments have broadened the possible applications enormously, so that the scope of the reaction partners is not restricted to aryls, but includes alkyls, alkenyls and alkynyls. Potassium trifluoroborates and organoboranes or boronate esters may be used in place of boronic acids. Some pseudohalides (for example triflates) may also be used as coupling partners.

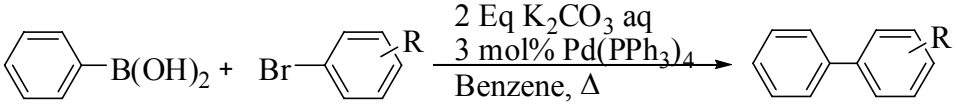

(2.11)

Boranes do not couple by themselves. To make them active, it is necessary to add a ligand to convert them into “ate” complexes (Scheme 2.12).

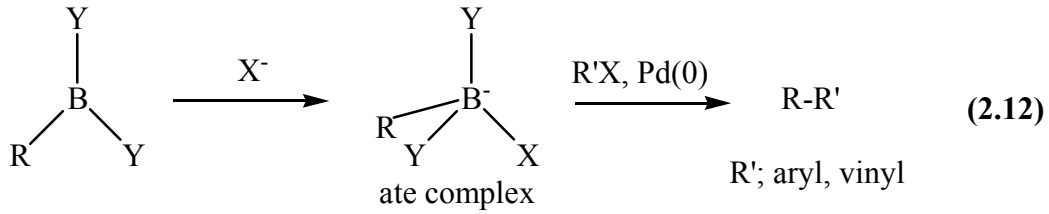

(2.12)

Suitable ligands are hard anions such as hydroxide, alkoxide, carbonate, fluoride [130] and phosphate. For base-sensitive compounds, such as esters, only the last of these, phosphate, is suitable. Boron compounds with four organic ligands, such as commercially available sodium tetraphenylborate ($NaBPh_4$), may be used without added ligands.

In comparison to the abundance of heteroarylstannanes, heteroarylboron reagents are not as prevalent. There are three major reasons why one should consider the Suzuki coupling when designing a Pd-catalyzed reaction in heteroaryl synthesis. First, a growing number of heteroarylboron reagents are now known. Second, judiciously designing the coupling partners will enable the use of a heteroaryl halide to couple with a known organoboron reagent for the synthesis of certain molecules. Third, there is no toxicity issue involved in organoboron reagents. Therefore, for a large-scale setting, a Suzuki coupling is a more attractive choice than a Stille coupling.

Since the carbon boron bond is almost completely covalent, transmetalation of an organoboron reagent to transfer the organic group will not occur without coordination of a negatively charged base or to the boron atom. As a consequence, the Suzuki reaction normally needs to be carried out in a basic solution, which poses some limitations to base-sensitive substrates. As each of the ensuing chapters will entail, pyrrolyl-, indolyl-, pyridinyl-, pyrimidinyl-, Ihienyl- and furylboron reagents have been documented, although those from thiazoles, oxazoles, imidazoles and pyrazines are yet to be seen. The most popular methods for synthesizing heteroarylboron reagents include: (a) halogen-metal exchange of a heteroaryl halide followed by treatment with a borate; (b) direct metalation of a heteroarene followed by quenching with a borate.

One difference between the Suzuki mechanism and that of the Stille Coupling is that the boronic acid must be activated, for example with base. This activation of the boron atom enhances the polarization of the organic ligand, and facilitates

transmetalation. If starting materials are substituted with base labile groups (for example esters), powdered KF effects this activation while leaving base labile groups unaffected.

In part due to the stability, ease of preparation and low toxicity of the boronic acid compounds, there is currently widespread interest in applications of the Suzuki Coupling, with new developments and refinements being reported constantly.

2.4.4. The Kumada Coupling; Grignard Reagent

The Kumada Coupling was the first Pd or Ni-catalyzed cross coupling reaction, developed in 1972.

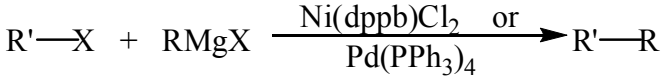

(2.13)

R ; aryl, vinyl, alkyl
R'; aryl, vinyl, X; Cl > Br > I

The Kumada coupling represents cross-coupling of a Grignard reagent with an electrophile such as an alkenyl-, aryl- and heteroaryl halide or triflate [131]. Advantage of this reaction is that numerous Grignard reagents are commercially available. Those that are not commercially available may be readily prepared from the corresponding halides. Another advantage is that the reaction can often be run at room temperature or lower. Drawback of this method is the intolerance of many functional groups by the Grignard reagents. In the synthesis of thienylbenzoic acid, interestingly, the carboxylic acid moiety survived under the coupling conditions [132].

2.4.5. The Hiyama Coupling; Organosilicon

In comparison to the transmetalation of organometallic reagents including RMg, RZn and RSn, transmetalation of an organosilicon reagent does not occur under normal palladium-catalyzed cross-coupling conditions because the C—Si bond is much less polarized. However, a C—Si bond can be activated by a nucleophile such as F^- or HO^- through formation of a pemacoordinated silicate, which weakens the C—Si bond by enhancing the polarization. As a result, the transmetalation becomes more facile and the cross-coupling proceeds readily. One of the advantages of the Hiyama

coupling is that organosilicon reagents are innocuous [133, 134] Another advantage is better tolerance of functional groups in comparison to other strong nucleophilic organometallic reagents. The combination of these two characteristics makes the Hiyama coupling an attractive alternative to other Pd-catalyzed cross-couplings. Therefore, this reaction has much promise for future exploration and exploitation.

$$R{-}X + R''_3Si\ R' \xrightarrow[F^- \text{ or base}]{\text{Pd (catal.)}} R'{-}R \qquad \textbf{(2.14)}$$

R''_3Si ; $(RO)_3Si$, $Me_{(3-n)}F_nSi$

The Hiyama couplings of heterocyclcs are still being developed to their full potential. There is no report yet on Pd-catalyzed cross-coupling using a heteroarylsilicon reagent. Nevertheless, several heteroaryl halides have been cross-coupled with arylsilicon reagents.

2.5. Carbon Fibers

Carbon fibers exhibit truly outstanding properties. As shown in Table 2.2, their strength, competes with the strongest steels; they can have stiffness, *E,* greater than any metal, ceramic or polymer; and they can exhibit thermal and electrical conductivities that greatly exceed those of competing materials. If the strength or stiffness values are divided by the low density, 1800-2100 kg m^{-3}, then their huge specific properties make this class of materials quite unique.

All carbon fibers sold commercially are fabricated from polyacrylonitrile (PAN) or from a coal, petroleum or synthetic pitch. PAN-based fibers are produced from a solubilized mixture that is wet or dry spun to produce a fiber, ostensibly for use in the textile industry. This fiber is stabilized and carbonized to produce a carbon fiber. Aerospace grade material can be obtained in tows that contain between 3000 and 12 000 fibers. Lower performance materials are usually formed using larger tows that contain up to 320 000 fibers. PAN-based carbon fibers are cheaper when produced from larger tows. Pitch fibers are melt spun products obtained in small tow sizes varying from 2000 to 4000 fibers. They are usually of larger diameter (~ 10-15 pm) than fibers formed from PAN.

The spinning process is controlled by the pitch-based carbon fiber producer; thus, microstructural features developed in the spinning process that also influence the stiffness, strength and the thermal and electrical properties of pitch can be optimized. Nevertheless, the tensile strength of PAN-based fibers has always been superior to pitch-based fibers; since PAN fibers were developed before pitch fibers, most structural materials and components use PAN-based fibers. The most important mechanical and physical properties exhibited by carbon fibers are the elastic modulus, tensile strength and the electrical and thermal conductivities. These properties are sensitive to the crystallite size and perfection of the graphene layers developed within the carbon fiber and depends for the most part on the degree of molecular alignment with respect to the fiber axis. Growth and alignment of such layers occur within the precursor and within the solid carbon fiber when it is heated to high temperature.

Carbon fibers, which are a new breed of high-strength materials, are mainly used as reinforcements in composite materials such as carbon fiber reinforced plastics, carbon-carbon composite, carbon fiber reinforced materials, and carbon fiber reinforced cement. Carbon fibers offer the highest specific modulus and highest specific strength of all reinforcing fibers. The fibers do not suffer from stress corrosion or stress rupture failures at room temperatures, as glass and organic polymer fibers do. Especially at high temperatures, the strength and modulus are outstanding compared to other materials [135]. Carbon fiber composites are ideally suited to applications where strength, stiffness, lower weight, and outstanding fatigue characteristics are critical requirements. They are also finding applications where high temperature, chemical inertness, and high damping are important. Carbon fibers also have good electrical conductivity, thermal conductivity, and low linear coefficient of thermal expansion [136].

The two main sectors of carbon fiber applications are high technology sector, which includes aerospace and nuclear engineering, and the general engineering and transportation sector, which includes engineering components such as bearings, gears, cams, fan blades, etc., and automobile bodies. However, the requirements of two sectors are fundamentally different. The large scale use of carbon fibers in aircraft and aerospace is driven by maximum performance and fuel efficiency, while the cost factor and the production requirements are not critical.

Table 2.3: Axial tensile properties of carbon fibers [137].

Carbon Fibers	Tensile strength (GPa)	Tensile modulus E, (GPa)	Elongation at break (%)	Density kg/m^3
Polyacrylonitrile	2.5–7.0	250–400	0.6–2.5	~1800
Mesophase pitch	1.5–3.5	200–800	0.3–0.9	~2100
Rayon	~1.0	~50	~2.5	-
Metals				
Aluminum	0.172	73	-	2720
Titanium	0.324	110	-	4500
Steel	0.414	199	-	7860

The use of carbon fibers in general engineering and surface transportation is dominated by cost constraints, high production rate requirements, and generally less critical performance needs. This necessitates two different approaches in the areas of production as well as research for two sectors. A number of achievements have been made in the past in the area of cost reduction as well as fiber quality improvement. After all the developments, we have been able to achieve 90–95% of the modulus of perfect graphite (~1025 GPa), a material with highest absolute and specific modulus of all the materials known [135]. However, carbon fiber in its current strength level range is 15–20 times below the theoretical strength limit. A common rule of thumb is that the strength of a fiber should be about 10% of the modulus of a single crystal. Thus, possible strength for carbon fiber is estimated to be about 100 Gpa. Though the theoretical tensile strength of single crystal of graphite is 150 Gpa [135], highest of all the materials known.

Carbon fibers when used without surface treatment produce composites with low interlaminar shear strength (ILSS). This has been attributed to weak adhesion and poor bonding between the fiber and matrix. All the carbon fibers are thus given a surface treatment, the exact nature of which is a trade secret. These treatments increase the surface area and surface acidic functional groups and thus improve bonding between the fiber and the resin matrix [138-140]. This tends to increase the wettability of the carbon fiber and enhances the ILSS.

A freshly prepared fiber does not bond well to polymeric glue (or to anything else for that matter); however, the tendency to bond can be significantly increased by subjecting the fiber surface to a controlled oxidation. This treatment essentially

etches the surface, cleans it, increases its surface area and produces polar hydrophilic oxygen-containing groups which bond to it.

Surface treatments may be classified into oxidative and non-oxidative treatments. Oxidation treatments involve gas-phase oxidation, liquid-phase oxidation carried out chemically [141] or electrochemically [142], and catalytic oxidation. The non-oxidative treatments involve deposition of more active forms of carbon, such as the highly effective whiskerization, the deposition of pyrolytic carbon, or the grafting of the polymers on the carbon fiber surface. Carbon fibers can also be plasma treated to improve bonding between the fiber and matrix. Liquid phase oxidation treatments are milder, very effective and are preferred.

Table 2.4: A summary of the carbon fiber composite materials.

	Fiber Composite Materials			
FIBERS	**Carbon Fibers**	**Glass Fibers**	**Aramid Fibers**	**Other Fibers**
Fiber types	HT, IM, HM } Acrylic based fibers	E glass R glass S glass C glass	Meta type Para type	PEK PES Al_2O_3 SiC
MATRICES	**Plastics**	**Metals**	**Ceramics**	**Other matrices**
Matrix types	Thermosets Thermoplasts Elastomers	Aluminum Magnesium Steel	Carbon Silicon Carbide Oxides Nitrides Silicides	Composites

2.5.1. Electropolymerizations onto carbon fiber microelectrodes

Surface characterizations of thin film coating of random poly(N-vinylcarbazole-co-vinylbenzenesulfonic acid), [143, 144] copolymer on carbon fiber was performed by Sarac et al. [143] Coatings of polymer thin films obtained, with different current densities, were characterized by scanning electron microscopy (SEM), atomic force microscopy (AFM), X-ray photoelectron spectroscopy (XPS), and Fourier transform infra red attenuated transform reflectometry (FT-IR-ATR).

Copolymer films of pyrrole and 3,4-ethylene-dioxythiophene (EDOT) were synthesized electrochemically on the carbon fiber microelectrodes (CFME). Deposition conditions on the carbon fiber and influence of the monomer concentrations to the copolymerization as well as the electrochemistry of the

resulting polymers and copolymers were studied using cyclic voltammetry, in-situ spectroelectrochemistry, FTIR-ATR and scanning electron microscopy [145].

Thin film electro-coated poly(N-vinylcarbazole-co-vinylbenzene sulfonic acid) [143, 146, 147] p(NVCzVBSA) [146], poly(carbazole-co-methylthiophene)[146], (p(CzMeTh)[146]) and polycarbazole (p(Cz)[148]) carbon fiber microelectrodes (CFMEs) were characterized by scanning electron microscopy (SEM) and FTIR-ATR spectroscopy. These modified carbon fiber electrodes were found to be effective systems for the determination of para-aminophenol (p-AP). Thin film coated p(NVCzVBSA) [146] was the most suitable modified electrode for the detection of p-AP [146].

3. EXPERIMENTAL WORK

3.1. Materials

Thiophene (Th), 3,4-ethylene dioxythiophene (2,3-Dihydrothieno[3,4-b]-1,4-dioxin = EDOT) were used as received from Sigma-Aldrich.

Electrolytes, tetrabutylammonium hexafluorophosphate (Bu_4NPF_6), tetraethylammonium hexafluorophosphate (Et_4NPF_6), tetrabutylammonium tetrafluoroborate (Bu_4NBF_4), and tetraethylammonium tetrafluoroborate (Et_4NBF_4) were supplied from Fluka Chemicals and were used after drying in vacuum oven without further purification with a ratio of 99% purity. $NaClO_4$ was used from Riedel-de Haen Chemicals as pure; $LiClO_4$ was used from Sigma-Aldrich Chemical with a purity of 99.99%. Monomers, thiophene and n-methyl pyrrole, were used from Lancester and Aldrich Chemicals with a purity of higher than 99%.

Chemicals: Synthesis procedures for all of the comonomers were given in the results and discussion chapter. All other chemicals were analytical grade and were used without further purification.

Dichloromethane (DCM), acetonitrile (ACN), propylene carbonate (PC) was used as received from either Riedel-de Haen Chemical or Merck. Tetrahydrofuran (THF) was received from Sigma-Aldrich and purified by refluxing with, and distilling with metallic sodium wire which removes water and other impurities. Double distilled water was used in aqueous reactions.

3.2. Characterizations

Polymerization reactions were performed electrochemically in proper solvent i.e., ACN, DCM, PC solution with different electrolyte systems such as containing 0.1M $LiClO_4$, 0.1M $NaClO_4$, 0.2M $NaClO_4$, 0.1M Et_4NBF_4 for various electrodes with different monomer concentrations and scan rates. Cyclic voltammogram (CV), of the polymers was performed on an Princeton Applied Research (PAR) branded, Parstat 2263 model potentiostat, which is a self-contained unit that combines potentiostatic

circuitry with phase-sensitive detection (Faraday cage that BAS Cell Stand C3). A three-electrode system employing CFME or a platinum button electrode or a gold button electrode (BASi stationary voltammetry electrodes; diameter 1.6 mm, area 0.02 cm^2) as working electrode, Platinum wire as counter electrode, and an Ag/AgCl (reference electrodes were stocked in 3.5M KCl). EIS measurements were also performed with Parstat 2263 Potentiostat with PowerSine software package. Both polymers and copolymers electrocoated onto carbon fiber surface were analyzed by FT-IR reflectance spectrophotometer. (Perkin Elmer, Spectrum One; with a Universal ATR attachment with a diamond and ZnSe crystal C70951).

Electrochemical Impedance Spectroscopy (EIS): EIS measurements were taken at room temperature (23±2ºC) using a conventional three electrode cell configuration. The electrochemical cell was connected to a Potentiostat (PAR 2263) with interfaced to a PC. An electrochemical impedance software PowerSine was used to carry out impedance measurements between 10 mHz and 16 kHz. The AC amplitude voltage used for the experiments was 10mV and DC potential referenced versus Ag/AgCl electrode. Galvanostatic DC charge/discharge experiments were carried out at constant current of ±1 mA cm^{-2}. The impedance spectra were analyzed using ZSimpWin V3.10.

Scanning Electron Microscopy: The morphological studies were analyzed using a SEM, AFM. The morphological features of the coated carbon fiber electrodes were performed by field emission scanning electron microscopy (FE-SEM) by using a Jeol JSM 6335F (TUBITAK) and a Jeol JSM-7000F SEM (ITU). The fibers were attached on copper plate by use of a double sided carbon tape.

^1H NMR spectra were collected on a Varian 400 MHz spectrometer and referenced to the residual proton solvent resonance.

A Canon (PowerShot S80) digital camera was used to take photographs and movie of the polymeric films at high resolution.

Electrical conductivity of the thin films of the prepared polymers was measured using four pint probe technique.

3.3. Preparation of Carbon Fiber Microelectrodes (CFMEs)

A high strength (HS) carbon fibers C 320.000A (CA) (Sigri Carbon, Meitingen, Germany) containing 320000 single filaments in a roving and a high modulus (HM) carbon fibers HM48004 were used as working electrodes. All of the electrodes were prepared by using 3 cm of the CFME (with average diameter of around 7 μm) attached to a copper wire with a Teflon tape. Generally number of carbon fibers was about 5-10. Roughly 1 cm of the CFME was dipped into the solution to keep the electrode area constant (~5.0 x 10^{-3} cm^2) and the rest of the electrode was covered with the Teflon tape. The CFMEs were firstly cleaned with acetone and then dried up with an air-dryer before the experiments.

3.4. Electropolymerizations and Characterizations of the Monomers

A platinum wire was used as a counter electrode and Ag/AgCl (was stocked in 3.5M KCl) was used as a reference electrode. Cyclic voltammetry (CV) experiments, spectroelectrochemistry and electropolymerizations were performed with a Princeton Applied Research Potentiostat model 2263 potentiostat/galvanostat interfaced to a PC computer and controlled PowerSuite software package in a three-electrode setup employing a carbon fiber microelectrode (CFME) or a platinum button electrode (BASi stationary voltammetry electrodes; diameter 1.6 mm, area 0.02 cm^2) or an indium tin oxide (ITO) coated glass slide as the working electrode, a platinum wire electrode as the counter electrode, and a silver wire as the pseudo reference electrode. The pseudo-reference was calibrated externally using a 5 mM solution of ferrocene/ferrocenium (Fc/Fc^+) couple in the electrolyte and the potentials are reported versus Ag/AgCl in this thesis, see Figure 3.1. for the comparison of the reference electrodes in 5mM ferrocene solution. The electrolyte used was 0.1 M of tetrabutylammonium hexafluorophosphate (Bu_4NPF_6) or tetraethylammonium tetrafluoroborate (Et_4NBF_4) in dicholoromethane (DCM).

Spectroelectrochemical data were recorded on a Perkin-Elmer Lambda 45 UV-vis spectrophotometer connected to a computer. A three-electrode cell system was used where the working electrode was a custom cut ITO-coated glass slide (8 mm x 50 mm x 1.1 mm, 30 mm of the ITO electrode immersed into the solution to keep electrode area constant at 2.4 cm^2, $R_s \leq 10\Omega/\square$ provided from Colorado Concept

Coatings LLC), the counter electrode was a platinum wire and an Ag wire was used as pseudo-reference electrode. Polymer films for spectroelectrochemical measurements were prepared by potentiodynamic deposition on ITO-coated glass slides.

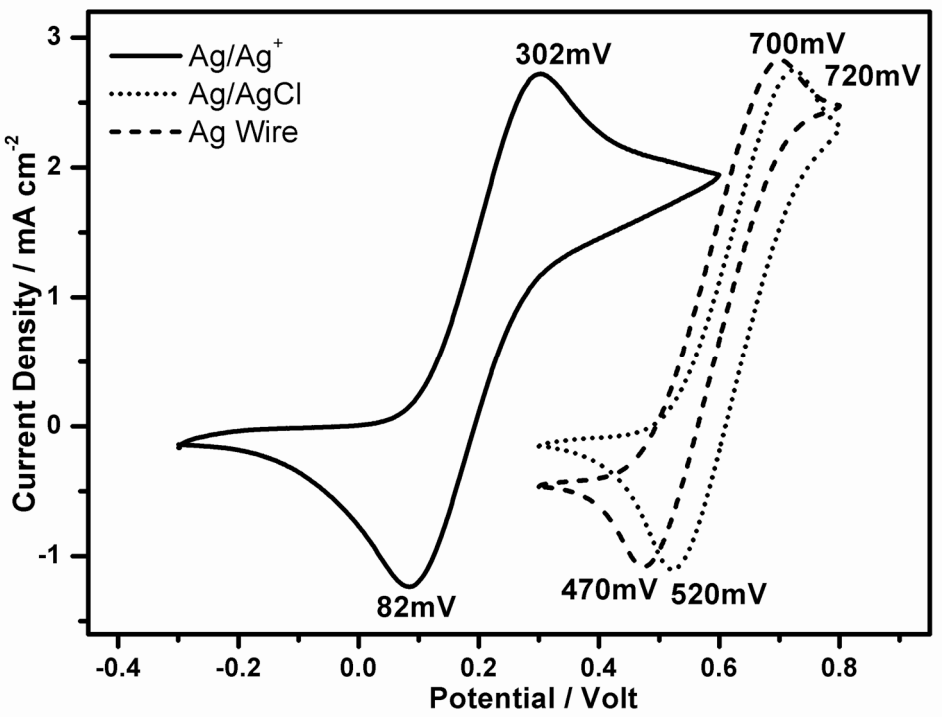

Figure 3.1: Comparison of the reference electrodes in 5mM ferrocene solution.

4. RESULTS AND DISCUSSION

4.1. Synthesis and Electrochemical Characterization of 2,2'-Bithiophene

4.1.1. Synthesis of 2,2'-Bithiophene

A dry 3-neck Schlenk flask was charged with ~50 mL of dry THF and 0.3462 g (16 mmol; ~ 1.4 mL) of thiophene. The mixture was cooled down to -78°C with methanol and liquid N_2 mixture. 9.412 mL (1.7M in Hexane; 1.5072 g) of butyllithium was added to the mixture and was stirred up for 45 minutes at -78°C. 2.1512 g (16 mmol) of anhydrous $CuCl_2$ was added and the system was heated to 40 ºC and was stirred two hours. Then the mixture was poured into water and was extracted with CH_2Cl_2. The organic phase was dried over K_2CO_3 and remaining solvent rotary evaporated. The raw product was washed with pentane and further purified with silica column using chloroform. 0.51 gram (yield 19.38 %) of 2,2'-bithiophene was obtained. The dimer was further purified with the aid of melting point differences to remove trimer and higher oligomers those are possibly coexist in the medium with 2,2'-bithiophene. Synthesis reaction of bithiophene is given in equation 4.1.

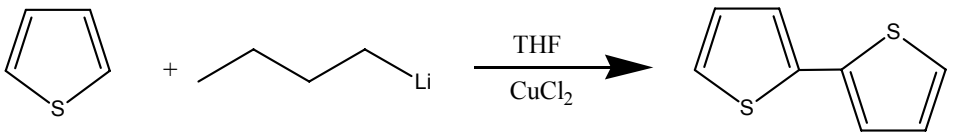

(4.1)

4.1.1.1. ATR-FTIR Characterization of 2,2'-Bithiophene

ATR-FTIR spectra were recorded for the 2,2'-bithiophene monomer a Perkin-Elmer Spectrum One ATR-FTIR spectrometer in the frequency range of 4000-650 cm^{-1}. FTIR measurement was made using solid 2,2'-bithiophene. The ATR-FTIR spectra of the samples were recorded at room temperature and at the laboratory humidity conditions. The ATR-FTIR spectrum of the 2,2'-bithiophene is presented given in Figure 4.1. The frequencies of the major absorption peaks are also listed in Table 4.1. Assignments of these frequencies have been done based upon literature tables [149,

150]. We observed absorption peaks belong to thiophene (See Appendix Figure A.1 for ATR-FTIR of thiophene) and new peaks appeared after dimerization reaction mostly corresponding to the $-C-H$ vibrations. The peak observed at 681 cm^{-1} is associated with the $C-S-C$ stretching vibration. The bands populated between 800 cm^{-1} and 1500 cm^{-1} are associated to symmetric asymmetric and in plane $-C-H$ vibrations. See the Table 4.1 for the systematic peak assignments.

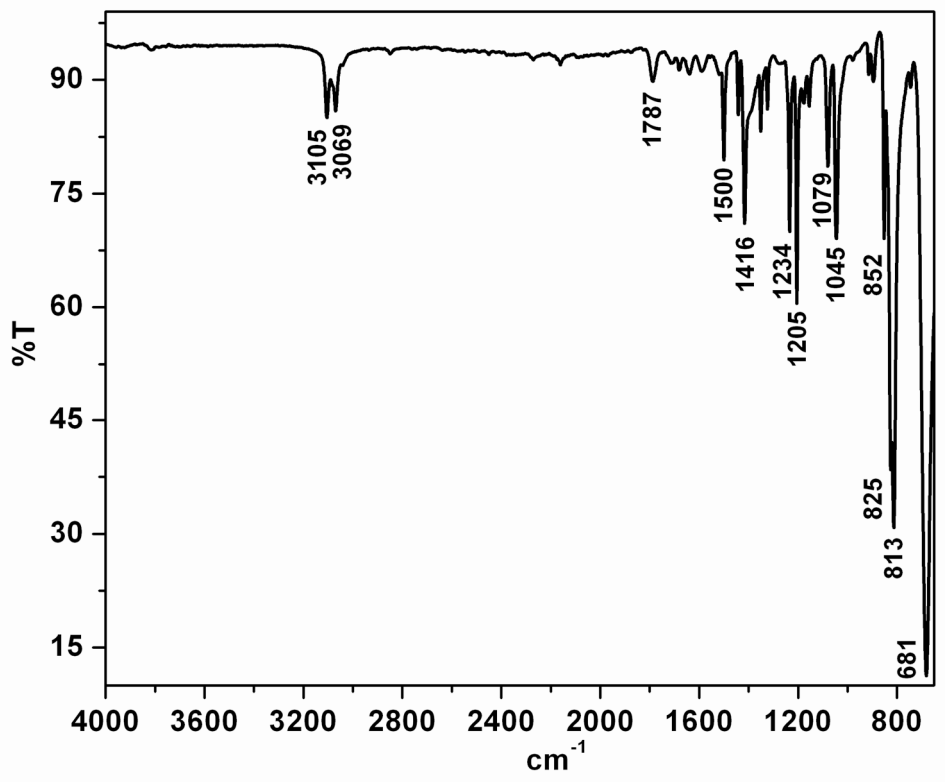

Figure 4.1: ATR-FTIR spectrum of the 2,2'-bithiophene monomer.

Table 4.1: ATR-FTIR absorption bands and peak assignment table for the BTh monomer. **vs**; very strong, **s**; strong, **m**; medium, **w**; weak

Peak / cm^{-1}	Fragment	Intensity / Comment
3105, 3069	Thiophene	**m** / $-C-H$ stretching vibration- asymmetric
1787	Dimer	**w** / $-C-H$ vibration overtone
1500	Dimer	**w** / $-C-H$ symmetric deformation vibration
1442	Dimer	**w** / $-C-H$ asymmetric deformation vibration-
1416	Thiophene	**m** / $=C-H$ and $-C=S$ in plane vibration
1234, 1205	Dimer	**w, m** / $-C-H$ deformation vibration
1079, 1045	Thiophene, Dimer	**w, m** / $S-H$ and $C-H$ deformation vibrations; due to six neighboring H atoms.
852,825,813	Dimer	**s** / $-C-H$ out of plane deformation vibration
681	Thiophene	**s** / $C-S-C$ stretching vibration

4.1.2. Electropolymerization of 2,2'-Bithiophene

PBTh (poly(2,2'-Bithiophene)) was first grown by cyclic voltammetry from Et_4NBF_4 / dichloromethane electrolyte solution containing 0.005 M of BTh. The electrodeposition of PBTh onto carbon fiber microelectrode (CFME) was performed by cyclic voltammetry at a scan rate of 50 mV s^{-1} between -0.3 V and 1.4V. The monomer oxidation onto bare electrode starts at (onset potential of the BTh E_{onset}) 1.246 mV vs. Ag/AgCl. A regular growth of the polymer is observed (see Figure 4.2). With repeated scanning, a reversible redox process grows in with half wave potential $E_{1/2}$ at 1.0 V vs. Ag/AgCl. It is evident that the polymer redox behavior develops rapidly and that the monomer polymerizes very efficiently to form electroactive polymers. Electrodeposition voltammogram of the monomer is given in Figure 4.2 and the current density versus time plot of the same electropolymerization is illustrated in Figure 4.3.

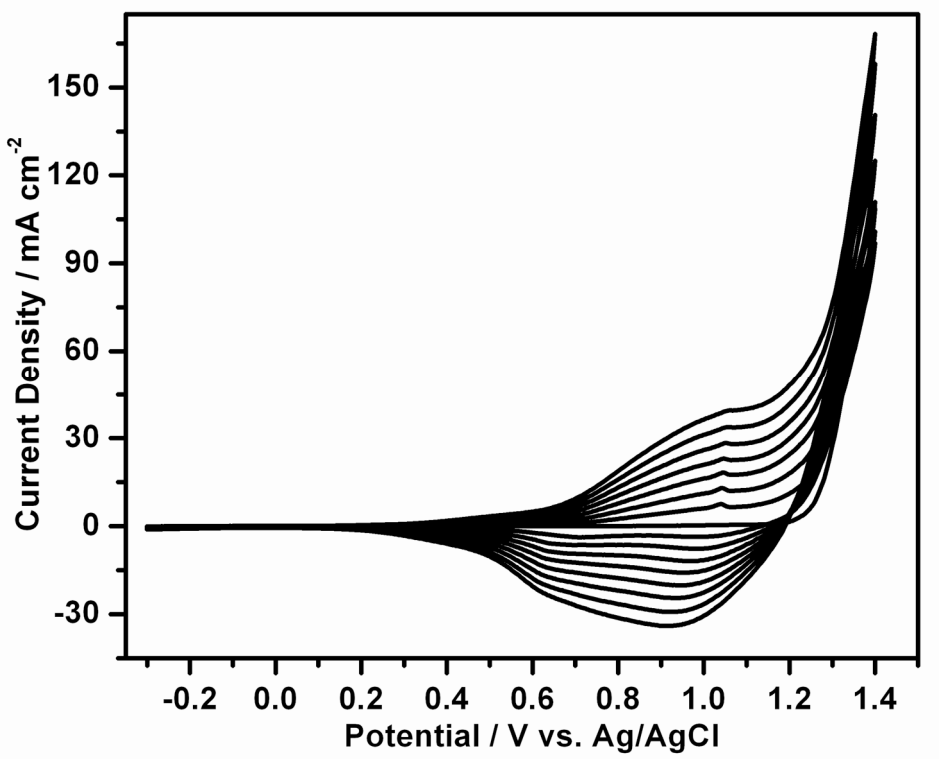

Figure 4.2: Electropolymerization of BTh monomer by cyclic voltammetry from a 0.005M solution of monomer in 0.1 M Et_4NBF_4/DCM at 50 mV s^{-1} onto CFME (area ~0.001 cm^2). Q_{dep}=3.7 C cm^{-2}.

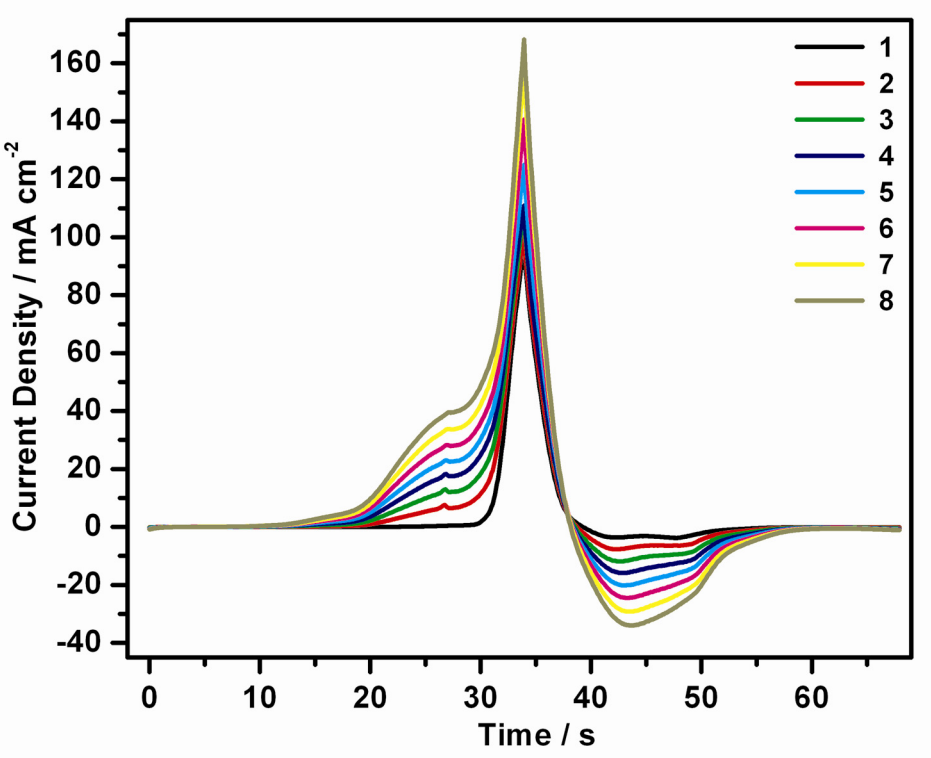

Figure 4.3: Variation of current density by time with increasing number of cycle during electrodeposition of the BTh onto carbon fiber microelectrode.

Figure 4.4a illustrates electroactivity of the polymer on carbon fiber microelectrode in monomer free solution. The polymer films were washed with monomer-free electrolyte solution, and scan rate dependence of the polymer redox was investigated. Scan rate dependencies of the both oxidation and reduction peaks of the polymer were calculated using current density values with respect to square root of the scan rate, and correlation coefficient of the oxidation peak and the reduction peak was calculated as 0.9936 and -0.9954 respectively, see Figure 4.4b. A linear relationship was found between the peak current density and scan rate, indicating that the electroactive polymer films are well adhered and the redox processes are non-diffusion limited. A sharper oxidation and a broad reduction peaks were monitored.

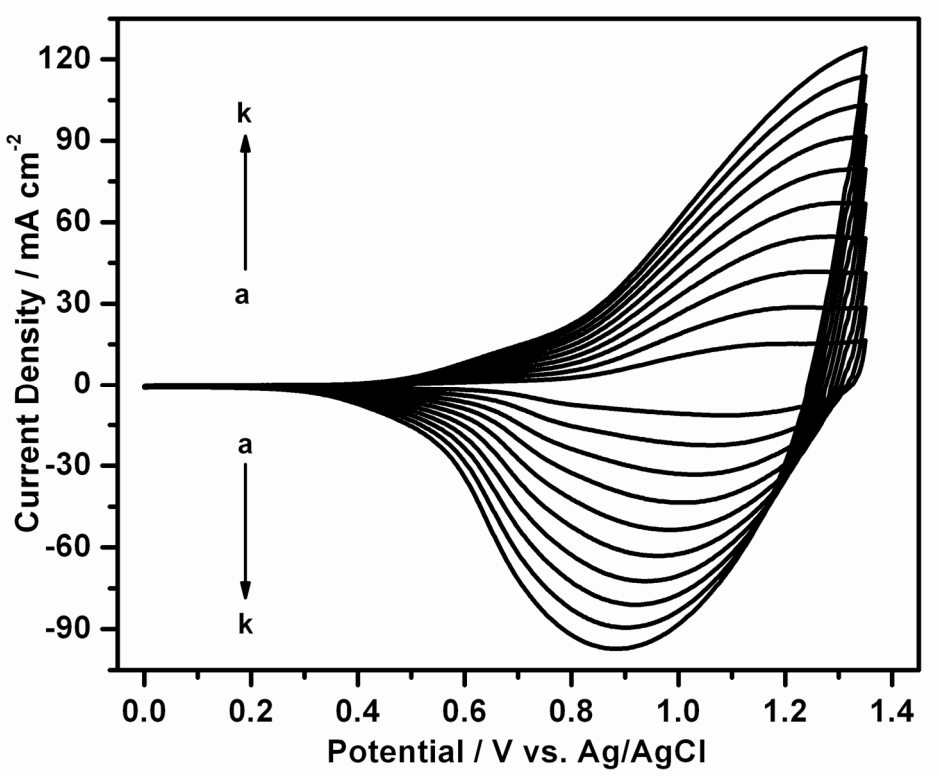

Figure 4.4: (**a)** CV of the PBTh film (electropolymerization CV of the film is given in the Figure 4.2) in a monomer free electrolyte solution scanned at (a) 20, (b) 40, (c) 60, (d) 80, (e) 100, (f) 120, (g) 140, (h) 160, (i) 180, and (k) 200 mV s^{-1}.

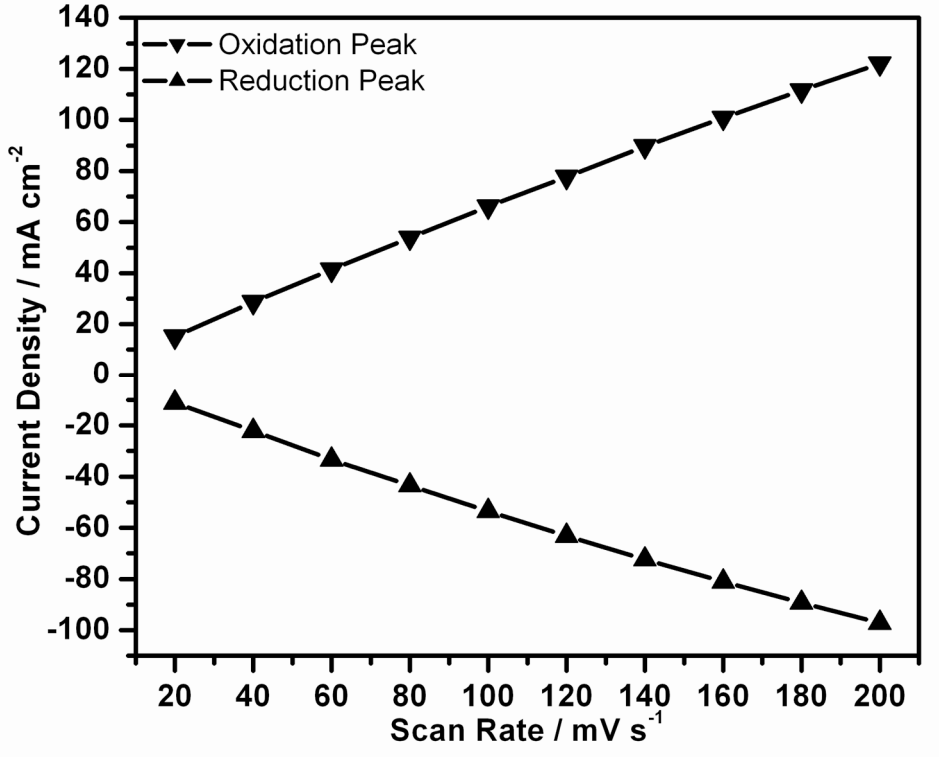

Figure 4.4: (b) Scan-rate dependence of the cyclic voltammogram which is given in Figure 4.4a.

4.1.3. Electrochemical Impedance Spectroscopy of Bithiophene on CFME

EIS measurements were performed at different applied potentials in the range of -0.2 to 1.2 V with a potential step of 0.1V in parallel to cyclic voltammogram of the PBTh in monomer free electrolyte solution (See Figure 4.4a) to fit entire electroactivity range of the polymer.

At low frequency, the redox reaction layer encompasses the whole polymer film, which therefore remains in equilibrium with the changing potential. Under these conditions the polymer-coated electrode behaves like a simple capacitor and the complex plane impedance plot becomes almost vertical. The extrapolation of this nearly vertical low frequency line on the real impedance axis is defined as low frequency intercept. The low frequency capacitance values of the polymer electrode from impedance spectroscopy were obtained from the slope of a plot of the imaginary component (Z_{IM}) of the impedance at low frequencies, versus inverse of the reciprocal frequency (f) using following equation [151].

$$C_{LF} = (2\pi f Z_{IM})^{-1} \qquad \textbf{(4.2)}$$

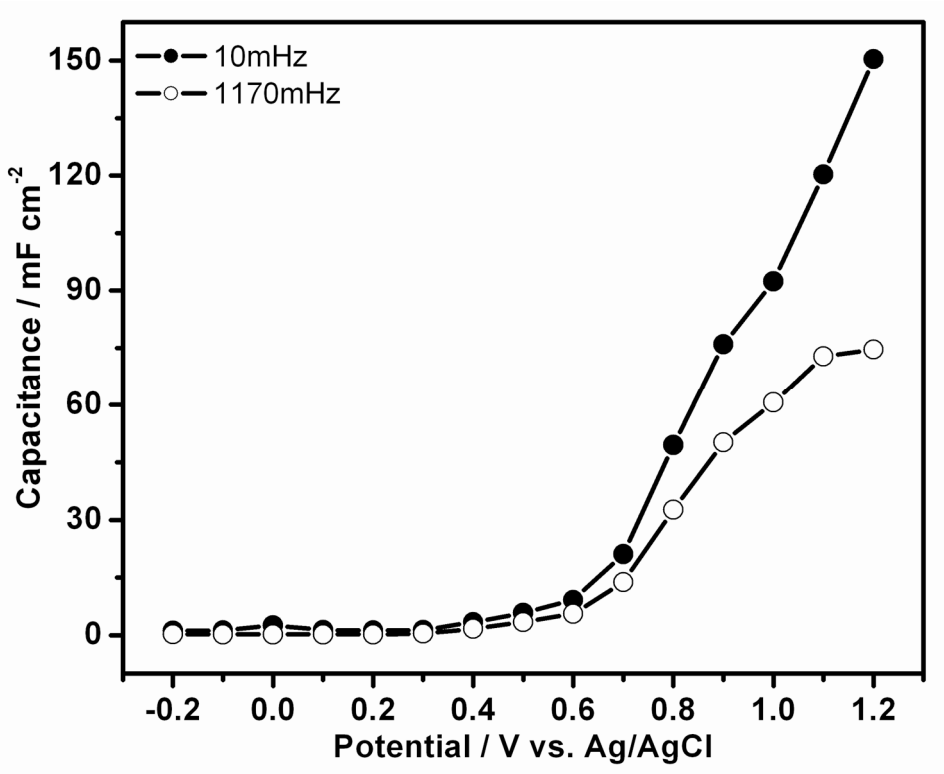

Figure 4.5: Variation of the specific capacitance values of galvanostatically deposited (Q_{dep}=1 C cm^{-2}) PBTh onto CFME.

Figure 4.5 illustrates the variation in the specific capacitance values of galvanostatically deposited (Q_{dep}=5 C cm^{-2}) PBTh film at 0.01 Hz and 1.170 Hz at DC potentials between -0.2V and 1.2V. The shape of the graph is in very good agreement with the corresponding CV of the polymer film in monomer free solution.

As illustrated in Figure 4.4.a CFME/PBTh/electrolyte system does not show electroactivity in the range of 0 V to 0.4V, current density starts to increase from this point. As shown Figure 4.5 we could not observe specific capacitance at low frequency (i.e. 10mHz), this system starts to show capacitive behavior at a DC potential around the 0.5 V and the maximum value 150 mF cm^{-2} obtained at around 1.2V. These results indicates that PBTh is not a very good polymer because of its very narrow electroactivity range and lower capacitance values compared to other conducting polymers.

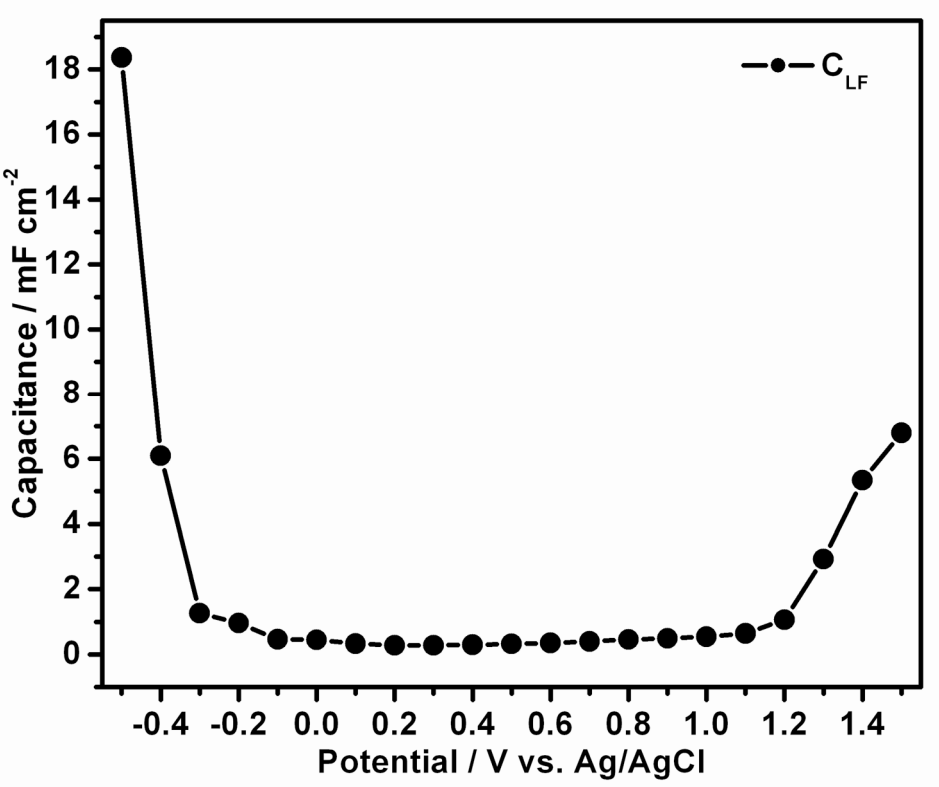

Figure 4.6: Variation of the low frequency (at 30 mHz) capacitance values of the CFME/electrolyte combination.

Contribution of the carbon fiber microelectrode to the low frequency capacitance is another intriguing question because carbon based materials is well known with their suitability as electrode material for supercapacitor applications for example porous

carbon is one of the most frequently selected electrode material due to its large surface area and very well polarization originated from the porosity [32, 152-154].

Figure 4.6 shows variation of the low frequency capacitance values calculated by equation (4.2). Low frequency capacitance of the bare CFME in the studied system is extremely low compared to the CFME/PBTh/electrolyte combination. In the range of -0.3V to 1.2V potential, low frequency capacitance is lower than 2 mF cm^{-2}.

Figure 4.7, 4.8a and 4.8b illustrate Nyquist, Bode Magnitude |Z| and Bode-phase angle plots of PBTh film which is galvanostatically deposited onto CFME with a charge of 1 C cm^{-2}, respectively. The complex plane impedance plots (Nyquist) demonstrate almost a vertical line with a phase angle very close to -80º. Highest phase angle obtained at 0.9V confirming the deviation point observed in Figure 4.5. Results of electrical equivalent circuit model calculation were also given in the Figure 4.5 symbols with open interior.

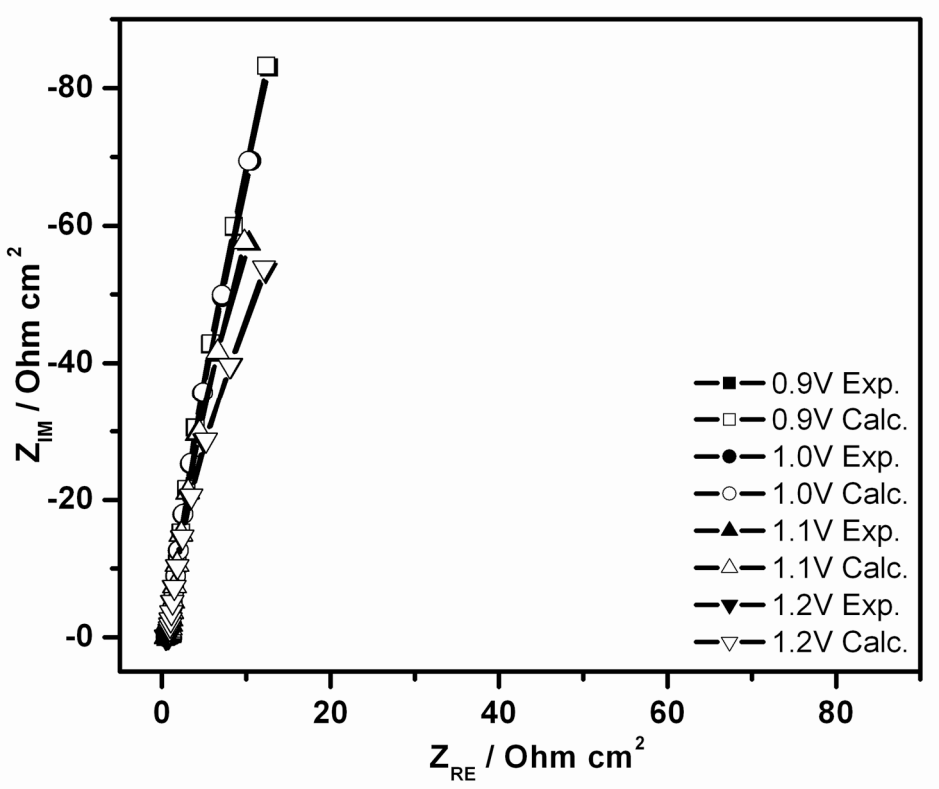

Figure 4.7: Impedance spectra of a PBTh film on CFME deposited with a charge of Q_{dep}= 1 C cm^{-2}. A complex plane representation (Nyquist) between 0.9V and 1.2V, symbols with open interior shows simulation results.

Bode phase angle plots, Figure 4.8b, show a maximum in the low frequency region of 100 to 200 mHz at all studied potential values, at lower potentials for instance 0.6

V a new maximum appears around 200 Hz and this maximum decreases by increasing potential and slightly shifts to higher frequencies.

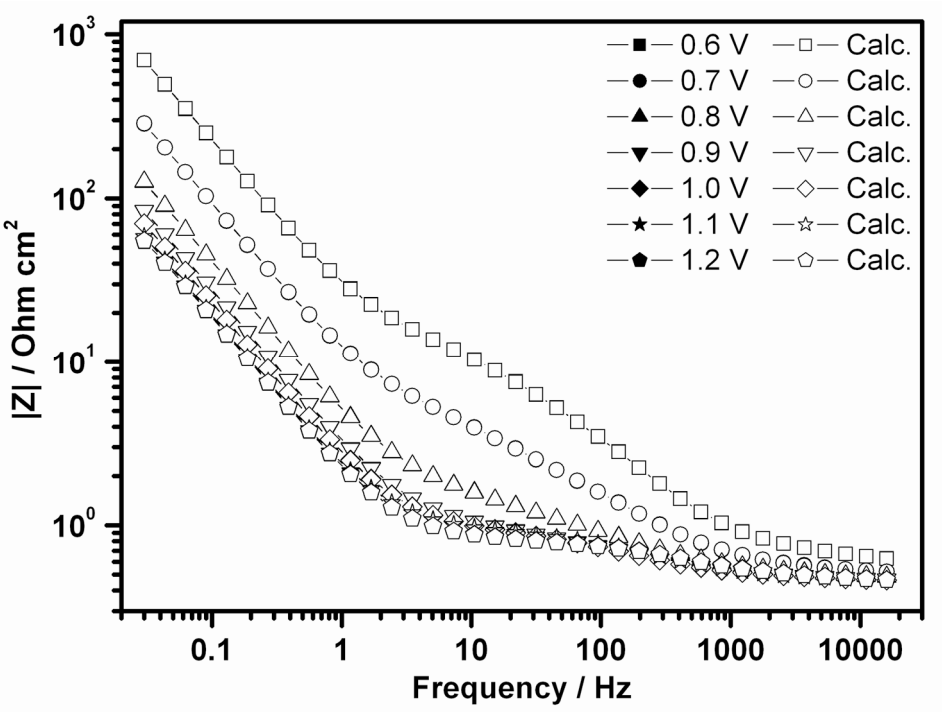

Figure 4.8: (a) Bode-magnitude |Z| plot with simulation results at 0.6V to 1.2V for a PBTh film on CFME deposited with a charge of Q_{dep}= 1 C cm^{-2}.

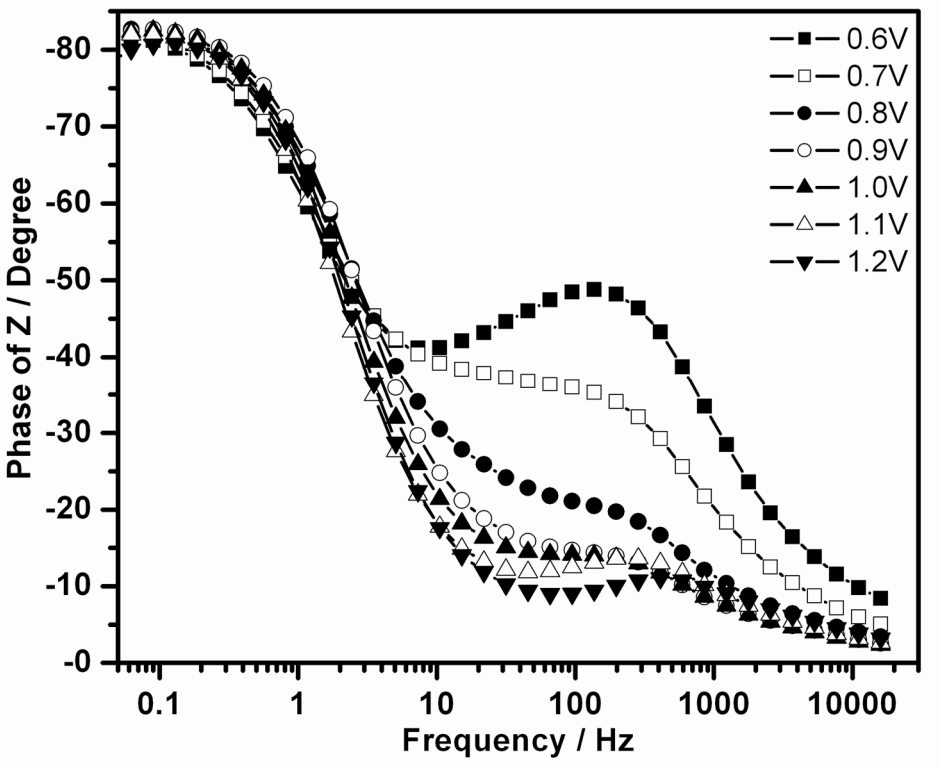

Figure 4.8: (b) Bode-phase angle plot at 0.6V to 1.2V for a PBTh film on CFME deposited with a charge of Q_{dep}= 1 C cm^{-2}.

4.1.4. Electrical Equivalent Circuit of CFME/PBTh/Electrolyte Configuration

The validity of the results obtained with EIS was verified using electrical equivalent circuit (Figure 4.9). The electrochemical parameters of this circuit representing CFME/PBTh/electrolyte configuration were evaluated by employing the ZSimpWin (version 3.10) software from Princeton Applied Research. We observed very good agreement between experimental results and the parameters obtained from the best fitting electrical equivalent circuit model, if the chi-squared (χ^2) minimized below 10^{-4}. χ^2 is the function defined as the sum of the squares of the residuals.

The electrical equivalent circuit model (see Figure 4.9) which is used in simulation of the impedance behavior of the film from the experimentally obtained impedance data was built using series components. The first component is the solution resistance between the polymer electrode and the electrolyte, R_S, second one the parallel combination of the double layer capacitance, C_{dl}, and, R_1 is the charge transfer, a series connection to R_1 constructed using a constant phase element Q_P (Y_o, CPE), in parallel with R_2 a series connection to R_2 made up using C_1 in parallel with R_3 and W, C_1 is the capacitance, R_3 is the charge transfer resistance, and W is the Warburg impedance of the polymer. The last component is a constant phase element (CPE) or represented as (Q_{CF}) in parallel to resistance of the carbon fiber electrode R_{CF}. Q_{CF} is given in admittance (Y_o, CPE) which is includes capacitance value of the carbon fiber. C_{DL} value in the Q_{CF} is very small compared to system's overall capacitance value.

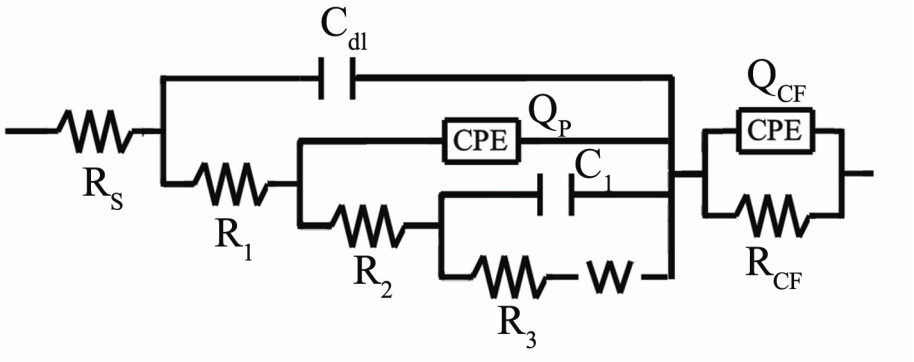

Figure 4.9: Equivalent electrical circuit for the CFME/PBTh/Electrolyte combination used in simulation.

Table 4.2 shows numerical values of simulation results for the porposed equivalent electrical circuit which applied to the experimental data to explain the interaction

between the CFME, the polymer film and the electrolyte in the potential region of 0.7V to 1.2V.

Table 4.2: Potential dependence of the parameters calculated from the equivalent circuit which is given in Figure 4.9.

	Potential / V vs. Ag/AgCl					
	E=0.7V	E=0.8V	E=0.9V	E=1.0V	E=1.1V	E=1.2V
R_S / Ohm cm^2	0.4949	0.4625	0.448	0.448	0.444	0.433
C_{dl} / F cm^{-2}	0.0039	0.0078	0.0101	0.0105	0.0058	0.0042
R_1 / Ohm cm^2	0.4011	0.1545	0.126	0.1209	0.1368	0.1021
CPE_1; Y_o/ S s^{-n} cm^{-2}	0.0035	0.0292	0.0459	0.0568	0.0747	0.0779
n	0.7719	0.9581	0.9559	0.9568	0.9606	0.9609
R_2 / Ohm cm^2	0.0244	213.2	749.4	647.9	476.9	294.7
C_1 / F cm^{-2}	0.0096	< 0.0001	0.0112	0.0129	0.2157	0.0037
R_2 / Ohm cm^2	5142	0.01	$7.25x10^{17}$	0.0225	2.989	213.4
W; Y_o / S $s^{-0.5}$ cm^{-2}	0.0004	0.002	< 0.0001	< 0.0001	< 0.0001	< 0.0001
CPE_2; Y_o/ S s^{-n} cm^{-2}	0.0169	0.0619	0.113	0.0795	0.0717	0.08962
n	0.6236	0.5373	0.4984	0.5466	0.5405	0.4828
R_{CF} / Ohm cm^2	5.452	1.446	0.6258	0.5069	0.4333	0.362
Chi-squared	$6.452x10^{-4}$	$7.559x10^{-5}$	$5.045x10^{-5}$	$5.436x10^{-5}$	$7.021x10^{-5}$	$5.591x10^{-5}$

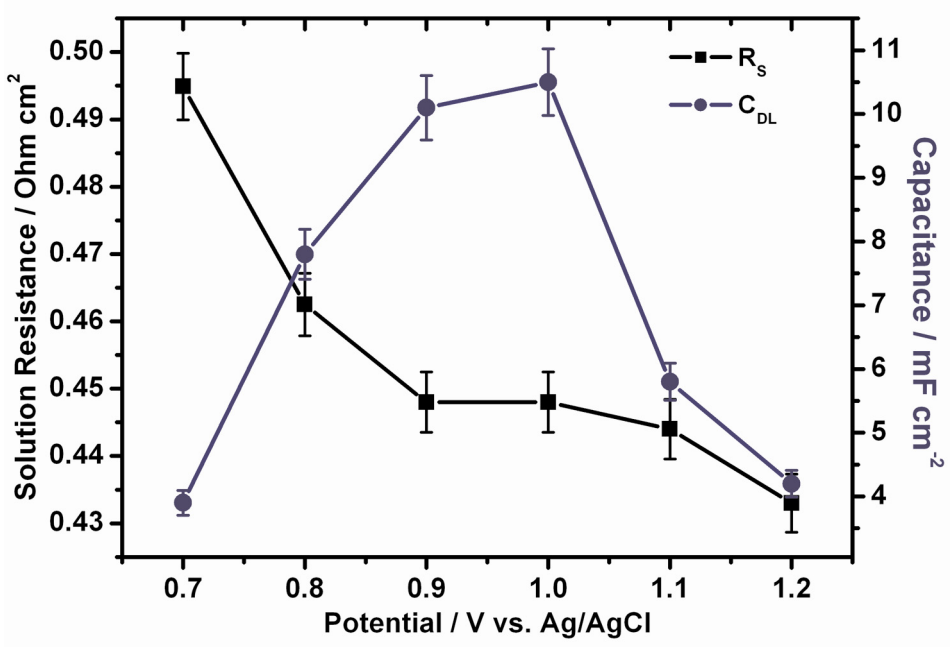

Figure 4.10: Variation of the solution resistance and double layer capacitance with respect to potential.

The obtained results showed that proposed electrical equivalent circuit for the CFME/PBTh/Electrolyte combination exhibits very good agreement with experimental data especially in the range of 0.8V to 1.2V, all chi squared values are smaller than 10^{-4}. Figure 4.7 shows a comparison of the experimental data and the calculated data by using proposed equivalent circuit. Symbols with solid interior

representing experimental data are completely covered by symbols with open interior showing calculated data. We can conclude that proposed equivalent circuit and the calculated values for the components of this circuit are quite reliable.

Figure 4.10 presents variation of the R_s and C_{DL} with respect to the potential. The bulk solution resistance varies in a very narrow range of 0.433 and 0.463 Ohm cm^2 and approximately independent of the potentials. The double layer capacitance that makes contribution to the specific capacitance of the system is quite low.

Figure 4.11a and Figure 4.11b illustrate complex plane capacitance and admittance plots of the PBTh which display the real and imaginary components in the x and y-axes, respectively, with each point associated with a frequency.

Admittance is a vector quantity which is composed of two independent scalar phenomena: conductance and susceptance. Conductance, denoted **G** (in Siemens) (real part) is given by G=1/R=I/E, is a measure of the ease with which charge carriers can pass through a component or substance. The more easily the charge carriers move in response to a given applied electric potential, the higher the conductance, which is expressed in positive real-number siemens.

Susceptance, denoted B (imaginary part), is an expression of the ease with which alternating current (AC) passes through a capacitance or inductance. Susceptance is expressed in imaginary number siemens. It is observed for AC, but not for DC. When AC passes through a component that contains susceptance, energy might be stored and released in the form of a magnetic field, in which case the susceptance is inductive (denoted $-jB_L$), or energy might be stored and released in the form of an electric field, in which case the susceptance is capacitive (denoted $+jB_C$).

Admittance is the vector sum of conductance and susceptance. Susceptance is conventionally multiplied by the positive square root of -1, the unit imaginary number called symbolized by j, to express Y as a complex quantity $G - jB_L$ (when the net susceptance is inductive) or $G + jB_C$ (when the net susceptance is capacitive). Admittance (Y) and the magnitude of admittance |Y| is given by following equations. Where X is reactance; imaginary part of the impedance in Ohms.

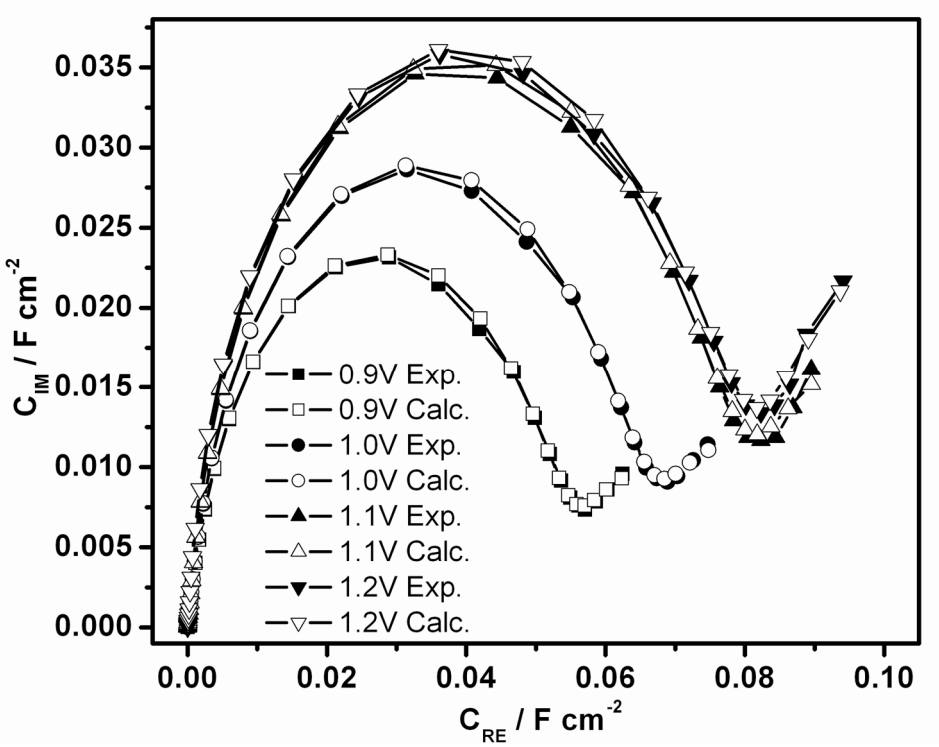

Figure 4.11: (a) Complex plane capacitance plot of the CFME/PBTh. Displays the real and imaginary components of in the x and y- axes.

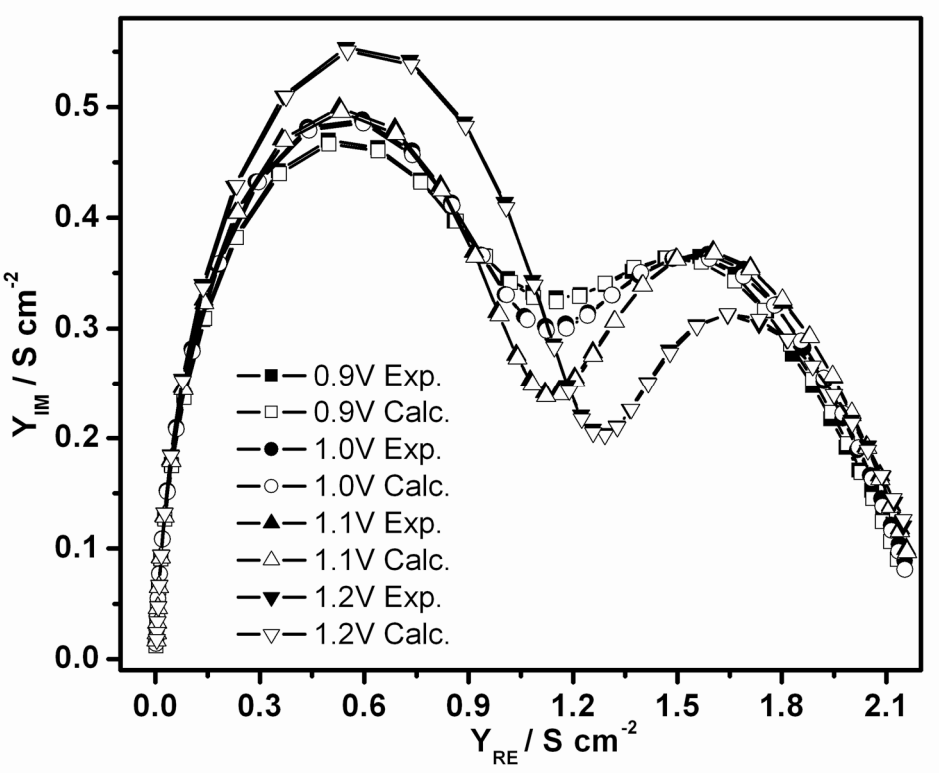

Figure 4.11: (b) Complex plane admittance plot of the CFME/PBTh. Displays the real and imaginary components of in the x and y- axes.

$$Y = Z^{-1} = (R + jX)^{-1} = G + iB \qquad |Y| = \sqrt{G^2 + B^2}$$

$$\mathrm{Re}(Y) = G = \frac{R}{R^2 + X^2} \qquad \mathrm{Im}(Y) = B = \frac{-X}{R^2 + X^2}$$

As the inductance of a component increases, its susceptance becomes smaller negatively (that is, it approaches zero from the negative side) in imaginary terms, assuming the frequency is held constant. As the frequency increases for a given value of inductance, the same thing happens. If L is the inductance in henries (H) and f is the frequency in hertz (Hz), then the susceptance $-jB_L$, in imaginary-number siemens, is given by: $-jB_L = -j(2\pi fL)^{-1}$

As the capacitance of a component increases, its susceptance becomes larger positively in imaginary terms, assuming the frequency is held constant. As the frequency increases for a given value of capacitance, the same thing happens. If C is the capacitance in farads (F) and f is the frequency in Hz, then the susceptance $+jX_C$, in imaginary-number ohms, is given by: $+jX_C = +j(2\pi fC)$.

In the light of this brief information about admittance and with the support of the Figure 4.11a and 4.11b one can conclude that susceptance is capacitive confirm the proposed equivalent circuit which does not contain an inductance (L) component.

4.1.5. Morphology of PBTh on CFME

The morphology of the galvanostatically electropolymerized PBTh from 0.005 M solution of the monomer with a charge of 1 C cm^{-2} onto carbon fiber electrode which is composed of five to ten single fibers were investigated using FE-SEM. Pictures of the obtained PENBTE films are presented in Figure 4.12. After electrodeposition of the PBTh, striations of the original carbon fiber which inherently exist are barely seen. This indicates very thin film of the BTh polymer was formed on the surface. (See Appendix Figure B.1 and Figure B.2 for FE-SEM pictures of the bare CFME). Thickness of the film was calculated about 0.1 micrometers from the SEM images.

Two types of formation observed on the CFME; first one is homogeneously distributed small granular formation on the surface with a variable size of 100-300 nm, and the second one irregular chunky structure with a size of 500-1000 nm.

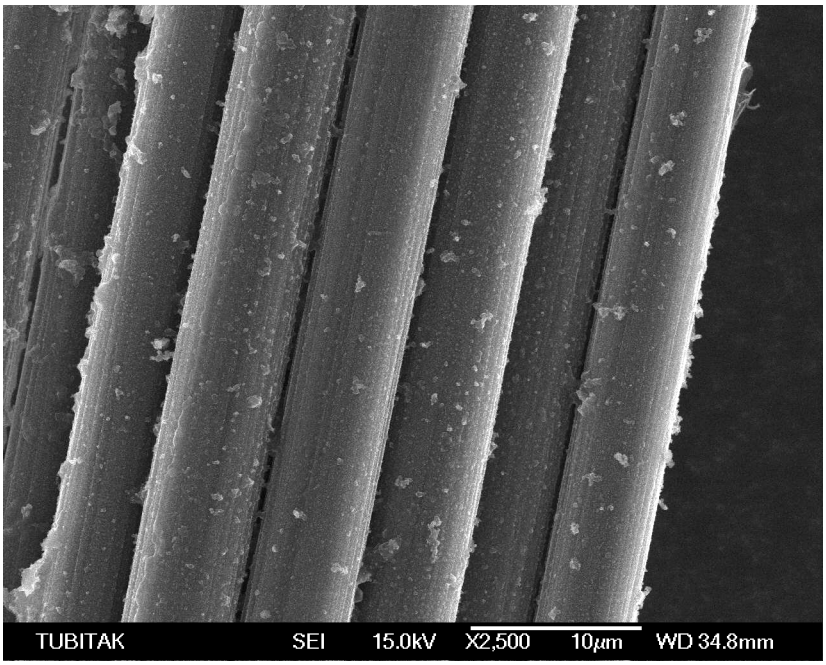

Figure 4.12: (a) FE-SEM images of the galvanostatically deposited PBTh films obtained by electropolymerization from a 0.005M solution of BTh in 0.1 M Et_4NBF_4/DCM with a charge of Q_{dep}= 1 C cm^{-2} a) at 2500 magnification,

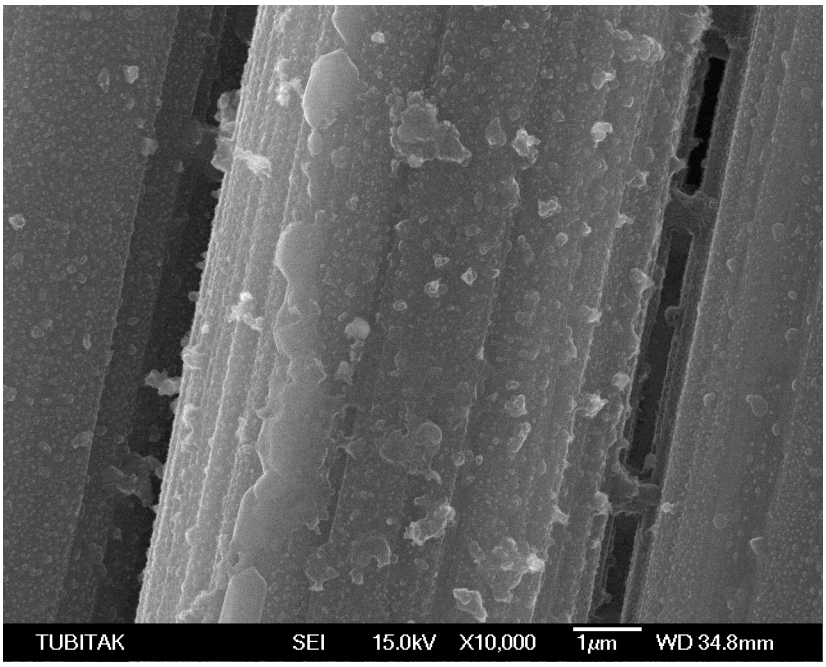

Figure 4.12: (b) FE-SEM image at 10000 magnifications.

4.2. Synthesis of 5,5'-bis-(4-methyl-thiazole)-[2,2']bithiophenyl

First step of the preparation of 5,5'-Bis-(4-methyl-thiazole)-[2,2']bithiophenyl is synthesis of 2,2 bithiophene. We have synthesized bithiophene as explained in the previous section.

4.2.1. Synthesis of 5,5'-bis-trimethylstannanyl-[2,2']bithiophenyl

A 250mL round bottom Schlenk flash equipped with an addition funnel, a stir bar, and kept under nitrogen atmosphere. 3.647 g (6.2 mmol) of butyllithium was added at -78 ºC during 30 minutes to the flask containing of solution of the 0.510 g (3.1 mmol) of 2,2'-bithiophenyl in Et_2O. Reaction mixture was stirred at this temperature for one hour and then the flask was heated up to 0 ºC, the reaction mixture was stirred for 15 more minutes and then the reaction mixture stirred for 5 hours at room temperature. 1.235 g (6.2 mmol) of $Sn(CH_3)Cl$ was added during 30 minutes and the resulting mixture was stirred for 17 hours at room temperature. Reaction mixture was then poured into water (20mL) containing 0.3mL of acetic acid. Organic phase was extracted CH_2Cl_2 and was washed with aqueous Na_2SO_4 and remaining solvent was removed by evaporation, 0.5027 g (yield 32.26 %) of product obtained after vacuumed overnight. Synthesis reaction of 5,5'-Bis-trimethylstannanyl-[2,2']-bithiophenyl is illustrated in equation 4.3.

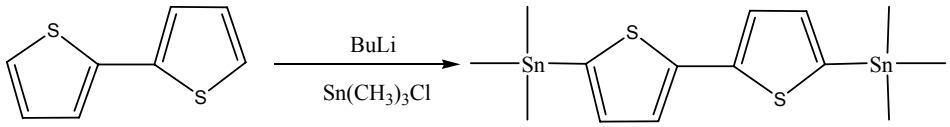

(4.3)

[2,2']Bithiophenyl

5,5'-Bis-trimethylstannanyl-[2,2']bithiophenyl

4.2.2. Bromination of 4-Methyl Thiazole; 5-bromo 4-methyl Thiazole

A 500 mL round bottom Schlenk flask equipped with a stir bar and an addition funnel was filled with 9.916 g (100 mmol) of 4-methylthiazole and 150 mL $CHCl_3$. 15.981 g (100 mmol; ~5.12 mL) of bromine was added in $CHCl_3$ (50mL) dropwise over 15 minutes at 0 ºC. The reaction mixture was refluxed for 10 hours. After the vacuum distillation three fractions were obtained.

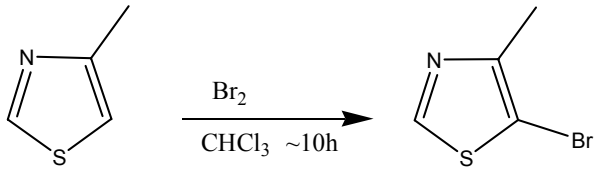

(4.4)

At full vacuum first and second fractions were collected at 20-30 ºC and 32-35 ºC consecutively, first two fractions showed an NMR shift at 6.9 PPM which is

attributed to proton of unreacted 4-methyl thiazole at five position. Third fraction, which is collected starting from 45 ºC, gave the final product and the NMR shift (see Figure 4.13) at 6.9 PPM was disappeared in this fraction. Bromination of 4-methyl thiazole is shown in equation 4.4. Yield = 64 %. H-NMR (in $CDCl_3$).

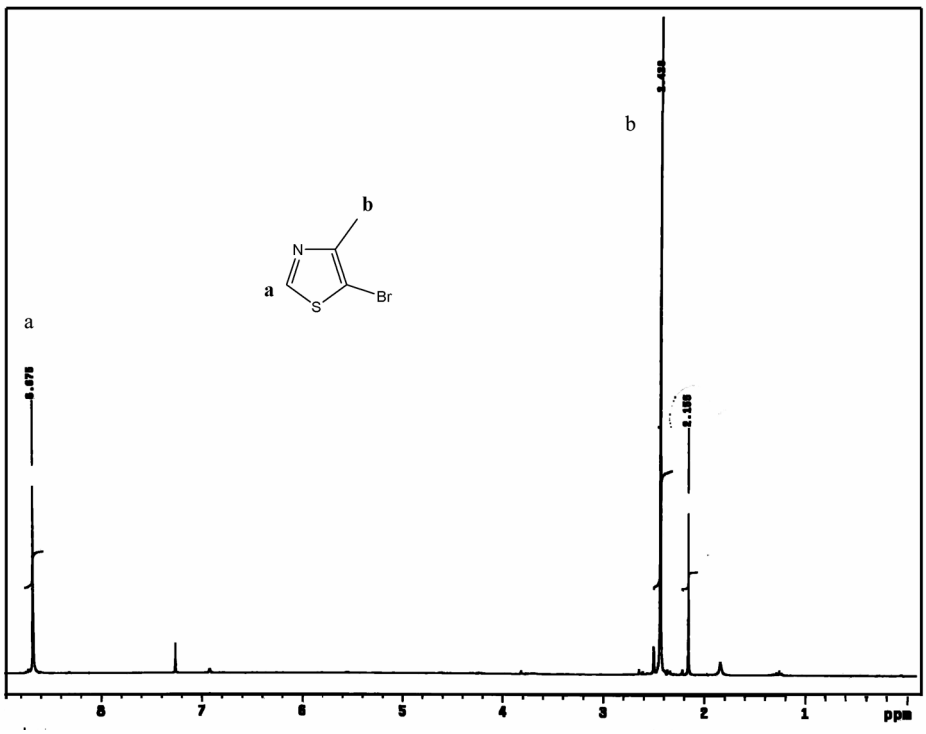

Figure 4.13: ^{1}H-NMR of the 5-Bromo 4-Methyl Thiazole in $CDCl_3$ obtained from the third fraction. 1. Fraction; a) δ 8.70-8.71 (d, 1H) ppm, b) δ 6.90-6.92 (q, 1H) ppm, c) δ 2.43 (m, 3H) ppm, 2. Fraction; a) δ 8.67 (s, 1H) ppm, b) δ 6.90-6.92 (q, 1H) ppm, c) δ 2.43 (m, 3H) ppm, 3. Fraction; a) δ 8.66 (s, 1H) ppm, b) none, c) 2.43 (s, 3H) δ ppm.

4.2.3. Synthesis of 5,5'-Bis-(4-methyl-thiazole)-[2,2']bithiophenyl

A dry Schlenk flask equipped with stir bar, N_2, condenser was added ~50mL of THF (dry), 0.5668 g (3.2 mmol) of 5-Bromo 4-Methyl Thiazole, 0.4918 g (1 mmol) of 5,5'-Bis-trimethylstannanyl-[2,2']bithiophenyl and 35.3 mg (0.05 mmol) of Pd(II) catalyst ($Pd(PPh_3)_2Cl_2$). Reaction mixture was refluxed overnight (~18h) and after cooling down to room temperature, reaction mixture was poured into water, CH_2Cl_2 was added and the organic phase was extracted, then organic phase was washed with water again and was dried with Na_2SO_4 and the solvent rotary evaporated. The product was re-crystallized in ethanol and dried in vacuum oven. Cross coupling reaction of 5,5'-Bis-(4-methyl-thiazole)-[2,2']bithiophenyl is given in equation 4.5.

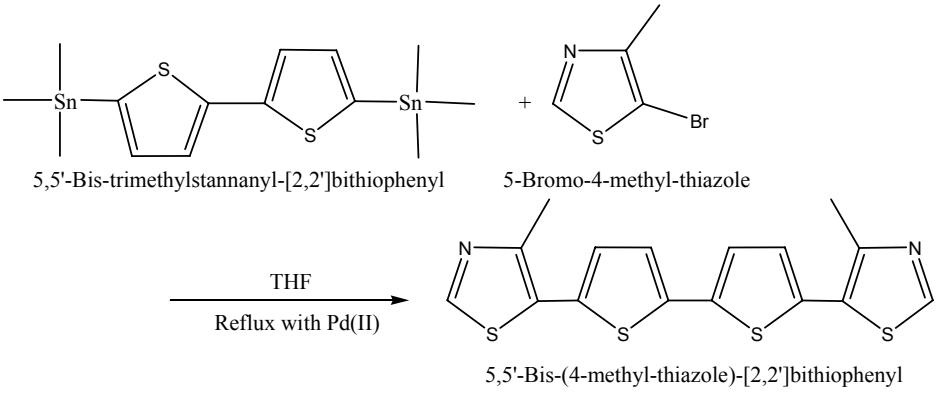

(4.5)

4.2.4. Electropolymerization of 5,5'-Bis-(4-methyl-thiazole)-[2,2']bithiophenyl

We have tried several ways to polymerize 3-methyl thiazole-bithiophene- 3-methyl thiazole (3MeTz-BTh-3MeTz) comonomer but all of the attempts were unsuccessful. Figure 4.14 shows a representative electropolymerization attempt of 3MeTz-BTh-3MeTz generally this type of cyclic voltammogram was obtained.

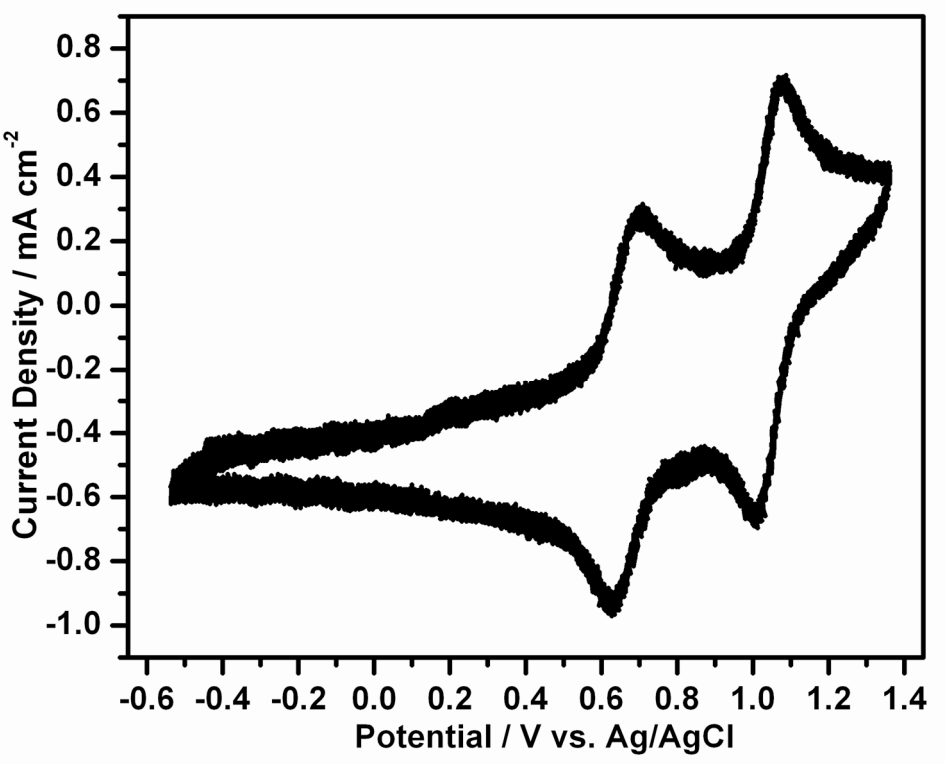

Figure 4.14: A cyclic voltammogram (25 cycles) for 0.001 M 3MeTz-BTh-3MeTz in CH_2Cl_2 0.1 M $TBAPF_6$/DCM solution; with a scan rate of 100 mVs^{-1}.

The cyclic voltammogram of the comonomer exhibits two reversible oxidation peaks attributed to the generation of the cation radical and the dication, and reduction peaks of the corresponding peaks as shown in Figure 4.14. The low oxidation potentials are mainly associated with the presence of the BTh portion of the molecule because of its electron-rich nature. The stability of the two oxidation states results from the thiazoles at the end caps, which not only block polymerization but also contribute to the stabilization of the cation by delocalization of the charge.

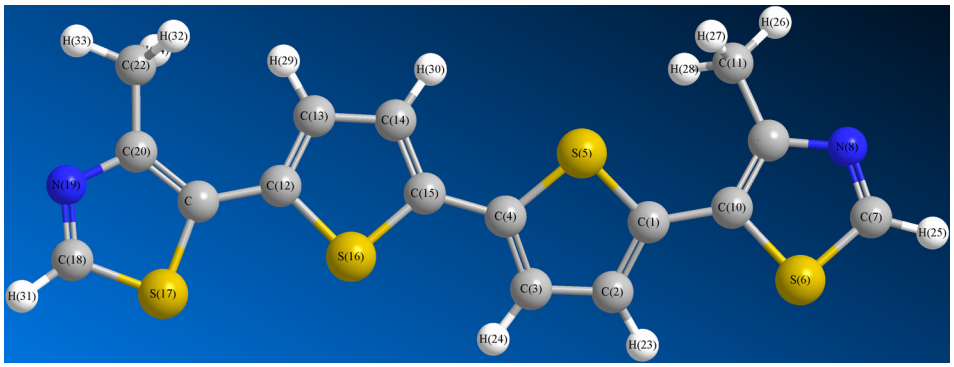

Figure 4.15: MM2 optimized geometry of the 5,5'-Bis-(4-methyl-thiazole)-[2,2']bithiophenyl. Geometry optimizations were performed ChemOffice3D Pro.

Table 4.3: Atomic charges of the 5,5'-Bis-(4-methyl-thiazole)-[2,2']bithiophenyl comonomer. Corresponding atom numbers are given in Figure 4.14.

Atom	Label	Charge	Atom	Label	Charge
C	[C(1)]	-0.104	C	[C(10)]	-0.16
C	[C(2)]	-0.241	C	[C(11)]	-0.154
C	[C(3)]	-0.237	C	[C(12)]	-0.112
C	[C(4)]	-0.11	C	[C(13)]	-0.237
S	[S(5)]	0.639	C	[C(14)]	-0.24
S	[S(6)]	0.623	C	[C(15)]	-0.099
C	[C(7)]	-0.048	S	[S(16)]	0.623
N	[N(8)]	-0.419	S	[S(17)]	0.622
C	[C(9)]	0.018	C	[C(18)]	-0.043

Atom	Label	Charge	Atom	Label	Charge
N	[N(19)]	-0.418	H	[H(27)]	0.049
C	[C(20)]	0.023	H	[H(28)]	0.047
C	[C(21)]	-0.17	H	[H(29)]	0.028
C	[C(22)]	-0.152	H	[H(30)]	0.023
H	[H(23)]	0.023	H	[H(31)]	0.013
H	[H(24)]	0.024	H	[H(32)]	0.048
H	[H(25)]	0.013	H	[H(33)]	0.039
H	[H(26)]	0.04	H	[H(34)]	0.048

The presence of the nitrogen in the bithiazole ring increases the oxidation potential and renders the materials unstable with respect to p-doping. Although n-doping is possible, the reduction potentials are near -2 V vs ferrocene/ferrocenium. [21, 155] Co-oligomers of bithiazoles and bithiophene was obtained with the aim of bithiazoles will possess the ease of oxidation characteristic of BTh. Compounds with similar structure to 3MeThz-BiTh-3MeThz may be classified as acceptor-donor-acceptor (A-D-A) type molecules because the bithiazole rings have relatively low-energy LUMOs (electron acceptor), and the thiophene rings have high-energy HOMOs (electron donor) [156].

To corroborate these assignments, extended Huckel calculations were used to calculate charge and results are given in Figure 4.15 and Table 4.3. In literature [157] this idea was supported with the measurements of low-temperature optical spectra and ESR measurements for similar thiazole end structures.

4.3. 4-Methyl-2-thiophene-2-yl-thiazole

4.3.1. Bromination of Thiophene

Because of the difficulty of the reaction itself and after some unsuccessful attempts 2-bromothiophene (2-thienylbromide) was provided from Aldrich and was used without further purification. Bromination of reaction thiophene is given in equation 4.6.

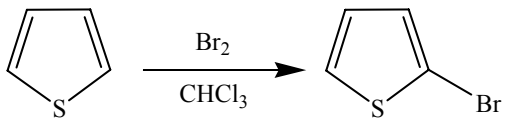

(4.6)

4.3.2. Synthesis of 2-trimethylstannanyl-4-methyl Thiazole

A 250 mL Schlenk flask equipped with an addition funnel was placed a 0.4958 g (5 mmol; ~ 0.55mL) of 3-methylthiazole in THF (50 mL, dry) and the flask was cooled to -78°C. A solution of (2.94 mL, 5 mmol) 2.5 M n-buthyllithium was added drop wise into the flask under nitrogen and the mixture was stirred at -78°C for one hour. 0.9963 g (5 mmol) of trimethylstannylchloride (in 40 mL THF) was added drop wise and the mixture was allowed to warm to ambient temperature with stirring overnight. Water (50 mL) was added followed by CH_2Cl_2 (50 mL). The phases were separated

and organic phase was dried with Na_2SO_4 and evaporated to dryness to give a reddish solid product. Synthesis of 2-trimethylstannanyl-4-methyl thiazole is presented in equation 4.7. Yield=0.6446 g.

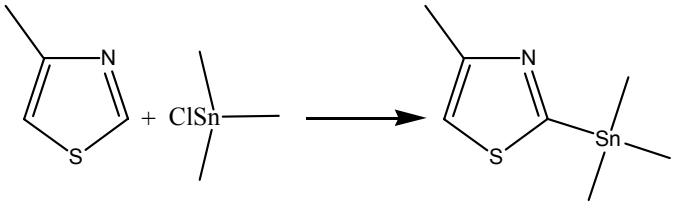

(4.7)

4.3.3. Synthesis of 4-Methyl-2-thiophen-2-yl-thiazole

In a 100 mL Schlenk flask equipped with a condenser and nitrogen, was charged with ~60 mL of THF (dry), 0.40 g (2.46 mmol; ~0.23 mL) of 2-bromothiophene, 0.6446 g (2.46 mmol) of 2-trimethylstannanyl-4-methyl thiazole and 86 mg (2.46 mmol) of Pd(II) catalyst ($Pd(PPh_3)_2Cl_2$). The mixture was refluxed for 18 h. After cooling to room temperature the reaction mixture was poured into water, and dichloromethane was added. Extracted organic phase was washed with water and dried over Na_2SO_4 and the solvent rotary evaporated. The final product was re-crystallized in ethanol. 0.2826 g (yield 63 %) of 4-Methyl-2-thiophen-2-yl-thiazole was obtained. Cross coupling reaction step of 4-methyl-2-thiophen-2-yl-thiazole synthesis is illustrated in equation 4.8.

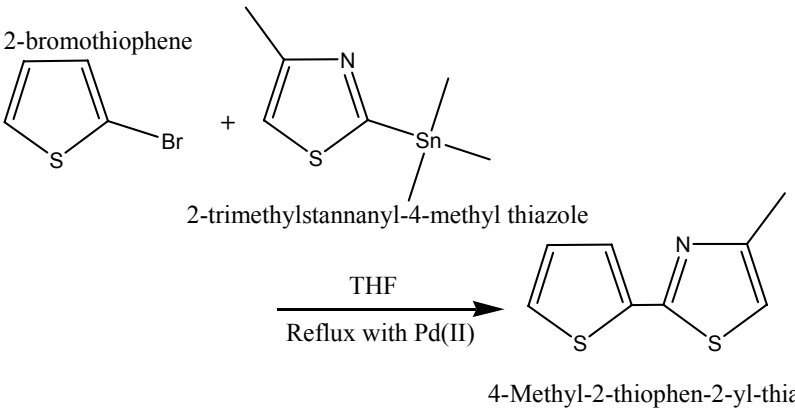

(4.8)

4.3.4. Electropolymerization of 4-Methyl-2-thiophen-2-yl-thiazole Comonomer

We have tried several ways to polymerize this novel thiophene and 4-methyl thiazole (Th-4MeTz) comonomer but all of the attempts were unsuccessful. We observed

similar results as explained in previous section. Atomic charges of the comonomer were calculated and results are given in Figure 4.16 and Table 4.4.

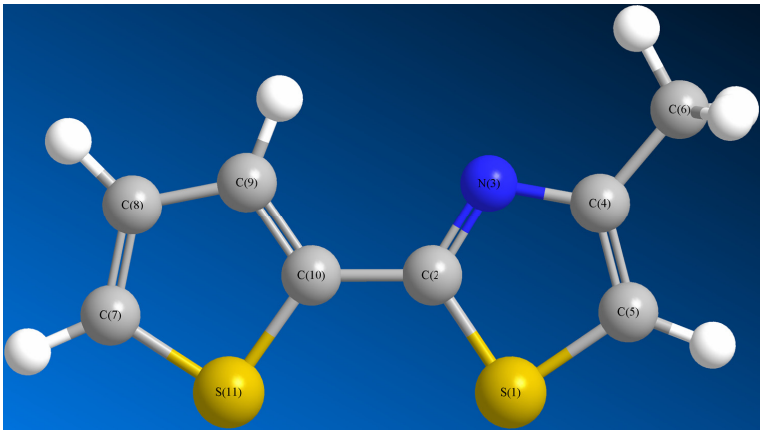

Figure 4.16: MM2 optimized geometry of thiophene-4-Methyl-thiazole. Geometry optimizations were performed ChemOffice3D Pro.

Table 4.4: Atomic charges of the 4-Methyl-2-thiophen-2-yl-thiazole comonomer. Corresponding atom numbers are given in Figure 4.14.

Atom	Label	Charge	Atom	Label	Charge
S	[S(1)]	0.62	C	[C(10)]	-0.115
C	[C(2)]	0.045	S	[S(11)]	0.66
N	[N(3)]	-0.452	H	[H(12)]	0.028
C	[C(4)]	0.059	H	[H(13)]	0.04
C	[C(5)]	-0.272	H	[H(14)]	0.049
C	[C(6)]	-0.154	H	[H(15)]	0.049
C	[C(7)]	-0.197	H	[H(16)]	0.028
C	[C(8)]	-0.205	H	[H(17)]	0.025
C	[C(9)]	-0.231	H	[H(18)]	0.024

4.4. Synthesis and Electrochemical Characterization of TNBTT Comonomer

In this part of the study we have completely changed our synthetic strategy and we have planned to synthesize donor-acceptor-donor type (DAD) comonomers. This section includes synthesis of a novel comonomer based on thiophene and thiazole moieties i.e., thiophene-nonylbithiazole-thiophene (TNBTT). It was anticipated that TNBTT would result in well-defined polymers with well-ordered linkages. The long alkyl chains on the thiazole moieties were expected to improve solubility of the comonomer and to reduce the polymer's band gap. Thus the comonomer is expected to yield regioregular polymers which should be well ordered and exhibit high conductivity.

In the first two steps, nonylbithiazole moiety of the target comonomer was synthesized via similar procedures as previously reported [16, 158]. A long alkyl chain was integrated to four position of the thiazole ring via 2-bromoundecanone, afterwards the 4,4'-dinonyl-2,2'-bithiazole was brominated. The synthesis of 2-trimethyltinthiophene was performed at the fourth step of the procedure and at the final step the palladium-catalysed cross coupling reaction were performed to integrate thiophene rings to the 4,4'-dinonyl-2,2'-bithiazole in order to obtain a mixed donor-acceptor comonomer based on thiophene and nonylthiazole rings. The product was re-crystallized in methanol and was characterized by ^{1}H-NMR. The TNBTT comonomer is soluble in DCM and insoluble or scarcely soluble in the other organic solvents tested.

4.4.1. Synthesis of Bis(thiophene)-(4,4'-dinonyl-2,2'-bithiazole)

Synthesis of bis(thiophene)-(4,4'-dinonyl-2,2'-bithiazole) or TNBTT (thiophene-nonylbithiazole-thiophene) comonomer was performed with a five consecutive step.

4.4.1.1. Synthesis of 1-bromoundecanone

A 500 mL Schlenk flask equipped with a magnetic stirring bar was filled with undecanone (100 mL, 484.4 mmol) and urea (50 g, 832.5 mmol) in acetic acid (260 mL). This mixture was stirred for 20 minutes. The Schlenk flask was equipped with pressure equalizing additional funnel, to this funnel 60mL of acetic acid and 27.4 mL of Br_2 was added dropwise over a period of about an hour. Then, the mixture was allowed to stir and come to room temperature. After 7 h, the mixture solution was poured into ice-water mixture and was filtered. And the final product was crystallized over ethanol. Synthesis of 1-bromoundecanone is given in equation 4.9.Yield = 73-75% white crystals.

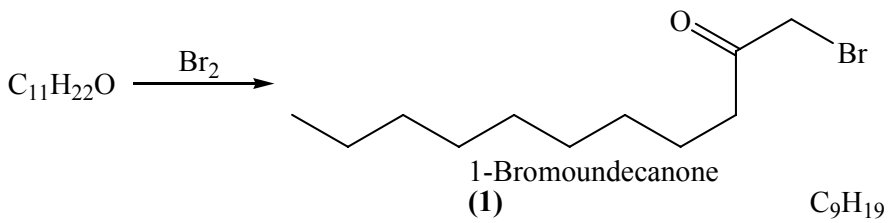

1-Bromoundecanone
(1)

(4.9)

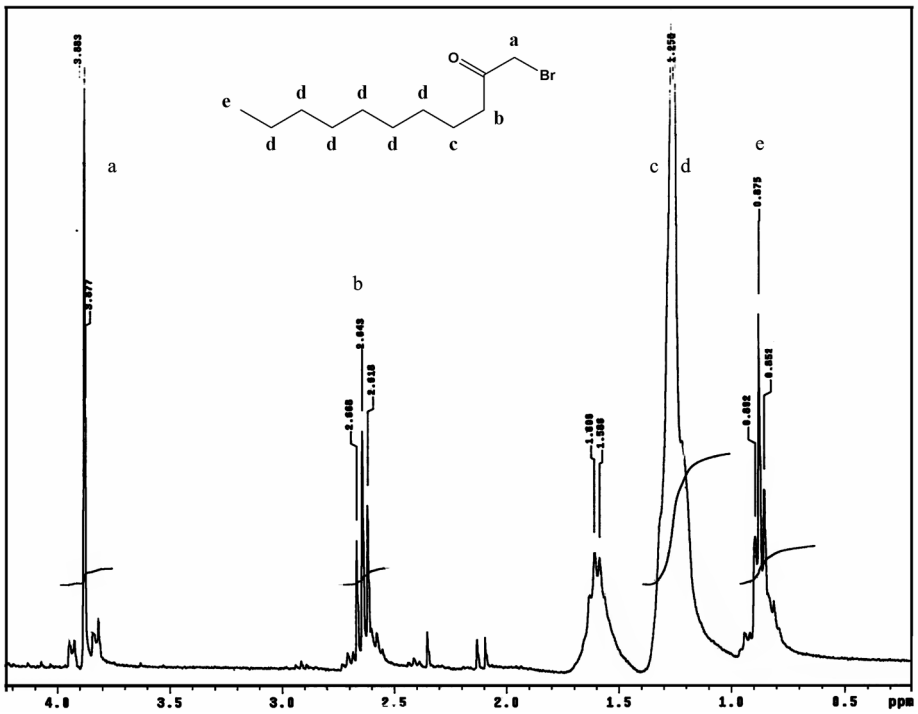

Figure 4.17: ^{1}H-NMR of the 1-bromoundecanone in $CDCl_3$. a) δ 3.88 (d, 2H).

4.4.1.2. Synthesis of Nonylbithiazole

A 250 mL 3-necked flash equipped with a condenser, a stir bar, N_2 was filled with 10.37 g of 1-bromoundecanon, 2.5 g of dithioxamide and absolute ethanol (100 mL). The mixture was heated to reflux for 5 hours, was poured into ice. The solid was filtered and stirred in CH_2Cl_2 over $NaSO_4$ and decolorizing carbon. The mixture was filtered and solvent removed by vacuum. The water layer was dried over $MgSO_4$ and the precipitate was crystallized in methanol. Synthesis of nonylbithiazole is illustrated in equation 4.10. Yield = 5.25 g (60.0%).

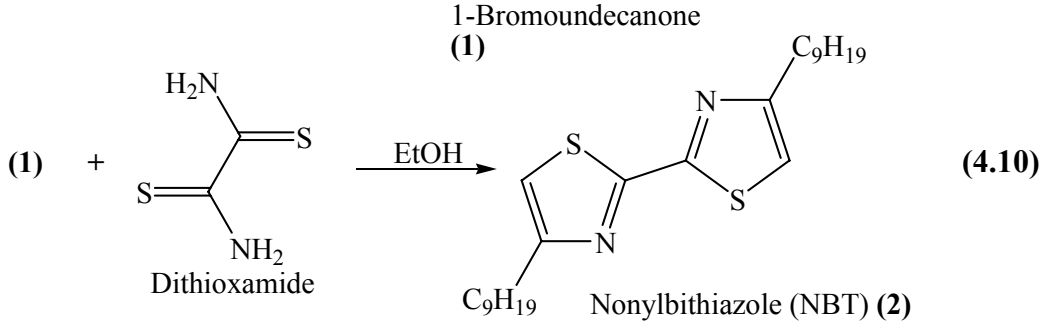

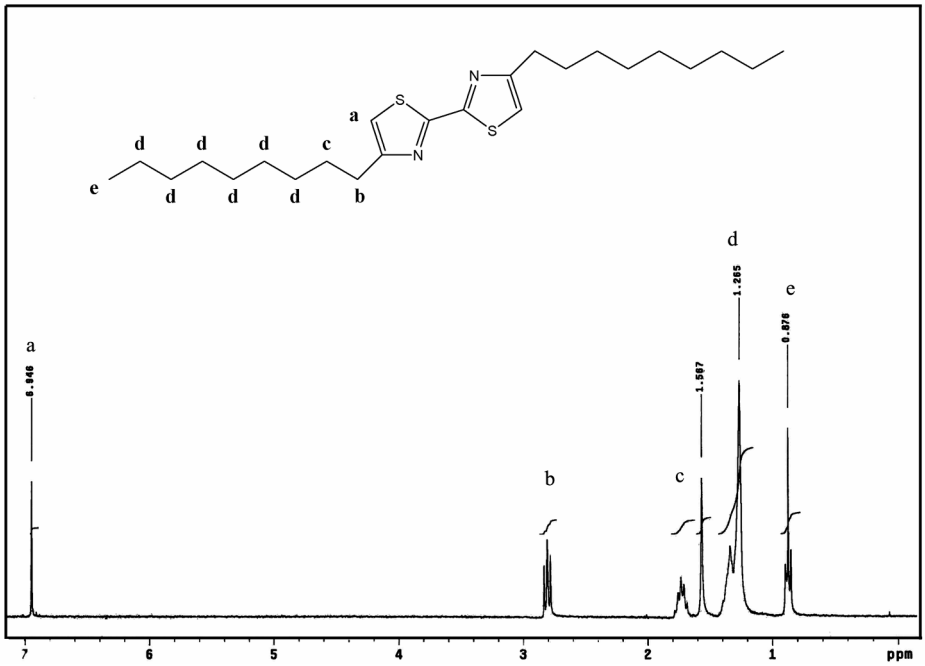

Figure 4.18: ^{1}H-NMR of the nonylbithiazole in $CDCl_3$. a) δ 6.95 (s, 1H) ppm, b) δ 2.78-2.80 (t, 2H) ppm, c) δ 1.73 (t, 2H) ppm, d) δ 1.33-1.26 (m, 12H) ppm, and e) δ 0.88-0.87 (t, 3H) ppm.

ATR-FTIR Characterization of Nonylbithiazole (NBT); FTIR measurement was made using solid NBT powder.

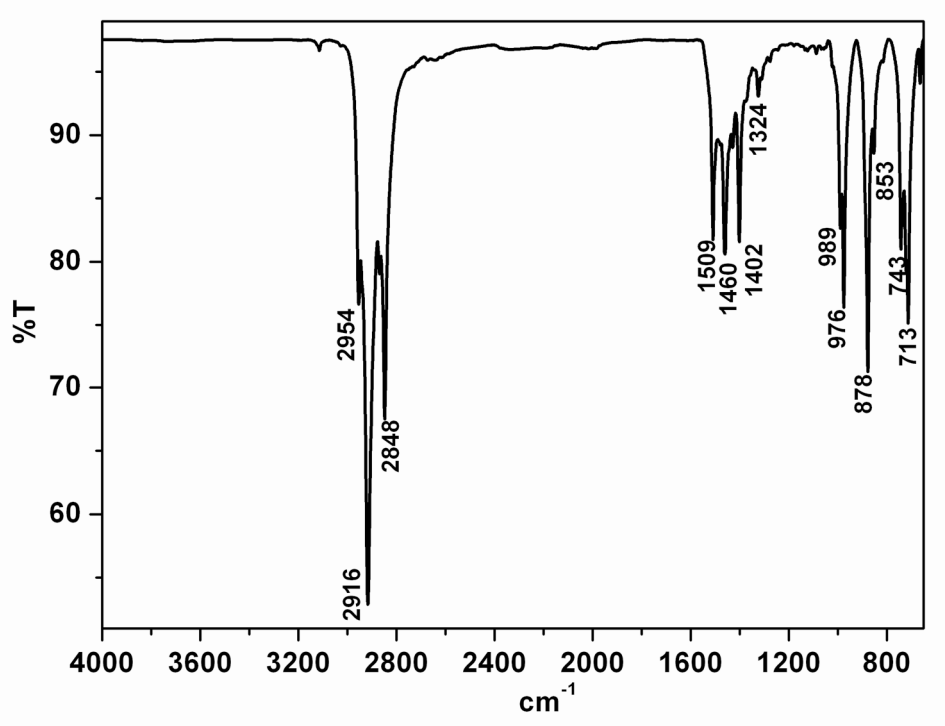

Figure 4.19: ATR-FTIR spectrum of the nonylbithiazole.

The ATR-FTIR spectra of the samples were recorded at room temperature and at laboratory humidity conditions. The ATR-FTIR spectrum of NBT sample recorded between 4000 and 650 cm^{-1}. The frequencies of the major absorption peaks are also listed in Table 4.5. Assignments of these frequencies have been done based upon literature tables [149, 150]. The peaks of the NBT populated in three region, the very strong absorption peaks appeared around 2840 – 2960 cm^{-1} assigned to long alkyl chain, the absorption in the region of 1509 cm^{-1} is ascribed to thiazole ring i.e. that is stretching and in-plane vibration of the $-C=N$ and in-plane vibration of the $-C=C-$ fractions of the thiazole ring. We observed peaks assigned to the long alkyl chain and definite peaks of thiazole ring.

Table 4.5: ATR-FTIR absorption bands and peak assignment table for the nonylbithiazole. **vs**; very strong, **s**; strong, **m**; medium, **w**; weak

Peak / cm^{-1}	Fragment	Intensity / Comment
2954	$R-CH_3$	**s** / $-C-H$ stretching vibration- asymmetric
2916	$R-CH_3$	**vs** / $-C-H$ stretching vibration- symmetric
2848	$-CH_2-$	**s** / $-C-H$ scissor vibration
1460	$R-CH_3$	**m** / $-C-H$ deformation vibration- asymmetric
1324	$R-CH_3$	**w** / $-C-H$ symmetric deformation vibration
989	Alkyl Chain	**s** / $-C-H$ deformation vibration
878	$R-CH_3$	**s** / $-C-H$ rocking vibration
3111	Thiazole	**w** / $=C-N-C-$ stretching vibration
1509	Thiazole	**m** / $-C=N$ stretching and in-plane vibration
1509	Thiazole	**m** / $-C=C-$ in-plane vibration
1402	Thiazole	**w** / C=C and C=N in-plane vibration
1260	Thiazole	**m** / $-C-N-$ stretching vibration
1014	$-S-$	**s** / $-C-S-$ stretching vibration
853	$-S-$	**s** / $-C-S-$ stretching vibration
713	$-S-$	**s** / $-C-S-$ stretching vibration

4.4.1.3. Bromination of Nonylbithiazole

A 100 mL round bottom 3-neck flask equipped with an addition funnel was charged with 1.00 g (2.38 mmol) NBT and 20 mL $CHCl_3$. 0.95 g (5.95 mmol) bromine was added in $CHCl_3$ (20 mL) dropwise over 15 minutes. A precipitate was formed during addition. The reaction was refluxed for 2 hours. At which time the solution was allowed to cool diluted with 40 mL of $CHCl_3$ and washed with (3x100 mL) $NaHSO_3$, (2x50 mL) K_2CO_3 and (2x100 mL) H_2O. The $CHCl_3$ layer was dried over $MgSO_4$

and filtered. Solvent was removed via vacuum to get pure product. The solid was recrystallized from acetone with a small amount $CHCl_3$. Bromination equation of nonylbithiazole is illustrated in equation 4.11. Yield = 1.06g (76.8%).

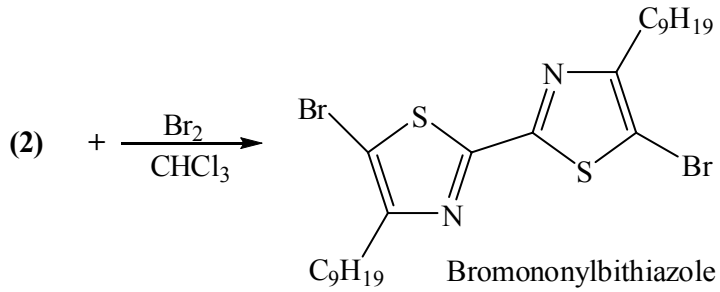

(4.11)

Bromononylbithiazole (BrNBTBr) **(3)**

Proton shifts of bromononylbithiazole in $CDCl_3$ is presented in Figure 4.20.

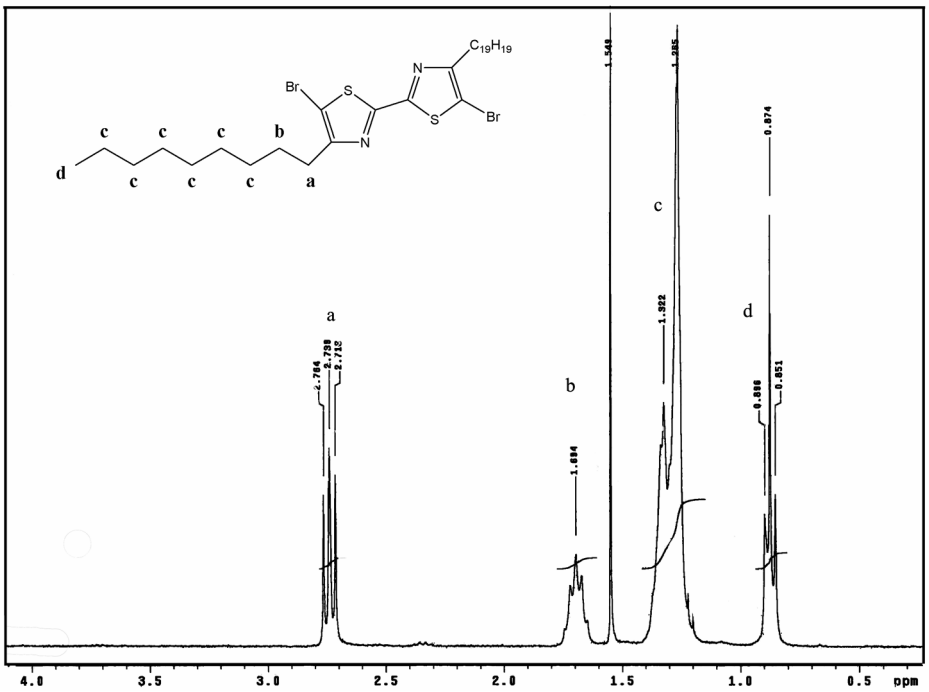

Figure 4.20: ^{1}H-NMR of the bromononylbithiazole in $CDCl_3$. a) δ 2.76-2.71 (t, 2H) ppm, b) δ 1.69 (m, 2H) ppm, c) 1.32-1.26 (m, 12H) ppm, d) δ 0.85-0.85 (t, 3H) ppm.

4.4.1.4. Synthesis of 2-trimethyltinthiophene

1.6 g of BuLi (2.5 M in hexane) was added drop wise to solution of 2.1 g of thiophene in Et-O-Et (40 mL) at -78°C, the mixture was stirred for one hour and system heated up to 0°C and stirred at this temperature for 15 minutes. After stirring for 30 minutes, 4.98 g of trimethyltinchloride (chlorotrimethylstannane) (in 40 mL ether) was added drop wise and the mixture was allowed to warm to ambient temperature with stirring overnight. Water (30 mL) was added followed by ether (40

mL). The phases were separated and organic phase was dried with $MgSO_4$ and evaporated to dryness to give the product. Synthesis of 2-trimethyltinthiophene is illustrated in equation 4.12.

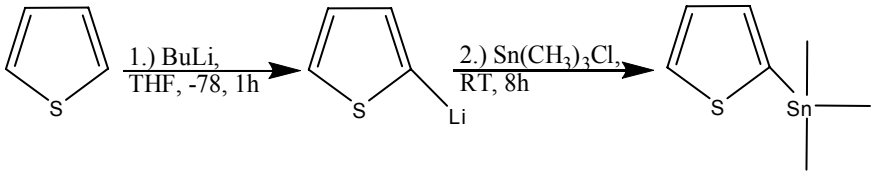

(4.12)

4.4.1.5. Synthesis of Thiophene-Nonylbithiazole-Thiophene (TNBTT)

In a dry schlenk flask equipped with stir bar, N_2, condenser was added ~60mL of THF (dry), 0.5785 g (2 mmol) of Br-NBT-Br, 0.4939 g of (4 mmol) of Th-$SnMe_3$ and 35.3 mg (0.05 mmol) of Pd(II) catalyst ($Pd(PPh_3)_2Cl_2$). After cooling down to room temperature, reaction mixture was poured into water. CH_2Cl_2, pentane, chloroform were added and the organic phase was extracted, then organic phase was washed with water again and was dried with $MgSO_4$ and the solvent rotary evaporated. The product was re-crystallized in ethanol. Cross coupling reaction of TNBTT synthesis is given in equation 4.13.

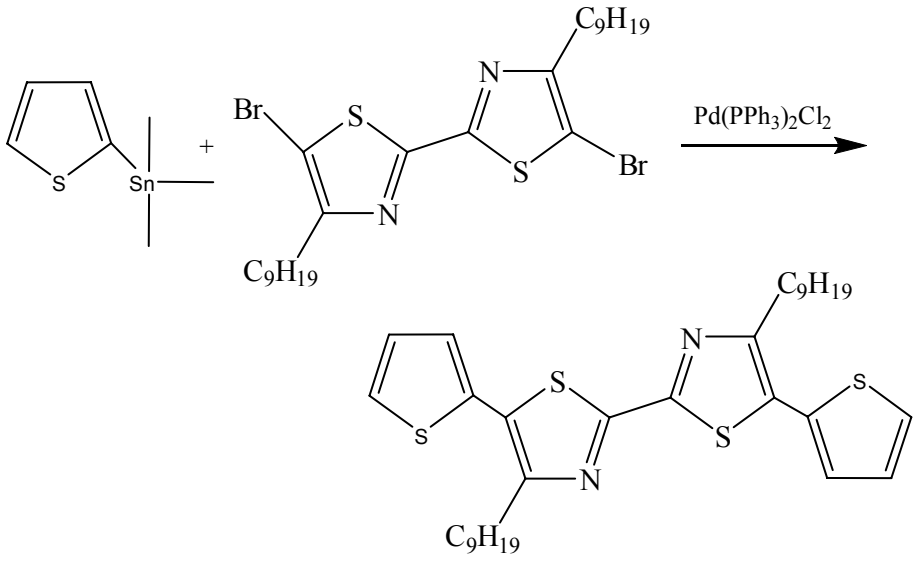

(4.13)

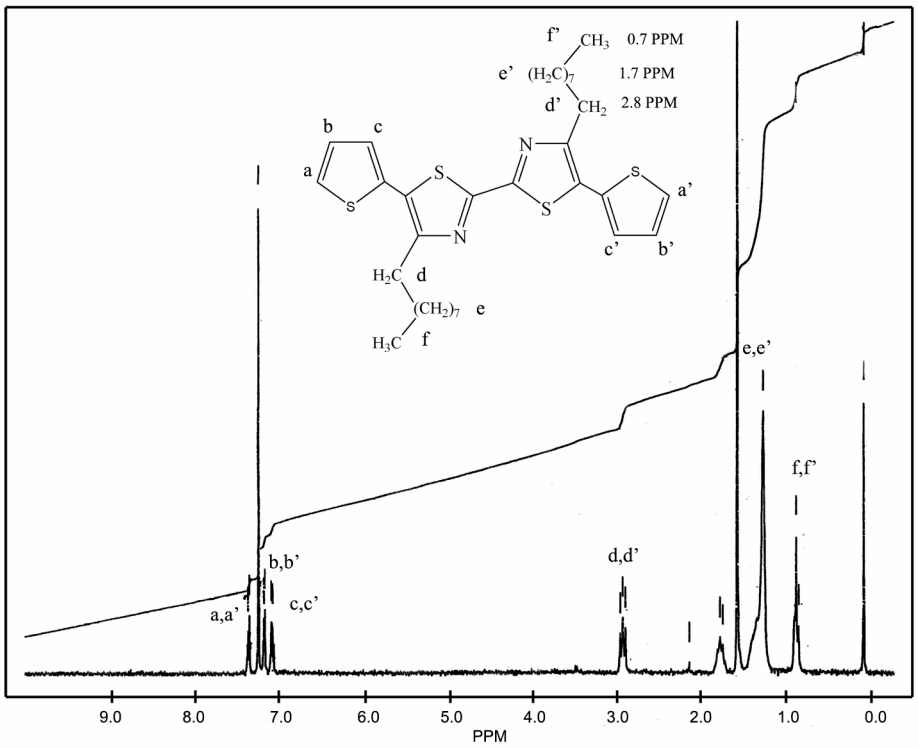

Figure 4.21: ^{1}H-NMR of the TNBTT in $CDCl_3$. a) δ 7.32 ppm (2H), c&b) δ 7.11 (4H), d) δ 2.96 – 2.90 ppm (t, 4H), e) δ 1.26 ppm (m, 28H), f) δ 0.83 ppm (t, 6H).

Spectroscopic characterization of TNBTT comonomer was performed by ^{1}H-NMR and ATR-FTIR. Results are presented in Figure 4.21 and 4.22, respectively.

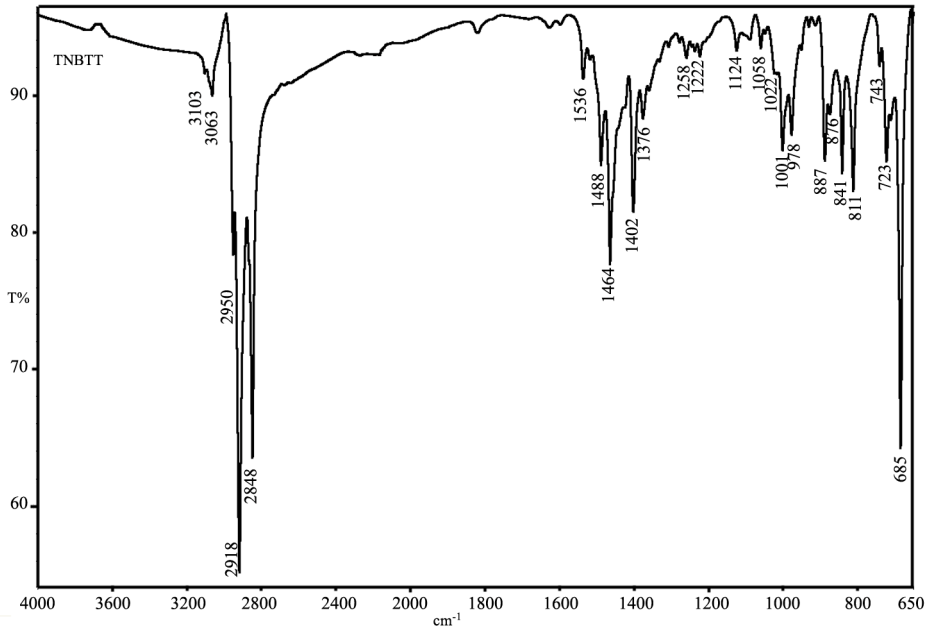

Figure 4.22: ATR-FTIR spectrum of the TNBTT monomer.

The ATR-FTIR a spectrum of the sample was recorded as previously described. The frequencies of the major absorption peaks are also listed in Table 4.6. Assignments

of these frequencies have been done based upon literature tables in a similar way as previously explained for bithiophene and nonylbithiazole.

Table 4.6: ATR-FTIR absorption bands and peak assignment table for the TNBTT. **vs**; very strong, **s**; strong, **m**; medium, **w**; weak

Peak / cm^{-1}	Fragment	Intensity / Comment
2950	$R-CH_3$	**s** / $-C-H$ stretching vibration- asymmetric
2918	$R-CH_3$	**vs** / $-C-H$ stretching vibration- symmetric
2848	$-CH_2-$	**s** / $-C-H$ scissor vibration
1464	$R-CH_3$	**s** / $-C-H$ deformation vibration- asymmetric
978	$-CH_2-$	**s** / $-C-H$ deformation vibration
876	$R-CH_3$	**s** / $-C-H$ rocking vibration
3103	Thiazole	**w** / $=C-N-C-$ stretching vibration
1509	Thiazole	**m** / $-C=N$ stretching and in-plane vibration
1509	Thiazole	**m** / $-C=C-$ in-plane vibration
1402	Thiazole	**w** / C=C and C=N in-plane vibration
1258	Thiazole	**m** / $-C-N-$ stretching vibration
1001	$-S-$	**s** / $-C-S-$ stretching vibration
841	$-S-$	**s** / $-C-S-$ stretching vibration
685	$-S-$	**vs** / $-C-S-$ stretching vibration

4.4.2. Electropolymerization of TNBTT

Due to the low solubility of the comonomer in commonly used solvents (acetonitrile, water, propylene carbonate, and nitrobenzene) for electrochemical polymerizations, dichloromethane was found to be the most suitable solvent for electrodeposition of PTNBTT. Figure 4.23 shows cyclic voltammograms on carbon fiber microelectrode containing 0.005 M of TNBTT in 0.1 M Et_4NBF_4/DCM solution. The electrodeposition of the comonomer was performed at scan rate of 20 mV s^{-1} between 0.0 V and 1.4V. The monomer oxidation onto bare electrode starts (E_{onset} of the TNBTT) at 1.096 mV vs. Ag/AgCl. In the scanning range of 0.0V to 1.4V, PTNBTT generates a broad cathodic peak at around 0.96V on the return scan. The increase in the size of this peak indicates that it is due to the electroactive film was formed on the surface of the carbon fiber microelectrode. A regular growth is not observed as seen from the inset plot of Figure 4.23. A linear increase in current densities of the consecutive cycles was not observed. This might be due to several reason for instance, instability of polythiophenes at the potentials for their formation

[159], low monomer concentration, possibility of the polymer formation more than one polymerization pathway on thiophene ring [160].

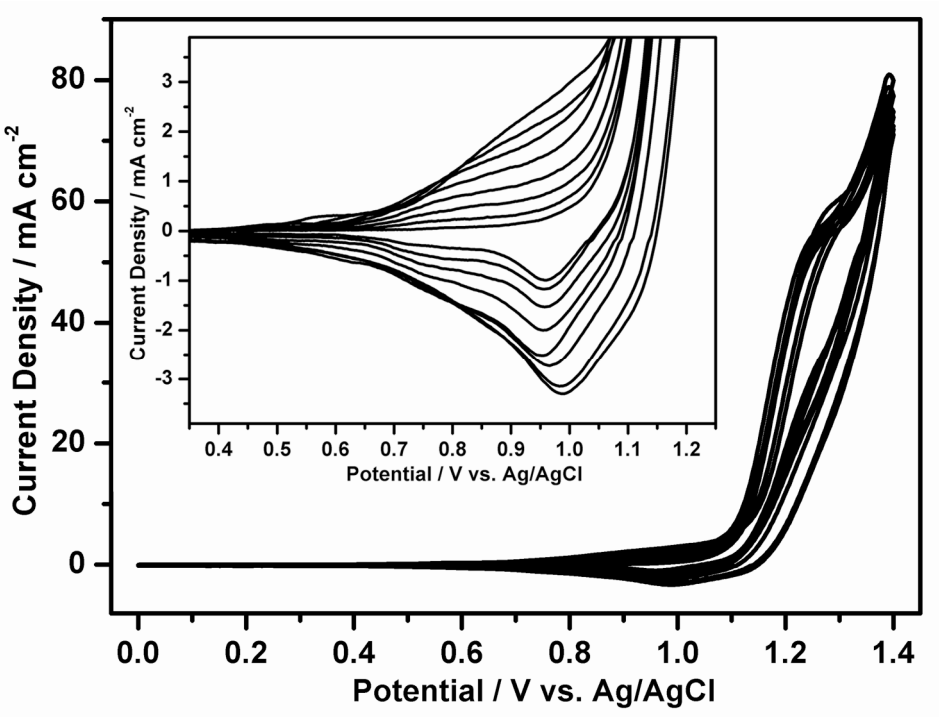

Figure 4.23: Electropolymerization of TNBTT monomer by cyclic voltammetry from a 0.005M solution of monomer in 0.1 M Et_4NBF_4/DCM at a scan rate of 20 mV s^{-1} onto CFME (area ~ 0.001 cm^2). Q_{dep}=8.7 C cm^{-2}.

The polymer films were washed with monomer-free electrolyte solution, and their redox behavior was investigated in the same solution by cyclic voltammetry. Figure 4.24a presents cyclic voltammogram of a PTNBTT polymer which is deposited with a charge of Q_{dep}=9.6 C cm^{-2} onto the carbon fiber microelectrode in the monomer free solution at different scan rates. Although irregular growth of the PTNBTT was observed during electropolymerization, in monomer free electrolyte solution it exhibits a well defined oxidation and reduction peaks and a linear increase in current densities were monitored. The scan rate of the polymer was investigated and the demonstrated in Figure 4.24b. Scan rate dependencies of the both oxidation and reduction peaks of the polymer were calculated using current density values with respect to square root of the scan rate and correlation coefficient of the oxidation peak and reduction was calculated as 0.9905 and -0.9941 respectively.

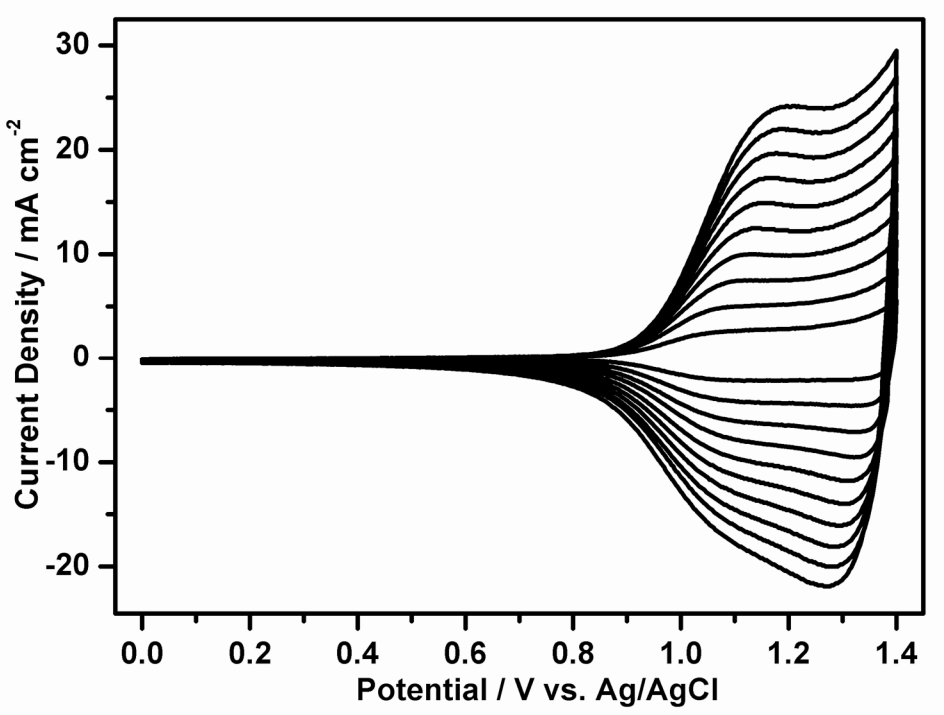

Figure 4.24: (a) Cyclic voltammogram of the electrochemically polymerized PTNBTT film (Q_{dep}=9.6 C cm^{-2}) in a monomer free electrolyte solution scanned at (a) 20, (b) 40, (c) 60, (d) 80, (e) 100, (f) 120, (g) 140, (h) 160, (i) 180, and (k) 200 mV s^{-1}.

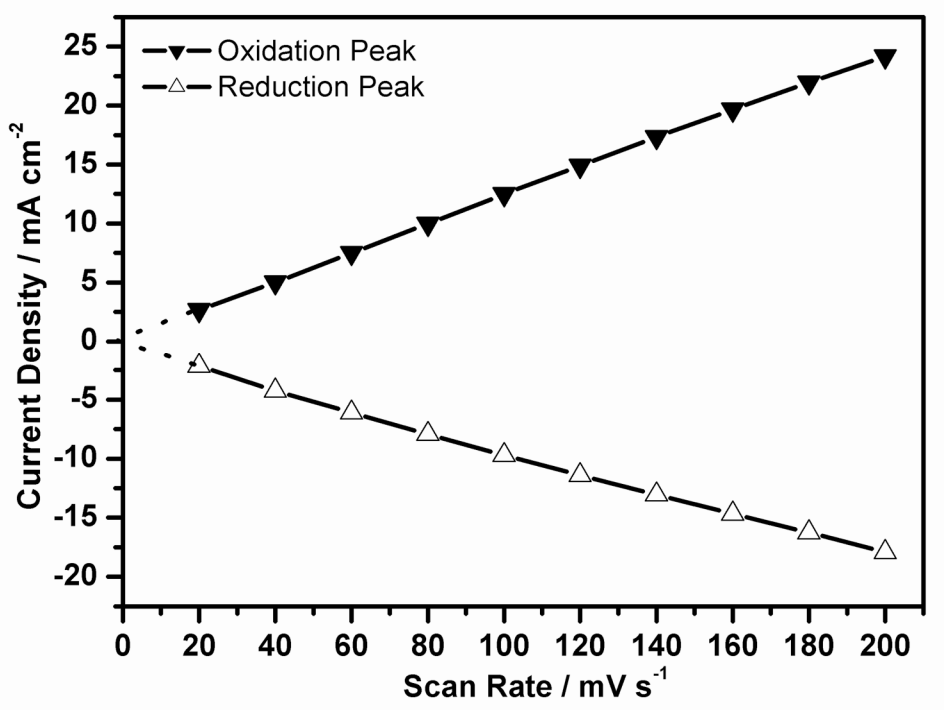

Figure 4.24: (b) Scan-rate dependence of the cyclic voltammogram which is given in Figure 4.24a.

A linear relationship was found between the peak current density and scan rate, indicating that the electroactive polymer films are well adhered and the redox

processes are non-diffusion limited. A sharper oxidation and a broad reduction peaks were also observed. We have observed more reversible oxidation and reduction peaks with almost same current densities and observed better scan rate dependency with thinner films of PTNBTT. An example of this kind of the films is given in Appendix Figure C.1 and C.2.

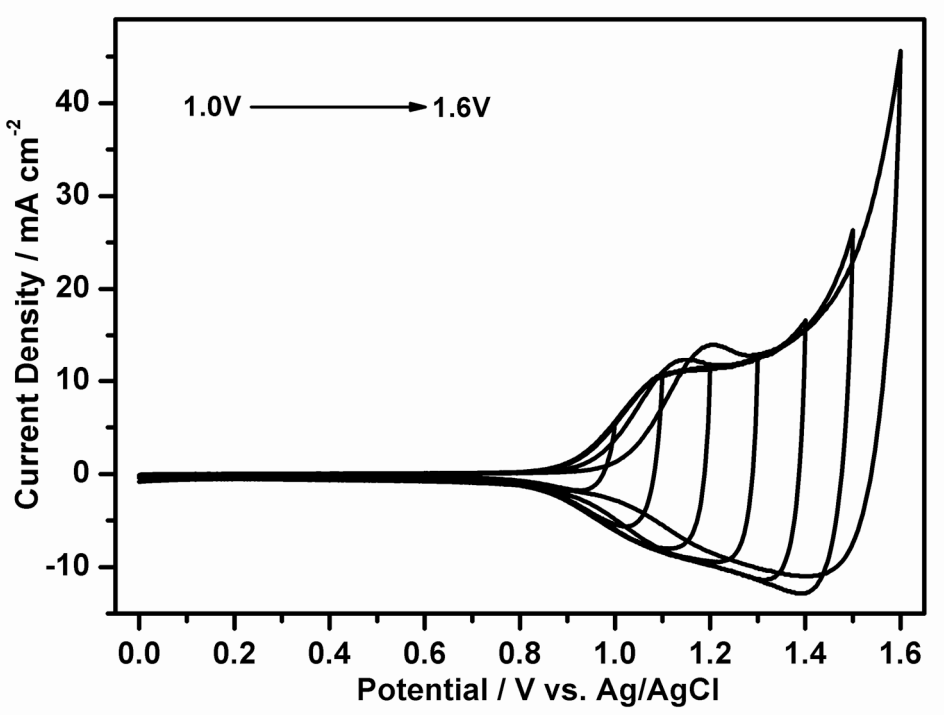

Figure 4.25: Stability test of PTNBTT films to over oxidation by cyclic voltammetry from 0.0V to a) 1.0V, b) 1.1V, c) 1.2V, d) 1.3V, e) 1.4V, f) 1.5V, and g) 1.6V. The polymer was cycled twice at a scan rate of 100mV s^{-1} in each potential, and the last cycle is presented.

Conducting polymers are known to be highly sensitive to overoxidation due to the degradation of their backbone at high potentials. A PTNBTT film has been exposed to a series of potentials above the half wave potential of the polymer by multiple cycling between its neutral (0.0 V) and oxidized forms at different upper potential limits (from +1.0 to +1.6 V). After cycling twice in each potential values, the second cyclic voltammogram was recorded. The results, presented in Figure 4.25, show the stability of PTNBTT to overoxidation without any electroactivity loss up to +1.6 V vs Ag/AgCl. This result shows that the PTNBTT film exhibits electroactivity between 0.9V to 1.5V without any significant deformation in shape of the anodic and cathodic peaks above the half wave potential of the polymer. Moreover, the polymer films have very large capacitive currents at potentials above $E_{1/2}$. Note that these

capacitive currents are very stable and can be an advantage for this polymer's in supercapacitor applications.

4.4.3. Electrochemical Impedance Spectroscopy of TNBTT on CFME

EIS measurements were performed at different applied potentials in the range of 0.2 to 1.5 V with a potential step of 0.1V in parallel to cyclic voltammogram of the PTNBTT in monomer free electrolyte solution (See Figure 4.25) where stability of the film exhibit electroactivity without undergoing deformation.

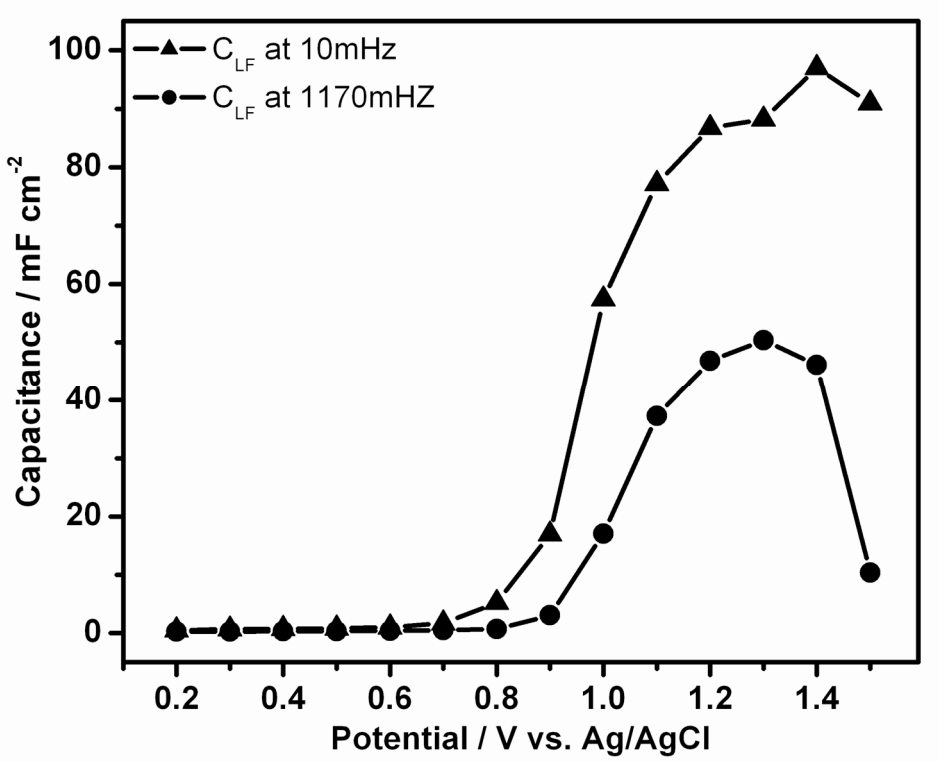

Figure 4.26: Variation of the low frequency capacitance values of the electrochemically polymerized PTNBTT film (Q_{dep}=9.6 C cm^{-2}).

The low frequency capacitance values of the PTNBTT film at 0.01 Hz and 1.170 Hz from impedance spectroscopy were calculated by the equation given in (4.2). The shape of the graph is in good agreement with the corresponding CV of the polymer film in monomer free solution (See Figure 4.24a). As illustrated in Figure 4.26 CFME/PTNBTT/electrolyte system does not show electroactivity in the range of 0 V to 0.8V, current density starts to increase from this point. As shown in the Figure 4.26, we could not observe low frequency capacitance, this system starts to show capacitive behavior starting from the 0.8V, and the maximum value obtained at around 100 mF cm^{-2}. Starting from the 1.4V, capacitance values drops drastically and

show a similar behavior as observed in Figure 4.26. Note that in Figure 4.26 at 1.6V shape of the CV deforms indicating that degradation of the PTNBTT film.

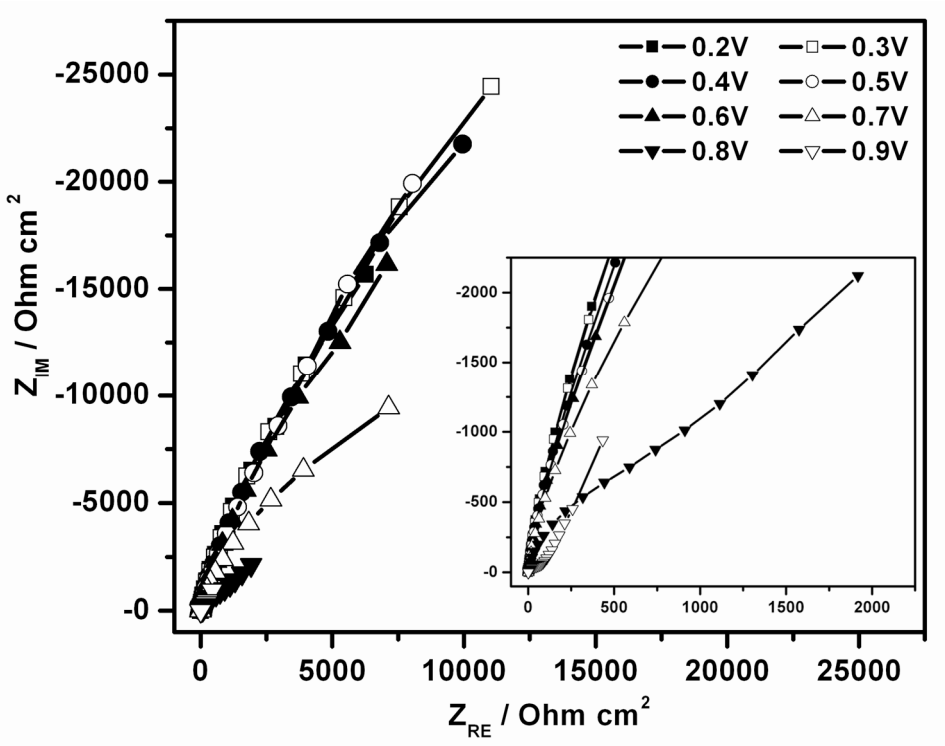

Figure 4.27: (a) Impedance spectra for a PTNBTT film on CFME deposited with a charge of of Q_{dep}= 9.6 C cm^{-2}. Nyquist plots at at (a) 0.9V to 1.2V.

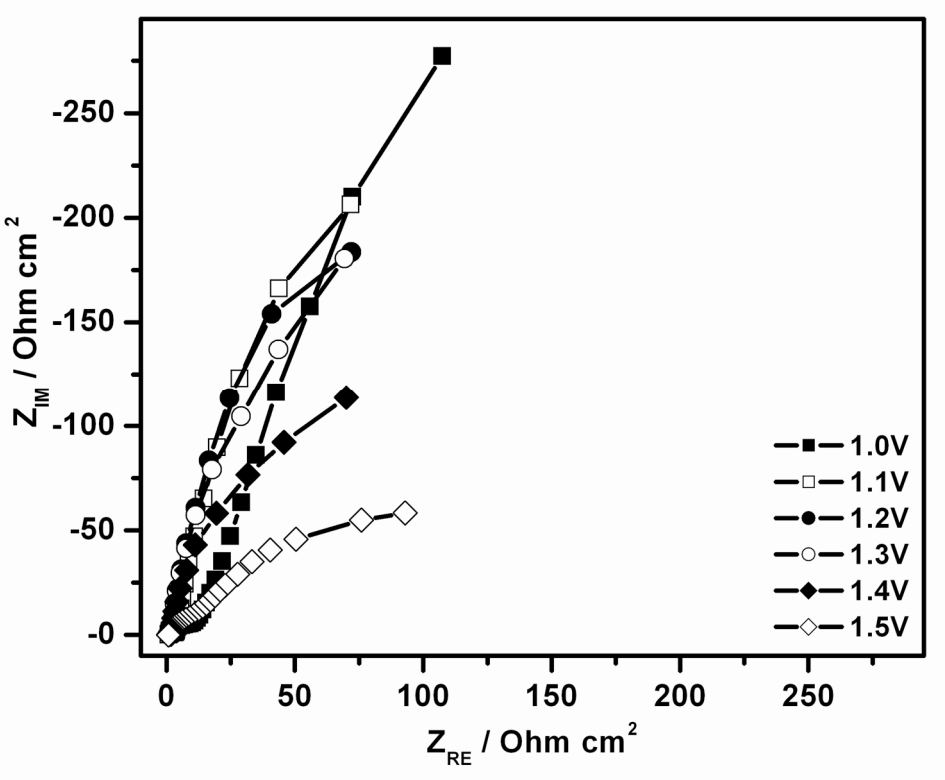

Figure 4.27: (b) Nyquist plots 1.0V to 1.5V.

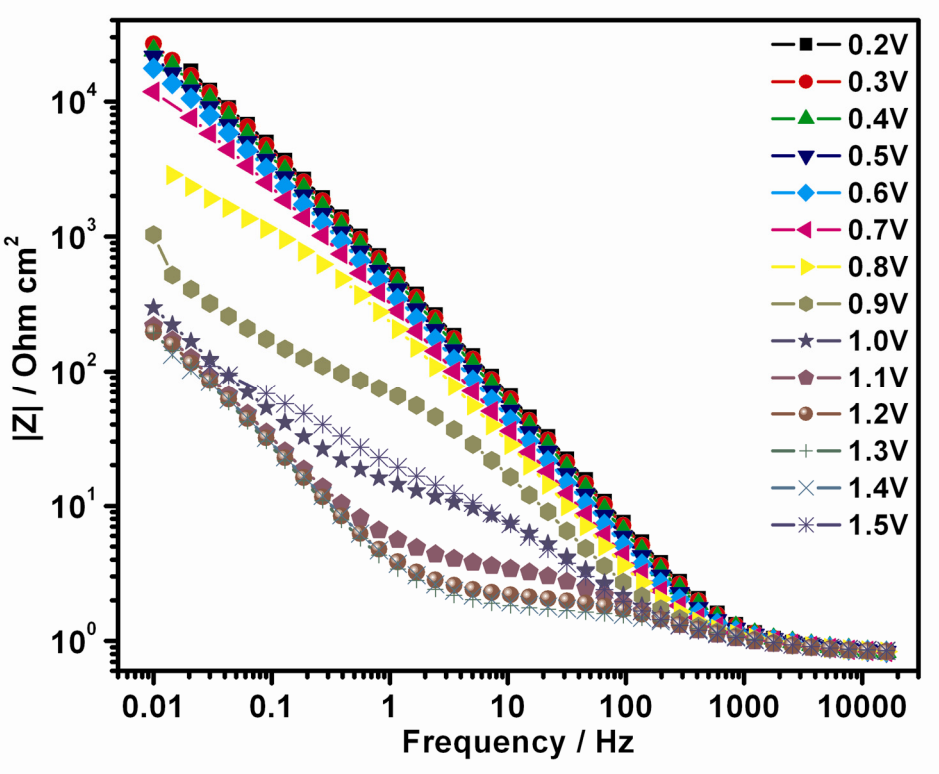

Figure 4.28: a) Bode magnitude |Z| plots at 0.2V to 1.5V for a PTNBTT film on CFME deposited with a charge of Q_{dep}= 9.6 C cm^{-2}.

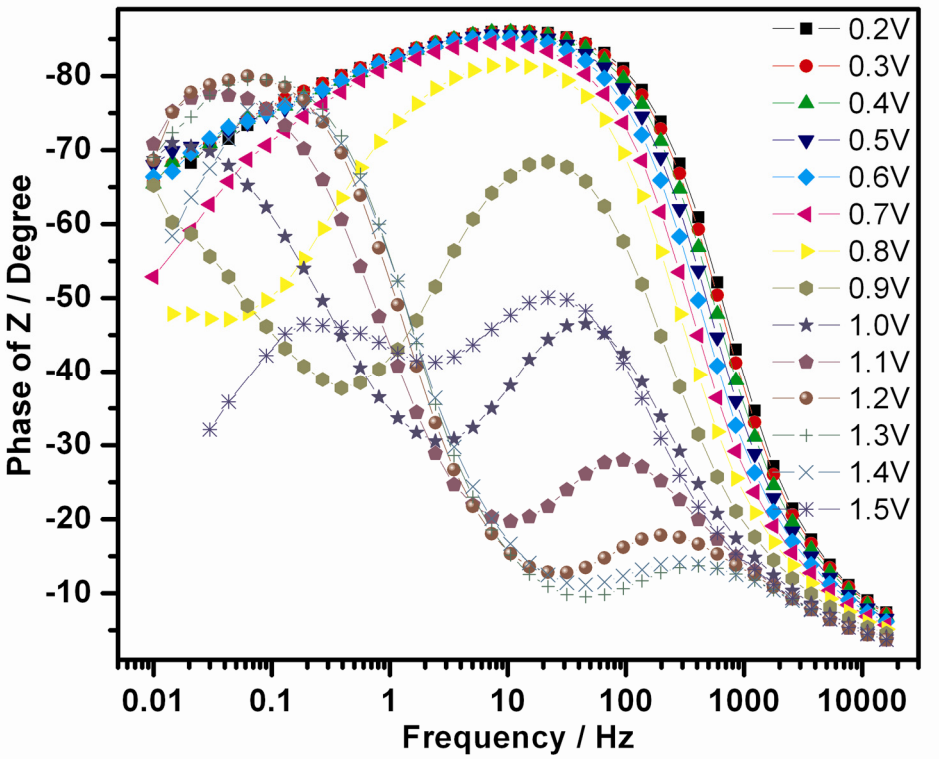

Figure 4.28 (b) Bode-phase angle plots at 0.2V to 1.5V for a PTNBTT film on CFME deposited with a charge of Q_{dep}= 9.6 C cm^{-2}.

Bode phase angle plots of the TNBTT film at different DC potentials are given in Figure 4.28b. We can be separated into three frequency regions namely low, medium and high frequency regions. Low frequency region is from 10 mHz to 1 Hz, in this region at higher potentials (1.1-1.4V) polymer film shows a maximum around 100 mHz with a phase angle of (-80°), starting from this frequency phase angle decreases and drops to (-45°) where electrode behaves in the low frequency region of 100 to 200 mHz at all studied potential values, at lower potentials for instance 0.6 V a new maximum appears around 200 Hz and this maximum decreases by increasing potential and slightly shifts to higher frequencies.

The frequency in which phase angle equal to -45° can be recognized as the frequency response to the ideally capacitive behavior (capacitor response frequency). The frequency of (-45°) phase angle values ranged from 1 to 10 Hz, giving the response time of the capacitor as 1s-100 ms.

Figure 4.27 illustrates Nyquist plots of the PTNBTT film. Figure 4.27a is complex plane impedance plots of the polymer in the range of 0.2V to 0.9V where polymer shows very little almost negligible electroactivity. Values of the imaginary part of very large and capacitance values is very small starting from the 0.9V (See inset Figure in 4.27a) phase angle starts to increase and reaches its maximum value at 1.1V.

Figure 4.28 shows Bode magnitude and phase angle plots in which the frequency dependence of the system is clearer compared to Nyquist plots. In the 0.2V to 0.8V region as the frequency increase from 10 mHz to 1000Hz magnitude of impedance exhibits a very large drop, i.e. from $2x10^4$ to 1 Ohm cm^{-2}, but in the case of higher electrode potentials drop in magnitude is a 200 to 20 Ohm cm^{-2} in a narrow frequency window 10mHz to 10Hz. From these observations we can conclude that the most capacitive potential range in terms of magnitude of the impedance by frequency is 1.1V to 1.4V.

Bode phase angle plots of the TNBTT film at different DC potentials are given in Figure 4.28b. This plot can be separated into three frequency regions namely low, medium and high frequency regions. In the low frequency region which is from 10 mHz to 1Hz, at higher potentials (1.1-1.4V) polymer film shows a maximum around 100 mHz with a phase angle of (-80°). Starting from 100 mHz phase angle decreases

and drops to (-45°) where electrode behaves in the low frequency region of 100 to 200 mHz at all studied potential values, at lower potentials for instance 0.6 V a new maximum appears around 200 Hz and this maximum decreases by increasing potential and slightly shifts to higher frequencies.

The frequency in which phase angle equal to -45° can be recognized as the frequency response to the ideally capacitive behavior (capacitor response frequency). The frequency of (-45°) phase angle values ranged from 1 to 10 Hz, giving the response time of the capacitor as 1s-100 ms.

4.4.4. Electrical Equivalent Circuit for PTNBTT

The validity of the results obtained with EIS was verified using electrical equivalent circuit which is given in Figure 8. The electrochemical parameters of this circuit representing CFME/PTNBTT/electrolyte configuration were evaluated by employing the ZSimpWin (version 3.10) software from Princeton Applied Research. We observed very good agreement between experimental results and the calculated results obtained from the best fitting electrical equivalent circuit model, if the chi-squared (χ^2) minimized below 10^{-4}. χ^2 is the function defined as the sum of the squares of the residuals.

Table 4.7: Potential dependence of the parameters calculated for PTNBTT film from the equivalent circuit which is given in Figure 4.9.

	Potential / V vs. Ag/AgCl					
	E=0.9V	E=1.0V	E=1.1V	E=1.2V	E=1.3V	E=1.4V
R_S / Ohm cm^2	0.820	0.767	0.781	0.816	0.814	0.797
C_{dl} / F cm^{-2}	0.0003	0.0019	0.0031	0.0002	0.0001	0.0066
R_1 / Ohm cm^2	0.1902	4.816	1.125	0.1511	0.0942	0.1566
CPE_1; Y_o/ S s^{-n} cm^{-2}	0.0092	0.0185	0.0461	0.0075	0.0069	0.0353
n	0.7856	0.7807	0.9095	0.6891	0.8000	0.9417
R_2 / Ohm cm^2	575.7	4.25	2260	1.271	0.8479	5.473
C_1 / F cm^{-2}	0.0060	0.1749	0.0043	0.0451	0.0494	0.0107
R_3 / Ohm cm^2	1277	2.3 $x10^{+07}$	211500	0.98	211	200.8
W; Y_o / S $s^{-0.5}$ cm^{-2}	<0.0001	<0.0001	<0.0001	0.0026	0.0044	0.0271
CPE_2; Y_o/ S s^{-n} cm^{-2}	0.0018	0.0469	0.0295	0.1818	0.1685	0.0114
n	0.8995	0.4859	0.5358	0.8392	0.8217	0.6208
R_{CF} / Ohm cm^2	60.27	18.2	2.376	0.4886	0.4328	0.9695
Chi-squared	$3.056x10^{-4}$	$4.197x10^{-5}$	$6.194x10^{-5}$	$9.075x10^{-5}$	$7.303x10^{-5}$	$1.018x10^{-4}$

The electrical equivalent circuit model (see Figure 4.9) which is used previously used to explain impedance behavior of PBTh was successfully applied to the CFME/TNBTT/Electrolyte combination and very good agreement was observed. Table 4.7 shows the simulation results of the electrical equivalent circuit which applied to the experimental data to explain the interaction between the carbon fiber microelectrode, the polymer film and the electrolyte in the potential region of 0.9V to 1.2V. The obtained results showed that the proposed electrical equivalent circuit is good enough to explain behavior of PTNBTT film because in the range of 1.0V to 1.3V, all chi squared values are smaller than 10^{-4}. Complex plane admittance and capacitance plots of the PTNBTT film were given in Appendix Figure D.1 and D.2.

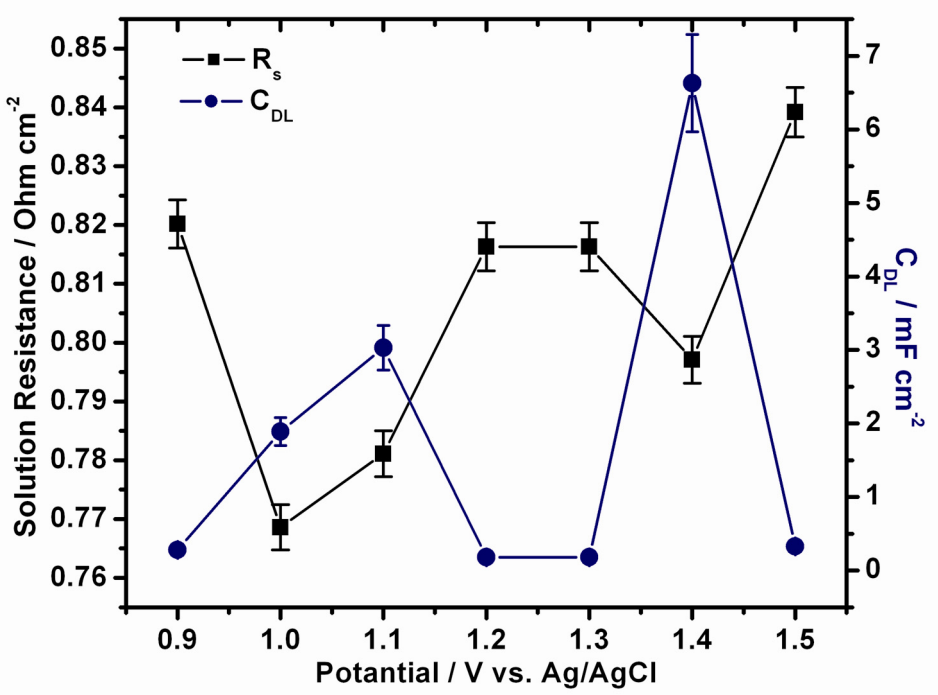

Figure 4.29: Variation of the solution resistance and double layer capacitance of the PTNBTT film with respect to the potential.

Figure 4.29 presents variation of the R_s and C_{DL} with respect to the potential. Variation of the solution resistance and contribution of the double layer capacitance to the specific capacitance of the system is almost negligible.

4.4.5. Morphology of the PTNBTT films on CFME

Morphology of the three films was investigated using FE-SEM. These films were deposited from 0.005 M solution of the TNBTT by cyclic voltammetry at a scan rate of 20mV s^{-1} with a different charge of 5.5 C cm^{-2}, 7.3 C cm^{-2} and 13.8 C cm^{-2}, Figure 4.30 (a), (b) and (c) respectively onto carbon fiber electrodes. After electrodeposition

of the PTNBTT striations of the original carbon fiber are not completely covered with the polymer indicting that the obtained electrode is a kind of composite electrode of CFME and PTNBTT. This also explains why we could not obtain high capacitance values for polymers deposited low number of cycles in other words low deposition charges.

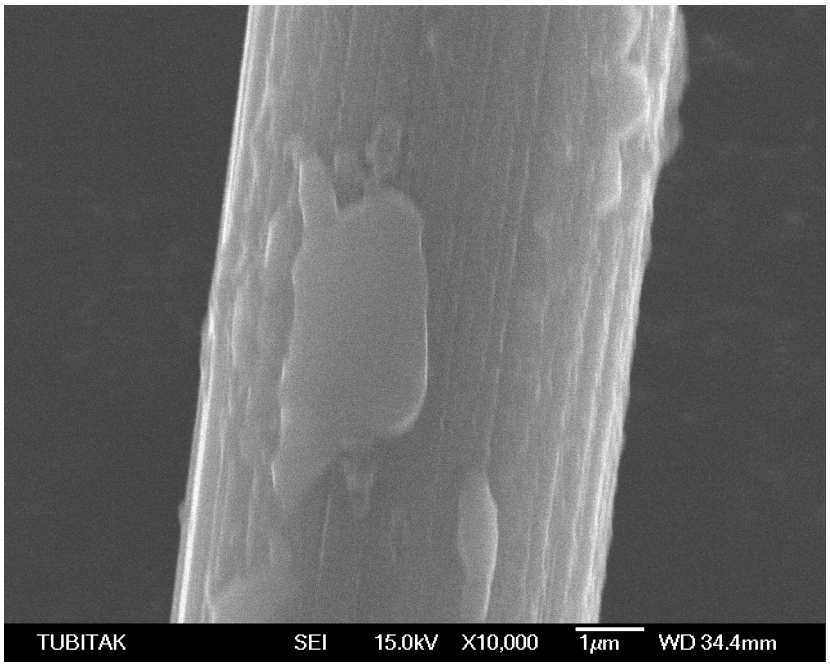

Figure 4.30: (a) FE-SEM image of a PTNBTT film deposited by cyclic voltammetry with a charge of 5.5 C cm^{-2} and 4 cycles.

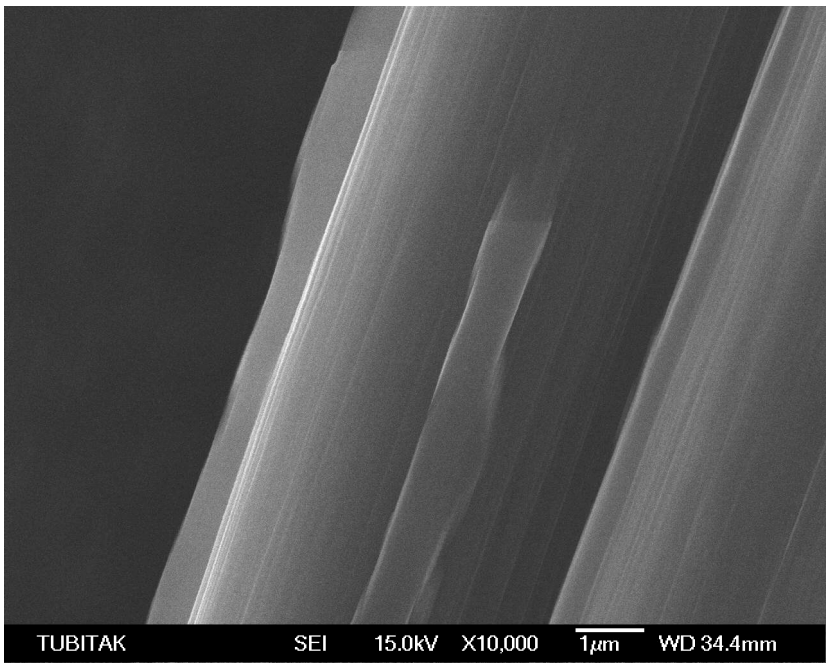

Figure 4.30: (b) FE-SEM image of a PTNBTT film deposited by cyclic voltammetry with a charge of 7.3 C cm^{-2} and 4 cycles.

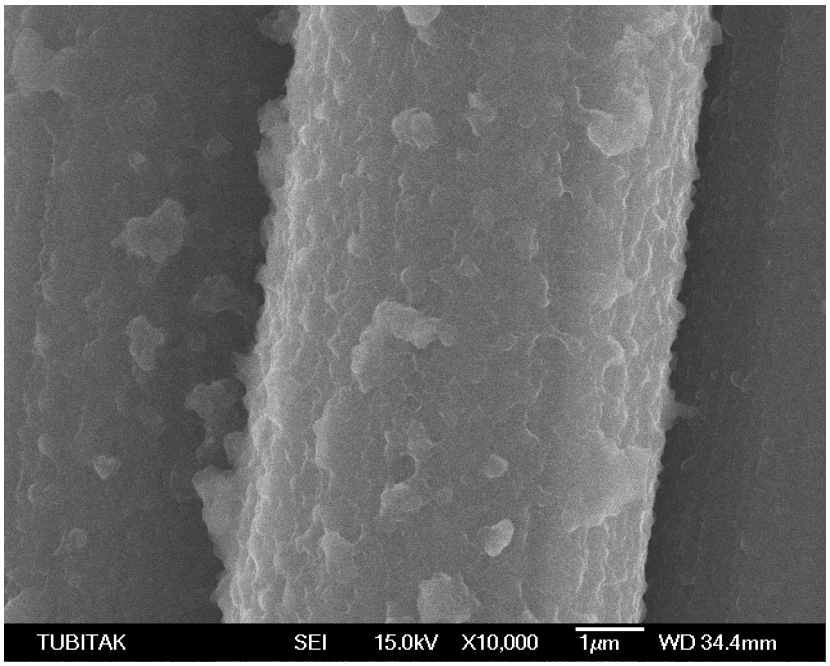

Figure 4.30: (c) FE-SEM image of a PTNBTT film deposited by cyclic voltammetry with a charge of 13.8 C cm^{-2} and 8 cycles.

Figure 4.30a and 4.30b are examples of the polymer electrodes which exhibits very low capacitance (Results are not given). At higher deposition currents very good deposition of PTNBTT was observed which indicates that surface of the electrode was completely covered by PTNBTT. Average thickness of the film was calculated as 0.15 micrometers.

4.5. Synthesis and Electrochemical Characterization of ENBTE Comonomer

4.5.1. Synthesis of The Bis(3,4-ethylene-dioxythiophene)-(4,4'-dinonyl-2,2'-bithiazole) Comonomer

Synthesis of the ENBTE comonomer and their bromine and trimethylstannyl derivatives are similar to the procedures previously described for first three steps as in the synthesis of TNBTT comonomer that is explained in the previous section. Only fourth and the fifth steps explained in here.

4.5.1.1. Synthesis of 2-trimethylstannyl-3,4-ethylenedioxythiophene

A 100 mL Schlenk flask was placed a 6.39 g (45 mmol) EDOT in THF (50 mL, dry) and the mixture was cooled to -78°C. A solution of (16.8 mL, 42 mmol) of 2.5 M n-buthyllithium was added into the mixture under nitrogen and the mixture was stirred

at -78°C for one hour and 8.78 g (45 mmol) of trimethylstannylchloride (in 40 mL THF) was added dropwise and the mixture was allowed to warm to ambient temperature with stirring overnight. Water (30 mL) was added followed by ether (50 mL). The phases were separated and organic phase was dried with $MgSO_4$ and evaporated to dryness to give the product as an oily brown solid. (75 % yield).

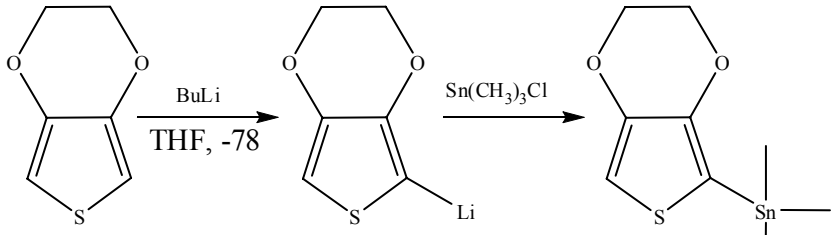

(4.14)

2-trimethylstannyl-3,4-ethylenedioxythiophene **(4)**

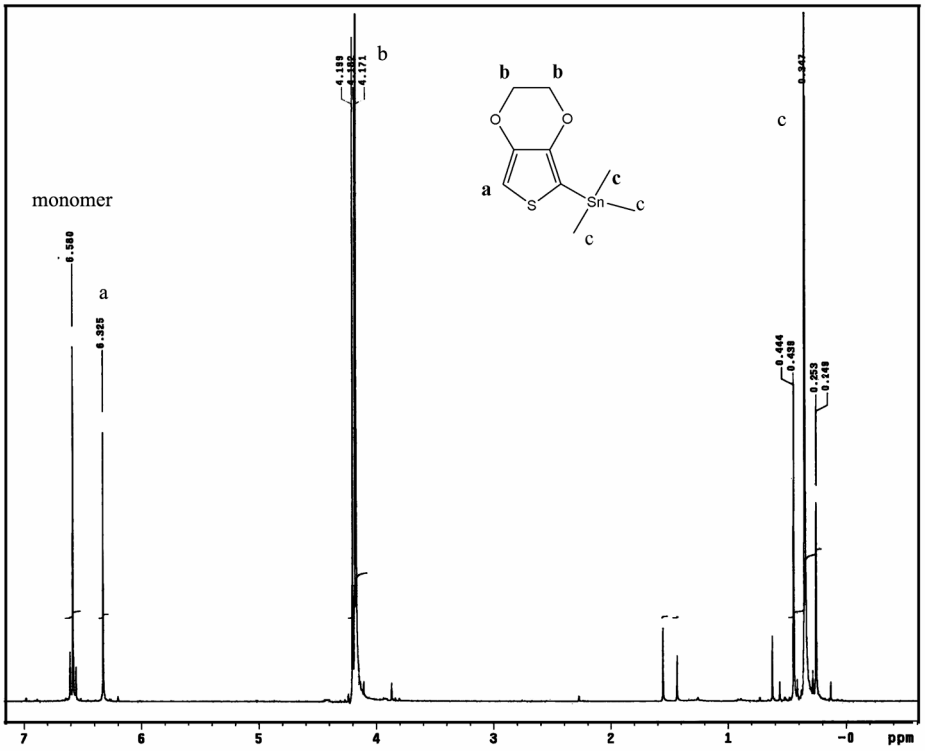

Figure 4.31: ^{1}H-NMR of the bromononylbithiazole in $CDCl_3$. a) δ 6.32 ppm (1H), b) δ 4.17 - 4.19 ppm (t, 4H), c) δ 0.44 – 0.25 ppm (m, 9H). The triplet at δ 6.58 ppm might be attributed to the proton of the monomer.

4.5.1.2. Synthesis of EDOT-NBT-EDOT

In the first three steps, thiazole moiety of the ENBTE comonomer was synthesized as a similar procedure described by Nanos [16]. A long alkyl chain was integrated to four position of the thiazole ring via 2-bromoundecanone with the hope of increasing

the regioregularity of polymeric films after electropolymerizations and 4,4'-dinonyl-2,2'-bithiazole was brominated. At the final step the palladium-catalysed cross coupling reaction were performed to attach electron donating EDOT rings to obtain a mixed donor-acceptor-donor type comonomer based on EDOT ring due to success of the EDOT derivatives. The raw product was further purified by crystallization and orange colored solid obtained in 65 % yield and was characterized by ^{1}H-NMR see Figure 4.32. The ENBTE comonomer is soluble in DCM and insoluble of scarcely soluble in the other organic solvents tested.

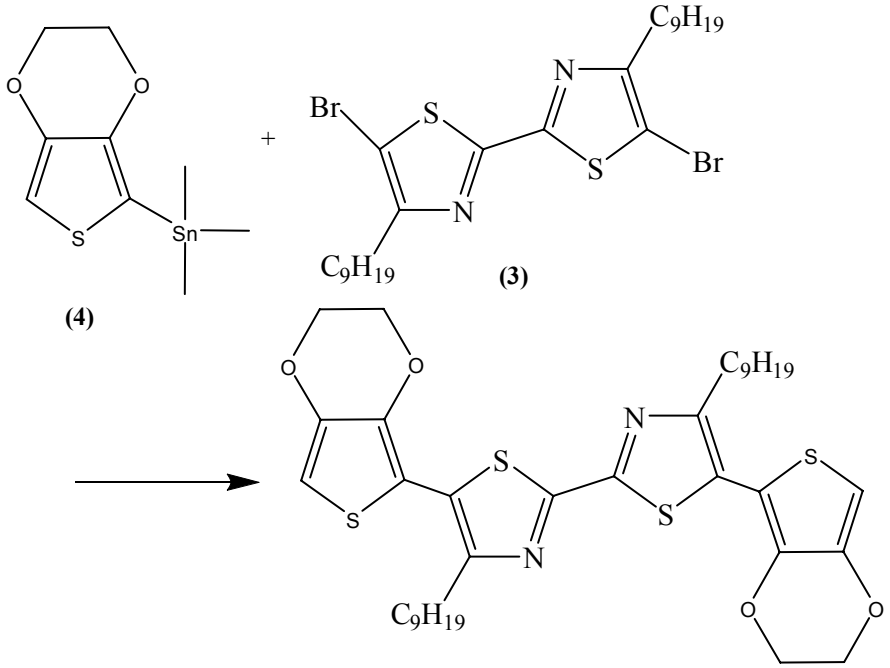

(4.15)

In a 100 mL Schlenk flask equipped with a condenser and nitrogen, was charged with ~60 mL of THF (dry), 0.6099 g (2 mmol) of Br-NBT-Br, 0.5785 g (1 mmol) of EDOT-$SnMe_3$ and 35.3 mg (0.05 mmol) of Pd(II) catalyst ($Pd(PPh_3)_2Cl_2$). The mixture was refluxed for 20 h. After cooling to room temperature the reaction mixture was poured into water, and dichloromethane, pentane and chloroform were added. Extracted organic phase was washed with water and dried over $MgSO_4$ and the solvent evaporated. The final product was re-crystallized in ethanol. ^{1}H-NMR spectrum of the final product is given in Figure 4.32. Yield=65 %.

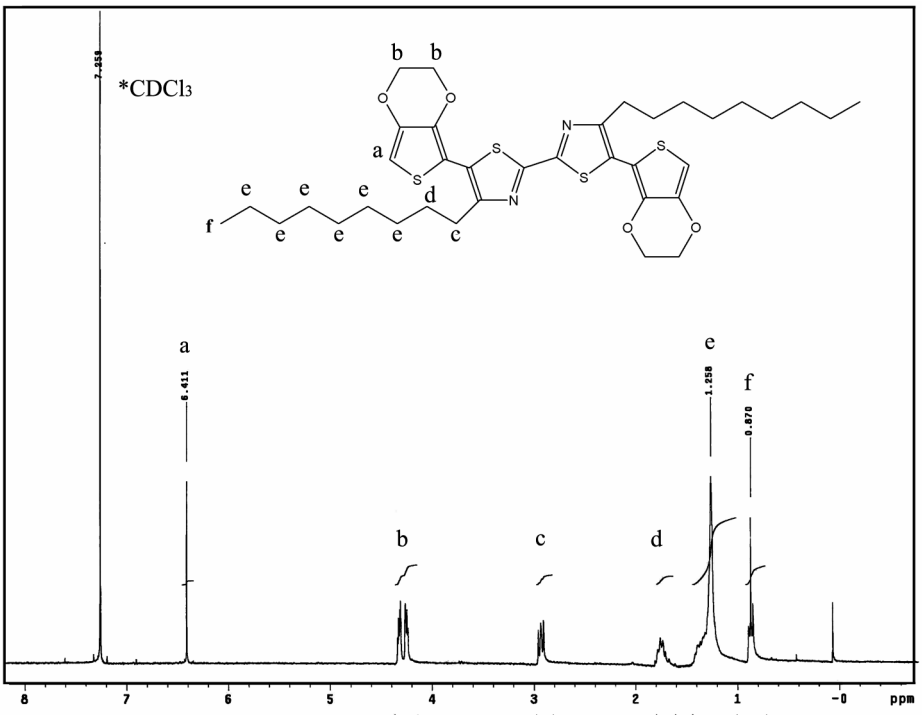

Figure 4.32: ^{1}H-NMR of the ENBTE in $CDCl_3$. a) δ 6.41 ppm (s, 2H), b) δ 4.33 - 4.25 ppm (m, 8H), c) δ 2.91 – 2.93 ppm (t, 4H), d) δ 1.80 - 1.70 ppm (m, 4H), e) δ 1.54 -1.29 ppm (m, 24H), f) δ 0.89 – 0.85 ppm (t, 6H).

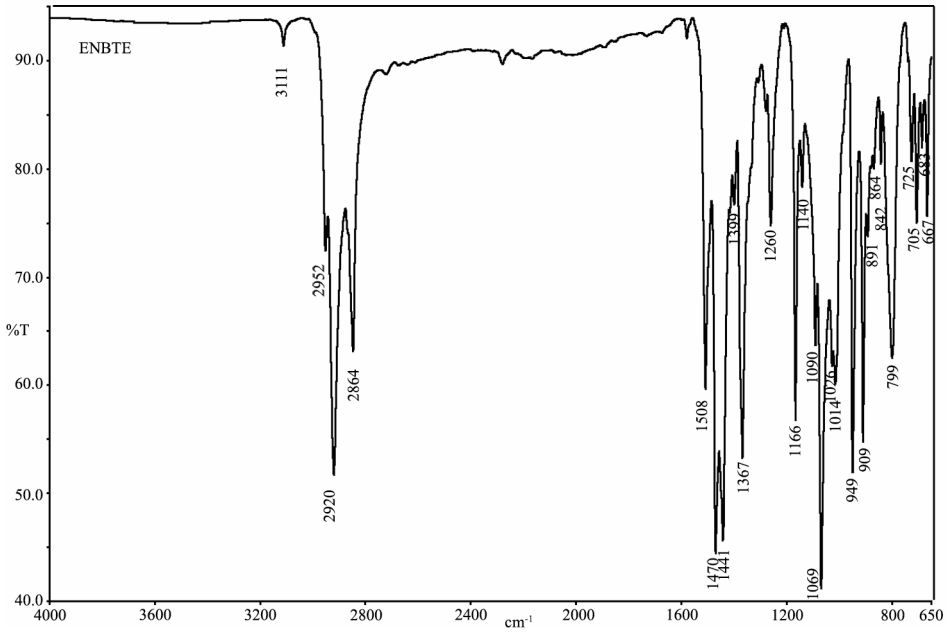

Figure 4.33: ATR-FTIR spectrum of the ENBTE monomer.

4.5.1.3. ATR-FTIR Characterization of ENBTE

ATR-FTIR spectrum was recorded for the ENBTE monomer using a Perkin-Elmer Spectrum One ATR-FTIR spectrometer in the frequency range 4000-650 cm-1. FTIR measurement was made using solid ENBTE powder. The ATR-FTIR spectra of the ENBTE was recorded at room temperature and at laboratory humidity conditions is

presented together in Figure 4.33. The frequencies of the major absorption peaks are also listed in Table 4.6. Assignments of these frequencies have been done based upon literature tables [149, 150].

Table 4.8: ATR-FTIR absorption bands and peak assignment table for the ENBTE monomer. **vs**; very strong, **s**; strong, **m**; medium, **w**; weak

Peak / cm^{-1}	Fragment	Intensity / Comment
2952	$R-CH_3$	**m** / $-C-H$ stretching vibration- asymmetric
2920	$R-CH_3$	**vs** / $-C-H$ stretching vibration- asymmetric
2864	$R-CH_3$	**s** / $-C-H$ stretching vibration- symmetric
1470	$-CH_2-$	**m** / $-C-H$ scissor vibration
1441	$R-CH_3$	**vs** / $-C-H$ deformation vibration- asymmetric
1367	$R-CH_3$	**s** / $-C-H$ deformation vibration- symmetric
1367	Alkyl Chain	**s** / $-C-H$ deformation vibration
1166	Alkyl Chain	**s** / $-C-C-$ stretching vibration
1140	Alkyl Chain	**w** / $-C-C-$ rocking vibration
799	Alkyl Chain	**s** / $-C-C-$ skeletal vibration
725	Alkyl Chain	**m** / $-C-C-$ skeleton rocking vibration
3111	Thiazole	**w** / $=C-N-C-$ stretching vibration
1508	Thiazole	**m** / $-C=N$ stretching and in-plane vibration
1508	Thiazole	**m** / $-C=C-$ in-plane vibration
1399	Thiazole	**w** / C=C and C=N in-plane vibration
1367	Thiazole	**s** / ring vibration
1260	Thiazole	**m** / $-C-N-$ stretching vibration
1470	$-O-CH_2-$	**vs** / $-CH_2-$ symmetric deformation vibration
1441	$-O-CH_2-$	**vs** / $-C-H$ asymmetric deformation vibration
1069	$-O-CH_2-$	**vs** / $-C-O-$ stretching vibration asymmetric
1026	$-O-CH_2-$	**m** / $-C-H$ deformation vibration
1026	$-O-CH_2-$	**m** / $-C-O-$ stretching vibration symmetric
1014	$-S-$	**s** / $-C-S-$ stretching vibration
842	$-S-$	**s** / $-C-S-$ stretching vibration
705	$-S-$	**s** / $-C-S-$ stretching vibration

We observed fairly intense absorption peaks belong to four component, i.e., long alkyl chain, thiazole, thiophene and 1,4-dioxin moieties of the EDOT, of the ENBTE comonomer. The peaks populated between 2850 and 2960 are associated to nonyl-chain. It may be seen that these peaks appear together and with another peak for example symmetric deformation vibration peak belong to 1,4-dioxin moiety appear

at around 1470 cm^{-1}. ATR-FTIR of the EDOT is given in Appendix Figure A.2 as a reference.

The absorption in the region of 1508 cm^{-1} is ascribed to thiazole ring i.e. that is stretching and in-plane vibration of the $-C=N$ and in-plane vibration of the $-C=C-$ fractions of the thiazole ring. See Table 4.8 for the systematic peak assignments.

4.5.2. Electropolymerization of ENBTE

Oxidative electropolymerization of ENBTE was carried out in DCM with 0.1 Et_4NBF_4 as electrolyte. Figure 4.34 shows the first 12 scans for the anodic electropolymerization by Cyclic Voltammetry (CV) at 20 mV s^{-1} of a 0.001M solution of ENBTE onto a CFME (area ~0.001 cm^2). The irreversible oxidation of the monomer appears clearly on the first cycle at 0.954 V versus Ag/AgCl.

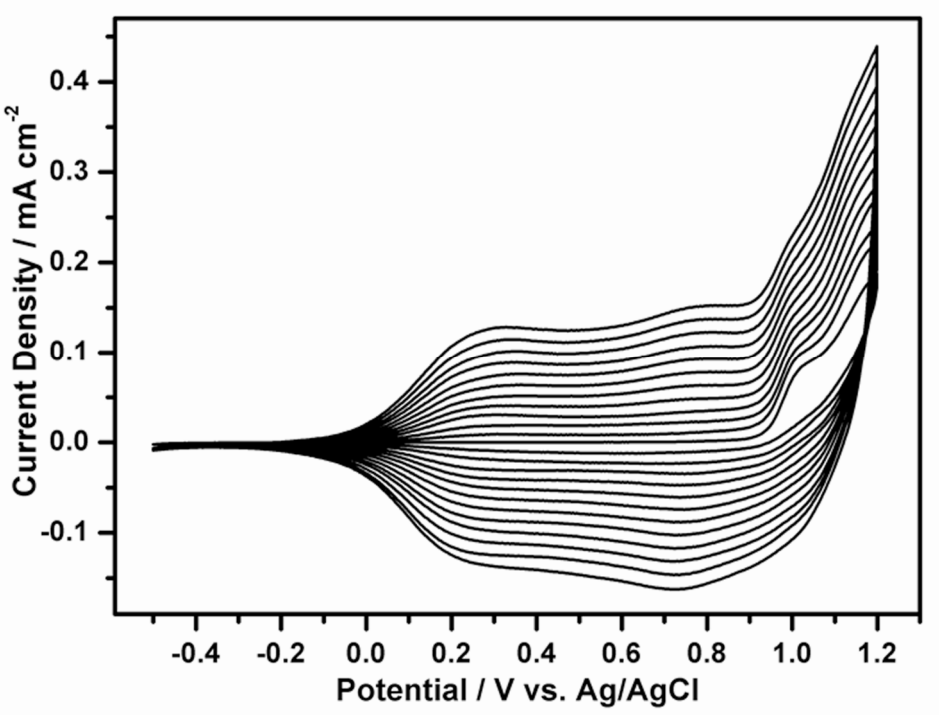

Figure 4.34: Electrodeposition of ENBTE by potentiodynamic deposition from a 0.001M solution of monomer in 0.1 M Et_4NBF_4/DCM at 20 mV s^{-1} onto CFME (area ~0.001 cm^2).

The polymeric films of PENBTE were deposited by CV over 4 cycles onto CFME (area≈0.001cm^2) from 0.001 M solution of monomer in 0.1 M Et_4NBF_4/DCM electrolyte. Investigation of the polymer films in monomer-free electrolyte solution for their redox switching showed a double well-defined redox process.

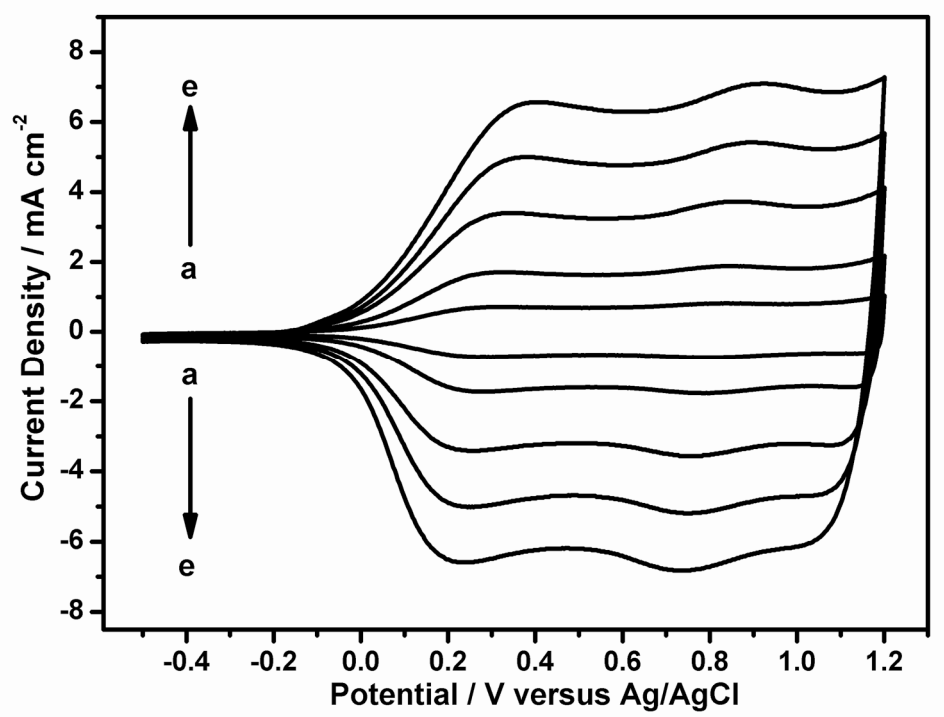

Figure 4.35: (a) Cyclic voltammogram of a PENBTE film in a monomer free solution of 0.1M Et_4NBF_4/DCM at scan rates of a) 20 mV s^{-1}, b) 50 mV s^{-1}, c) 100 mV s^{-1}, d) 150 mV s^{-1}, e) 200 mV s^{-1}.

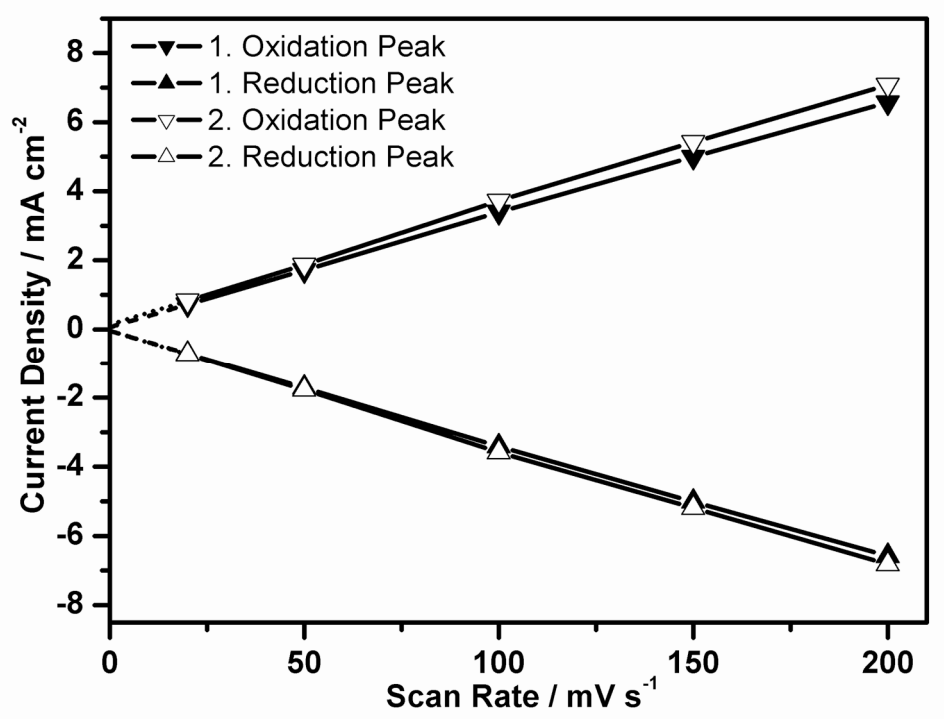

Figure 4.35: (b) Scan rate dependence graph of the voltammogram given in Figure 4.35a. (First oxidation ▼ and reduction ▲ peaks, and second oxidation ∇ and reduction Δ peaks.)

Figure 4.35 shows the cyclic voltammogram of this polymer film at scan rates of 20, 50, 100, 150, and 200 mV s^{-1} in 0.1 M Et_4NBF_4/DCM. It is significant that the polymer exhibits very well defined and reversible redox processes.

The half-wave oxidation potentials of the polymer ($E_{1/2}$) was observed at 0.303 V and 0.814 V versus Ag/AgCl ($E_{ox1/p}$=0.354 V, $E_{ox2/p}$=0.867 V and $E_{red1/p}$=0.254 V, $E_{red2/p}$=0.761 V versus Ag/AgCl) at the scan rate of 100 mV s^{-1}.

The current response of the film was directly proportional to the scan rate, indicating that the polymer film is electroactive and very well adhered to the electrode. The scan rate dependence of the peak currents of the both anodic and cathodic peaks shows a linear dependence, for the first oxidation peak correlation coefficient (r) is 0.9999 and for reduction of the same peak r is calculated as 0.9999, for the second oxidation peak same behavior was observed with a linear correlation of r=0.9998 and reduction of the same peak is r=0.9997, as a function of the scan rate (see Figure 4.35b). The extrapolated lines pass through the origin indicate that there is no constant term in the linear correlation.

Shape of the CV of a PENBTE film on CFME in a monomer free solution, (see Figure 4.35a), in the form of a rectangle which is the behavior of an ideal double layer capacitance as suggested in literature[32]. Electrochemical impedance studies were used to consider the low frequency capacitance properties of the ENBTE polymer electrode and it is found that complex plane impedance plot of PENBTE yields slope as high as 90° at low frequencies. These preliminary studies suggested the idea that PENBTE coated CFMEs is a good candidate as active electrode material in supercapacitors.

Figure 4.36a shows a CV of the PENBTE in 0.1 M Bu_4NPF_6/DCM solution. Sweep was started from an initial potential of -0.35V, and at 1.2V the anodic scan was reversed the final potential at cathodic scanning was -1.72V, at a scan rate of 100 mV/s versus Ag/AgCl. The PENBTE film exhibited two oxidation peaks (or p-doping) peak at 0.36 and 0.88 V versus Ag/AgCl and a reduction (or n-doping) peak at -1.67 V versus Ag/AgCl in a 0.1 M Bu_4NPF_6/DCM solution, and the peaks were coupled with p-dedoping and n-dedoping peaks at 0.35 V and 0.86 V and -1.48 V versus Ag/AgCl, respectively.

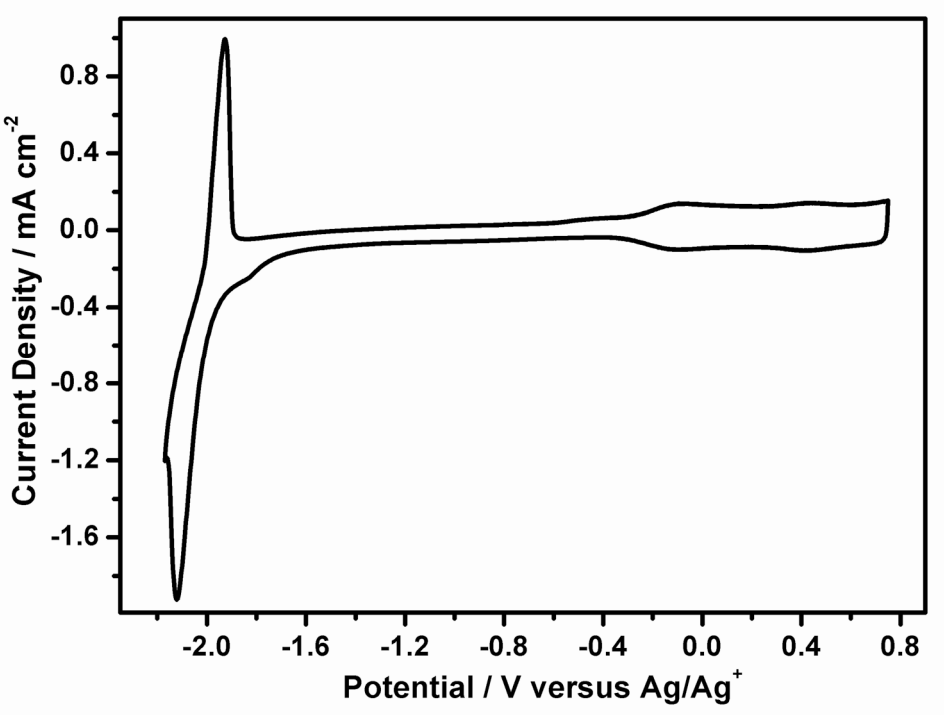

Figure 4.36: (a) Cyclic voltammetry (second scan) of the PENBTE on a Pt wire electrode in 0.1 M Bu_4NPF_6/DCM at a scan rate of 100 mV/s from -0.35V to 1.20V to -1.72V versus Ag/AgCl,

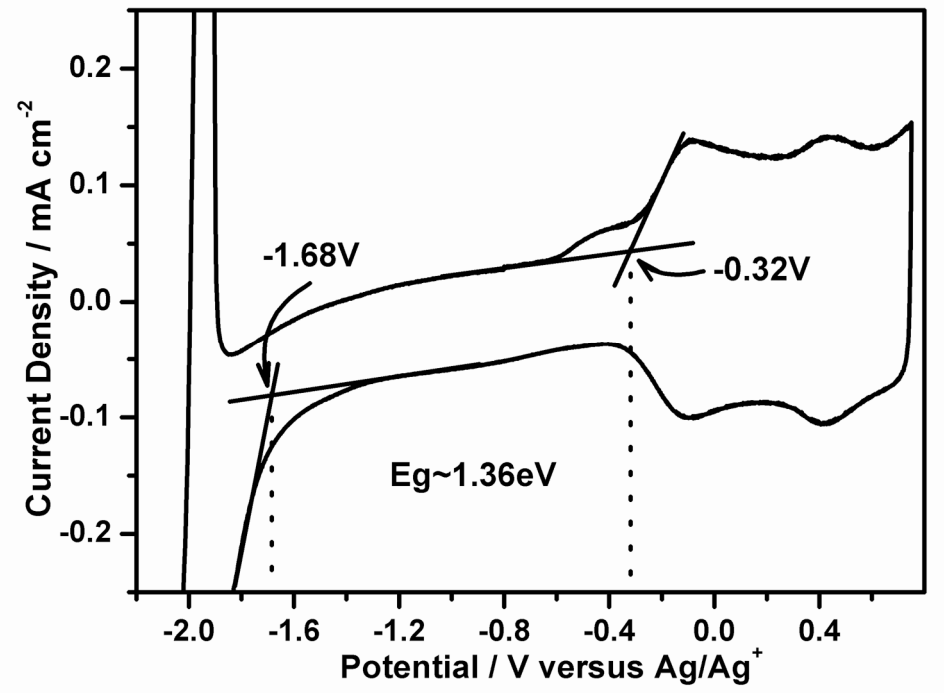

Figure 4.36: (b) calculation of band gap from CV shown in Figure 4.36a.

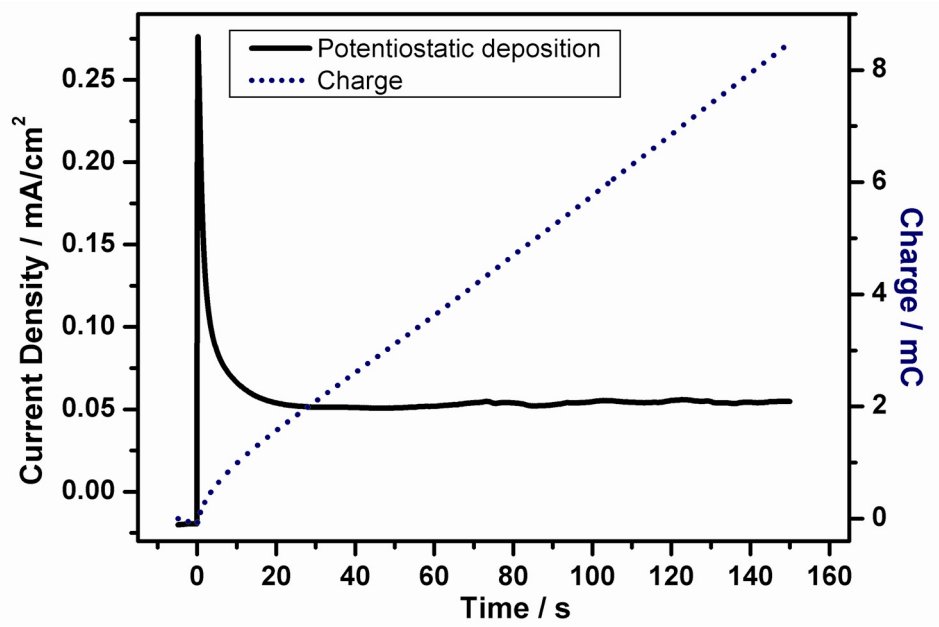

Figure 4.37: Potentiostatically deposition of ENBTE comonomer onto ITO electrode Y axis on the right shows charge and on the left current density.

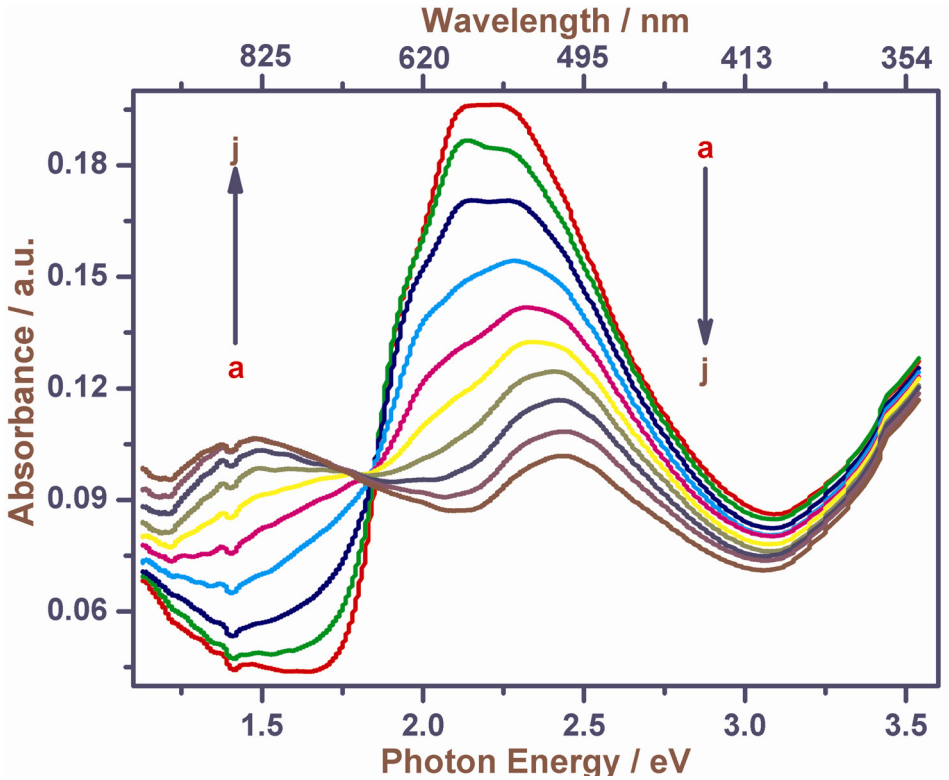

Figure 4.38: *In-situ* spectroelectrochemistry in 0.1M Et_4NBF_4/DCM for PENBTE potentiostatically deposited at 1.1V vs Ag/AgCl on a ITO coated glass slide, (a) -400 mV (b) 0 mV (c) 100 mV (d) 200 mV (e) 300 mV (f) 400 mV (g) 500 mV (h) 600 mV (i) 700 mV, and (j) 800 mV potentials are referenced against Ag/AgCl. And corresponding colors of the polymer film at -400 mV and 800 mV were given in Figure 4.40.

These results support the structure of the polymer having both the electron-donating EDOT unit and the electron-accepting thiazole unit. The n-doping peak was larger than the p-doping peak, since p-doping proceeds only with the thiazole unit and n-doping can proceed not only in the thiazole unit but also in the EDOT as previously explained [161]. From the potential difference between the onset of the p-doping and that of the main n-doping peak (see Figure 4.36b), the band gap of PENBTE is determined at about 1.36 eV, which is lower as expected that of calculated from the UV-Vis absorption band of PENBTE (1.75 eV).

4.5.3. Spectroelectrochemistry of PENBTE

Spectroelectrochemistry of PENBTE films were studied on the potentiodynamically deposited (Figure 4.37) ITO-coated glass slides, as shown in Figure 4.38.

At an applied potential of -0.40 V (vs Ag/AgCl), at which the polymer is in its fully neutral form, the onset for the π to π^* transition (Eg) is 1.75 eV with a λ_{max} at 2.15 eV. Relative to other polymers of this type, this transition is narrow and distinct with a difference between the onset for the π to π^* transition and λ_{max} of only 0.4 eV. This is attributed to the efficient polymerization process of the ENBTE monomer and is suggestive of a regular, defect-free structure.

4.5.4. Differential Pulse Voltammetry (DPV) of PENBTE

The Eg value for the PENBTE obtained by spectroelectrochemistry (UV-vis) and CV was verified by DPV analysis. Differential-pulse voltammetry of PENBTE was carried out in 0.1 M monomer-free electrolyte solution. Polymer was grown potentiodynamicallay on CFME, rinsed in 0.1M Et_4NBF_4/DCM. DPV shows onset potentials of n- and p- doping at -0.970 V and 0.140 V respectively (see Figure 4.39). The E_g of the polymer calculated from the difference of these onset potentials is ~1.1 eV.

The different Eg values estimated from the three approaches, i.e., spectroelectrochemical measurements, cyclic voltammetry and differential pulse voltammetry, Figure 4.39b, ITO coated glass slide electrode, platinum electrode and carbon fiber microelectrodes were used for the polymer deposition respectively, would be expected to lead to significantly different that might be due to substrate, structure of the deposited film and measurement method.

4.5.5. Switching Properties of PENBTE

The experiments, carried out by spectroelectrochemical methods, have demonstrated the ability of PENBTE to switch between its neutral and doped states (i.e. coloring/bleaching process of the PENBTE) with a significant change in transmittance at 555 nm. To investigate the switching time of these polymers and the stability of their electrochromic changes, double potential pulse switching experiments were performed between -0.4 and +0.80V vs Ag/AgCl. The polymer were switched 5 second step time between the absorbing, neutral state and the transmissive, oxidized state as shown in Figure 4.40. The polymer exhibited effectively fast switching time since the time between coloration and bleaching processes (see Figure 4.41a) was less than 0.25 s, Figure 4.41b shows an expanded spot of the Figure 4.41a at tenth seconds dotted line represent 90% of the full switch. The observed net result is that PENBTE yields a homogeneous and high quality film overall and favorably stable of its optical properties offering fast switching time.

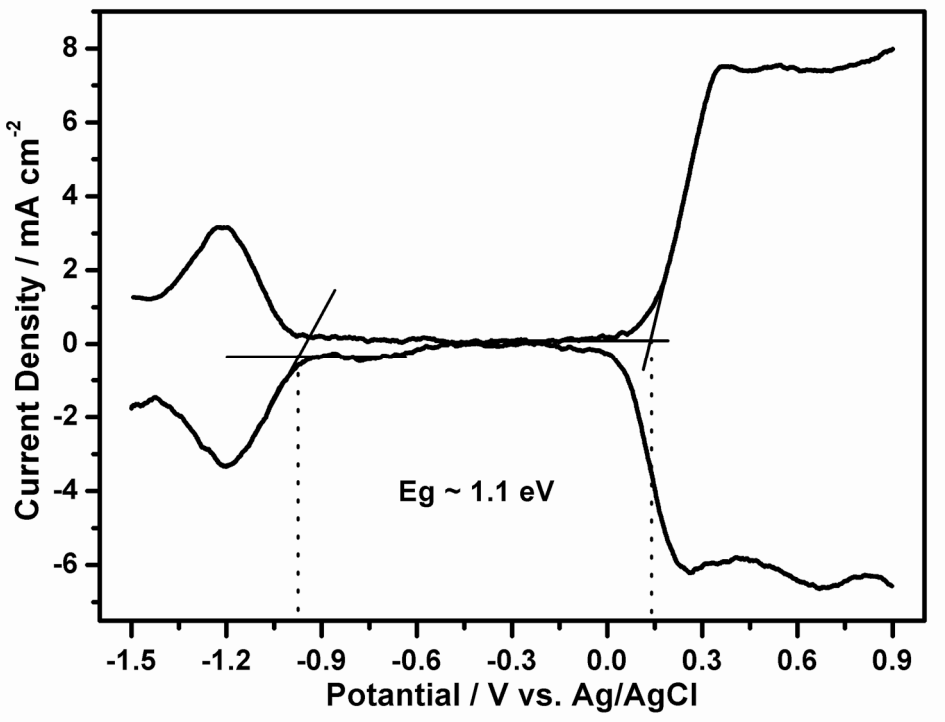

Figure 4.39: (a) Differential-pulse voltammetry of PENBTE in 0.1 M monomer-free electrolyte solution. Polymer was grown potentiodynamically on CFME, rinsed in 0.1M Et_4NBF_4/DCM,

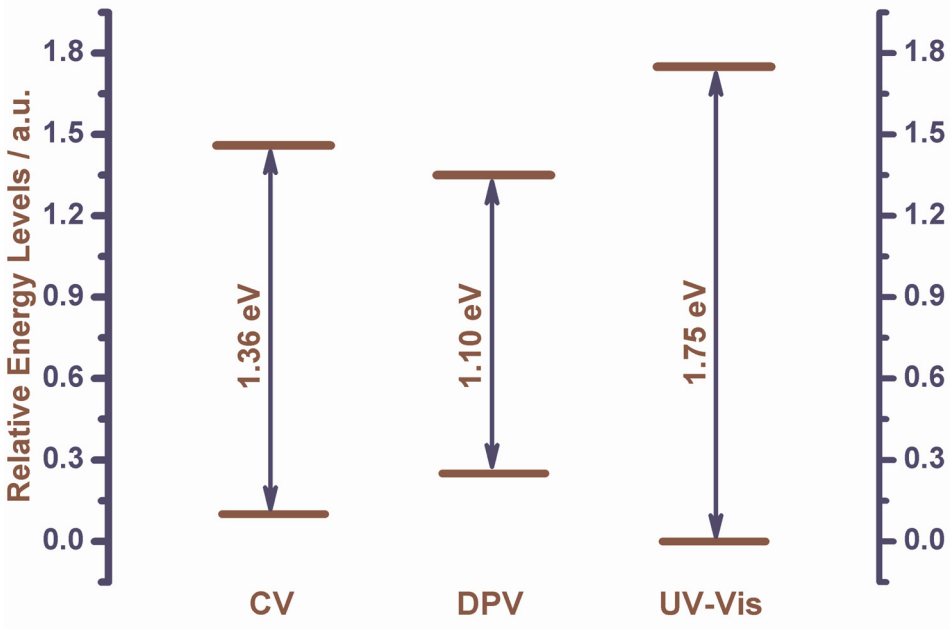

Figure 4.39: (b) Comparison of the different Eg values obtained from the three approaches.

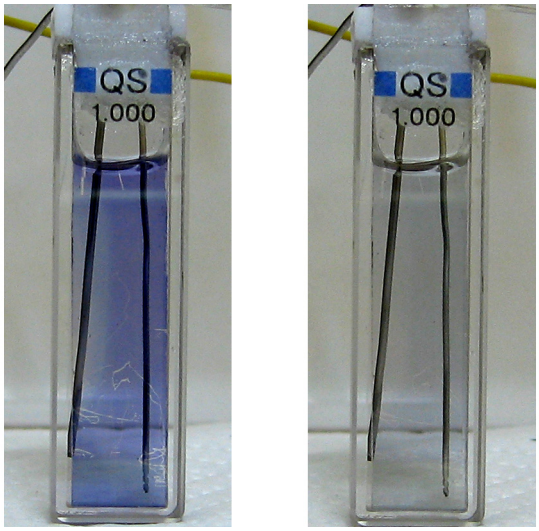

Figure 4.40: A PENBTE film on an ITO coated glass slide electrode reduced at -0.4 V (colored), and oxidized at 0.8 V (bleached) vs. Ag/AgCl.

Figure 4.42a and 4.42b shows chronocoulometry and chronoamperometry plots obtained during the switching measurements confirms the stability and the quality of the prepared film there is loss in the charges and peak values of the current densities almost equal.

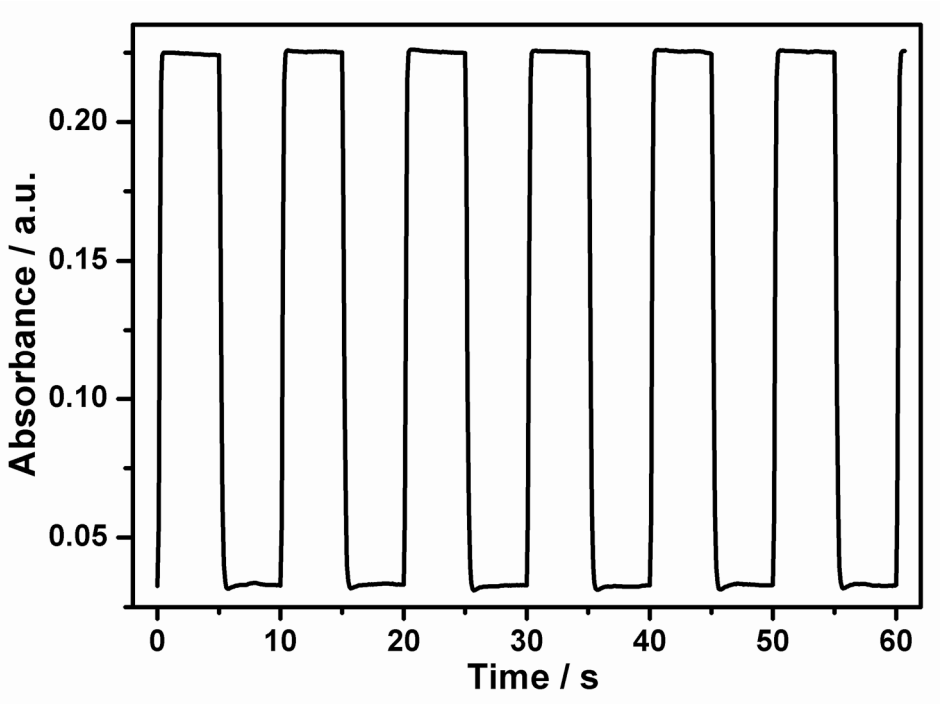

Figure 4.41: (a) Chronoabsorptometry of PENBTE monitored at 555nm the full coloration and bleaching occurs upon polymer oxidation from -0.4 to +0.8 V vs Ag/AgCl in a monomer free solution of 0.1M Et_4NBF_4/DCM only the first six double pulses for chronoabsorptometry of a total 1000 switches that were taken are shown.

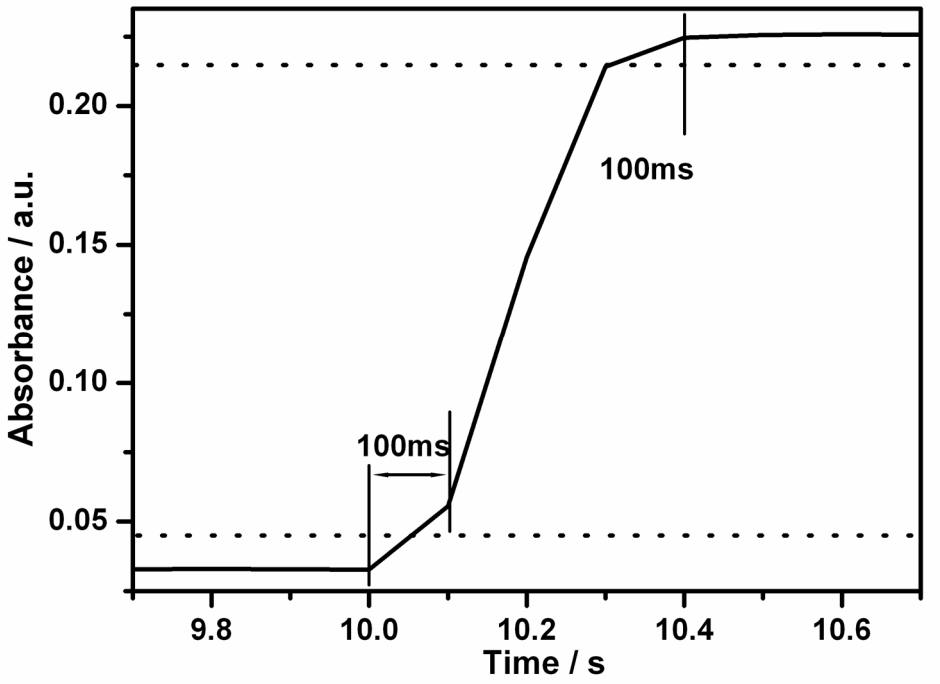

Figure 4.41: (b) An expanded spot of the Figure 4.41a at tenth seconds

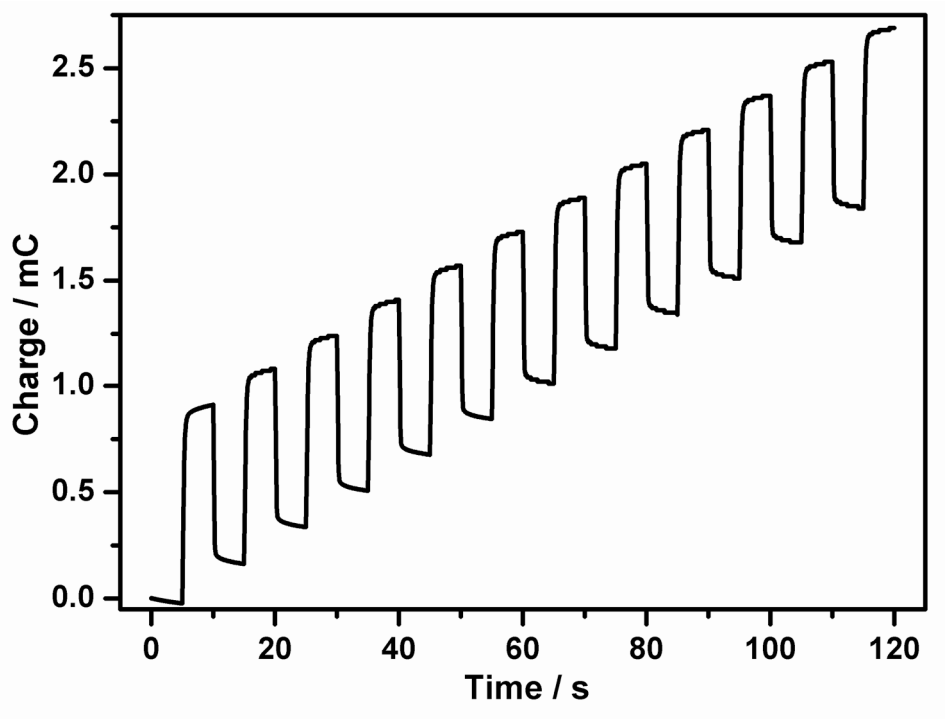

Figure 4.42: (a) Chronocoulometry plot of the PENBTE film which is measured during the switching experiment. The first twelve double pulses of a total 1000 switches that were taken are shown.

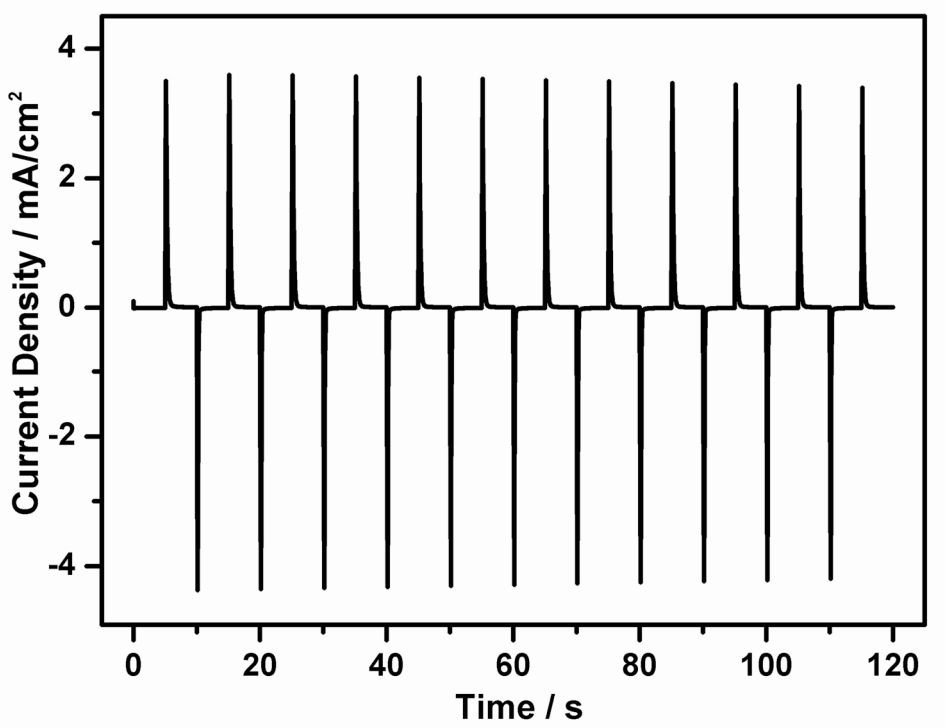

Figure 4.42: (b) Chronoamperometry plot of the same measurement which is given in Figure 4.42b.

4.5.6. Morphological Study

The morphology of the PENBTE films obtained by electropolymerization with increasing number of deposition cycle were analyzed using FE-SEM. Pictures of the obtained PENBTE films are presented in Figure 4.43. We observed that the thickness of the polymer film is a function of number of cycles and increases linearly with the number of deposition cycle during the electrosynthesis as expected. The original carbon fiber exhibits striations along the fiber axis which are typical for PAN-based carbon fibers. As shown in Figure 4.43 (a), the striations barely seen after deposition four cycles of PENBTE, however at this number of deposition cycle homogeneous coating was observed, and the polymer was deposited as a continuous and very well adhering film to the fiber surfaces. Further increase in the number of deposition cycle, e.g. eight cycles, led to thicker and the most homogeneous, tight and smooth coatings, and the striations were also disappeared with this number of deposition cycle, (see Figure 4.43b). With a twelve cycle of deposition, (see Figure 4.43c), the polymer coating deposited on the CFME similarly exhibited homogeneous and uniformly distributed polymer globules along the carbon fiber. Such structures have formed by grafting of growing polymer molecules on the fiber surface. In a higher magnification of a spot of the film, (see Figure 9d), clearly shows that surface of the polymer coating quite smooth and has an even thickness. See Appendix Figure B.3 and Figure B.4 for further SEM images.

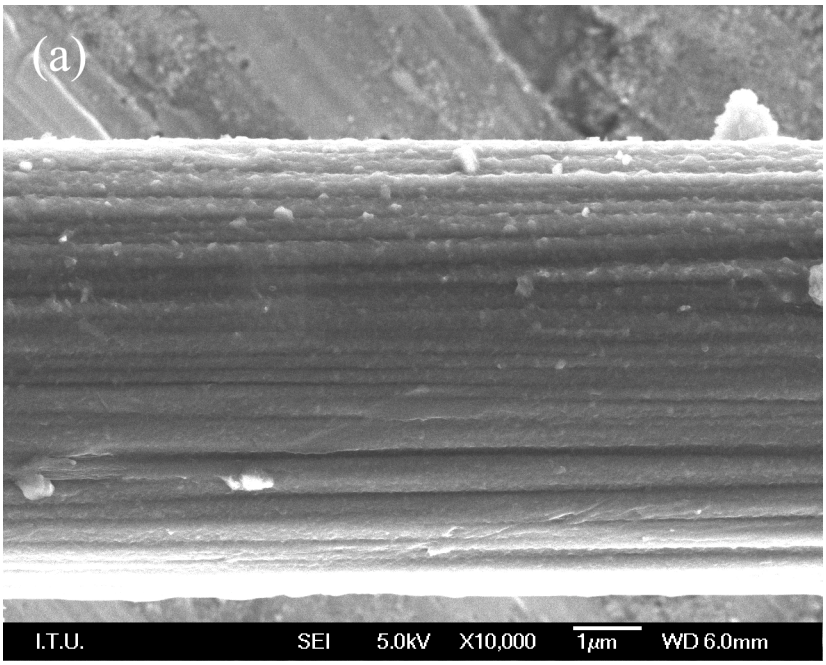

Figure 4.43: (a) FE-SEM images of the PENBTE films obtained by electropolymerization with increasing number of deposition cycle from a 0.001M solution of ENBTE in 0.1 M Et_4NBF_4/DCM at 20 mV s^{-1}, **(a)** 4 cycles deposition at x10000 magnifications.

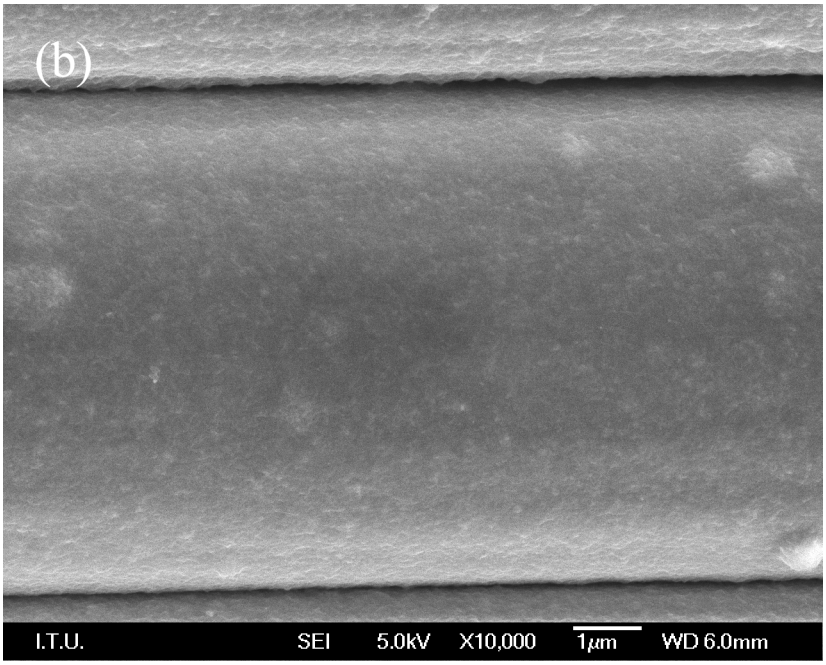

Figure 4,43: (b) 8 cycles deposition at x10000 magnifications.

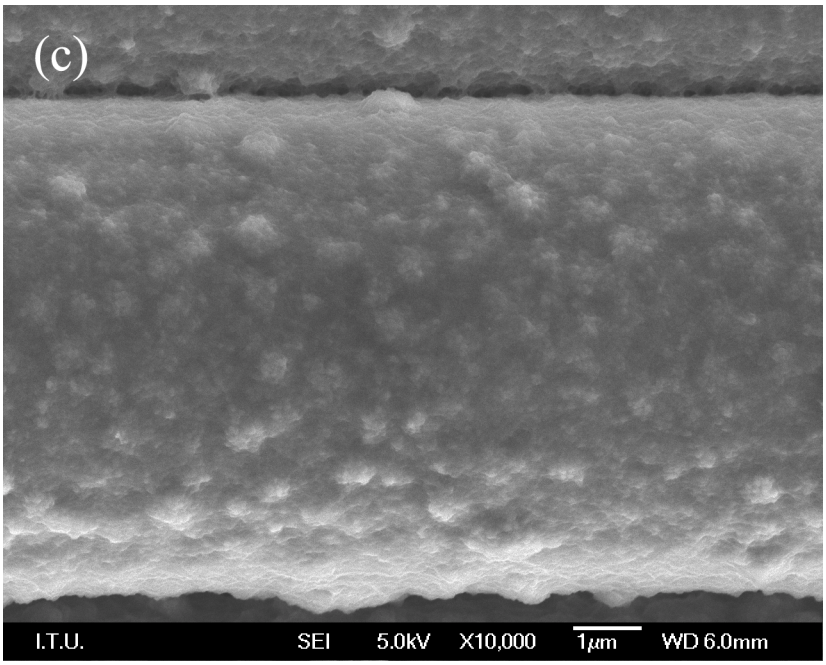

Figure 4.43: (c) 12 cycles deposition at x10000 magnifications.

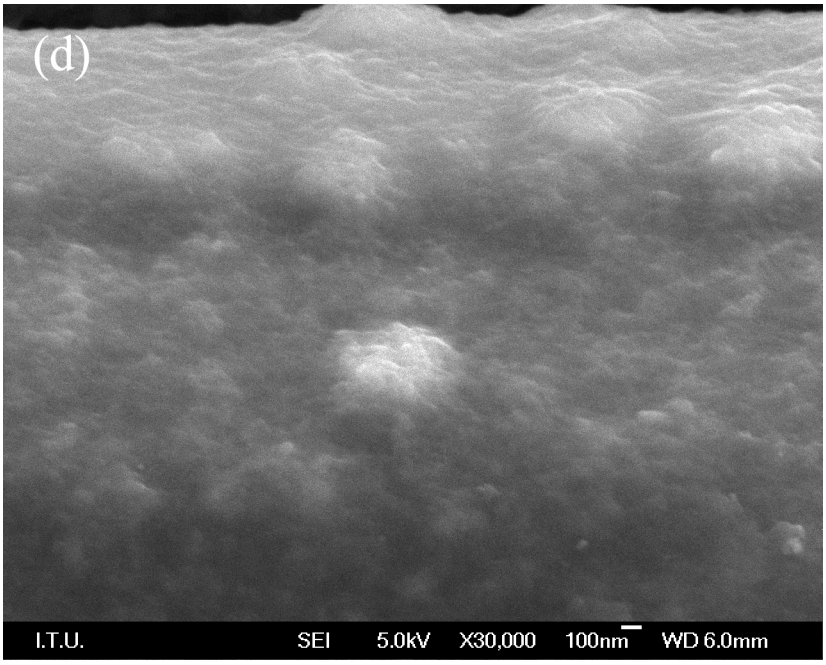

Figure 4.43: (d) A high magnification spot on the film which is shown in (b) at x30000 magnifications.

4.6. EIS Investigation of ENBTE as an Active Electrode Material for Supercapacitor Applications

Supercapacitors [32, 33] can be classified into two types the double-layer which store the energy within the electrochemical double-layer at the electrode-electrolyte interface and the redox supercapacitors. For redox supercapacitors, among several

types of electrode materials employing of conducting polymers has received much attention due to their use in both aqueous and organic electrolytes and their wide potential working range [34-37].

The electrochemical impedance spectroscopy (EIS) is one of the most effective and the reliable method to extract information about electrochemical characteristics of the electrochemical system for instance double-layer capacitance, diffusion impedance, determination of the rate of the charge transfer and charge transport processes, solution resistance etc. [38, 39]. EIS was used to explain behavior of the polymer coated electrodes by established theories employing two models which are known as uniform [40-44] and porous medium [2, 45-47].

Conducting polymers, such as, polypyrrole, polyaniline, polythiophene, and their derivatives, were reported as electrode materials for supercapacitors. [12, 162-165] Among the conducting polymers poly(3,4-ethylenedioxythiophene) (PEDOT) has been much more investigated due to its good electrochemical properties and unusual thermal stability in the oxidized state [7, 8], conductivity and stability of PEDOT makes it useful as a conducting electrode in electrochemical supercapacitors [12, 165, 166]. The poly(alkylbithiazoles) exhibit interesting thermochromic and electrochemical behavior [15-22] especially nonyl derivative shows unusual optical properties as a result of its crystallinity and π-π stacking behavior. The π-stacking of thiazole rings between neighboring chains and increased planarity along the backbone causes well ordered polymer films [16, 18, 19, 23, 24].

Carbon based materials are popular for the electrochemical applications, as an electrode material, carbon has several advantages compared to other electrode materials, i.e. well polarization of the electrode, high surface area, processability, low cost, accessibility, thermal and chemical stability [32, 33]. Porous carbon is the most frequently selected electrode material which offer large surface area and very good polarization due to porosity which makes porous carbon is one of the most promising electrode material for supercapacitors applications [32, 152-154].

Carbon fibers have unique properties such as high strength, high modulus and low density. The surface properties of carbon fibers were studied recently and modification of carbon fiber surfaces by electropolymerizing 3-methyl-thiophene [25], ter-thiophene [26], pyrrole, 3,4-ethylene-dioxythiophene (EDOT) and their

copolymers [27] onto the fibers have investigated in detail. EDOT-Ethylcarbazole-EDOT was electrochemically coated onto carbon fiber microelectrodes and very stable films were obtained at high potentials [31].

In this part of the study, an impedance study of a novel donor acceptor donor type comonomer [158] which is created combining a well known p-type electron donating EDOT monomer and an n-type electron accepting nonylbithaizole monomer on carbon fiber microelectrode was performed. We have investigated the electrochemical characteristics of PENBTE on carbon fiber microelectrode (CFME) in an electrolyte solution of tetraethylammonium tetrafluoroborate (Et_4NBF_4) in dicholoromethane (DCM) as an active electrode material for electrochemical capacitor applications.

4.6.1. Electropolymerizations of ENBTE onto CFME

Oxidative electropolymerization of ENBTE was carried out either potentiodynamically between -0.5V and 1.2V vs. Ag/AgCl or galvanostatically (See Figure 4.44a) at a constant current of 10 mA cm^{-2} in DCM with 0.1 Et_4NBF_4 as electrolyte. Figure 4.44b shows the cyclic voltammogram (CV) of the polymer film which is deposited by the anodic electropolymerization by cyclic voltammetry at 20 mV s^{-1} of a 0.001M solution of ENBTE onto a CFME (area ~ 0.001 cm^2) at scan rates from 20 mV s^{-1} to 200 mV s^{-1} in 0.1 M Et_4NBF_4/DCM. Typical CV of the polymeric film exhibits a double very well-defined and reversible redox processes as shown in Figure 4.44b. The current response of the film was directly proportional to the scan rate indicating a diffusion limited process , showing that the polymer film is electroactive from 0.1 V to 1.2 V and sufficiently well to ensure a rapid film charging and discharging.

Capacitive behavior of the CFME/PENBTE film was firstly noticed from CV experiments which exhibits a rectangular shape in a monomer free solution, (see Figure 4.44b). The rectangular shape of the CV is expected for an ideal double layer capacitance behavior [32]. Figure 4.45 shows the variation of specific capacitance (C_{CV}) values calculated from CV with respect to potential and the scan rate of the CFME/PENBTE/electrolyte system which is given in Figure 4.45b. Capacitance values from CV were calculated applying the equation $C_{CV} = j / v$ (where j is the current density and v is the scan rate) to the current density values obtained from the

oxidation and reduction peaks[167]. Dependency of the C_{CV} on the film thickness (i.e. polymerization charge) will be discussed later.

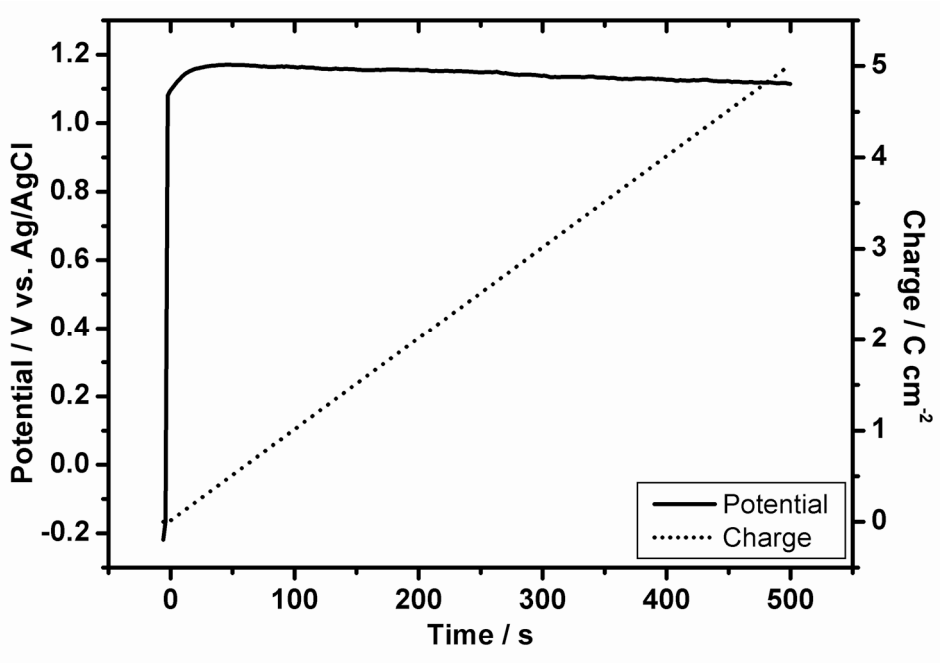

Figure 4.44: (a) Galvanostatic deposition of a PENBTE film at 10 mA cm^{-2}.

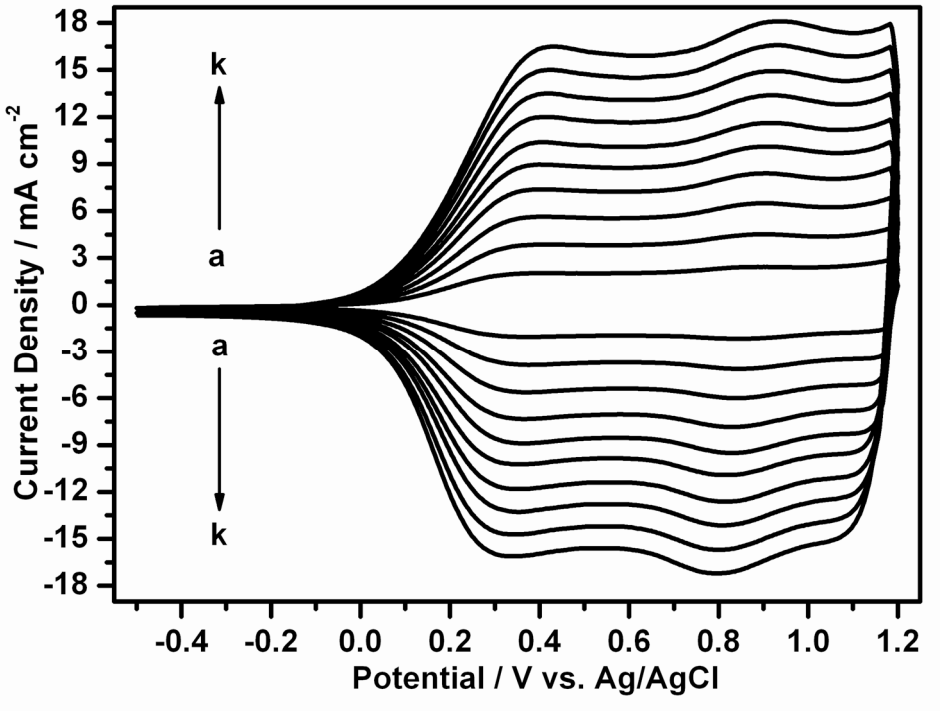

Figure 4.44: (b) Cyclic voltammogram of a PENBTE film (Deposited from 1mM ENBTE in 0.1 M Et_4NBF_4/DCM solution at a scan rate of 20mV s^{-1}; Q_{dep}=731.7mC) in a monomer free solution of 0.1M Et_4NBF_4/DCM at scan rates of a) 20, b) 40, c) 60, d) 80, e) 100, f) 120, g) 140, h) 160, i) 180, and k) 200 mV s^{-1}.

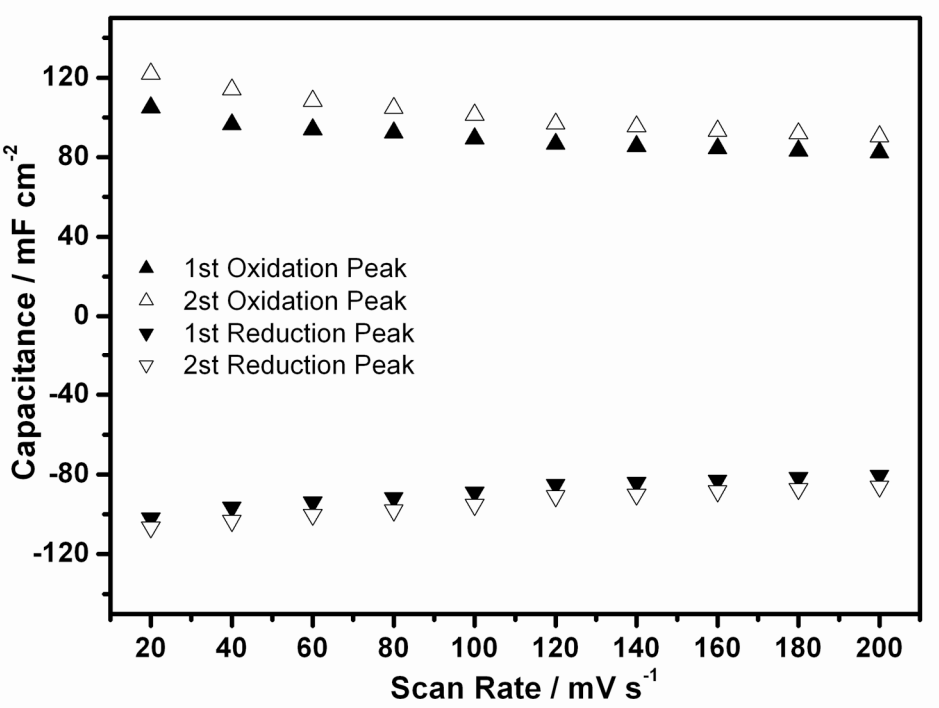

Figure 4.45: Variation of the capacitance (C_{CV}) values by scan rate capacitance values were calculated from oxidation and reduction peak current densities of the CFME/PENBTE/electrolyte system which is given in Figure 4.44.

As expected voltammetric capacitance values obtained for the CFME/PENBTE film was directly proportional to the scan rate. The scan rate dependence of the capacitance values shows a linear dependence, for example at 0.3V correlation coefficient (r) of the positive capacitance is 0.997 and negative capacitance at the same DC potential is calculated as 0.999 as a function of the scan rate. Dependency of the C_{CV} on the film thickness (i.e. polymerization charge) will be discussed later.

4.6.2. EIS Studies on PENBTE Films on CFMEs

EIS measurements were performed at different applied potentials in the range of -0.5 to 1.2 V with a potential step of 0.1V to cover entire polymerization range of the ENBTE comonomer.

The low frequency capacitance values of the polymer electrode from impedance spectroscopy were obtained from the slope of a plot of the imaginary component (Z_{IM}) of the impedance at low frequencies, versus inverse of the reciprocal frequency (f) using following equation [151].

$$C_{LF} = (2\pi f Z_{IM})^{-1} \qquad \textbf{(1)}$$

Figure 4.46 illustrates the variation in the specific capacitance values of galvanostatically deposited (Q_{dep}=5 C cm^{-2}) on PENBTE film at 0.01 Hz and 1.170 Hz at DC potentials between -0.5V and 1.2V. The shape of the plot has a very good agreement with the corresponding CV of the polymer film in monomer free solution. Capacitance values have two peaks at 0.4V and 0.8V. These two maximum points converge very well those of two oxidation peaks observed in CV of the PENBTE film at 0.4V and 0.9V for 100 mV s^{-1}.

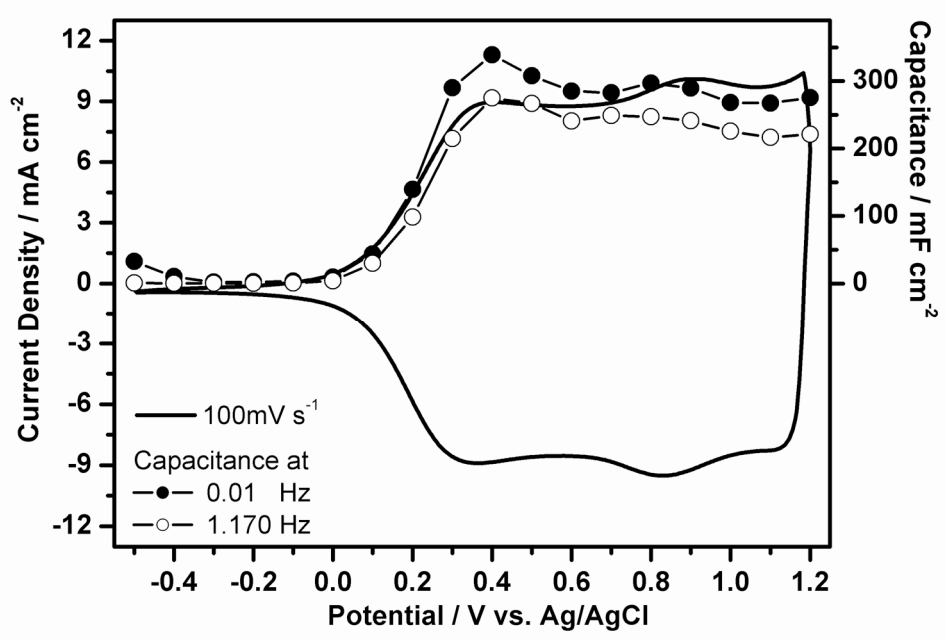

Figure 4.46: Variation of the specific capacitance values of galvanostatically deposited (Q_{dep}=5 C cm^{-2}) PENBTE onto CFME and CV of a PENBTE film at 100mV s^{-1}.

Results of the EIS measurements are given as Nyquist and Bode plot in Figure 4.47 at different potentials for PENBTE. The complex plane impedance plots demonstrate a vertical line with a phase angle very close to -90º. Impedance behavior of the film quite similar in the range of 0.3V to 1.2V starting from the 1.1V a negligible deviation is observed. Nyquist and Bode plots for 0V and 0.1V are almost identical. Starting from -0.1V (See Figure 4.47a) PENBTE far from the capacitive behavior due to limited electroactivity.

After these screening results we mainly focused on the range of 0.3 to 1.2 V where the PENBTE/CFME/electrolyte system shows electroactivity and capacitive behavior.

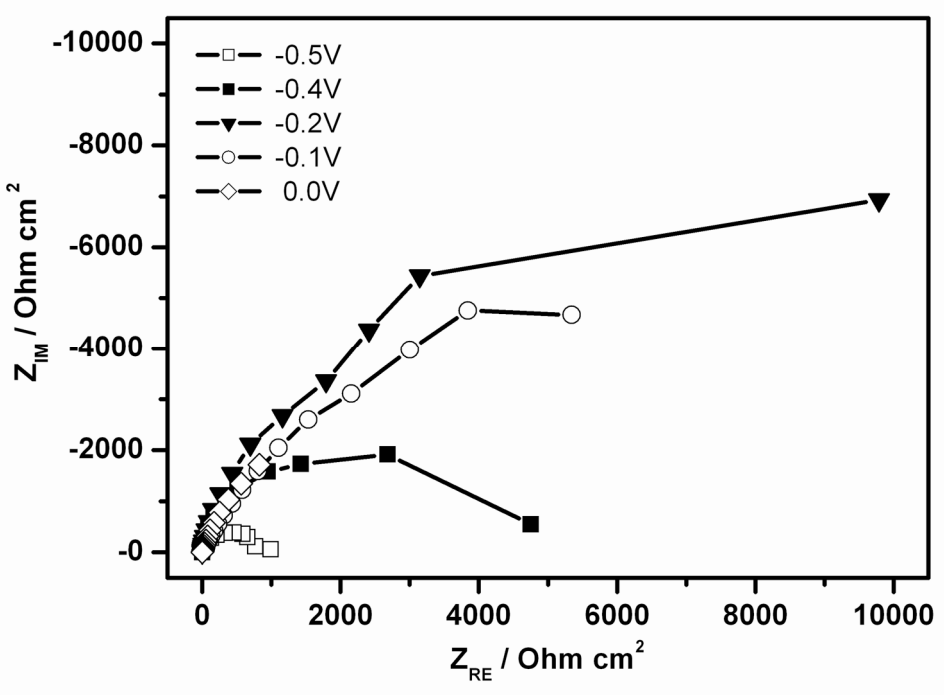

Figure 4.47: (a) The complex plane impedance plots (Nyquist) of the CFME/ PENBTE/0.1M Et_4NBF_4 in DCM in various potential between -0.5V and 0V.

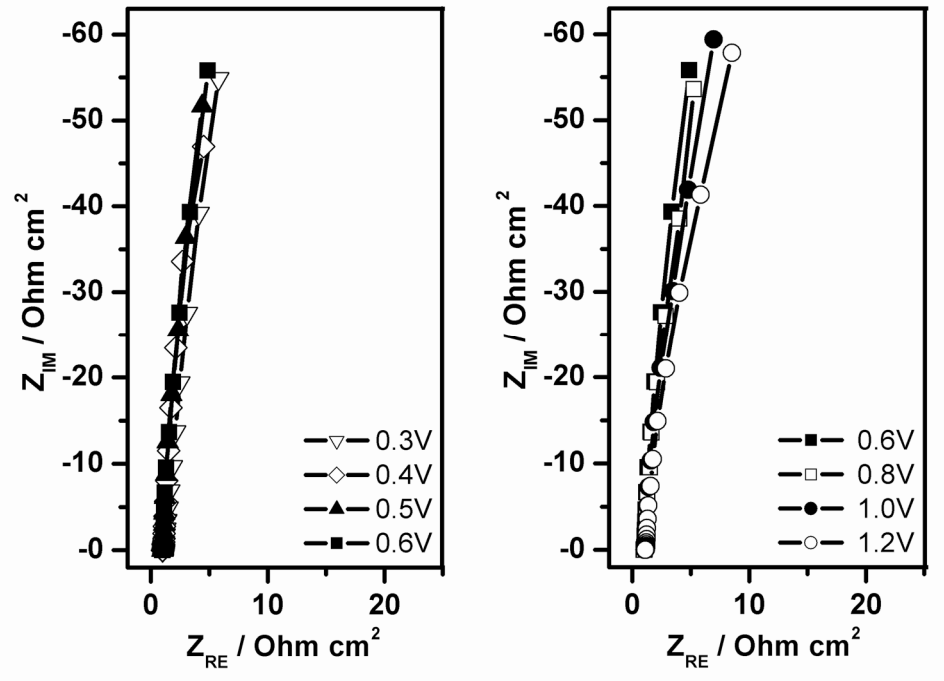

Figure 4.47: (b) Nyquist plots between 0.2V and 1.2V. Q_{dep}=5 C cm^{-2}.

The Bode magnitude plots shown in Figure 4.48a can be divided into a high frequency component (bended at -45º) and a low frequency component (near vertical) with the transition between the two regions. The resistive and capacitive impedances are equal at the transition i.e. -45º. For example at 0.6V; transition between high frequency and low frequency observed at -45.6º and 562.2 mHz (see

magnitude |Z| vs. frequency plot, Figure 4.48a) slope of the linear fit for the data between 10 mHz and 562.2 mHz is -0.9154 and the correlation of this data set is -0.9988. The slope is close to unity supporting an ideal capacitor behavior of the film; note that in the range of 0.3V and 1.2V all Bode Magnitude plots overlap.

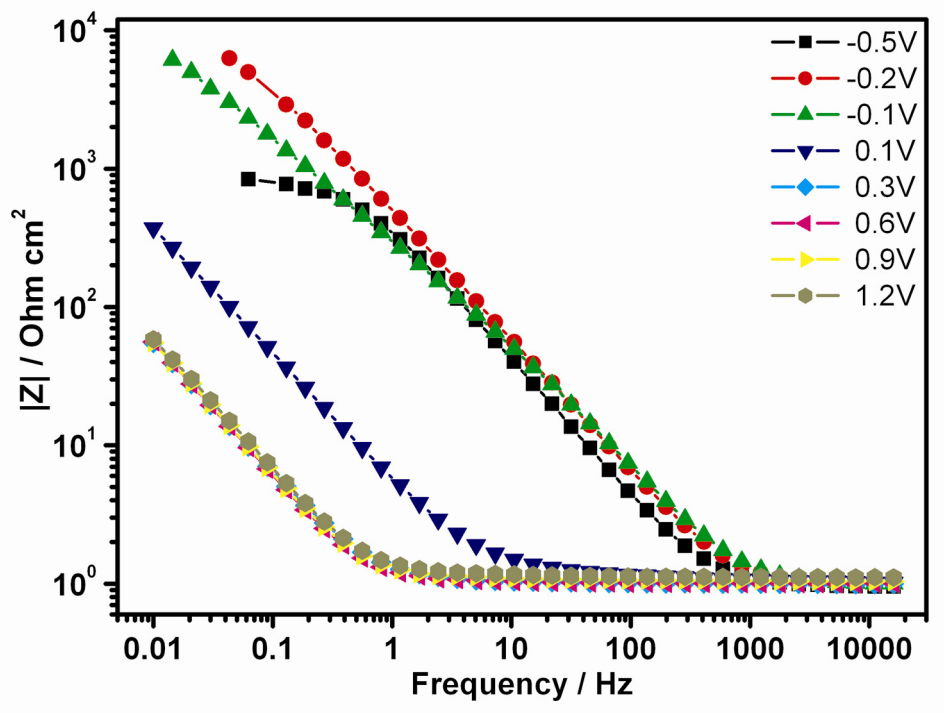

Figure 4.48: (a) Bode magnitude |Z| plots of the CFME/PENBTE/0.1M Et_4NBF_4 combination in DCM at various potentials.

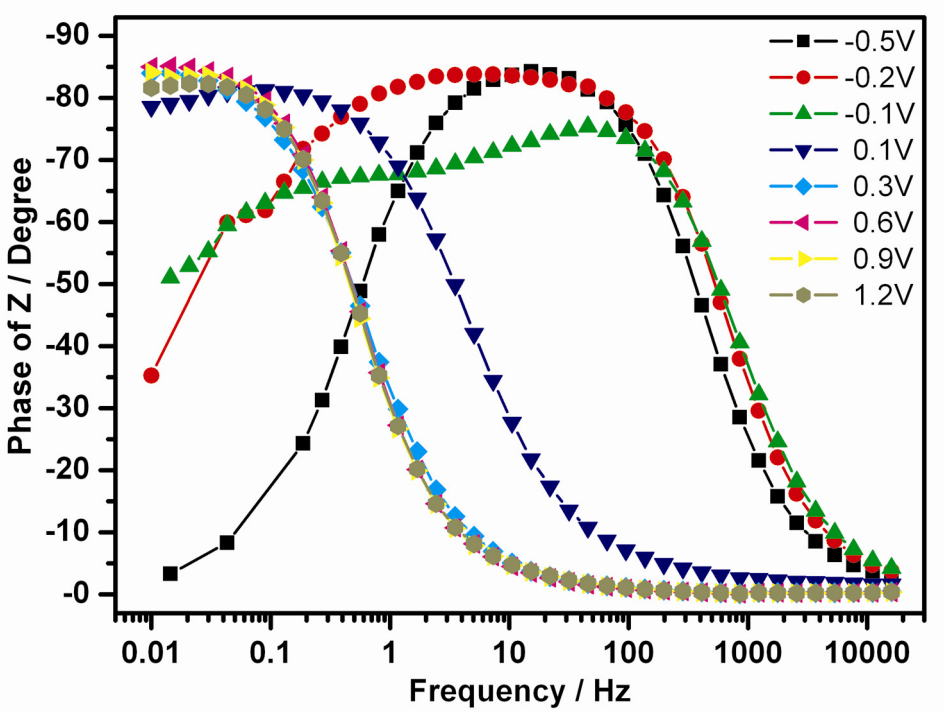

Figure 4.48: (b) Bode phase angle plots.

Figure 4.48b shows the variation of the Bode plots of the CFME/PENBTE film (Q_{dep}=5 C cm^{-2}) by potential. Impedance response of the CFME/PENBTE film divided into three regions by the variation of the potential. First region is between -0.5V and -0.1, second region is 0V and 0.2V, and the third region covers 0.3V and 1.2V. Third region is the most electroactive region of the CFME/PENBTE film. Bode plots at the all studied potentials in this range look same. In the low frequency region (10 mHz to 1Hz) for example at 0.6V phase angle reaches to -87º which is close to that of an ideal capacitor (−90º). Transition frequency is observed lower than 0.5Hz in this potential range. In the middle frequency region (1 Hz to 100Hz) phase angle decreases from −24.5º (1.17Hz) to -1º (94.84 Hz) with increasing frequency, the phase angle approaches to zero at frequencies higher than 100Hz. Bode plot of the 0.1V and 0.0V (not shown) is almost identical. For these two potential values electrode shows a maximum (−81º) at 90 mHz. Transition frequency shifts from 0.5Hz to 5Hz. In the first region CFME/PENBTE film behaves as a resistor as expected.

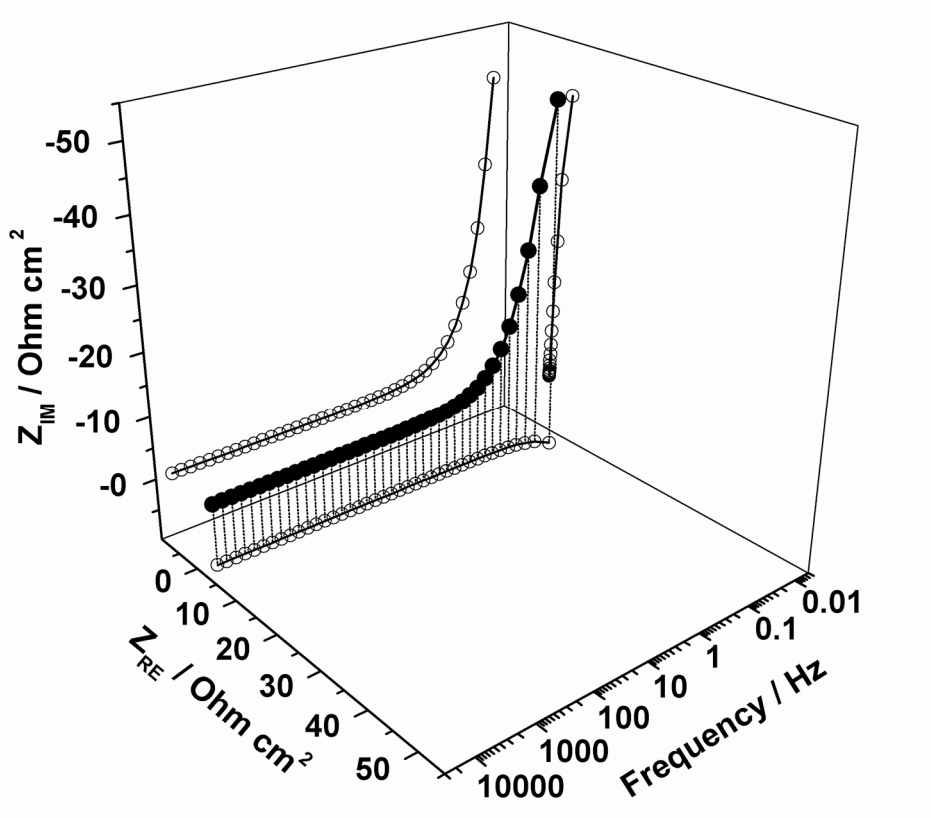

Figure 4.49: (a) The perspective 3D impedance plots of the CFME/PENBTE film (Q_{dep}=5 C cm^{-2}) at 0.4V.b) capacitance and c) admittance.

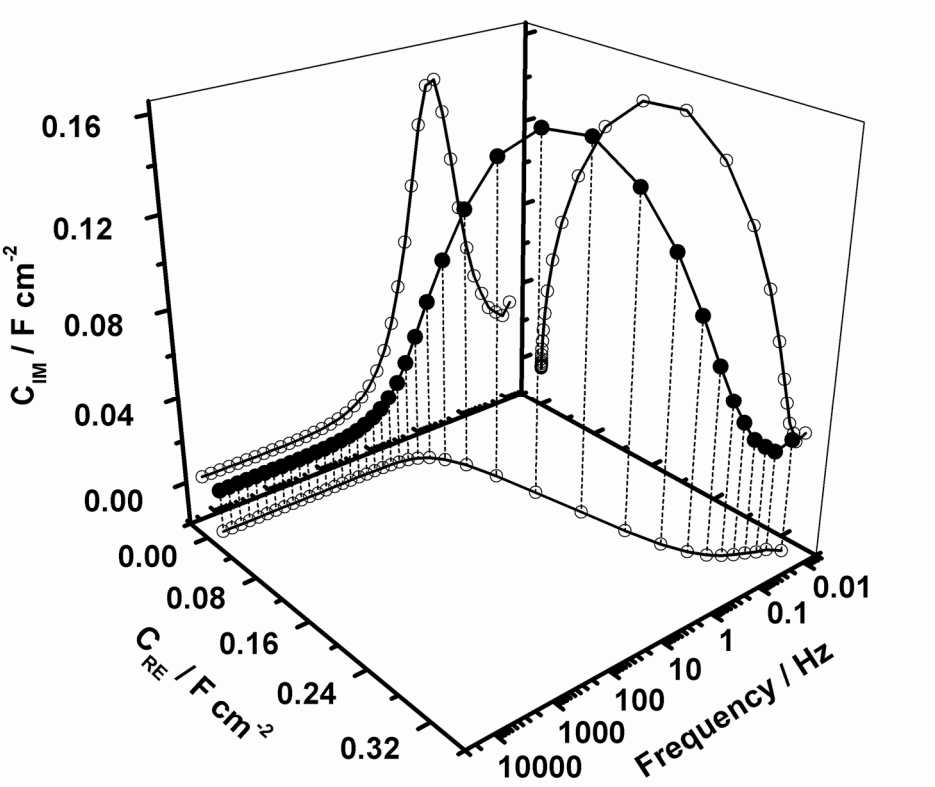

Figure 4.49: (b) The perspective 3D capacitance plots of the CFME/PENBTE film.

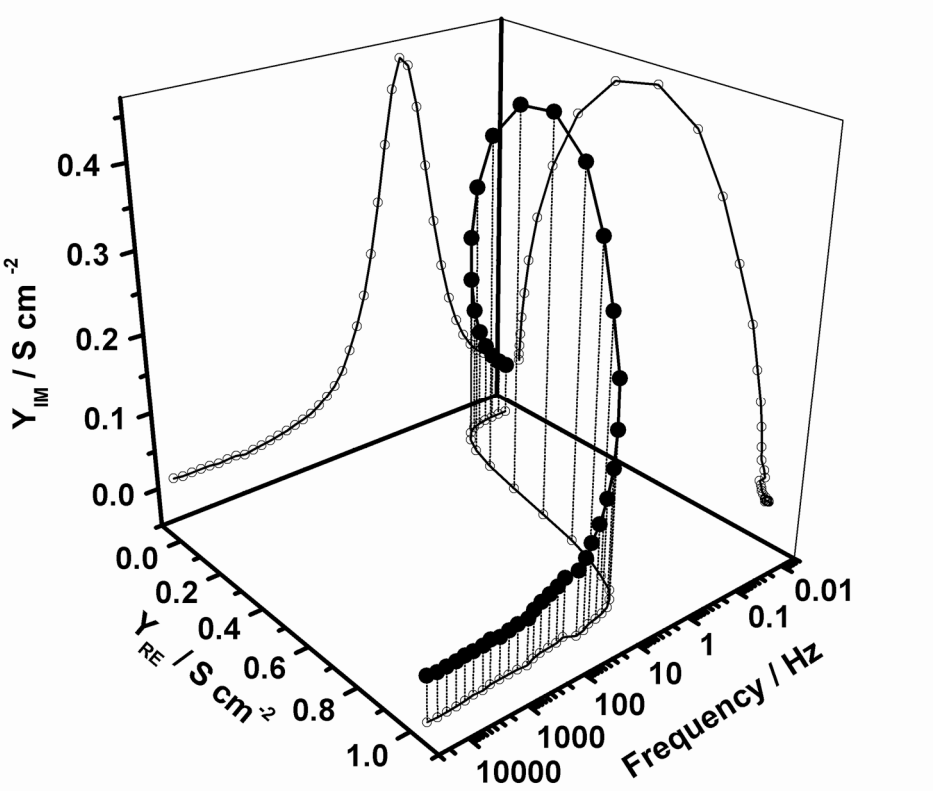

Figure 4.49: (c) The perspective 3D admittance plots of the CFME/PENBTE film.

The perspective 3D plots of impedance, capacitance and admittance of the CFME/PENBTE film (Q_{dep}=5 C cm^{-2}) at 0.4V where the highest capacitance value

was observed is given in the Figure 4.49. These plots very well presents variation of the imaginary and real component as function of frequency of the each investigated response.

4.6.3. Equivalent Circuit

The electrochemical parameters of the CFME/PENBTE/electrolyte system were evaluated by employing the ZSimpWin (version 3.10) software from Princeton Applied Research. We observed excellent agreement between experimental results and the parameters obtained from the best fitting electrical equivalent circuit model, if the chi-squared (χ^2) minimized below 10^{-4}. χ^2 is the function defined as the sum of the squares of the residuals.

Two electrical equivalent circuits were used in simulation of the impedance behavior of the film from the experimentally obtained impedance data. First model (See Figure 4.50a) was used in the electroactive region (i.e. 0.3V to 1.2V) of the electrode. This model was built using series components; the first one is the solution resistance of the polymer and the electrolyte, R_S, second one the parallel combination of the double layer capacitance, C_{dl}, and, R_1 is the charge transfer resistance. The series connection to R_1 made up using CPE in parallel with R_2 and W, R_2 is the charge transfer, and W is the Warburg impedance of diffusion of the ions in the electrolyte. The last component a capacitor element (C_{CF}) is introduced in parallel with a charge transfer resistor (R_{CF}) corresponding to the carbon fiber microelectrode is equivalent to the charge transfer from the polymer coating to the carbon fiber. Simulation results are given in Table 4.9 show that this electrical equivalent circuit was successfully applied to the experimental data to explain the interface between the carbon fiber microelectrode, the polymer film and the electrolyte in this potential region. The potentials given in the table were chosen to cover entire area of the electrochemical activity of the polymer film deposited from the comonomer.

The proposed electrical equivalent circuit (for Model 2 see figure 4.50b) in the region of the -0.5 V to 0.1V was constructed using the Constant Phase Element (Y_o, CPE) instead of all capacitance components in the Model 1 to have better fit with experimental data. In the Model 2 due to the very low electroactivity of the polymer electrode, in order to get better agreement for the interaction of the carbon fiber

electrode and the polymer last component of the Model 1 constructed into the second component. Numerical results of the Model 2 are presented in the Table 4.10.

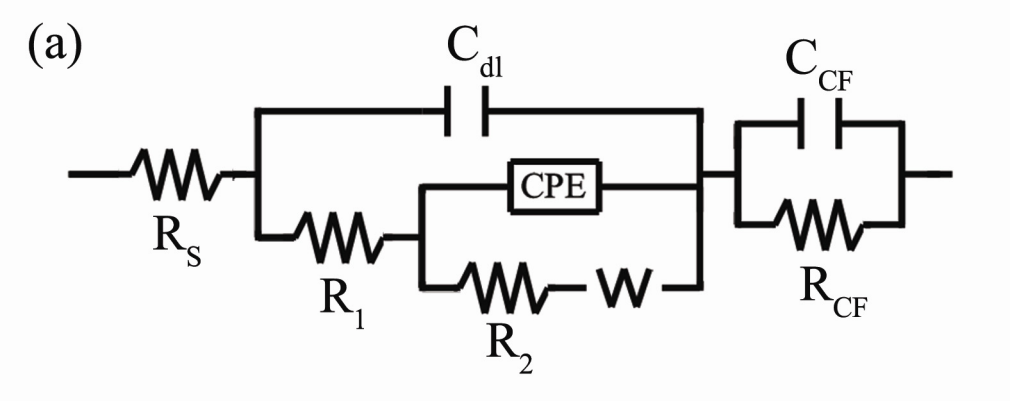

Figure 4.50: (a) Electrical equivalent circuit used for simulating the experimental impedance data from 0.2 V to 1.2V (Model 1).

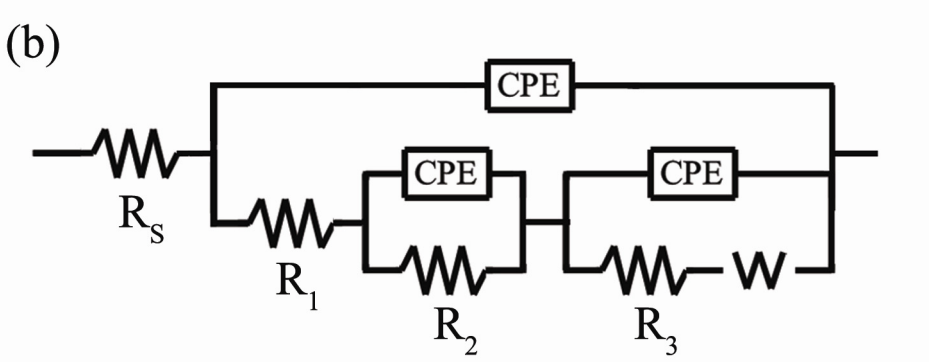

Figure 4.50: (b) Electrical equivalent circuit used for simulating the experimental impedance data from -0.5 V to 0.1V (Model 2).

Table 4.9: Potential dependence of the parameters calculated from the Model 1 which is given in **Figure 4.50a.**

	Potential / V vs. Ag/AgCl				
	E=0.3 V	**E=0.4 V**	**E=0.6 V**	**E=0.9 V**	**E=1.2 V**
R_S / Ohm cm^2	0.999	1.006	0.999	1.040	1.113
C_{dl} / F cm^{-2}	0.182	0.224	0.171	0.127	0.131
R_1 / Ohm cm^2	1.537	0.941	0.389	0.216	0.297
CPE_1; Y_o/ S s^{-n} cm^{-2}	0.073	0.087	0.092	0.131	0.104
n	0.862	0.943	0.973	0.976	0.976
R_2 / Ohm cm^2	15.4	438.5	175.6	146.5	67.3
W; Y_o / S $s^{-0.5}$ cm^{-2}	0.0001	0.0047	0.0056	0.0075	0.0111
C_{CF} / F cm^{-2}	0.0953	0.0342	0.1028	0.0069	0.0639
R_{CF} / Ohm cm^2	0.0301	0.0218	0.0157	0.0181	0.0201
Chi-squared	$4.08x10^{-5}$	$7.96x10^{-5}$	$3.87x10^{-5}$	$7.68x10^{-5}$	$6.68x10^{-5}$

Table 4.10: Potential dependence of the parameters calculated from the Model 1 which is given in **Figure 4.50b.**

	Potential / V vs. Ag/AgCl				
	E=-0.5 V	**E=-0.2 V**	**E=-0.1 V**	**E=0.0 V**	**E=0.1 V**
R_S / Ohm cm^2	0.953	0.991	0.992	0.919	0.956
CPE; Y_o/ S s^{-n} cm^{-2}	$3.67x10^{-4}$	$3.42x10^{-4}$	$3.52x10^{-4}$	$8.77x10^{-4}$	$4.40x10^{-4}$
n	0.977	0.949	0.931	0.424	0.618
R_1 / Ohm cm^2	1.902	6901	137.4	0.045	0.061
CPE; Y_o/ S s^{-n} cm^{-2}	$0.49x10^{-4}$	$4.25x10^{-4}$	$27.9x10^{-4}$	$49.7x10^{-4}$	$296.9x10^{-4}$
n	1	0.8	1	0.8	0.978
R_2 / Ohm cm^2	762.1	752.7	3088	$2.11x10^{14}$	$2.67x10^{17}$
CPE; Y_o/ S s^{-n} cm^{-2}	0.0135	0.0053	0.0005	0.0054	0.7476
n	0.561	1	0.642	0.666	0.320
R_3 / Ohm cm^2	0.010	46870	7561	6.196	5.683
W; Y_o / S $s^{-0.5}$ cm^{-2}	0.0001	0.0018	0.0011	0.0260	0.0270
Chi-squared	$1.88x10^{-5}$	$5.42x10^{-5}$	$1.47x10^{-5}$	$7.42x10^{-5}$	$4.49x10^{-5}$

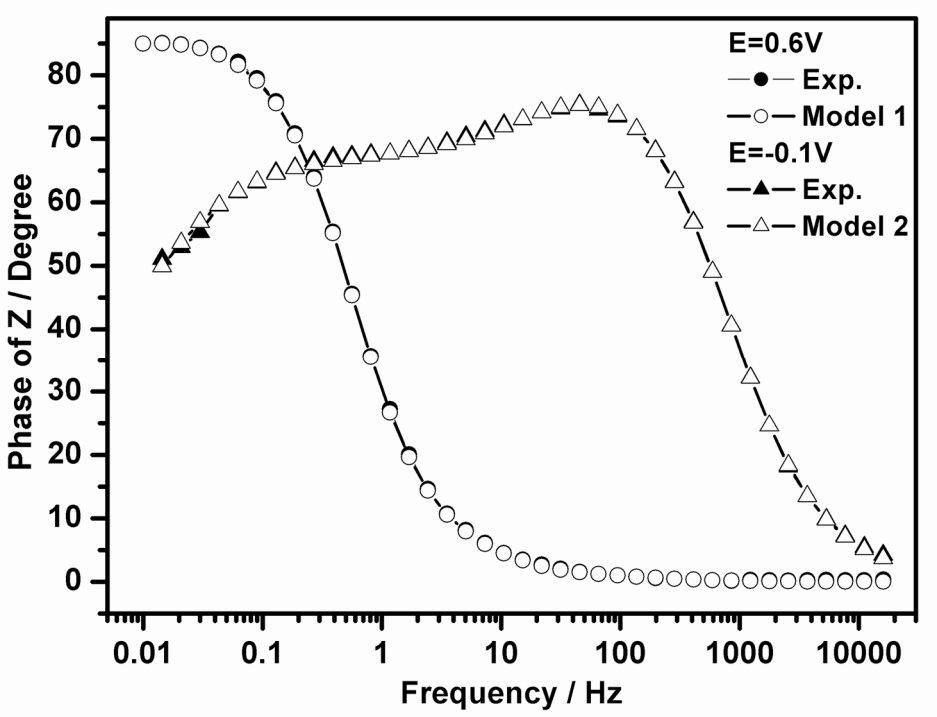

Figure 4.51: Bode plot results of the fitting.

Figure 4.51 shows a representative comparison of the experimental data and the fitting results at 0.6V for Model 1 and -0.1V for Model 2. After applying Model 1 all of the calculated chi-squared values are smaller than $1x10^{-4}$ indicating very good agreement between experimental data and simulation results in the 0.3V to 1.2V range. Symbols with solid interior representing experimental data are completely covered symbols with open interior showing simulation results. Model 2 yields better

results through to the positive potentials of the -0.5V to 0.1V scale. As shown in Figure 4.50b, Model 2 as a general (except for the low frequency values from 10 mHz to 90 mHz) shows very good correlation with experimental data.

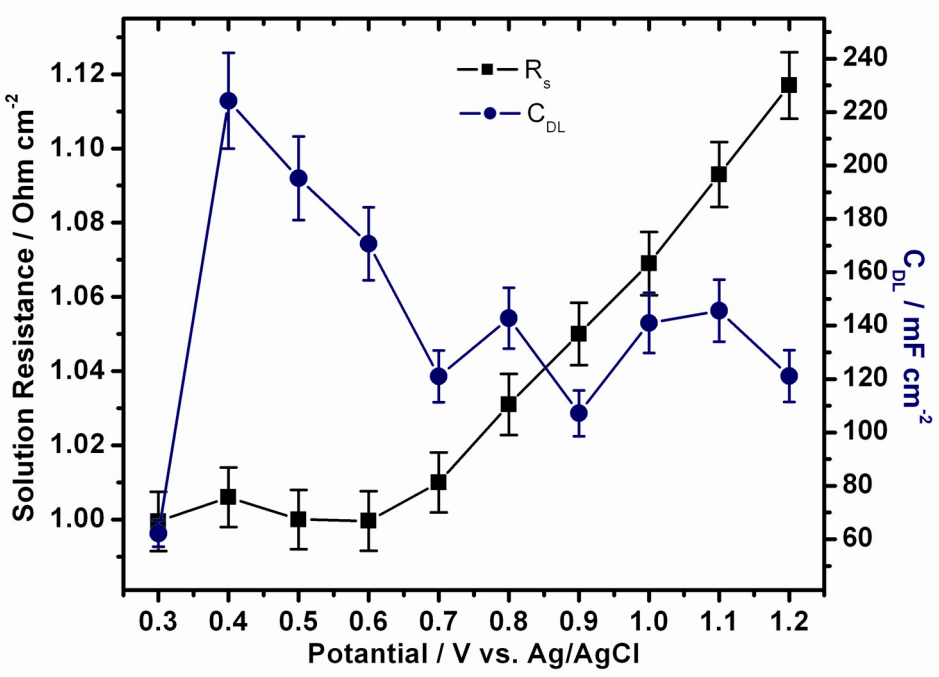

Figure 4.52: Variation of the solution resistance and double layer capacitance with respect to potential values obtained from the Table 4.8.

Figure 4.52 presents variation of the R_s and C_{DL} with respect to the potential. The solution resistance varies in a very narrow range of 1.00 and 1.12 Ohm cm^2 and slightly increases as the potential increase. The double layer capacitance has great influence on the capacitance of the CFME/PENBTE/Electrolyte system that makes contribution to the specific capacitance of the system. Variation of the C_{DL} by potential shows similar behavior as explained previously in Figures 4.45 and 4.46. With a rough estimation one can conclude that low capacitance of the film at 0.4V vs. Ag/AgCl is 300 mF cm^{-2} (see Figure 4.46) and 220 mF cm^{-2} of the total capacitance comes from the double layer capacitance.

4.6.4. Effect of Solvent

Figure 4.53 shows variation of low frequency capacitance values in different solvents of ENBTE comonomer. CFME/PENBTE film has capacitance values higher in propylene carbonate (PC) and in DCM compared to acetonitrile (ACN). Shape of the capacitance curves at various potentials in PC and in ACN exhibits similar fashion, specific capacitance values which are measured in ACN is almost half of those of

measured in PC. This result suggested by the findings that were reported by Otero et. al.[168] in terms of dipole moment and dielectric constant. Dielectric (ε) and dipole moment (μ/D) values of propylene carbonate, acetonitrile and dichloromethane are 66.14 and 4.9, 36.64 and 3.92, 8.93 and 1.6, respectively.

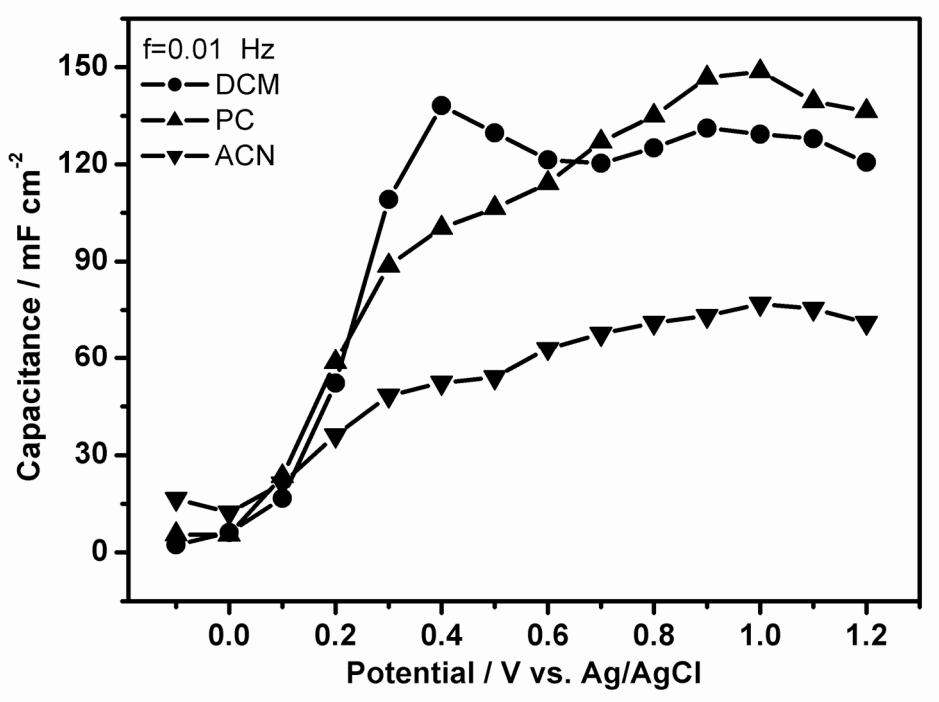

Figure 4.53: (a) Variation of low frequency capacitance values by potential at 10 mHz in different solvents of ENBTE comonomer deposited from 1mM ENBTE in 0.1 M Et_4NBF_4/DCM solution at a scan rate of 20mV s^{-1}; Q_{dep}=1205 mC cm^{-2}.

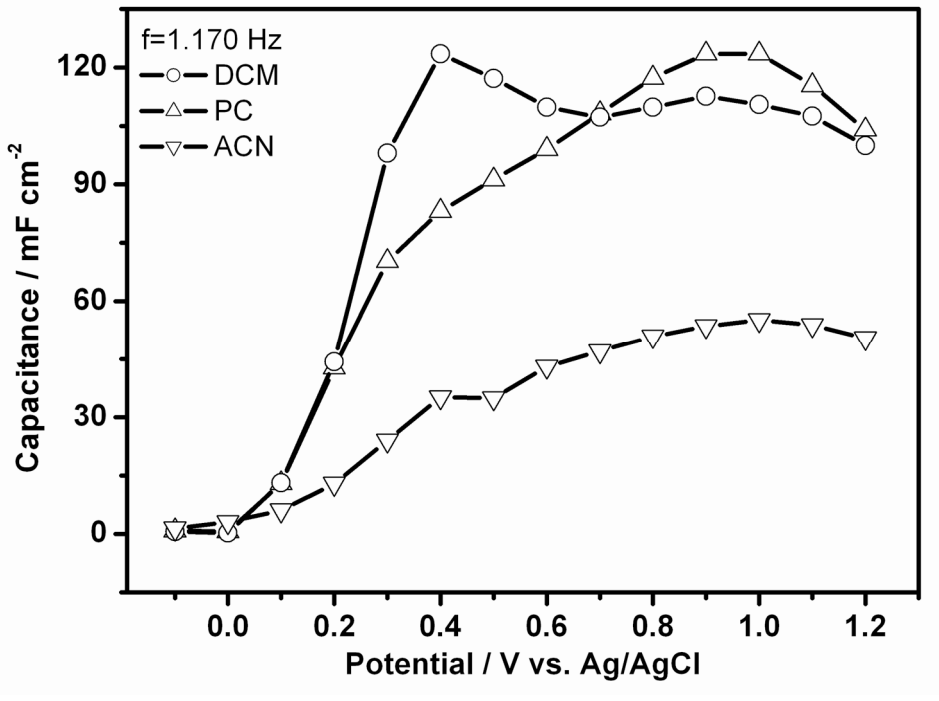

Figure 4.53: (b) Variation of C_{LF} capacitance values by potential at 1170mHz.

High capacitance was observed in the case of DCM which has the lowest dielectric constant among the used solvents; this might be due to low dielectricity of the solvent which might promote ion formation in double-layer while high dielectricity solvents reduce. The peak which is observed in DCM at around 0.4V corresponding to the first oxidation peak of the polymer (see Figure 4.44b), was not clearly observed in PC and ACN, these two solvents exhibits higher specific capacitance at the second oxidation peak of the polymer at around 0.9V at where in DCM shows lower capacitance than that of 0.4V.

4.6.5. Effect of Deposition Charge and Method

As shown in the Figure 4.54 the specific capacitances increase with increasing deposited charge (film thickness). PENBTE was deposited from 1mM ENBTE in 0.1 M Et_4NBF_4/DCM by chronopotantiometry with a charge of 1 to 5 C cm^{-2} at a current density of 10mA cm^{-2}. There is no linear correlation with specific capacitance values and the charge. This might be due to morphology of the deposited film (see morphology section) film thickness also does not exhibit a linear increase due to formation of the polymer globules with deposited charge.

In the EIS studies part of this thesis we generally prepared electrodes by galvanostatic deposition, because controlling amount of the deposited charges in other words film thickness can be readily done with this method. Morphology of the films, surface roughness and porosity of the surface might show differences depending on deposition method. In order to examine effect of the deposition method to the capacitance behavior of the CFME/PENBTE/Electrolyte combination we prepared a set of electrodes by cyclic voltammetry at different deposition charges. We know from the FE-SEM studies (see section 4.5.2.) that ENBTE exhibits homogeneous deposition as a continuous and very well adhering film to the fiber surfaces.

Figure 4.55 shows variation of the specific capacitance values at low frequency region by deposited charge. As observed from the there is critical film thickness at which specific capacitance of the system drastically increase our unpublished results also support this idea. All of the studied charge values electrodes exhibits same pattern by potential.

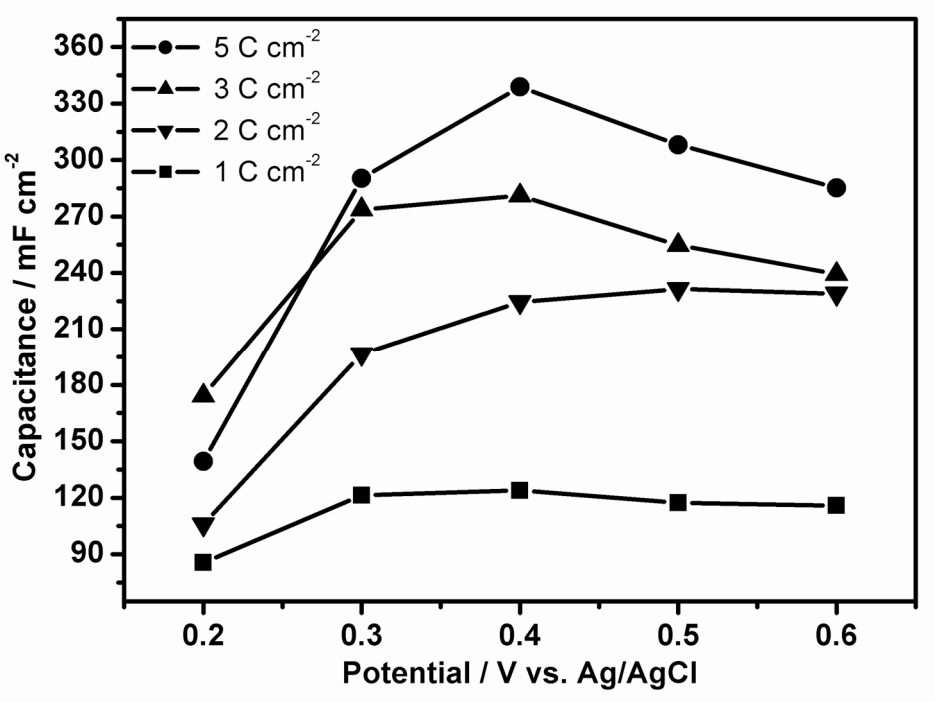

Figure 4.54: (a) Variation of capacitance values by potential at 10 mHz by deposited charge (film thickness). The polymer deposited from 1mM ENBTE in 0.1 M Et_4NBF_4/DCM solution by chronopotantiometry at a current density of 10mA cm^{-2}.

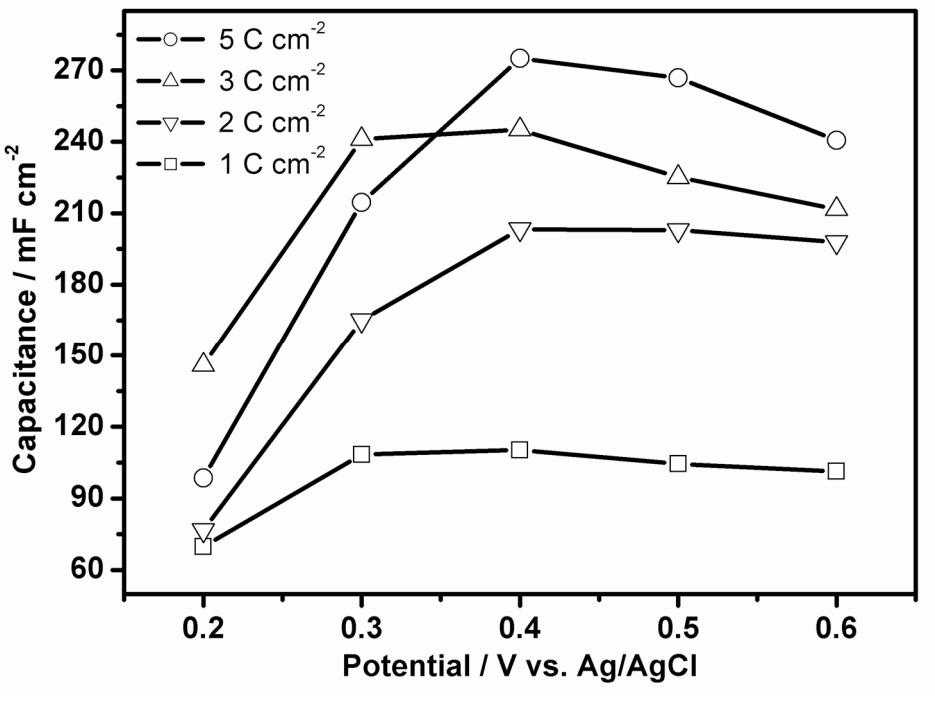

(b) Variation of capacitance values by potential at 1170 mHz.

We have successfully applied electrical equivalent circuit that is given in Figure 4.50a to the PENBTE film deposited by cyclic voltammetry without any extra component calculated results of the model fit exhibits excellent agreement with the experimental data. Deposition charge dependence of the parameters calculated for

the PENBTE film from the equivalent circuit which is given in Table 4.11 at 0.4V dc potential. See Appendix Table A.1-A.6 for potential dependence of the films deposited at different charges.

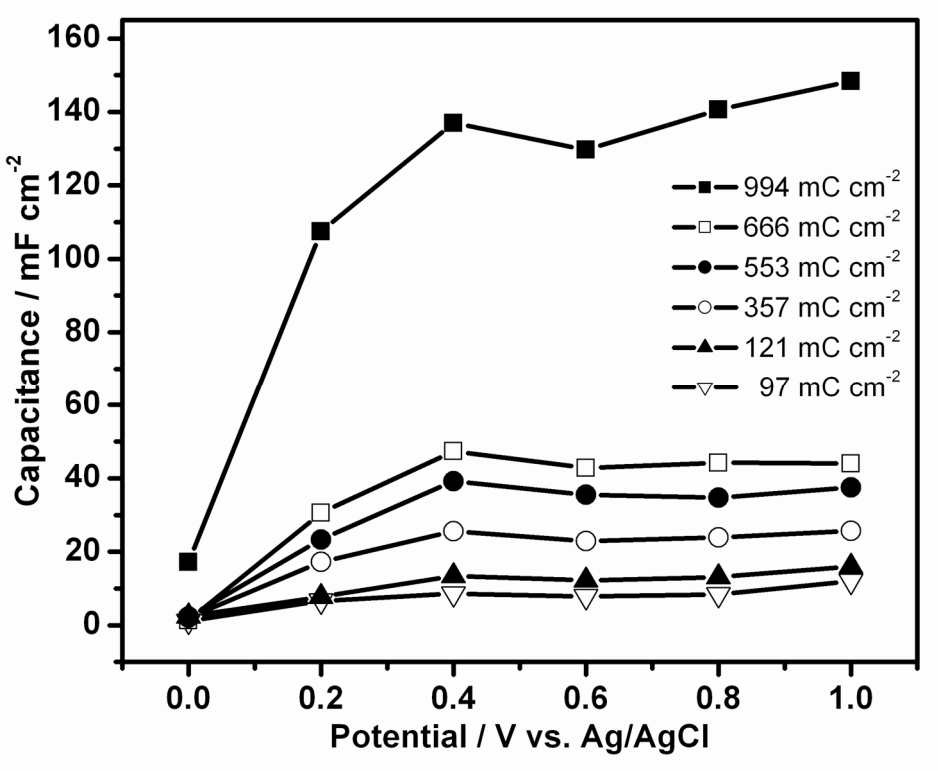

Figure 4.55: Variation of the specific capacitance values at 10mHz by deposited charge and electrode potential. PENBTE films deposited from 1mM solution of the monomer by cyclic voltammetry.

Figure 4.56 illustrates variation of the solution resistance, double layer capacitance calculated by model fit and low frequency capacitance obtained from equation 4.1 of the PENBTE film with respect to deposition charge. Double layer capacitance (C_{DL}) and low frequency (C_{LF}; specific capacitance) of the PENBTE electrodes deposited with a charge of between 97 mC cm^{-2} and 666 mC cm^{-2} increase linearly. Contribution of the double layer capacitance to the specific capacitance is lower than 35% of between 357 mC cm^{-2} and 666 mC cm^{-2}. This very small contribution might be an indication of homogenous and even surface of the electrode at this deposition charges. At the highest deposition charge contribution of the double layer capacitance approaches 75% and specific capacitance of the electrode drastically increases and solution resistance decreases.

Table 4.11: Deposition charge dependence of the parameters calculated for PENBTE film from the equivalent circuit which is given in Figure 4.50a.

	Deposition Charge / mC cm^{-2}					
	Q_{dep}=97	Q_{dep}=121	Q_{dep}=357	Q_{dep}=553	Q_{dep}=666	Q_{dep}=994
R_S / Ohm cm^2	2.277	2.109	2.696	2.296	2.833	0.6897
C_{dl} / F cm^{-2}	0.00551	0.00728	0.00864	0.03454	0.01667	0.1005
R_1 / Ohm cm^2	0.9101	166.9	0.1469	60.86	0.1623	0.7853
CPE_1; Y_o/ S s^{-n} cm^{-2}	0.00267	0.00565	0.01619	0.00317	0.02914	0.0034
n	0.9725	0.9714	0.9832	0.8911	0.9817	0.9761
R_2 / Ohm cm^2	14060	0.2398	7540	$1.03x10^{+08}$	2.148	0.3079
W; Y_o / S $s^{-0.5}$ cm^{-2}	$4.73x10^{-05}$	$6.38x10^{-17}$	$5.44x10^{-14}$	$1.25x10^{-17}$	$3.91x10^{-18}$	$1.00x10^{-20}$
C_{CF} / F cm^{-2}	$1.46x10^{-04}$	0.2772	0.8991	0.01565	$7.28x10^{-05}$	0.02209
R_{CF} / Ohm cm^2	0.04295	34.65	15.58	0.07328	0.06913	0.02474
Chi-squared	$6.28x10^{-05}$	$7.05x10^{-05}$	$6.89x10^{-05}$	$4.75x10^{-05}$	$5.83x10^{-05}$	$5.44x10^{-05}$

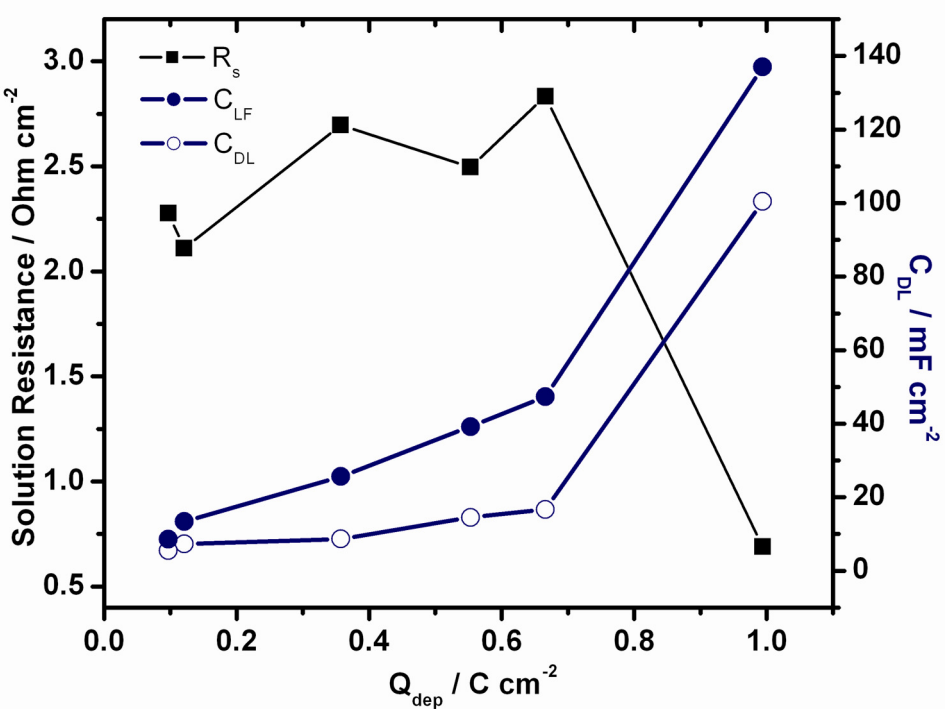

Figure 4.56: Variation of the solution resistance, double layer capacitance and low frequency capacitance of the PENBTE film with respect to deposition charge at 0.4V DC potential vs. Ag/AgCl.

Figure 4.57 illustrates the complex plane impedance plots PENBTE films deposited at deposition charges. Phase angle of these films are higher than -88º and the highest deposition condition see inset 1 phase angle higher than (-89.5º) can be considered as (-90º) that of an ideal capacitor which exhibits same angle (-90º). Inset Figure also illustrates simulation results which were performed using equivalent circuit given in Figure 4.50a. Proposed models demonstrate excellent consent with experimental data

as illustrate in the Figure simulation data represented with empty interior symbol completely covers symbol of the experimental data shown with solid interior.

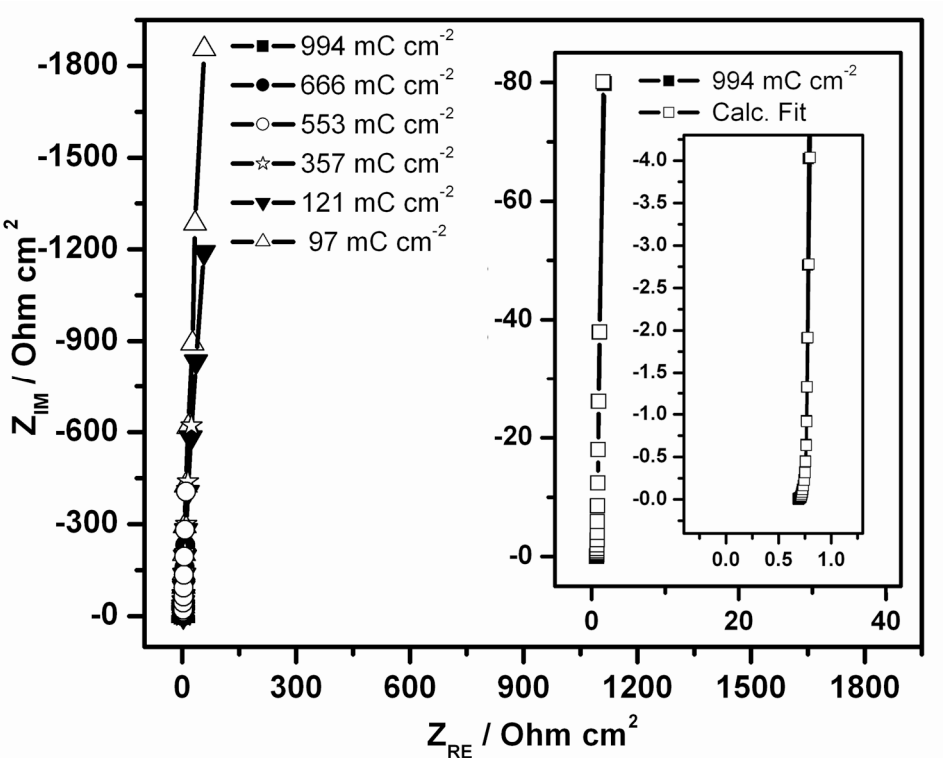

Figure 4.57: The complex plane impedance plots (Nyquist) of the CFME/ PENBTE/0.1M Et_4NBF_4 in DCM at various deposition charges. Inset 1 show Nyquist plot at deposition charge of 994 mC cm^{-2} and Inset 2 shows expanded complex plane plot 4 x 4 ohm cm^2 of Inset 1.

Figure 4.58 shows the variation of the Bode plots of the CFME/PENBTE film (Q_{dep}=5 C cm^{-2}) by deposition charge at 0.4V DC potential vs. Ag/AgCl. Bode magnitude |Z| plots Figure 4.58a are given with simulation data, simulation data completely covers the experimental data indicating quality of the simulation results at entire frequency range.

Transition frequency is observed between 1 Hz and 2 Hz for thicker films shift 10 Hz and 20 Hz for thinner films. For the thickest film Bode Magnitude of the impedance becomes smaller than 1 Ohm cm^{-2} at frequencies higher than 1 Hz and behaves free of frequency and drop of the Bode magnitude is around 60 Ohm cm^{-2}.

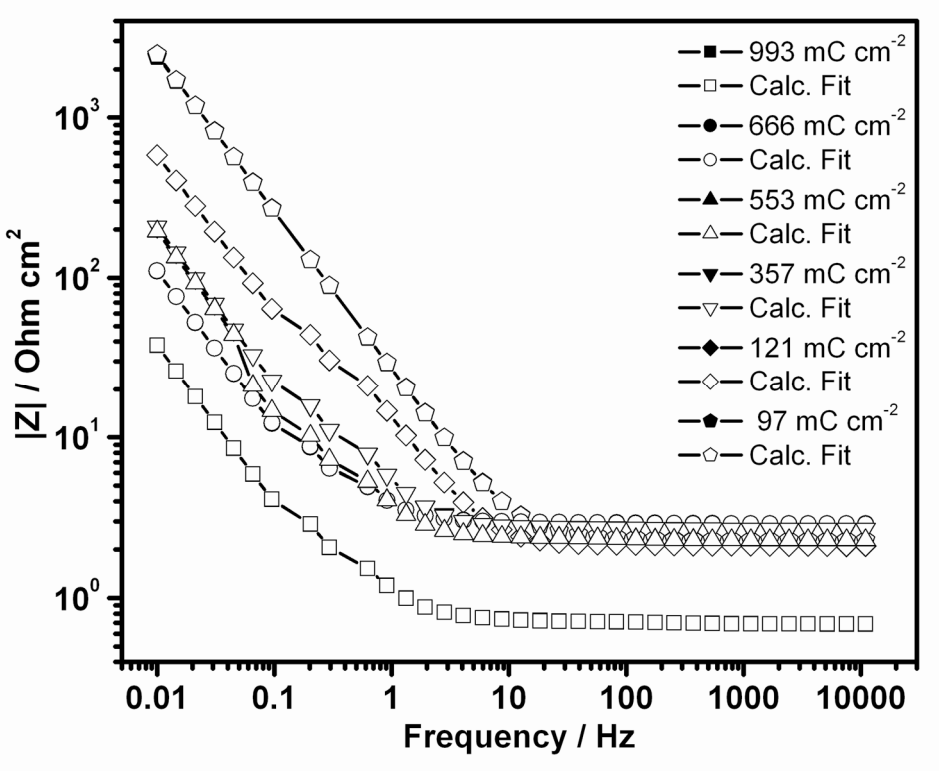

Figure 4.58: (a) Bode magnitude |Z| plots of the CFME/PENBTE/0.1M Et_4NBF_4 in DCM in various deposition charges at 0.4V DC potential with simulation results.

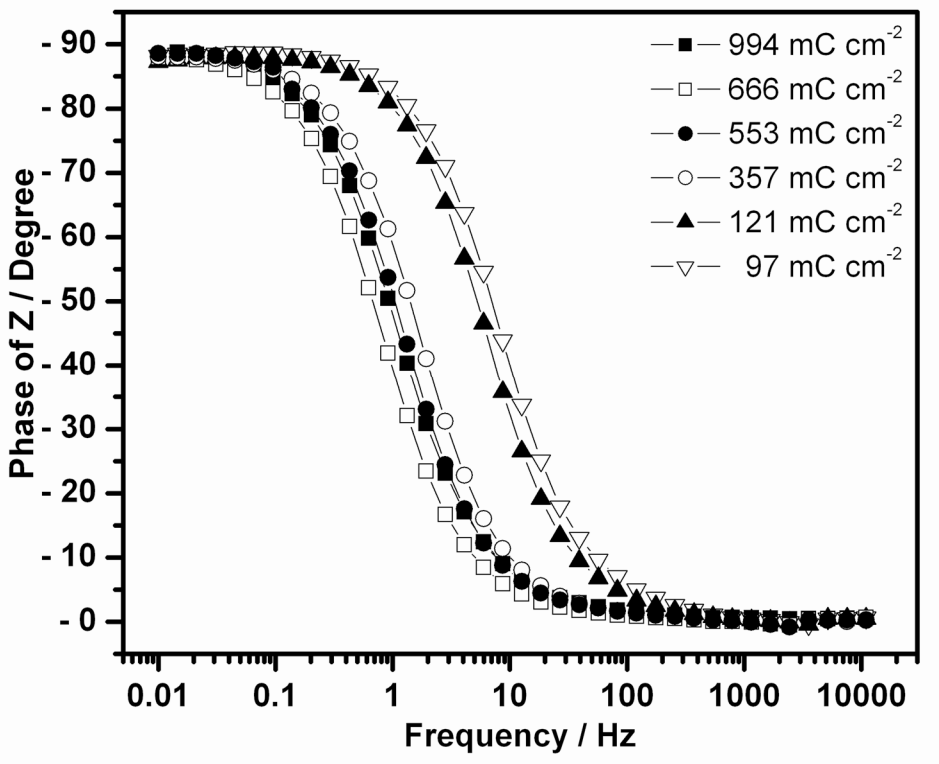

Figure 4.58: (b) Bode phase angle plots.

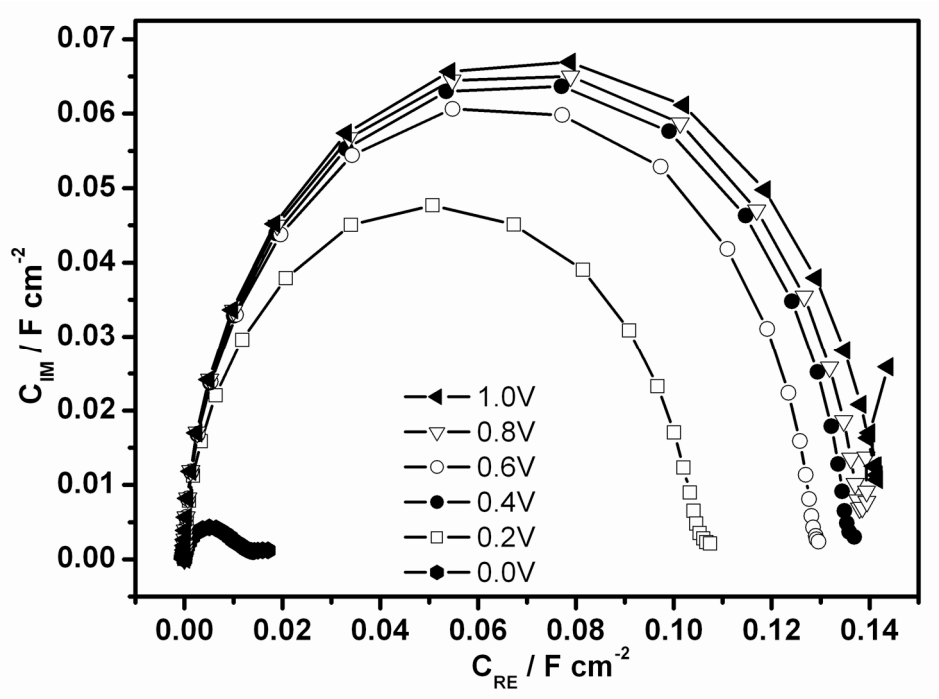

Figure 4.59: (a) Potential dependence of complex plane capacitance plots of the of the CFME/PENBTE film which is deposited with a charge of 994 mC cm^{-2}.

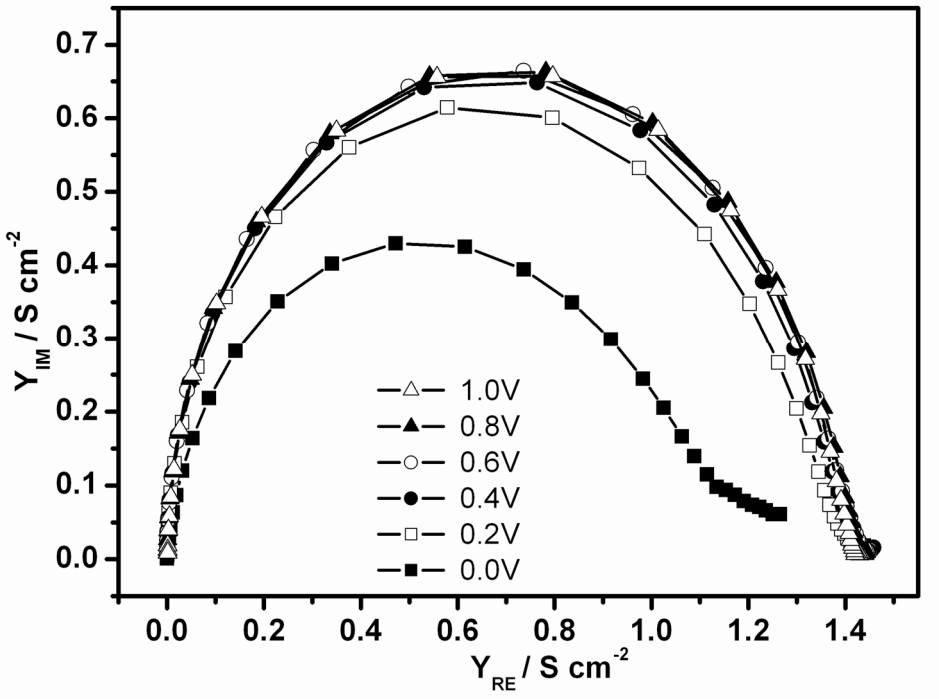

Figure 4.59: (b) And complex plane admittance plots.

Figure 4.59 displays variation of the real and imaginary components of the capacitance and admittance plots with each point associated with a frequency.

The galvanostatic charge/discharge characteristic of a film (Q_{dep}= 1000 mC cm^{-2}) is given in Figure 4.60b. Slope of the charge/discharge curve is 0.9985 and -0.9998

respectively indicates that IR drop is negligible and triangular shape of the charge discharge curve is typical for ideal capacitor behavior indicates that very good capacitive performance.

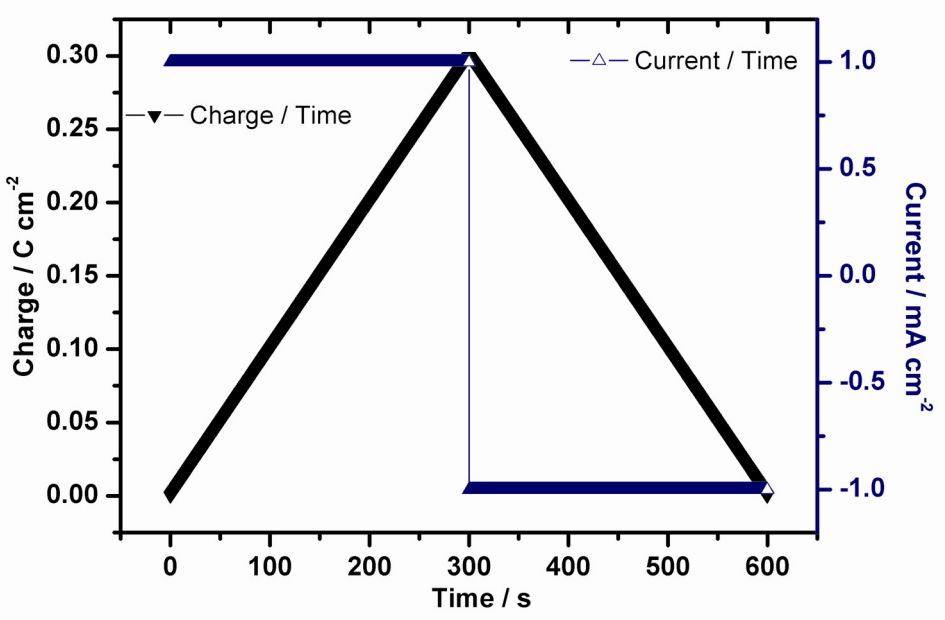

Figure 4.60: (a) Variation of the charge during charging and discharging, y axis on the right hand side shows current density of charge/discharge.

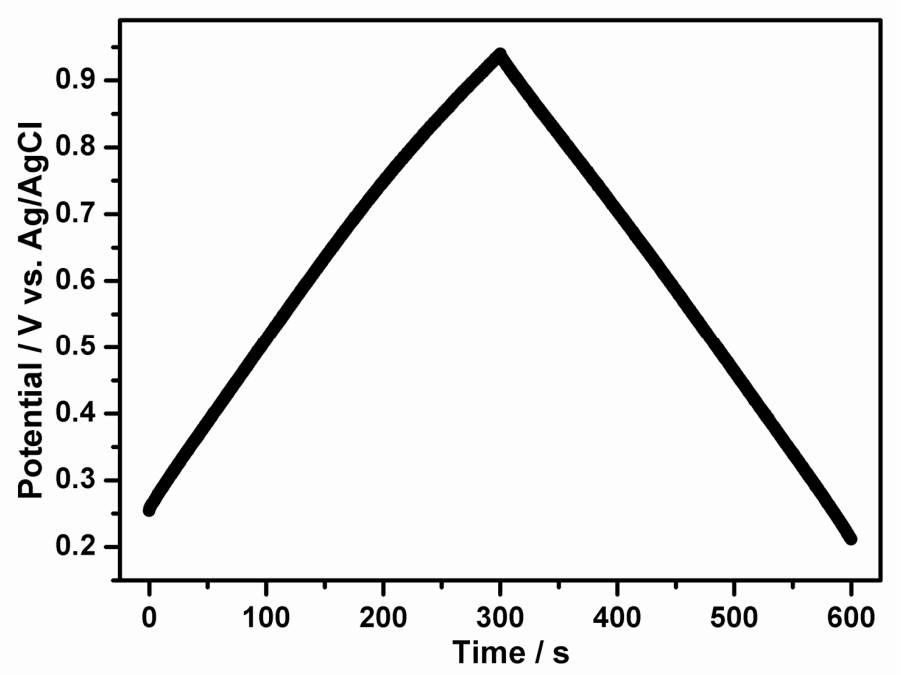

Figure 4.60: (b) Galvanostatic charge/discharge curve of chronopotentiostatically deposited (Q_{dep}= 1000 mC cm^{-2}) PENBTE. Galvanostatic conditions; 0.1 M Et_4NBF_4/DCM solution.

4.6.6. Morphology of The Films

The morphology of the films electrodeposited at different deposition charges were analyzed using FE-SEM pictures of the obtained films are presented in Figure 6.61.

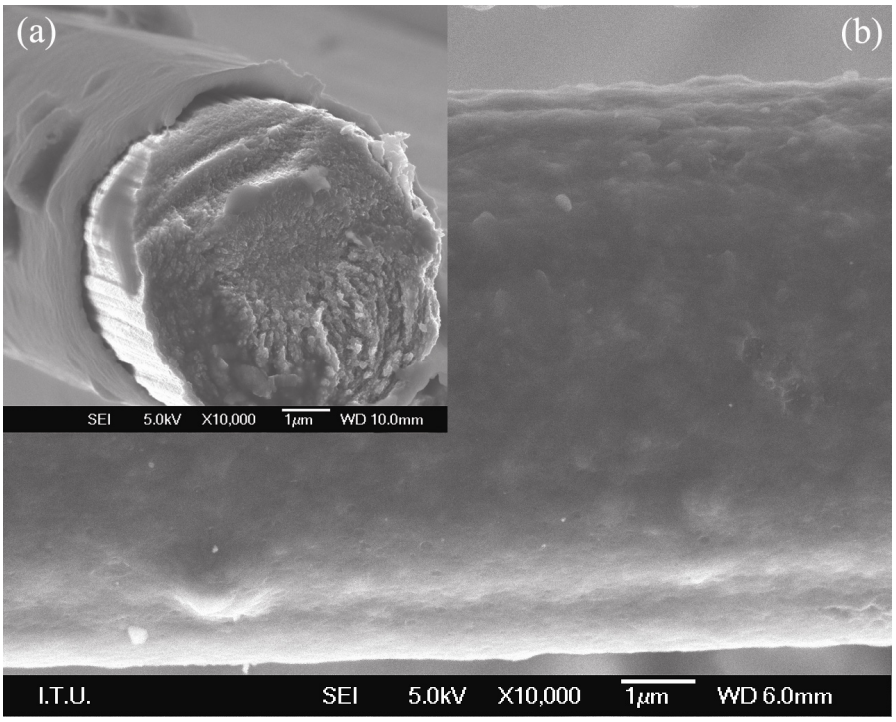

Figure 4.61: SEM images of ENBTE coated CFMEs; **(a)** Cross section image of ENBTE comonomer deposited from 1mM ENBTE in 0.1 M Et_4NBF_4/DCM solution at a scan rate of 20mV s^{-1}; Q_{dep}=268.8mC cm^{-2}, **(b)** Side view of image (a).

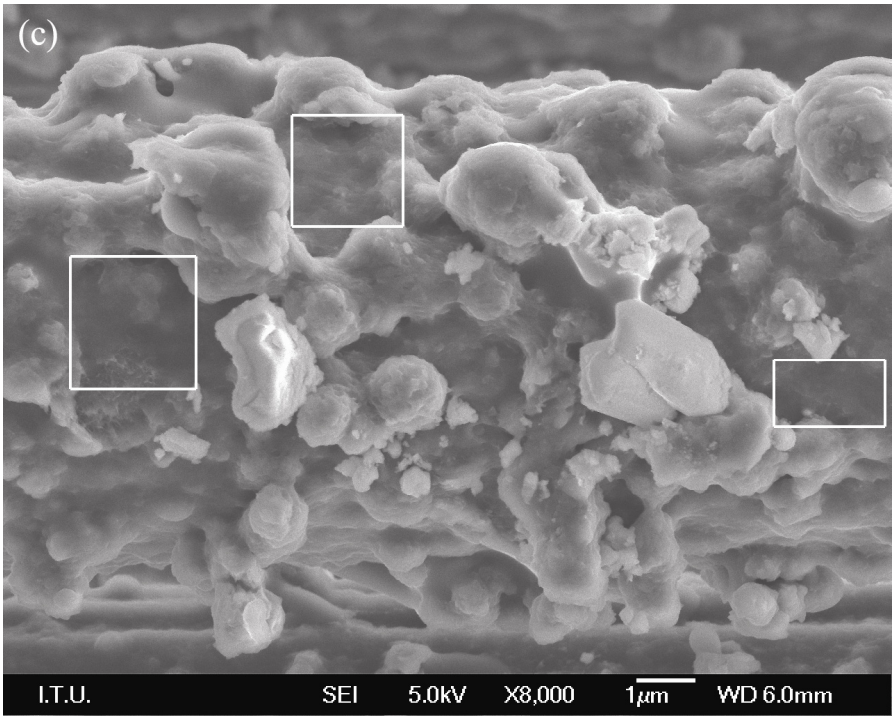

Figure 4.61: (c) PENBTE film deposited under similar conditions with a charge of almost five times higher, Q_{dep}= 1385 mC cm^{-2}.

Figure 4.61(a) and 4.61(b) show cross section and side view image of the film deposited with a charge of 268.8mC cm^{-2} and the average thickness of the film about 0.3μm. The polymer was deposited homogeneously as a continuous and very well adhering film which is exhibiting even thickness on the fiber surfaces. Increase in the deposition charge, for example a film which is deposited with a charge of five times higher than the film shown in Figure 4.61 (a) and (b) (Q_{dep}= 1385 mC cm^{-2}) yields 0.7 μm thick film, causes formation of the polymer globules along the carbon fiber over the homogeneous polymer coating spots marked out with white rectangles show homogeneous lower background of the film. Note that bare carbon fiber exhibits striations along the fiber (see cross section image Figure 4.61(a)) firstly a homogenous coating forms on the carbon fiber and than globular structures appear.

Morphology of the coated films strongly depends on the deposition charge but film thickness does not show a linear fashion with the increase of deposition charge.

4.7. Electrocopolymerization and Characterization of BTh and ENBTE

4.7.1. Electrochemical Copolymerization.

The oxidative electrochemical copolymerization of bithiophene and ENBTE comonomers was carried out via cyclic voltammetry and chronopotentiometry. A structural representation of the reaction taking place during electrochemical copolymerization is illustrated in equation (4.16).

Copolymerization is initiated at the electrode surface following the one-electron oxidation of monomer. Combination of the radical species with neutral monomer, followed by proton elimination, forms the neutral oligomer. The polymerization proceeds through subsequent oxidation of oligomer at the electrode to generate the radical species. The resulting polymer film can be repeatedly cycled between the insulating neutral form and the oxidized conductive bipolaron state [169].

We have prepared homopolymers of BTh and ENBTE comonomers, as explained in previous sections and have observed that their oxidation potentials adequate to ensure copolymerization. Monomer oxidation potential of BTh in the case of CFME as a working electrode is 1.246 V vs. Ag/AgCl and ENBTE comonomer as monomer oxidation potential of +0.954 V vs Ag/AgCl. We have prepared a set of copolymers with different mole fractions using BTh and ENBTE comonomers. The copolymer

films were deposited by CV over 4 cycles onto CFME (area≈0.001cm^2) from 0.001 M solution of the both comonomers in 0.1 M Et_4NBF_4/DCM electrolyte solution.

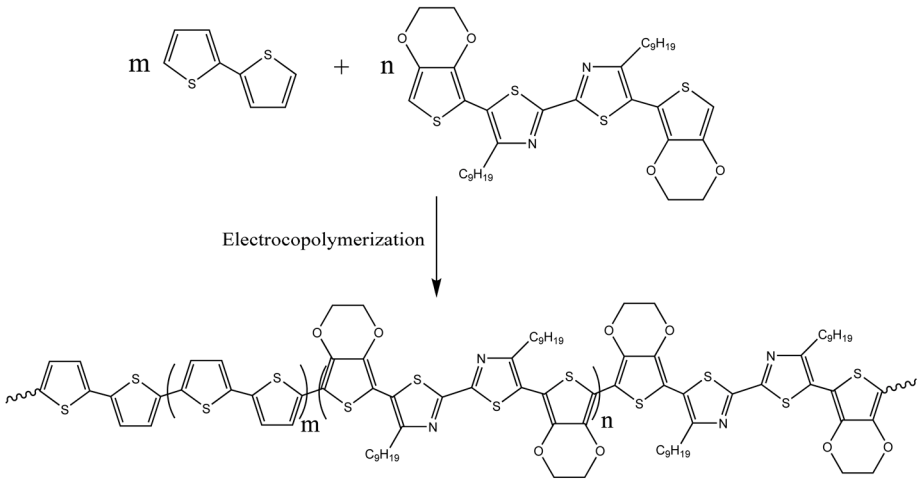

(4.16)

Figure 4.62 illustrates electropolymerization of BTh and ENBTE comonomer with a mole fraction ratio of 0.5. Mole fractions (***x)*****,** onset potentials of the monomer and half wave potentials of the prepared polymers are given in Table 4.12. Polymer growth CV's at some other fractions are given in Appendix Figure E.1 and E.2.

After the films were rinsed in the electrolyte solution, to remove surface bound monomers and oligomers and then two voltammograms of the copolymer films were recorded over the potential range for complete copolymer oxidation and reduction as shown in Figure 4.63.

Copolymers were characterized in monomer-free electrolyte solution at the following scan rates: 20, 40, 60, 80, 100, 120, 140, 160, 180 and 200 mV s^{-1}. (Scan rate dependency plots of some selected mole fractions are given in Appendix Figure F.1 and F.2) All of the copolymer films exhibit reversible oxidation processes and their half wave potentials of the corresponding oxidation and reduction peaks are given in Table 4.10. The anodic and cathodic peak currents are linear in scan rate dependence between 20 mV s^{-1} and to 200 mV s^{-1}. This demonstrates that the electrochemical processes are not diffusion-limited and are reversible, even at high scan rates.

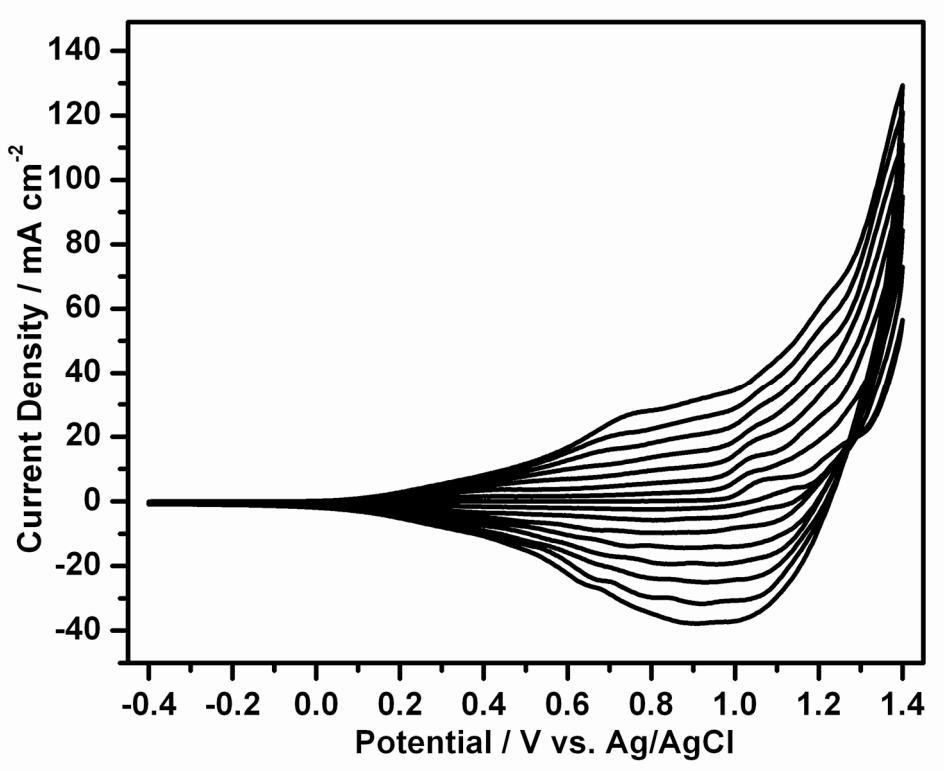

Figure 4.62: Electrocopolymerization of 1mM BTh and 1mM ENBTE (x=0.5) onto CFME in 0.1M Et_4NBF_4 /DCM solution. Deposition charge of 7.7 C cm^{-2}.

Table 4.12: Mole fractions, the on set potentials of polymerizations, and half wave potentials of the BTh and ENBTE comonomers.

$x_{BTh} = \frac{m_{BTh}}{m_{BTh} + m_{ENBTE}}$	$E_{onset,\,m}$	1. peak $E_{1/2}$	2. peak $E_{1/2}$
$x = 1$	1.246	-	1.137
$x = 0.925$	0.998	0.413	1.023
$x = 0.875$	1.008	0.333	0.955
$x = 0.850$	0.994	0.342	0.950
$x = 0.50$	0.972	0.295	0.998
$x = 0$	0.954	0.304	0.814

The oxidation of PENBTE domains are present in all copolymers shown in Figure 4.63, indicating that each comonomer is being incorporated into the copolymer chain. As the concentration of ENBTE increased, redox peaks belong to this comonomer becomes clearer. Due to high concentration of BTh comonomer at the mole ratios of 0.875 and 0.925, current densities produced by this comonomer is higher, for this reason as a result redox peaks of the ENBTE comonomer looks smaller. As the mole fraction of ENBTE is increased a significant decrease in onset potential of ENBTE was observed as expected.

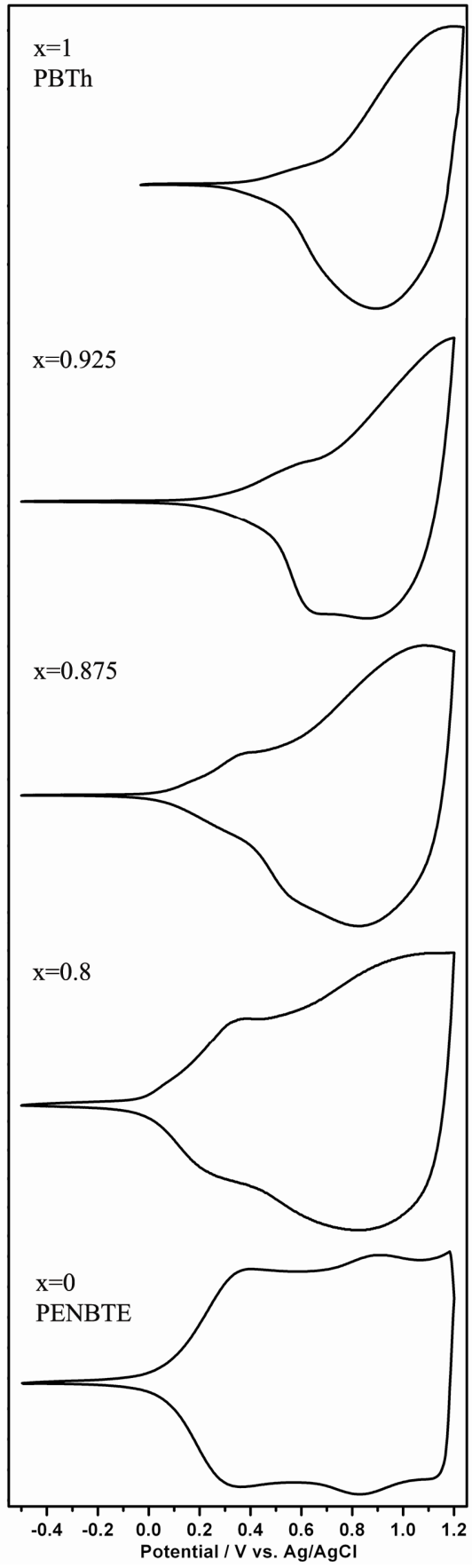

Figure 4.63: Redox behavior of the BTh and ENBTE comonomers in monomer free electrolyte solution at a scan rate of 100 mV s^{-1}.

4.7.2. EIS Studies on BTh and ENBTE Copolymers

EIS measurements were performed to find out electrochemical characteristics of the prepared copolymers for all studied mol fractions at different applied potentials in the range of -0.2 to 1.2 V with a potential step of 0.1V to cover entire electroactivity range of the prepared copolymers. As a first step we have calculated low frequency capacitance values for a set of copolymers to have an idea about their capacitance behavior. As we stated in previous sections deposition charge plays an important role on capacitance behavior of polymer electrodes, so that we have prepared a set of copolymer electrodes that were deposited with a charge of 3 C cm^{-2}. Figure 4.64 illustrates specific capacitance values of copolymer electrodes which are prepared with a charge of 3 C cm^{-2}. The low frequency capacitance values from impedance spectroscopy were obtained from slope of a plot of the imaginary component (Z_{IM}) of impedance at low frequencies versus inverse of the reciprocal frequency.

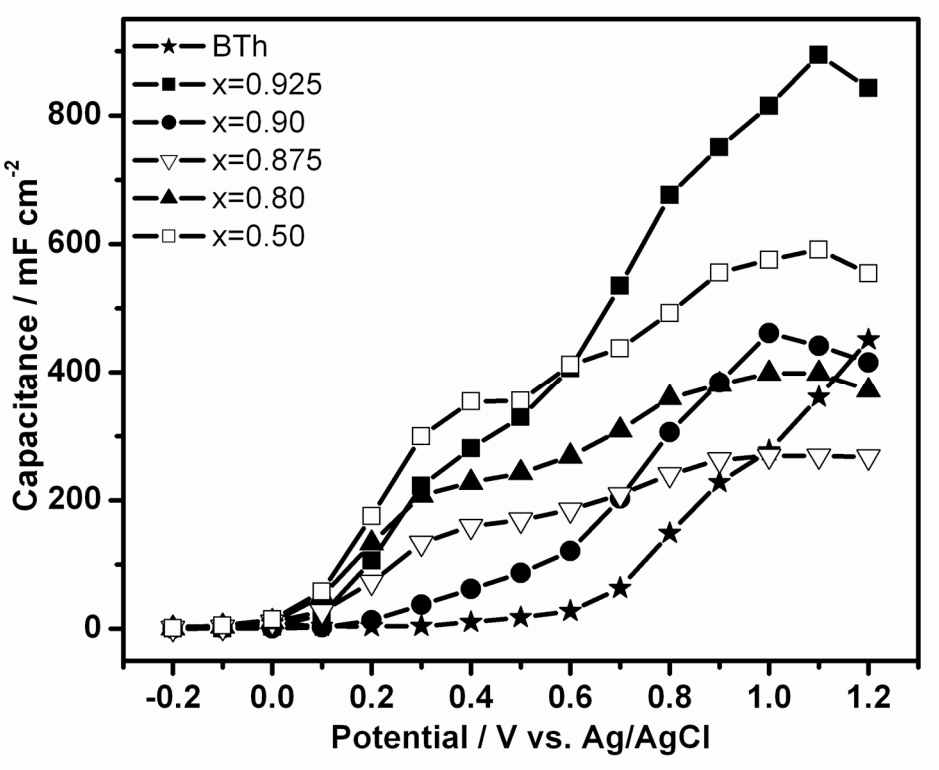

Figure 4.64: Variation of specific capacitance values of BTh and ENBTE comonomers by potential at different mole fractions on CFME with a deposition charge of 3 C cm^{-2}.

Specific capacitance curves present similar pattern with their redox behavior in monomer free solution. For instance specific capacitance of the PBTh starts to increase at 0.6 V which is similar to that of at same potential current density of the

PBTh increases. The copolymer which was prepared with a mole fraction of 0.5 exhibits quite similar behavior like PENBTE due to at this mole fraction both comonomers found in same amount in the solution but onset potential of monomer oxidation for ENBTE starts about 0.3V lower than that of BTh, presumably incorporation of ENBTE into the copolymer structure is more favorable. At the mole fraction of 0.925 it looks from the Figure 4.64, this fraction is the best combination for the comonomers in connection with capacitance. But as will be discussed later this combination is not suitable for supercapacitor applications. The other combinations of the comonomers show an increase in their capacitance behavior as the mole fraction of ENBTE is increased.

We have successfully applied electrical equivalent circuit model 1 (See Figure 4.50a) which is previously suggested for PENBTE polymer electrodes. The excellent agreement found with experimental and results are given in Table 4.13.

Table 4.13: Values of the equivalent circuit components which given in Figure 4.50a for the copolymer electrode of BTh an ENBTE prepared with a mole ratio of 0.925 and deposition charge of 4.6 C cm^{-2}.

	Potential / V vs. Ag/AgCl					
	0.4V	**0.6V**	**0.8V**	**1.0V**	**1.2V**	**1.4V**
R_S / Ohm cm^2	0.8365	0.8056	0.8039	0.8044	0.8113	0.8276
C_{dl} / F cm^{-2}	0.2199	0.1188	0.1554	0.5842	0.3175	0.1203
R_1 / Ohm cm^2	0.7349	0.03761	0.03391	0.15	0.06118	0.02745
CPE_1; Y_o/ S s^{-n} cm^{-2}	0.1876	0.44	0.7431	0.5133	11.93	0.3786
n	0.9633	0.9731	0.9677	0.9232	0.9444	0.9498
R_2 / Ohm cm^2	3358	132.5	100.5	1249	1.916	9.222
W; Y_o / S $s^{-0.5}$ cm^{-2}	$1.35x10^6$	0.00498	0.02569	0.00213	$1.41x10^{-14}$	1.411
C_{CF} / F cm^{-2}	0.03432	1.902	3.084	0.1216	3.121	0.00605
R_{CF} / Ohm cm^2	0.04943	0.06473	0.04262	0.01499	6.857	0.01013
Chi-squared	$7.292x10^{-5}$	$5.139x10^{-5}$	$6.479x10^{-5}$	$5.603x10^{-5}$	$9.44x10^{-5}$	$2.677x10^{-4}$

Figure 4.65 and Figure 4.66a and 4.66b presents Nyquist and Bode phase and Bode magnitude of the copolymer electrode which was prepared with a mole fraction of x=0.925 and Q_{dep}=4.6 C cm^{-2} at different potentials with simulation results. Open interiors show data which were obtained from model fit calculations. At lower potentials copolymer electrode shows more capacitive behavior compared to the higher potentials i.e. 1.2V whereas specific capacitance values which were calculated for low frequencies higher at high potentials. We know that PENBTE shows very high capacitances in the range of 0.4 to 0.8V which is also an indication of the

incorporation of ENBTE into the copolymer structure where PBTh does not show much capacitive behavior see Figure 4.5. The highest phase angle at this mole fraction observed in the region of 0.4V-0.6V but as a combination of good properties for supercapacitor applications for example lowest magnitude drop, highest imaginary component of impedance, high phase angle observed at 1.0V in this copolymerization condition. Nyquist, Bode phase, and Bode magnitude plots of some other mole fractions are given in Appendix Figure G1 and G2.

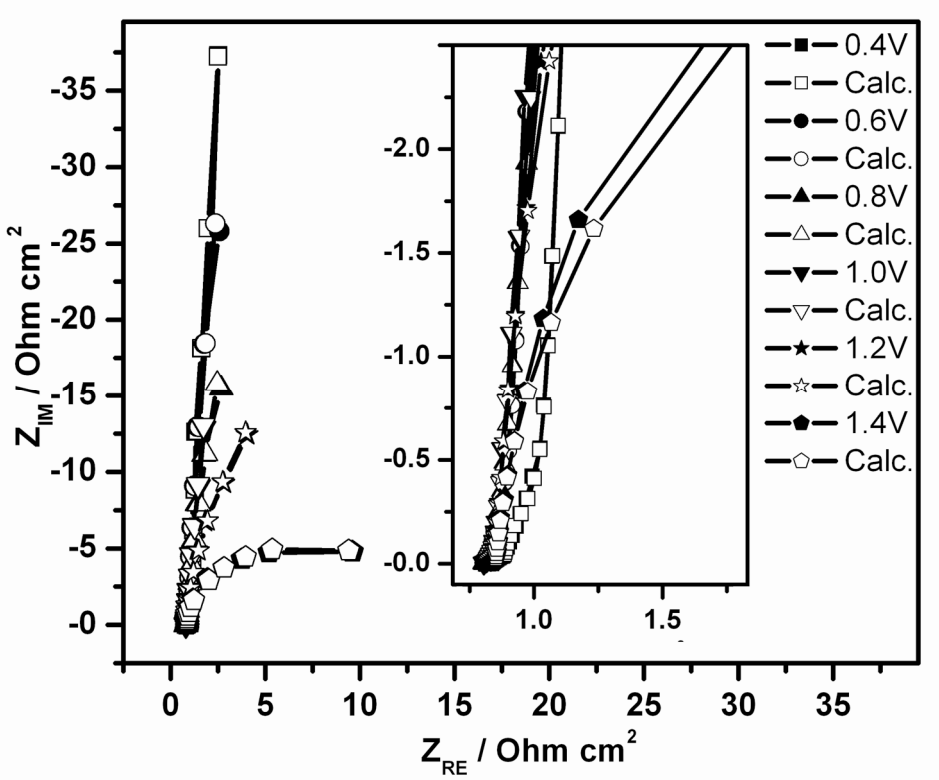

Figure 4.65: Complex plane impedance plots of the copolymer (x=0.925 and Q_{dep}=4.6 C cm^{-2}) at different potentials. Inset: An expanded complex plane view of the high frequency region.

The galvanostatic charge discharge characteristics of the copolymer electrodes were investigated with a current density of 1 mA cm^{-2} and results are presented in the Figure 4.67. Charge discharge characteristics of a capacitor determines suitability for application, in ideal case shape of the charge discharge curve is a triangle, slope of the both sides must be very close to unity.

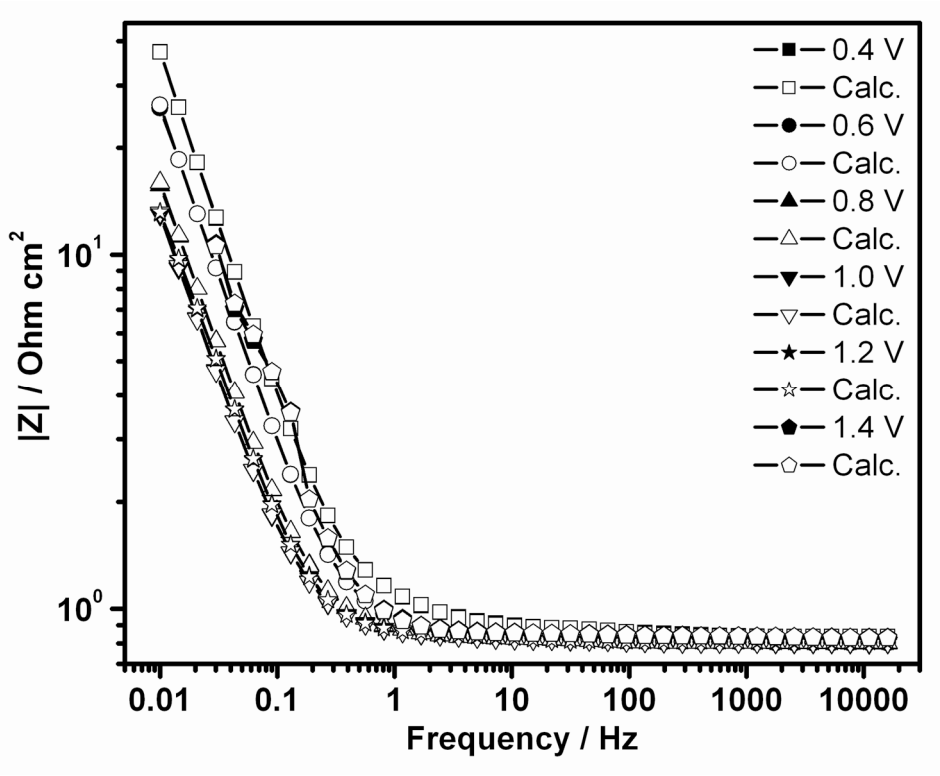

Figure 4.66: (a) Variation of Bode magnitude |Z| plots by electrode potential of the BTh and ENBTE copolymer (x=0.925 and Q_{dep}=4.6 C cm^{-2}) at different potentials.

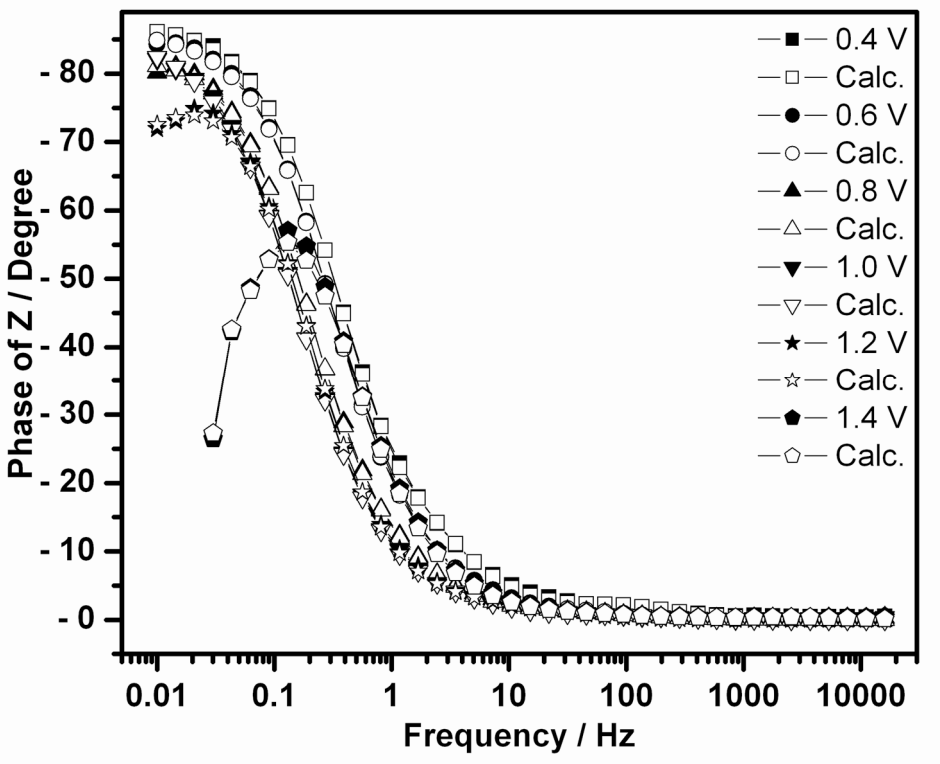

Figure 4.66: (b) Variation of Bode phase angle plots by electrode potential.

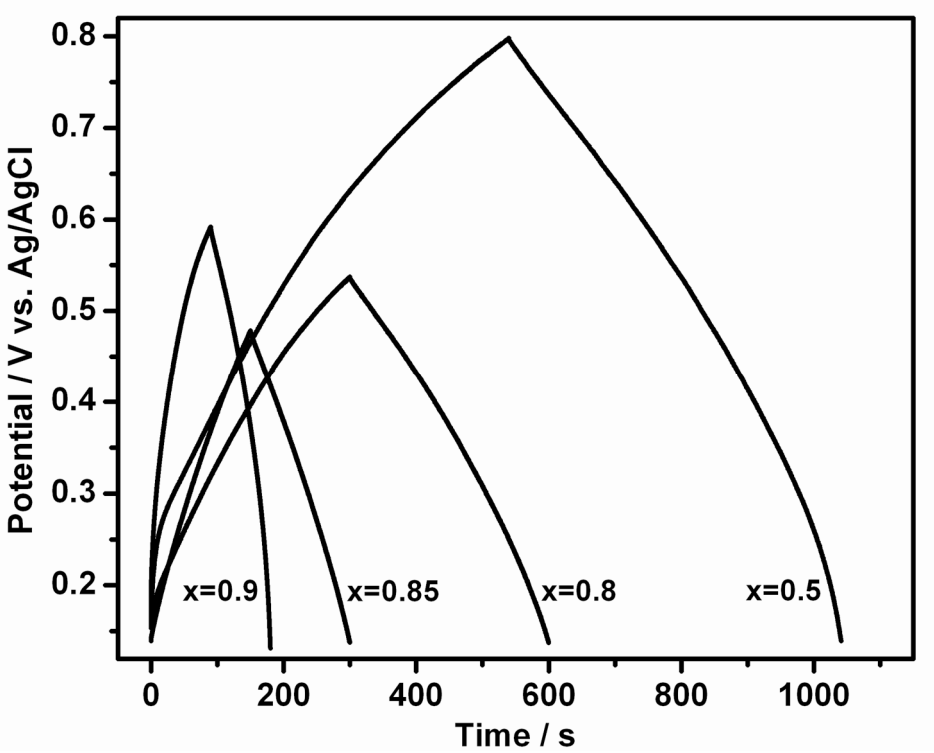

Figure 4.67: Galvanostatic charge/discharge curve of BTh and ENBTE copolymers with different mole fractions.

The other important parameters are loading and unloading current, discharge time and the potential change during the discharge process. The specific gravimetric capacitances can be calculated from the following equation where, C_g is the specific capacitance (F/g), I is the loaded current, Δt is the discharge time and ΔV is the potential change during the discharge process.

$$C_g = I\Delta t / \Delta V \qquad \textbf{(4.17)}$$

Slope of the charge/discharge curve is 0.9985 and -0.9998 respectively indicates that IR drop is negligible and triangular shape of the charge discharge curve is typical for ideal capacitor behavior indicates that very good capacitive performance.

After this brief information one can conclude from the Figure 4.67 as the mole fraction of the BTh in the solution increase that also means increase in BTh in the copolymer composition, specific gravimetric capacitance of the copolymer electrode is decreased as expected. Specific gravimetric capacitances calculated as 830 mF g^{-1}, 770 mF g^{-1}, 462 mF g^{-1}, and 196 mF g^{-1} for the mole fractions of x=0.5, 0.8, 0.85 and 0.90 respectively.

4.7.3. ATR-FTIR characterizations of the BTh and ENBTE copolymers

Copolymer films of bithiophene and ENBTE prepared by potentiostatic deposition method onto carbon fiber micro electrodes were analyzed by ATR-FTIR spectroscopy to confirm the presence of the both monomers inside the copolymer. Figure 4.68 shows the corresponding spectra between 4000 and 650 cm^{-1}. Comparison of the ATR-FTIR spectra of the CFME (see Appendix Figure A.3 for the ATR-FTIR of bare CFME), BTh and ENBTE show the incorporation of both BTh and ENBTE comonomers to the resulting copolymer. The very sharp peak just above the 1000 cm^{-1} is assigned to the CFME. The dotted lines in the Figure are characteristics peaks belong to the PENBTE and intensity of these peaks increase as the mole fraction of the PENBTE is increase in the composition of the copolymer.

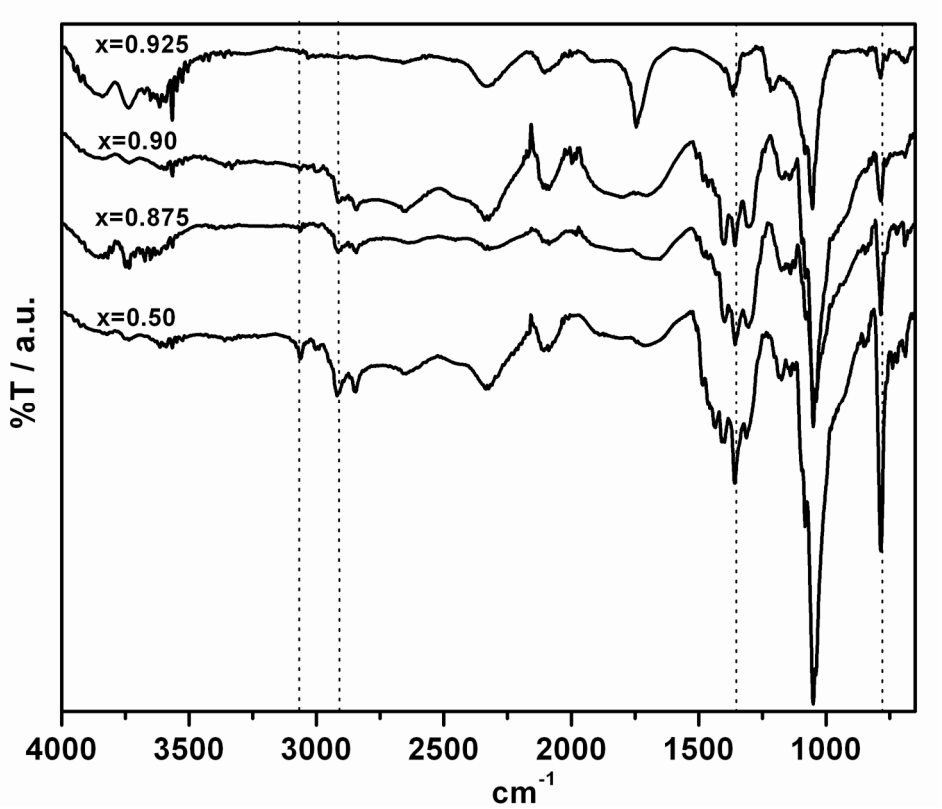

Figure 4.68: ATR-FTIR spectra of the copolymers of BTh and ENBTE which were prepared onto CFME with different mole ratios.

4.7.4. Morphology of the BTh and ENBTE copolymers

The morphologies of the oxidized copolymers of BTh and ENBTE on CFME were investigated comparatively by FE-SEM. We have previously presented FE-SEM of the homopolymer of BTh in Figure 4.12 which yields very thin films. In this case copolymerization with ENBTE at higher mole ratios of BTh a globular structure

resulting from a three-dimensional nucleation growth is observed (See Figure 4.69b and 4.70).

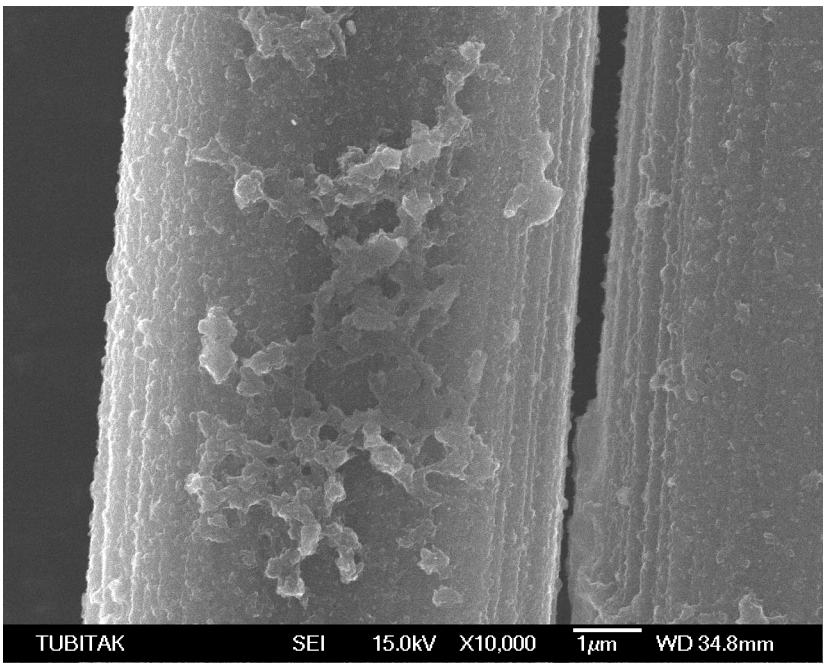

Figure 4.69: FE-SEM images of the BTh and ENBTE copolymers deposited with a charge of **(a)** 2.262 C cm^{-2} and mole ratio of 0.5 at 10000 magnification.

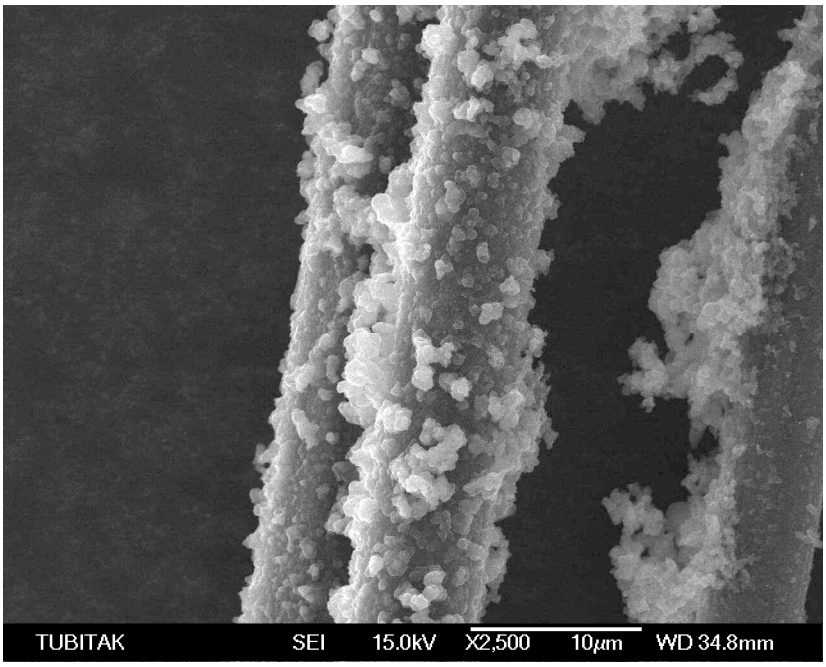

Figure 4.69: (b) 3.076 C cm^{-2} and mole ratio of 0.8 at 2500 magnification.

The morphology of PENBTE (see Figure 4.43) is different from PBTh. At a mole ratio of x=0.5 presumably the highest incorporation of ENBTE into the copolymers structure more homogenous film was observed. Sizes of the globules are almost same size at the mole ratios of 0.8 and 0.875. FE-SEM pictures of these films have shown

that incorporation of more ENBTE to the resulting copolymer makes the surface smoother and less globular structure and fewer voids monitored on the surface of the electrode. This surface morphology might be an explanation of why better capacitive behavior was observed at lower mole ratios of BTh.

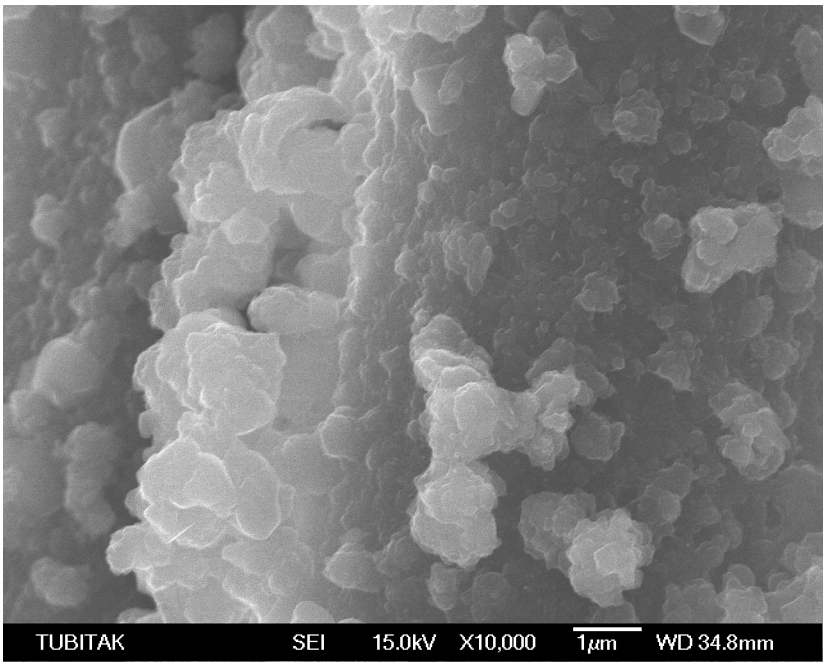

Figure 4.70: FE-SEM images of the BTh and ENBTE copolymers deposited with a charge of **(a)** 3.076 cm^{-2} and mole ratio of 0.8.

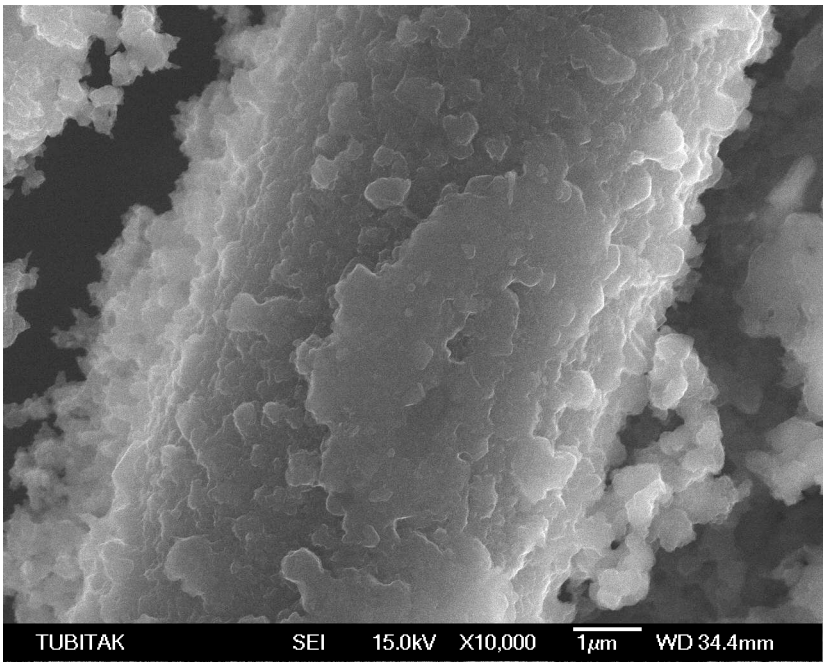

Figure 4.70: (b) 5.539 C cm^{-2} and mole ratio of 0.875 at 10000 magnifications.

4.8. Electrocopolymerization and Characterization of EDOT and ENBTE

4.8.1. Electrochemical Copolymerization

The oxidative electrochemical copolymerization of EDOT monomer and ENBTE comonomer was carried out via cyclic voltammetry and chronopotentiometry. A structural representation of the reaction taking place during electrochemical copolymerization is illustrated in equation (4.18).

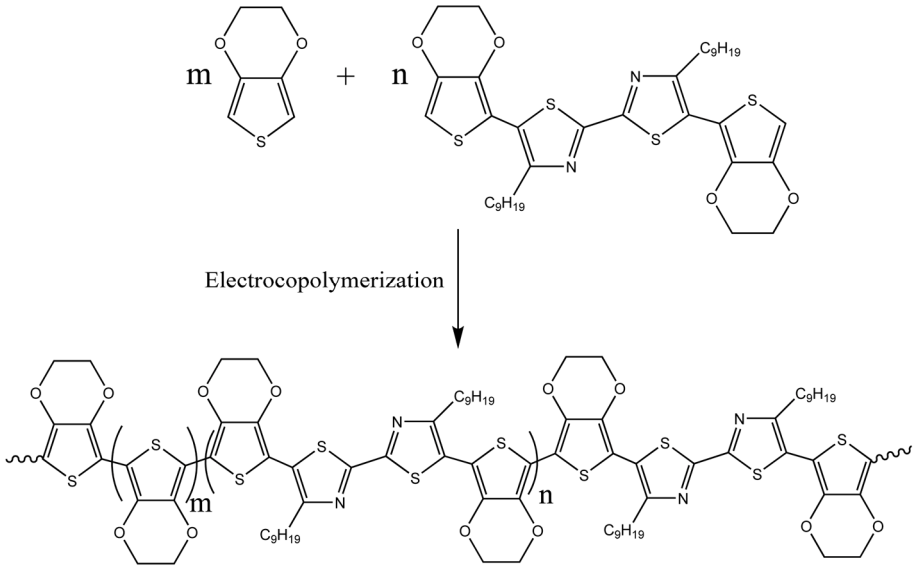

(4.18)

If it is assumed that both EDOT and ENBTE oxidize at the same potential, then radical cations of both monomers are formed simultaneously at the working electrode surface which then reacts with each other. It is expected that since both radical cations will be form on the EDOT so there is no preference shown between reactive species, resulting in the formation of a random copolymer.

We have prepared homopolymer of the ENBTE comonomer, as explained in previous sections and prepared homopolymer of the EDOT as shown in Figure 4.71, to confirm both their oxidation potentials adequate to ensure copolymerization so that both monomers must oxidize to form their reactive radical cations at oxidation potentials close to each other. Monomer oxidation potential of EDOT in the case of CMFE as a working electrode is 1.307 V vs. Ag/AgCl and ENBTE comonomer as monomer oxidation potential of +0.954 V vs Ag/AgCl.

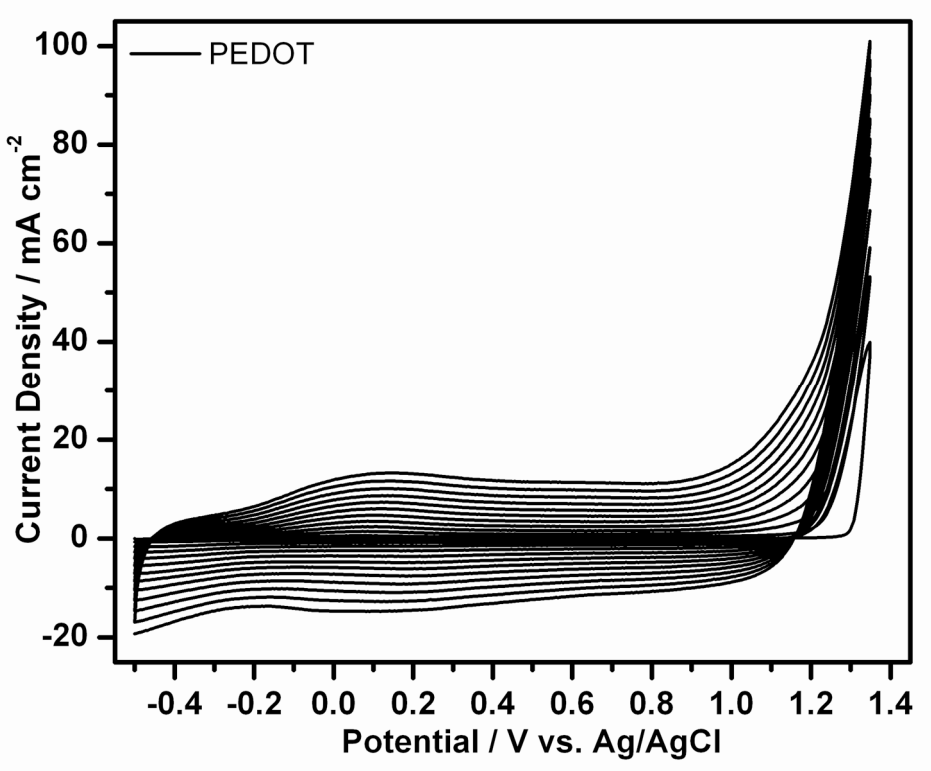

Figure 4.71: Electropolymerization of EDOT on CFME from 0.005 M in 0.1M Et_4NBF_4/ DCM solution by potential sweep between -0.5 V and 1.35 at a scan rate of 20mV s^{-1}. Q_{dep}=7.074 C cm^{-2}.

Thin films of PEDOT, PENBTE and copolymers of EDOT and ENBTE with different mole fractions were deposited on CFMEs both potentiodynamically and galvanostatically. Figure 4.72 represents potentiodynamic electrocopolymerization of the EDOT and ENBTE with a mole ratio of x=0.6. Copolymer films were obtained from the mixture of both monomers with different mole fractions. The mole fractions, monomer oxidation onset potentials of copolymerizations, and half wave potentials of the polymers are given Table 4.14. The cyclic voltammograms of these films are compared for different mole fractions and are given in Appendix Figure H.1 and H.2.

Following electrocopolymerizations, polymer films were rinsed in monomer free electrolyte solution to remove surface bound monomers and oligomers and then two voltammograms of the copolymer films were recorded over the potential range for complete copolymer oxidation and reduction as shown in Figure 4.73. The second cycles are reported in each case. All the copolymers are electroactive with different characters depending on the mole fractions. As we explained earlier that EDOT and ENBTE comonomer monomers have different oxidation potentials (1.307 V and

0.954 V vs Ag/AgCl., respectively) and $E_{1/2}$ of their polymer films. This characteristic of monomers and polymers suggest the use of different mole fractions of monomer solutions for the copolymerizations. Since EDOT monomer is more difficult to oxidize, the concentration of this monomer was kept high compared to ENBTE. The reason for use of high concentrations of EDOT can easily be seen from Figure 4.73.

Table 4.14: Mole fractions, the on set potentials of polymerizations, and half wave potentials of the EDOT and ENBTE comonomers.

$x_{EDOT} = \frac{m_{EDOT}}{m_{EDOT} + m_{ENBTE}}$	$E_{onset,\ m}$	1. peak $E_{1/2}$	2. peak $E_{1/2}$	3. peak $E_{1/2}$
$x = 1$	1.307	-0.186	0.420	-
$x = 0.95$	1.025	-0.167	0.395	0.772
$x = 0.90$	0.998	-0.114	0.347	0.778
$x = 0.85$	0.987	-0.104	0.434	0.860
$x = 0.60$	0.953	-0.145	0.235	0.742
$x = 0$	0.954	-	0.304	0.814

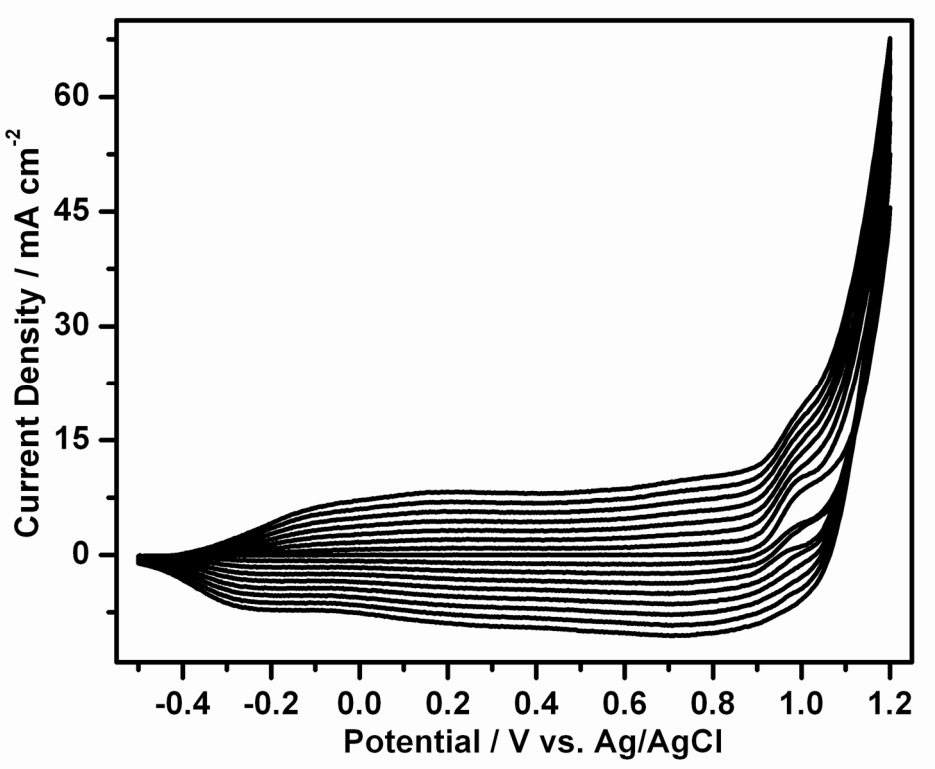

Figure 4.72: Electrocopolymerization of EDOT and ENBTE at a mole ratio of (x=0.6) in 0.1M Et_4NBF_4/ DCM solution by potential sweep between -0.5 V and 1.2 at a scan rate of 20mV s^{-1}. Q_{dep}=3.810C cm^{-2}.

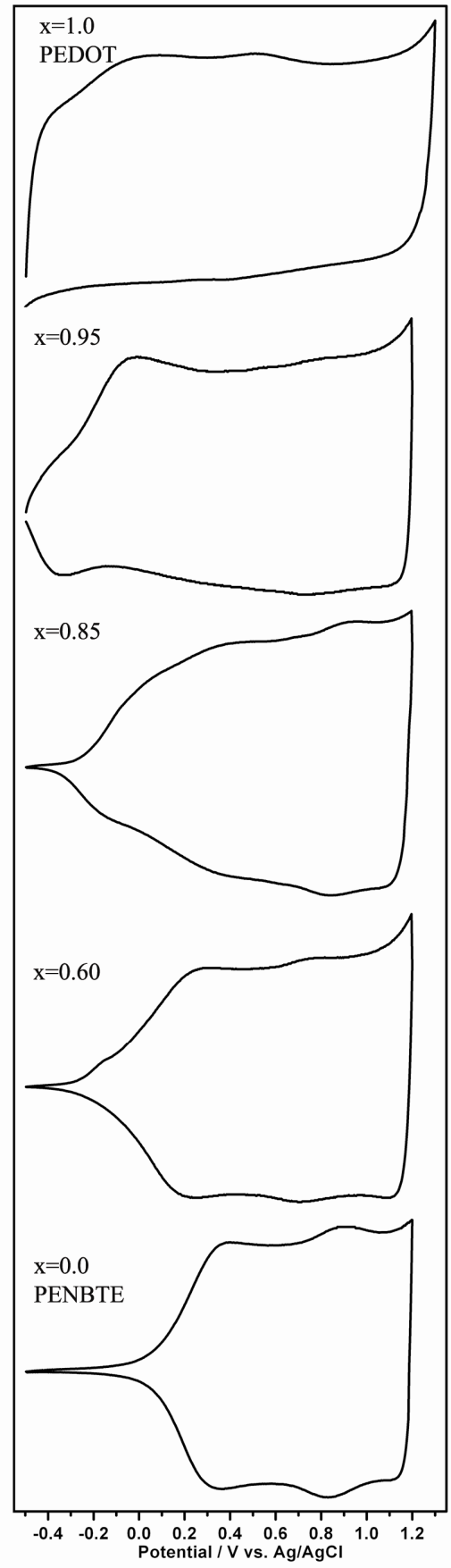

Figure 4.73: Redox behavior of the EDOT and ENBTE comonomers at different mole ratios in monomer free electrolyte solution at a scan rate of 100 mV s^{-1}.

Copolymers were characterized in monomer-free electrolyte solution at the following scan rates: 20, 40, 60, 80, 100, 120, 140, 160, 180 and 200 mV s^{-1}. (Scan rate dependency plots of some selected mole fractions are given in Appendix I.1 and I.2) All of the copolymer films of the all of the copolymers exhibits very well defined reversible oxidation processes and half wave potentials of the corresponding oxidation and reduction peaks are given in Table 4.14. The anodic and cathodic peak currents are linear in scan rate dependence between 20 mV s^{-1} and 200 mV s^{-1}. This demonstrates that the electrochemical processes are not diffusion-limited and are reversible, even at high scan rates.

Homopolymers of both monomers exhibits two redox peaks at different potentials. Redox peaks of PEDOT appear at -0.186V and 0.420V, and redox peaks of PENBTE were observed at 0.304V and 0.814V in our experimental condition that is CFME and in 0.1M Et_4NBF_4/DCM solution. Peaks that are observed in the middle of the -0.5 and 1.2V sweep range slightly overlap yielding a broader peak.

The three peak oxidation of EDOT and ENBTE are present in all copolymers shown in Figure 4.64, in the low potential region redox behavior characteristics for EDOT an overlapping peak for both monomers and redox peak belong to ENBTE comonomer indicating that each comonomer is being incorporated into the copolymer chain. As the concentration of ENBTE increased redox peaks belong to this comonomer becomes clearer, and current density of the redox peaks in the lower potential region. Due to high concentration of the EDOT comonomer, current densities produced by this monomer is higher at higher concentrations (for example x=0.95) first peaks produces high current density. Onset potential of copolymerization significantly decreases as the mole fraction of ENBTE in solution is increased.

4.8.2. EIS Studies on EDOT and ENBTE Copolymers

EIS measurements were performed to find out electrochemical characteristics of the prepared copolymers for all studied mole fractions of at different applied potentials in the range of -0.5 to 1.2 V with a potential step of 0.1V to cover entire electroactivity range of the prepared copolymers. As we explained in previous sections PENBTE shows electroactivity and starts exhibit capacitive behavior at an electrode potential of 0.3V. Incorporation of the EDOT which demonstrates

electroactivity in lower potential range compared to the PENBTE into the copolymer chain might bring an advantage to cover wider potential range. Capacitance calculations from the CV of the copolymer (results are not given) support this idea.

We have prepared a set of copolymer electrodes that were prepared with a charge of 3 C cm^{-2} as we previously done. Figure 4.74 illustrates specific capacitance values of copolymer electrodes which are prepared with a charge of 3 C cm^{-2}. The low frequency capacitance values from impedance spectroscopy were obtained from the slope of a plot of the imaginary component (Z_{IM}) of the impedance at low frequencies versus inverse of the reciprocal frequency (*f*).

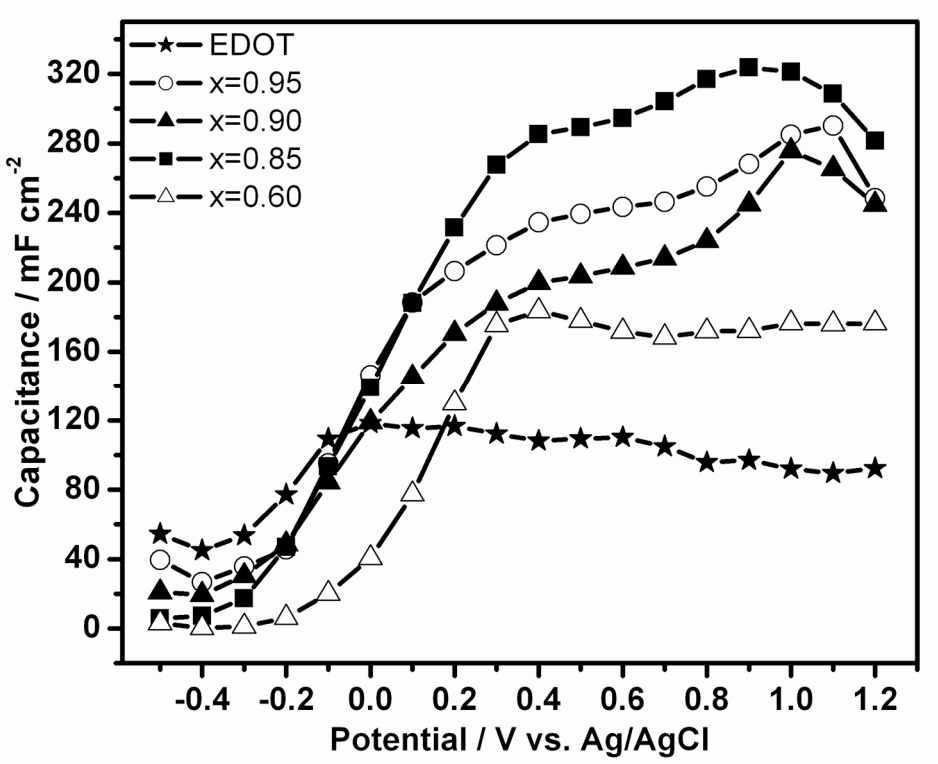

Figure 4.74: Low frequency capacitance values of the copolymers of EDOT and ENBTE at different mole fractions deposited with a charge of 3 C cm^{-2}.

Specific capacitance curves present obtained at low frequencies perfectly overlaps with their redox behavior in monomer free solution. For instance specific capacitance behavior of the PEDOT which symbolized with stars in Figure 4.74 is a good example. As it can barely seen from the Figure 4.74 low frequency capacitance values confirms that incorporation of the EDOT into the copolymer structure broadens capacitance behavior of the PENBTE monomer to lower potential region. The highest capacitance behavior of the copolymer was obtained at the mole fraction of 0.85. The copolymer electrode which starts to exhibit capacitive behavior at a

potential of -0.3V to 1.2V with a total range of 1.5V that is 0.4V wider potential range compared to PENBTE itself.

We have successfully applied electrical equivalent circuit model 1 (See Figure 4.50a) which is previously suggested for PENBTE polymer electrodes. We have obtained best results in correlation between experimental data and calculated in this thesis. The excellent agreement with experimental and calculation results can be seen from chi-squared values in Table 4.15 and very well overlapping data points in Figures 4.75 and 4.76.

Table 4.15: Values of the equivalent circuit components which given in Figure 4.50a by mole fraction of EDOT and ENBTE copolymer.

	Mole Fraction					
	EDOT	**x=0.95**	**x=0.90**	**x=0.85**	**x=0.60**	**ENBTE**
R_S / Ohm cm^2	1.109	0.765	0.6134	0.5525	1.125	0.7508
C_{dl} / F cm^{-2}	0.06277	0.03689	0.04461	0.1894	0.1234	0.18
R_1 / Ohm cm^2	0.294	0.2579	0.5113	0.3401	0.7674	0.4223
CPE_1; Y_o/ S s^{-n} cm^{-2}	0.08442	0.0365	1.989	0.08327	0.05016	0.083
n	0.9734	0.9672	0.9703	0.9702	0.9665	0.9557
R_2 / Ohm cm^2	3.516	$3.03x10^{+4}$	0.01	985.1	1053	992.4
W; Y_o / S $s^{-0.5}$ cm^{-2}	$2.71x10^{-11}$	0.000115	$2.17x10^{-17}$	0.002832	0.002371	0.001883
C_{CF} / F cm^{-2}	2.66	0.03756	0.002297	0.09676	0.04006	0.01738
R_{CF} / Ohm cm^2	0.6534	0.0149	0.0544	0.01202	0.02927	0.01
Chi-squared	$5.12x10^{-5}$	$4.67x10^{-5}$	$5.28x10^{-5}$	$3.41x10^{-5}$	$3.95x10^{-5}$	$4.70x10^{-5}$

Figure 4.75 shows complex plane impedance plot of the copolymers, all of the copolymers demonstrate very high phase angle almost vertical line to the imaginary part of the impedance. Highest imaginary impedance obtained at a mole fraction of 0.85. Inset 2 very well demonstrates impedance behavior of the copolymers. Nyquist plots of the PEDOT and the copolymer prepared with a mole fraction 0.60 was perfectly converged. The copolymer which prepared with a mole fraction of 0.85 exhibits best capacitive behavior that was observed in the left hand side of inset 2 with a phase angle of higher than (-88°)

The Bode magnitude plots shows linear drop in the low frequency region with a slope of -1 which is typical for ideal capacitors to (-45°) phase angle where bending occurs in the Bode magnitude plot and electrode starts to behave as a resistor. The frequency of -45° phase angle values ranged from 0.5 to 1 Hz, giving the response time of the capacitor as 2s to 1s. Drop in Bode magnitude of 0.85 mole fraction

condition is less than 60 Ohm cm^2 and is around 200 Ohm cm^2 at 0.95 mole fractions. Bode phase angle graphs show similar tendencies. Their shapes demonstrate similar fashion at higher mole fractions in the middle frequency region a 10 Hertz shift was observed.

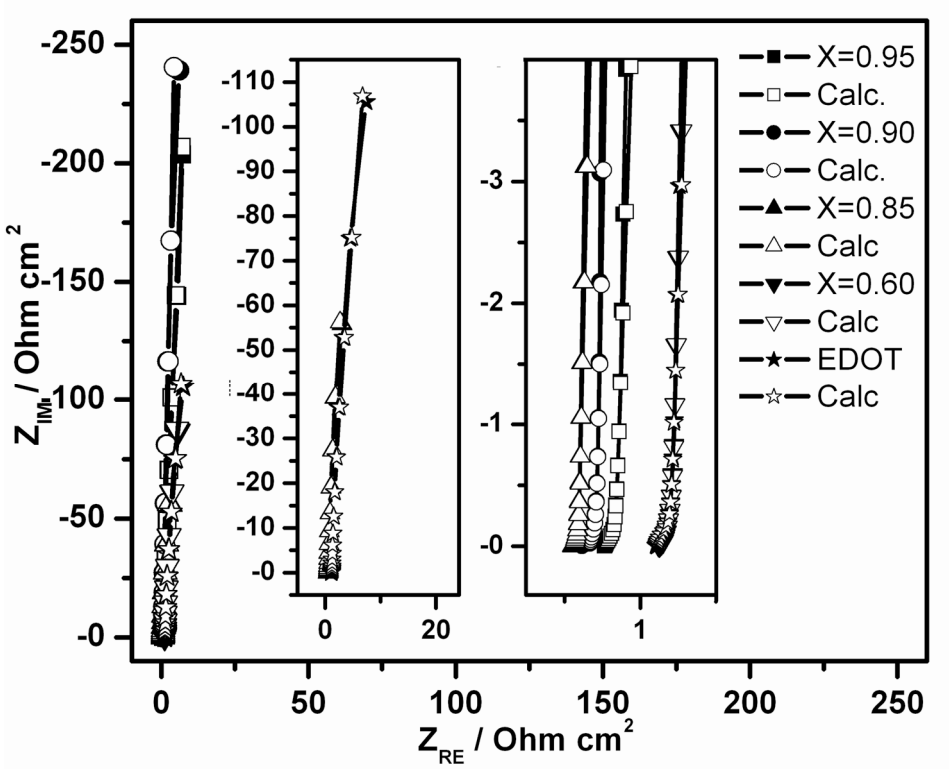

Figure 4.75: Complex plane impedance plots of the copolymers at different mole fractions and homopolymer of EDOT. Inset 1: An expanded view for EDOT and the copolymer at 0.60 mole ratio. Inset 2: An expanded complex plane view of the high frequency region. Results are given with calculation fit in open interior symbols.

The galvanostatic charge discharge characteristics of the copolymer electrodes of EDOT and ENBTE were investigated with a current density of 1 mA cm^{-2} and results are presented in the Figure 4.77. Triangular charge discharge curves were observed in all of the investigated mole fractions which show excellent behavior of both monomers for capacitor applications. At higher mole fractions, i.e. 0.95 and 0.90, charge discharge curves quite similar. As the inclusion of more ENBTE into the structure is an increase specific gravimetric capacitances is increase.

After this brief information one can conclude from the Figure 4.77 as the mole fraction of the ENBTE in the solution is increased, specific gravimetric capacitance of the copolymer electrode is increased. Specific gravimetric capacitances around 6200 mF g^{-1}, 480 mF g^{-1}, 400 mF g^{-1}, and 360 mF g^{-1} for the mole fractions of x=0.6, 0.8, 0.9 and 0.95 respectively.

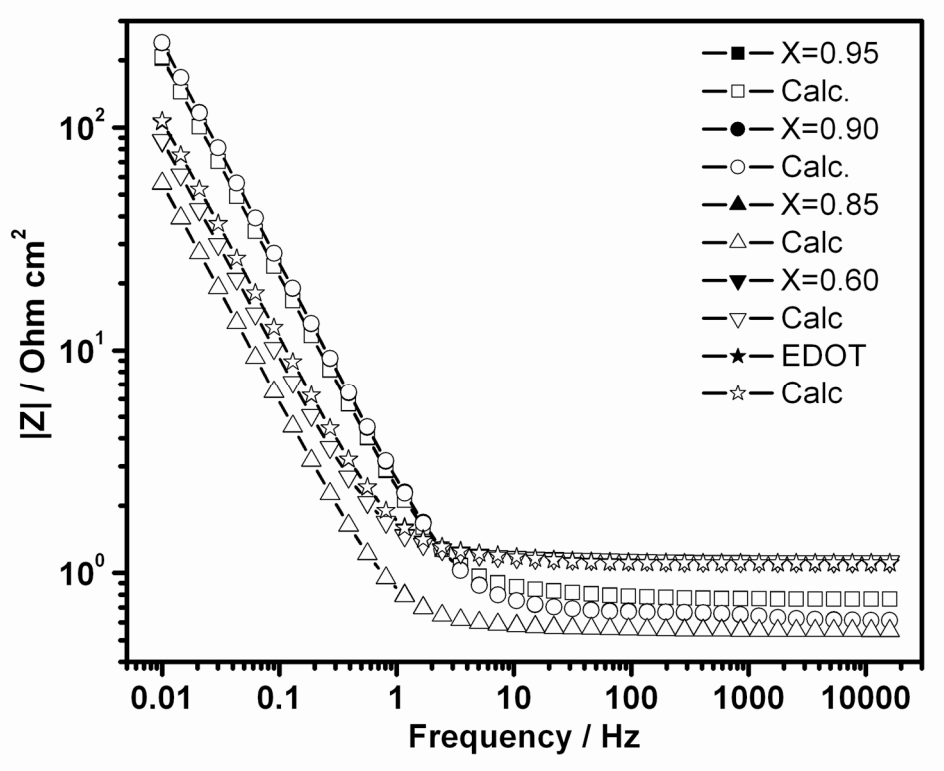

Figure 4.76: Frequency dependency plots of the copolymers at different mole fractions and homopolymer of EDOT **(a)** Bode magnitude |Z| plots.

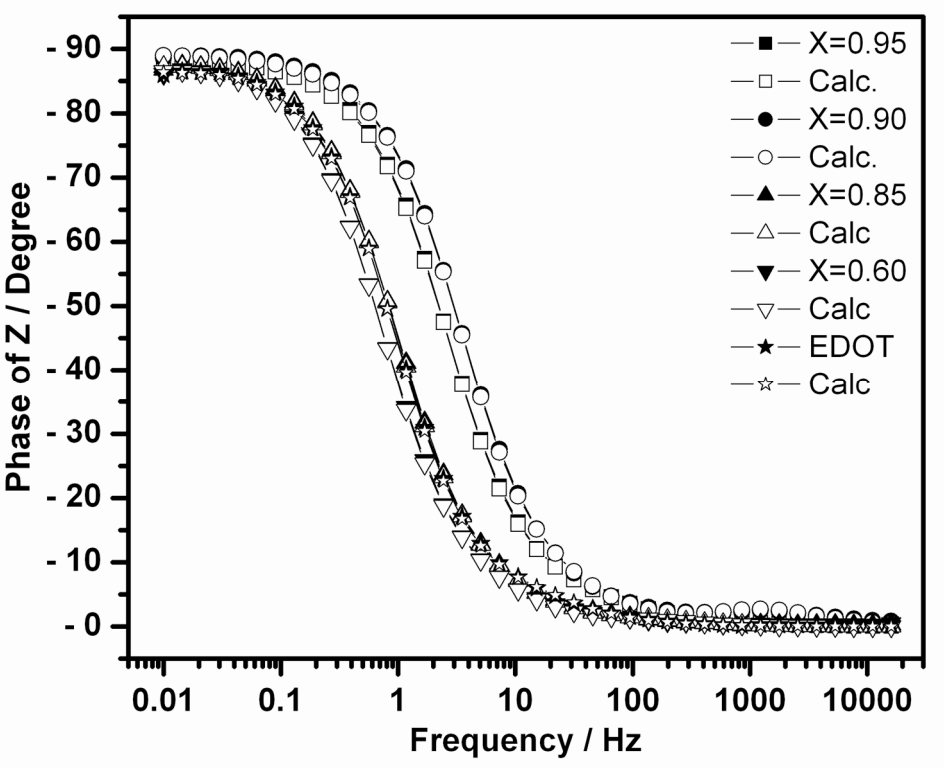

(b) Bode phase angle plots with calculation data.

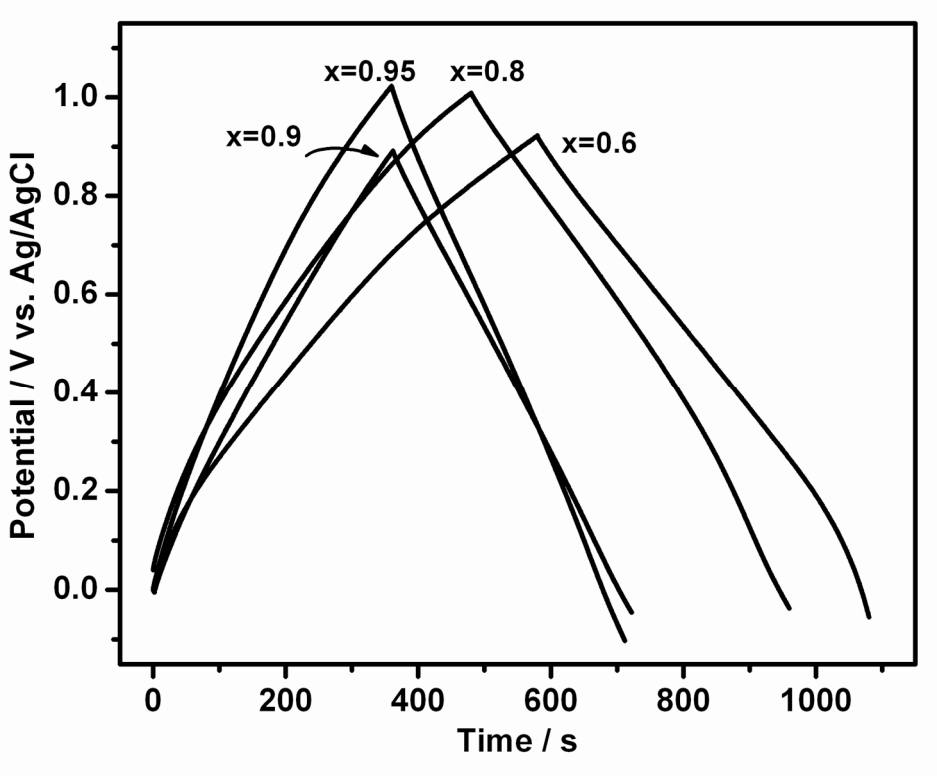

Figure 4.77: Galvanostatic charge/discharge curve of EDOT and ENBTE copolymers with different mole fractions.

4.8.3. FE-SEM study on the copolymers of EDOT and ENBTE

The morphologies of EDOT and ENBTE copolymers on CFME were investigated comparatively by FE-SEM. Figure 4.78a illustrates image of FE-SEM a galvanostatically deposited PEDOT homopolymer with a charge of 2 C cm^{-2}. PEDOT homogeneously covers the surface of the carbon fiber with a thin film average thickness of the film is around 0.1 micrometers. As the incorporation of the ENBTE into copolymer structure at 5 percentage 4.78b morphology of the copolymer completely changes huge globular structures form on the surface which are typical for PENBTE at high deposition charges see Figure 4.61c, at this mole ratio irregular distribution of the polymer globules were observed. Distribution of globular very homogeneous which was produced very thin films. In this case copolymerization with ENBTE at higher mole ratios of BTh a globular structure resulting from a three-dimensional nucleation growth is observed (See Figure 4.69b and 4.70). As the mole ratio of ENBTE increase in the solution very homogenously distributed interesting cubic structures were observed. This might be incorporation of the electrolyte into the structure but crystalline structures and the π-stacking properties of the alkylbithiazole structures are reported in the literature [18], we

believe in ENBTE promotes formation of this type formations. See more FE-SEM images in Appendix Figure B.5 and B.6.

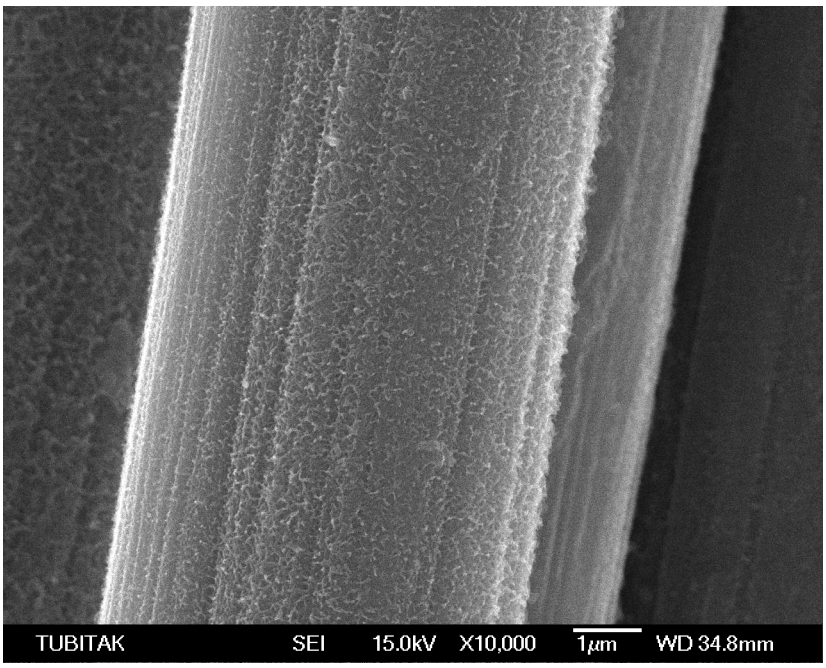

Figure 4.78: FE-SEM image of **(a)** EDOT galvanostatically deposited with a charge of 2 C cm^{-2} and

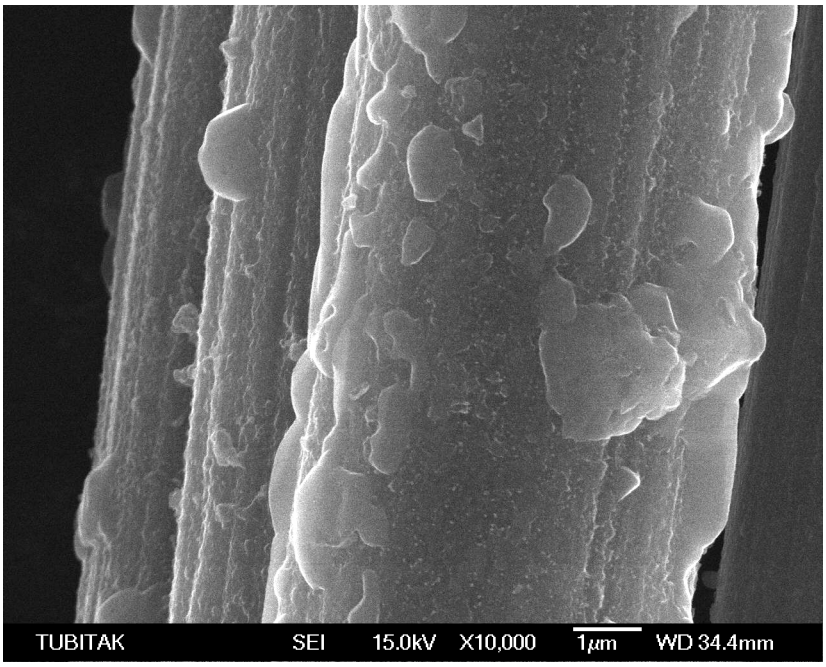

Figure 4.78: (b) FE-SEM image of EDOT and ENBTE copolymer with a deposition charge 1.663 C cm^{-2} and mole ratio of 0.95 on CFME at 10000 magnifications.

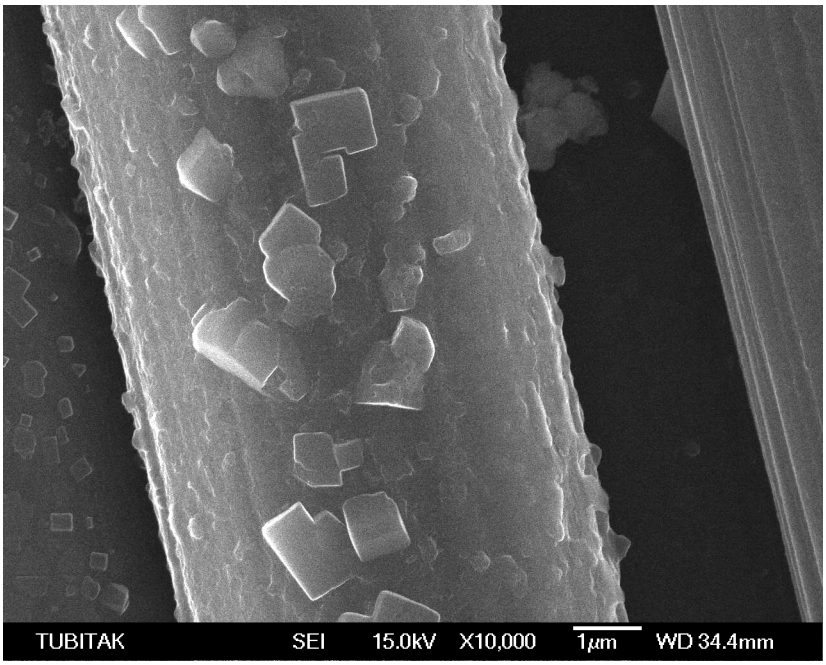

Figure 4.79: FE-SEM image of **(a)** EDOT galvanostatically deposited with a charge of 2 C cm^{-2} and mole ratio of 0.85.

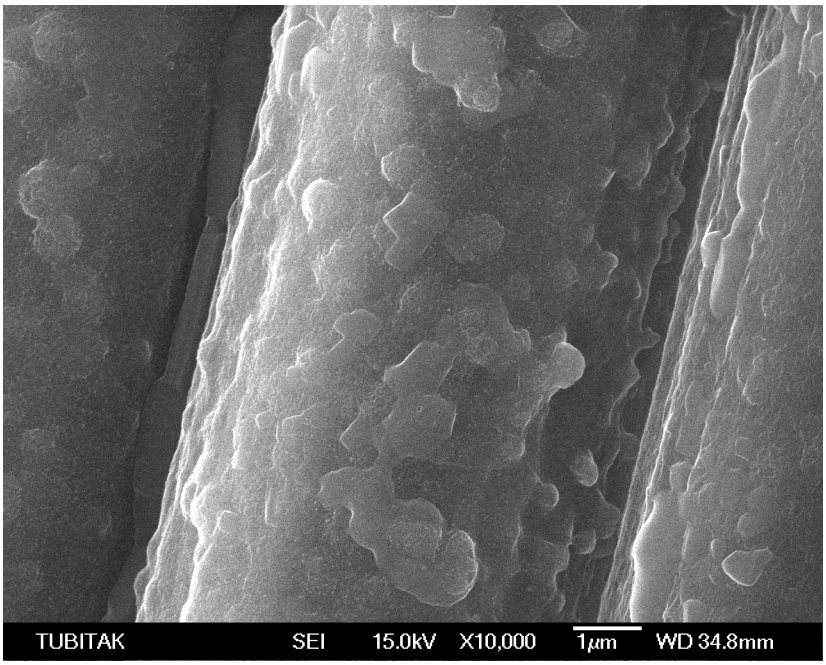

Figure 4.79: (b) FE-SEM image of a potentiodynamically deposited copolymer of EDOT and ENBTE charge 2.262 C cm^{-2} and mole ratio of 0.60 on CFME at 10000 magnifications.

5. CONCLUSIONS

This thesis was concentrated on synthesis and characterizations of novel thiophene and alkylbithiazole based comonomers, preparation of their polymers onto carbon fiber microelectrodes by electrochemical polymerization and including their electrochemical characterizations and morphological studies. Testing the polymer films in the use electrochromic device construction and polymer electrodes on CFME as an active electrode material in supercapacitor applications are the final steps of this thesis.

In the first step of this thesis five different comonomers based on thiophene and alkylbithiazole moieties were synthesized. We observed that two of these comonomers which were prepared at the early stages of this study are not electrochemically polymerizable. After this unsuccessful synthesis studies we have adopted a new strategy and integrated long alkyl chains on thiazole rings and added thiophene and a popular thiophene derivative namely EDOT outer part of the moiety. EDOT has only one site allow to formation of radical cation after comonomer synthesis this is a superior advantage to have extremely regular polymer formation.

Electrochemical polymerizations of 2,2'-bithiophene, thiophene-nonylbithiazole-thiophene and edot-nonylbithiazole-edot comonomers were successfully carried out. Especially ENBTE comonomer was produced very high quality polymers offering several multifunctional advantages. In order to further increase these properties of PENBTE, we have prepared and investigated copolymers of this comonomer with bithiophene and EDOT.

Electrochemical Impedance Spectroscopy is a very powerful tool for the analysis of electrochemical systems. We have soberly used this technique to explain electrochemical characteristics of the polymer electrodes like resistance, capacitance impedance. Then we have proposed several electrical equivalent circuits corresponding to the polymer electrodes and calculated values of the each component of these circuits using a simulation program which we found excellent agreements with experimental and calculation data.

Initial device properties based on PENBTE were checked with switching properties and results shows that 0.25 s is short enough to use as electrochromic applications. Stability of the film was supported from the spectroelectrochemical and FE-SEM measurements. Typical CV of the polymeric film exhibits a double very well-defined and reversible redox processes. The current response of the film was directly proportional to the scan rate indicating a diffusion limited process [38], showing that the polymer film is electroactive from 0.1 V to 1.2 V and sufficiently well to ensure a rapid film charging and discharging. All results suggest the high quality film deposition that results in desired electronic properties due to the presence of long alkyl chain as initially it was aimed. The impedance study on capacitive properties of the EDOT and novel ENBTE comonomer on CFME revealed that high capacitance values observed in low frequency region.

Several equivalent circuits were used in simulation of the impedance behavior of the polymer films from the experimentally obtained impedance data. The model (See Figure 4.50a) was used in the electroactive region (i.e. 0.3V to 1.2V) of the polymer electrodes of TNBTT, PENBTE and its copolymers with BTh and EDOT. This electrical equivalent circuit was successfully applied to the experimental data to explain the interface between the carbon fiber microelectrode, the polymer film and the electrolyte in this potential region.

Charge discharge characteristics of a capacitor determines suitability for application in ideal case shape of the charge discharge curve is a triangle, slope of the both sides must be very close to unity. The slope the galvanostatic charge/discharge curve for PENBTE and its copolymers was found as high as 0.998 and -0.999 respectively indicates that IR drop is negligible and triangular shape of the charge discharge curve is typical for ideal capacitor behavior suggest that films offer very good capacitive performance.

We observed that the thickness of the polymer film is a function of number of cycles and increases linearly with the number of deposition charge during the electrodeposition as expected. A homogeneous coating was observed in the case of PENBTE film, and the polymer was deposited as a continuous and very well adhering film to the fiber surfaces. At higher deposition charges coating deposited on the CFME similarly exhibited homogeneous and uniformly distributed polymer globules along the carbon fiber. Such structures have formed by grafting of growing

polymer molecules on the fiber surface. Incorporation of BTh and EDOT into the structure of PENBTE changes the morphology of the resulting copolymer

From the obtained results, we can conclude that use of synthesized novel comonomers in polymer electrode shows very good capacitive behavior on carbon fiber microelectrode. The measured capacitance values are quite promising for supercapacitor constructions with a good engineering.

Table 5.1: A comparison of the capacitance results and onset potentials is given in the table.

	PBTh	**PTNBTT**	**PENBTE**	**PBTh-co-PENBTE**	**PEDOT-co-PENBTE**
C_g	-	-	500 mF g^{-1}	830 mF g^{-1}	620 mF g^{-1}
C_{DL}	10.5 mF cm^{-2}	6.6 mF cm^{-2}	224 mF cm^{-2}	584 mF cm^{-2}	189 mF cm^{-2}
C_{LF}	120 mF cm^{-2}	90 mF cm^{-2}	300 mF cm^{-2}	600 mF cm^{-2}	320mF cm^{-2}
Electroactivity Range	0.8-1.2V Range 0.4V	0.8-1.5V Range 0.7V	0.3-1.2V Range 0.9V	0.1-1.2V Range 1.1V	-0.2-1.2V Range 1.4V
Onset Potential	E=1.246V	E=1.096V E_{Th}=1.8V	E=0.954V E_{EDOT}=1.307V	E=0.972V X=0.5	E=0.987V X=0.85

REFERENCES

[1] **Shirakawa, H., Louis, E. J., Macdiarmid, A. G., Chiang, C. K. and Heeger, A. J.,** 1977. Synthesis of Electrically Conducting Organic Polymers - Halogen Derivatives of Polyacetylene, (Ch)X,

[2] **Inzelt, G., Pineri, M., Schultze, J. W. and Vorotyntsev, M. A.,** 2000. Electron and proton conducting polymers: recent developments and prospects, *Electrochimica Acta,* **45,** 2403-2421.

[3] **Halls, J. J. M., Walsh, C. A., Greenham, N. C., Marseglia, E. A., Friend, R. H., Moratti, S. C. and Holmes, A. B.,** 1995. Efficient Photodiodes from Interpenetrating Polymer Networks, *Nature,* **376,** 498-500.

[4] **Kraft, A., Grimsdale, A. C. and Holmes, A. B.,** 1998. Electroluminescent conjugated polymers - Seeing polymers in a new light, *Angewandte Chemie-International Edition,* **37,** 402-428.

[5] **Rauh, R. D., Wang, F., Reynolds, J. R. and Meeker, D. L.,** 2001. High coloration efficiency electrochromics and their application to multi-color devices, *Electrochimica Acta,* **46,** 2023-2029.

[6] **Sonmez, G., Meng, H., Zhang, Q. and Wudl, F.,** 2003. A highly stable, new electrochromic polymer: Poly(1,4-bis(2-(3(,)' 4 ' ethylenedioxy)thienyl)-2-methoxy-5-2 "-ethylhexyloxybenzene), *Advanced Functional Materials,* **13,** 726-731.

[7] **Jonas, F. and Schrader, L.,** 1991. Conductive Modifications of Polymers with Polypyrroles and Polythiophenes, *Synthetic Metals,* **41,** 831-836.

[8] **Heywang, G. and Jonas, F.,** 1992. Poly(Alkylenedioxythiophene)S - New, Very Stable Conducting Polymers, *Advanced Materials,* **4,** 116-118.

[9] **Granstrom, M., Berggren, M. and Inganas, O.,** 1995. Micrometer-Sized and Nanometer-Sized Polymeric Light-Emitting-Diodes, *Science,* **267,** 1479-1481.

[10] **Heuer, H. W., Wehrmann, R. and Kirchmeyer, S.,** 2002. Electrochromic window based on conducting poly (3,4-ethylenedioxythiophene)poly(styrene sulfonate), *Advanced Functional Materials,* **12,** 89-94.

[11] **Kvarnstrom, C., Neugebauer, H., Blomquist, S., Ahonen, H. J., Kankare, J. and Ivaska, A.,** 1999. In situ spectroelectrochemical characterization of poly(3,4-ethylenedioxythiophene), *Electrochimica Acta,* **44,** 2739-2750.

[12] **Carlberg, J. C. and Inganas, O.,** 1997. Poly(3,4-ethylenedioxythiophene) as electrode material in electrochemical capacitors, *Journal of the Electrochemical Society,* **144,** L61-L64.

[13] **Sapp, S. A., Sotzing, G. A., Reddinger, J. L. and Reynolds, J. R.,** 1996. Rapid switching solid state electrochromic devices based on complementary conducting polymer films, *Advanced Materials,* **8,** 808-&.

[14] **Sotzing, G. A., Reynolds, J. R. and Steel, P. J.,** 1997. Poly(3,4-ethylenedioxythiophene) (PEDOT) prepared via electrochemical polymerization of EDOT, 2,2'-bis(3,4-ethylenedioxythiophene) (BiEDOT), and their TMS derivatives, *Advanced Materials,* **9,** 795-&.

[15] **Gonzalez-Ronda, L., Martin, D. C., Nanos, J. I., Politis, J. K. and Curtis, M. D.,** 1999. Structural characterization of electrooptically active poly(nonlbithiazole), *Macromolecules,* **32,** 4558-4565.

[16] **Nanos, J. I., Kampf, J. W. and Curtis, M. D.,** 1995. Poly(alkylbithiazoles): A new class of variable-bandgap, conjugated polymer, *Chemistry of Materials,* **7,** 2232-2234.

[17] **Koren, A. B., Curtis, M. D. and Kampf, J. W.,** 2000. Crystal engineering of conjugated oligomers and the spectral signature of pi stacking in conjugated oligomers and polymers, *Chemistry of Materials,* **12,** 1519-1522.

[18] **Yamamoto, T., Suganuma, H., Maruyama, T., Inoue, T., Muramatsu, Y., Arai, M., Komarudin, D., Ooba, N., Tomaru, S., Sasaki, S. and Kubota, K.,** 1997. pi-conjugated and light emitting poly(4,4'-dialkyl-2,2'-bithiazole-5,5'-diyl)s and their analogues comprised of electron-accepting five-membered rings. Preparation, regioregular structure, face-to-face stacking, and electrochemical and optical properties, *Chemistry of Materials,* **9,** 1217-1225.

[19] **Yamamoto, T., Suganuma, H., Maruyama, T. and Kubota, K.,** 1995. Poly(4,4'-Dialkyl-2,2'-Bithiazole-5,5'-Diyl) - New Electron-Withdrawing Pi-Conjugated Polymers Consisting of Recurring 5-

Membered Rings, *Journal of the Chemical Society-Chemical Communications,* 1613-1614.

[20] **Yamamoto, T., Maruyama, T., Zhou, Z. H., Ito, T., Fukuda, T., Yoneda, Y., Begum, F., Ikeda, T., Sasaki, S., Takezoe, H., Fukuda, A. and Kubota, K.,** 1994. Pi-Conjugated Poly(Pyridine-2,5-Diyl), Poly(2,2'-Bipyridine-5,5'-Diyl), and Their Alkyl Derivatives - Preparation, Linear Structure, Function as a Ligand to Form Their Transition-Metal Complexes, Catalytic Reactions, N-Type Electrically Conducting Properties, Optical-Properties, and Alignment on Substrates, *Journal of the American Chemical Society,* **116,** 4832-4845.

[21] **Politis, J. K., Curtis, M. D., Gonzalez, L., Martin, D. C., He, Y. and Kanicki, J.,** 1998. Synthesis and characterization of conjugated, n-dopable, bithiazole-containing polymers, *Chemistry of Materials,* **10,** 1713-1719.

[22] **Stille, J. K.,** 1986. The Palladium-Catalyzed Cross-Coupling Reactions of Organotin Reagents with Organic Electrophiles, *Angewandte Chemie-International Edition in English,* **25,** 508-523.

[23] **Curtis, M. D., Cheng, H. T., Johnson, J. A., Nanos, J. I., Kasim, R., Elsenbaumer, R. L., Ronda, L. G. and Martin, D. C.,** 1998. N-methylated poly(nonylbithiazole): A new n-dopable, conjugated poly(ionomer), *Chemistry of Materials,* **10,** 13-16.

[24] **Curtis, M. D., Cheng, H. T., Nanos, J. I. and Nazri, G. A.,** 1998. Reversible n-doping of poly(nonylbithiazole) and oligomeric model compounds. Application as a Li battery electrode, *Macromolecules,* **31,** 205-207.

[25] **Sarac, A. S. and Springer, J.,** 2002. Electrografting of 3-methyl thiophene onto carbon fiber: characterizatioi and carbazole random copolymer by FTIR-ATR, SEM, EDX, *Surface & Coatings Technology,* **160,** 227-238.

[26] **Sarac, A. S., Evans, U., Serantoni, M., Clohessy, J. and Cunnane, V. J.,** 2004. Electrochemical and morphological study of the effect of polymerization conditions on poly (terthiophene), *Surface & Coatings Technology,* **182,** 7-13.

[27] **Sarac, A. S., Sonmez, G. and Cebeci, F. C.,** 2003. Electrochemical synthesis and structural studies of polypyrroles, poly(3,4-ethylenedioxythiophene)s and copolymers of pyrrole and 3,4-

ethylenedioxythiophene on carbon fibre microelectrodes, *Journal of Applied Electrochemistry,* **33,** 295-301.

[28] **Sarac, A. S., Bismarck, A., Kumru, M. E. and Springer, J.,** 2001. Electrografting of poly(carbazole-co-acrylamide) onto several carbon fibers - Electrokinetic and surface properties, *Synthetic Metals,* **123,** 411-423.

[29] **Kumru, M. E., Springer, J., Sarac, A. S. and Bismarck, A.,** 2001. Electrografting of thiophene, carbazole, pyrrole and their copolymers onto carbon fibers: electrokinetic measurements, surface composition and morphology, *Synthetic Metals,* **123,** 391-402.

[30] **Sarac, A. S., Serantoni, M., Tofail, S. A. M. and Cunnane, V. J.,** 2005. Nanoscale characterization of carbazole-indole copolymers modified carbon fiber surfaces, *Journal of Nanoscience and Nanotechnology,* **5,** 1677-1682.

[31] **Sezer, E., Sarac, A. H. S. and Parlak, E. A.,** 2003. Electrochemical synthesis of EDOT-ECZ-EDOT copolymer on carbon fiber micro-electrodes, *Journal of Applied Electrochemistry,* **33,** 1233-1237.

[32] **Frackowiak, E. and Beguin, F.,** 2001. Carbon materials for the electrochemical storage of energy in capacitors, *Carbon,* **39,** 937-950.

[33] **Kotz, R. and Carlen, M.,** 2000. Principles and applications of electrochemical capacitors, *Electrochimica Acta,* **45,** 2483-2498.

[34] **Rudge, A., Davey, J., Raistrick, I., Gottesfeld, S. and Ferraris, J. P.,** 1994. Conducting Polymers as Active Materials in Electrochemical Capacitors, *Journal of Power Sources,* **47,** 89-107.

[35] **Ferraris, J. P., Eissa, M. M., Brotherston, I. D. and Loveday, D. C.,** 1998. Performance evaluation of poly 3-(phenylthiophene) derivatives as active materials for electrochemical capacitor applications, *Chemistry of Materials,* **10,** 3528-3535.

[36] **Arbizzani, C., Mastragostino, M., Meneghello, L. and Paraventi, R.,** 1996. Electronically conducting polymers and activated carbon: Electrode materials in supercapacitor technology, *Advanced Materials,* **8,** 331-334.

[37] **Mastragostino, M., Arbizzani, C., Paraventi, R. and Zanelli, A.,** 2000. Polymer selection and cell design for electric-vehicle supercapacitors, *Journal of the Electrochemical Society,* **147,** 407-412.

[38] **Bard, A. J. and Faulkner, L. R.,** 2001. Electrochemical Methods : Fundamentals And Applications, John Wiley, New York.

[39] **Barsoukov, E. and Macdonald, J. R.,** 2005. Impedance spectroscopy : theory, experiment, and applications, Wiley-Interscience, Hoboken, N.J.

[40] **Mathias, M. F. and Haas, O.,** 1992. An Alternating-Current Impedance Model Including Migration and Redox-Site Interactions at Polymer-Modified Electrodes, *Journal of Physical Chemistry,* **96,** 3174-3182.

[41] **Deslouis, C., Musiani, M. M. and Tribollet, B.,** 1994. Ac-Impedance Study of Transport Processes in Polyaniline Membranes, *Journal of Physical Chemistry,* **98,** 2936-2940.

[42] **Inzelt, G. and Lang, G.,** 1994. Model Dependence and Reliability of the Electrochemical Quantities Derived from the Measured Impedance Spectra of Polymer-Modified Electrodes, *Journal of Electroanalytical Chemistry,* **378,** 39-49.

[43] **Lang, G. and Inzelt, G.,** 1999. An advanced model of the impedance of polymer film electrodes, *Electrochimica Acta,* **44,** 2037-2051.

[44] **Vorotyntsev, M. A., Daikhin, L. I. and Levi, M. D.,** 1994. Modeling the Impedance Properties of Electrodes Coated with Electroactive Polymer-Films, *Journal of Electroanalytical Chemistry,* **364,** 37-49.

[45] **Lang, G. G., Ujvari, M., Rokob, T. A. and Inzelt, G.,** 2006. The brush model of the polymer films-analysis of the impedance spectra of Au,Pt/poly(o-phenylenediamine) electrodes, *Electrochimica Acta,* **51,** 1680-1694.

[46] **Paulse, C. D. and Pickup, P. G.,** 1988. Chronoamperometry of Polypyrrole - Migration of Counterions and Effect of Uncompensated Solution Resistance, *Journal of Physical Chemistry,* **92,** 7002-7006.

[47] **Bisquert, J., Garcia-Belmonte, G., Fabregat-Santiago, F., Ferriols, N. S., Bogdanoff, P. and Pereira, E. C.,** 2000. Doubling exponent models for the analysis of porous film electrodes by impedance. Relaxation of TiO2 nanoporous in aqueous solution, *Journal of Physical Chemistry B,* **104,** 2287-2298.

[48] **Roncali, J.,** 1997. Synthetic principles for bandgap control in linear pi-conjugated systems, *Chemical Reviews,* **97,** 173-205.

[49] **Groenendaal, B. L., Jonas, F., Freitag, D., Pielartzik, H. and Reynolds, J. R.,** 2000. Poly(3,4-ethylenedioxythiophene) and its derivatives: Past, present, and future, *Advanced Materials,* **12,** 481-494.

[50] **Sotzing, G. A., Reynolds, J. R. and Steel, P. J.,** 1996. Electrochromic conducting polymers via electrochemical polymerization of bis(2-(3,4-ethylenedioxy)thienyl) monomers, *Chemistry of Materials,* **8,** 882-889.

[51] **Fu, Y. P., Cheng, H. T. and Elsenbaumer, R. L.,** 1997. Electron-rich thienylene-vinylene low bandgap polymers, *Chemistry of Materials,* **9,** 1720-1724.

[52] **Sezer, E., Van Hooren, M., Sarac, A. S. and Hallensleben, M. L.,** 1999. Synthesis and electrochemical polymerization of ter-arenes based on N-ethyl carbazole and thiophene, *Journal of Polymer Science Part a-Polymer Chemistry,* **37,** 379-386.

[53] **Nalwa, H. S.,** 1997. Handbook of Organic Conductive Molecules and Polymers, John Wiley & Sons, New York.

[54] **Reddinger, J. L. and Reynolds, J. R.,** 1999. Molecular engineering of pi-conjugated polymers, *Radical Polymerisation Polyeletrolytes,* **145,** 57-122.

[55] **Skotheim, T. A., Elsenbaumer, R. L. and Reynolds, J. R.,** 1998. Handbook Of Conducting Polymers, M. Dekker, New York.

[56] **Friend, R. H., Gymer, R. W., Holmes, A. B., Burroughes, J. H., Marks, R. N., Taliani, C., Bradley, D. D. C., Dos Santos, D. A., Bredas, J. L., Logdlund, M. and Salaneck, W. R.,** 1999. Electroluminescence in conjugated polymers, *Nature,* **397,** 121-128.

[57] **Brotherston, I. D., Mudigonda, D. S. K., Osborn, J. M., Belk, J., Chen, J., Loveday, D. C., Boehme, J. L., Ferraris, J. P. and Meeker, D. L.,** 1999. Tailoring the electrochromic properties of devices via polymer blends, copolymers, laminates and patterns, *Electrochimica Acta,* **44,** 2993-3004.

[58] **Lee, Y. S. and Kertesz, M.,** 1988. The Effect of Heteroatomic Substitutions on the Band-Gap of Polyacetylene and Polyparaphenylene Derivatives, *Journal of Chemical Physics,* **88,** 2609-2617.

[59] **Bredas, J. L., Cornil, K., Meyers, F. and Beljonne, D.,** 1998. Electronic Structure and Optical Response of Highly Conducting and

Semiconducting Conjugated Polymers and Oligomers, *Handbook of conducting polymers,* xiii, 1097 p., Skotheim, T. A., Elsenbaumer, R. L. and Reynolds, J. R., M. Dekker, New York.

[60] **Peierls, R.,** 1955. In Quantum Theory Of Solids, Oxford Universtiy Press, Oxford.

[61] **Shimamura, K., Karasz, F. E., Hirsch, J. A. and Chien, J. C. W.,** 1981. Crystal-Structure of Trans-Polyacetylene, *Makromolekulare Chemie-Rapid Communications,* **2,** 473-480.

[62] **Bauerle, P., Segelbacher, U., Maier, A. and Mehring, M.,** 1993. Electronic-Structure of Monomeric and Dimeric Cation Radicals in End-Capped Oligothiophenes, *Journal of the American Chemical Society,* **115,** 10217-10223.

[63] **Hill, M. G., Penneau, J. F., Zinger, B., Mann, K. R. and Miller, L. L.,** 1992. Oligothiophene Cation Radicals - Pi-Dimers as Alternatives to Bipolarons in Oxidized Polythiophenes, *Chemistry of Materials,* **4,** 1106-1113.

[64] **Bryce, M. R., Chissel, A., Kathirgamanathan, P., Parker, D. and Smith, N. R. M.,** 1987. Soluble, Conducting Polymers from 3-Substituted Thiophenes and Pyrroles, *Journal of the Chemical Society-Chemical Communications,* 466-467.

[65] **Bayer-AG,** 1988. *European Patent,* 339340.

[66] **Winter, I., Reese, C., Hormes, J., Heywang, G. and Jonas, F.,** 1995. The Thermal Aging of Poly(3,4-Ethylenedioxythiophene) - an Investigation by X-Ray-Absorption and X-Ray Photoelectron-Spectroscopy, *Chemical Physics,* **194,** 207-213.

[67] **Dietrich, M., Heinze, J., Heywang, G. and Jonas, F.,** 1994. Electrochemical and Spectroscopic Characterization of Polyalkylenedioxythiophenes, *Journal of Electroanalytical Chemistry,* **369,** 87-92.

[68] **Bayer-AG,** 1991. *European Patent,* 440957.

[69] **Gogte, V. N., Shah, L. G., Tilak, B. D., Gadekar, K. N. and Sahasrabudhe, M. B.,** 1967. Synthesis of potential anticancer agents—I Synthesis of substituted thiophenes *Tetrahedron,* **23,** 2437-2441.

[70] **Bolognesi, A., Catellani, M., Destri, S. and Porzio, W.,** 1987. Polythiazole - a New Semiconducting Polymer Having a Heteroatom in the Conduction Pathway, *Synthetic Metals,* **18,** 129-132.

[71] **Catellani, M., Destri, S., Porzio, W., Themans, B. and Bredas, J. L.,** 1988. Thiazole-Based Polymers - Synthesis, Characterization and Electronic-Structure, *Synthetic Metals,* **26,** 259-265.

[72] **Bredas, J. L.,** 1986. Electronic Structure of Highly Conducting Polymers, *Handbook of conducting polymers,* 559-567, Skotheim, T. A., M. Dekker, New York.

[73] **Dall'Olio, A., Dascola, Y., Varacco, V. and Bocchi, C. R.,** 1968. CRC Seances Acad. Sci. Ser. C, 466.

[74] **Kanazawa, K. K., Diaz, A. F., Geiss, R. H., Gill, W. D., Kwak, J. F., Logan, J. A., Rabolt, J. F. and Street, G. B.,** 1979. Organic Metals - Polypyrrole, a Stable Synthetic Metallic Polymer, *Journal of the Chemical Society-Chemical Communications,* 854-855.

[75] **Schnoller, M., Wersing, W. and Naarman, H.,** 1987. Intrinsically Conductive Organic Polymers as Electrode Material for Functional Ceramics in Electronics, *Makromolekulare Chemie-Macromolecular Symposia,* **8,** 83-95.

[76] **Patil, A. O., Ikenoue, Y., Wudl, F. and Heeger, A. J.,** 1987. Water-Soluble Conducting Polymers, *Journal of the American Chemical Society,* **109,** 1858-1859.

[77] **Bittihn, R., Ely, G. and Woeffler, F.,** 1987. Polypyrrole as an Electrode Material for Secondary Lithium Cells, *Makromolekulare Chemie-Macromolecular Symposia,* **8,** 51-59.

[78] **Burroughes, J. H., Bradley, D. D. C., Brown, A. R., Marks, R. N., Mackay, K., Friend, R. H., Burns, P. L. and Holmes, A. B.,** 1990. Light-Emitting-Diodes Based on Conjugated Polymers, *Nature,* **347,** 539-541.

[79] **Roth, S.,** 1995. One-Dimensional Metals, Weinheim VCH,

[80] **Salaneck, W. R., Lundstrom, I. and Randby, B.,** 1993. Nobel Symposium in Chemistry: Conjugated Polymers and Related Materials, Oxford Sci, Oxford.

[81] **Berggren, M., Inganas, O., Gustafsson, G., Rasmusson, J., Andersson, M. R., Hjertberg, T. and Wennerstrom, O.,** 1994. Light-Emitting-Diodes with Variable Colors from Polymer Blends, *Nature,* **372,** 444-446.

[82] **Argun, A. A., Audebert, P., Thompson, B. C., Schwendeman, I., Gaupp, C. L., Hwang, J., Pinto, N. J., Tanner, D. B., Macdiarmid, A. G. and Reynolds, J. R.,** 2004. Multicolored Electrochromism in Polymers: Structures and Devices, *Chemistry of Materials,* **16,** 4401-4412.

[83] **Lyons, M. E. G.,** 1997. Advances in Chemical Physics, Polymeric Systems, John Wiley & Sons, New York.

[84] **Levi, M. D., Lopez, C., Vieil, E. and Vorotyntsev, M. A.,** 1997. Influence of ionic size on the mechanism of electrochemical doping of polypyrrole films studied by cyclic voltammetry, *Electrochimica Acta,* **42,** 757-769.

[85] **Andrieux, C. P., Audebert, P., Hapiot, P. and Saveant, J. M.,** 1991. Observation of Some Reactive Pyrrolic Radical-Cations by Use of Fast Voltammetry at Ultramicroelectrodes, *Synthetic Metals,* **43,** 2877-2880.

[86] **Beelen, E., Riga, J. and Verbist, J. J.,** 1991. Electrochemical Doping of Polypyrrole - Xps Study, *Synthetic Metals,* **41,** 449-454.

[87] **Kassim, A., Davis, F. J. and Mitchell, G. R.,** 1994. The Role of the Counterion during Electropolymerization of Polypyrrole Camphor Sulfonate Films, *Synthetic Metals,* **62,** 41-47.

[88] **Warren, L. F. and Anderson, D. P.,** 1987. Polypyrrole Films from Aqueous-Electrolytes - the Effect of Anions Upon Order, *Journal of the Electrochemical Society,* **134,** 101-105.

[89] **Kuwabata, S., Nakamura, J. and Yoneyama, H.,** 1988. The Effect of Basicity of Dopant Anions on the Conductivity of Polypyrrole Films, *Journal of the Chemical Society-Chemical Communications,* **12**, 779-780.

[90] **Imanishi, K., Satoh, M., Yasuda, Y., Tsushima, R. and Aoki, S.,** 1988. Solvent Effect on Electrochemical Polymerization of Aromatic-Compounds, *Journal of Electroanalytical Chemistry,* **242,** 203-208.

[91] **Waltman, R. J., Diaz, A. F. and Bargon, J.,** 1984. Electroactive Properties of Polyaromatic Molecules, *Journal of the Electrochemical Society,* **131,** 1452-1456.

[92] **Cross, M. G., Walton, D., Morse, N. J., Mortimer, R. J., Rosseinsky, D. R. and Simmonds, D. J.,** 1985. A Voltammetric Survey of Steric and Beta-Linkage Effects in the Electropolymerization of Some

Substituted Pyrroles, *Journal of Electroanalytical Chemistry,* **189,** 389-396.

[93] **Diaz, A. F., Castillo, J. I., Logan, J. A. and Lee, W. Y.,** 1981. Electrochemistry of Conducting Polypyrrole Films, *Journal of Electroanalytical Chemistry,* **129,** 115-132.

[94] **Merz, A., Schwarz, R. and Schropp, R.,** 1992. 3,4-Dimethoxpyrrole - Monomer Synthesis and Conducting Polymer Formation, *Advanced Materials,* **4,** 409-411.

[95] **Gaupp, C. L., Zong, K. W., Schottland, P., Thompson, B. C., Thomas, C. A. and Reynolds, J. R.,** 2000. Poly(3,4-ethylenedioxypyrrole): Organic electrochemistry of a highly stable electrochromic polymer, *Macromolecules,* **33,** 1132-1133.

[96] **Thomas, C. A., Zong, K., Schottland, P. and Reynolds, J. R.,** 2000. Poly(3,4-alkylenedioxypyrrole)s as highly stable aqueous-compatible conducting polymers,vith biomedical implications, *Advanced Materials,* **12,** 222-225.

[97] **Audebert, P. and Bidan, G.,** 1985. Polyhalopyrroles - Electrochemical Synthesis and Some Characteristics, *Journal of Electroanalytical Chemistry,* **190,** 129-139.

[98] **Waltman, R. J. and Bargon, J.,** 1985. The Electropolymerization of Polycyclic-Hydrocarbons - Substituent Effects and Reactivity Structure Correlations, *Journal of Electroanalytical Chemistry,* **194,** 49-62.

[99] **Park, S. M. and Yoo, J. S.,** 2003. Electrochemical impedance spectroscopy for better electrochemical measurements, *Analytical Chemistry,* **75,** 455A-461A.

[100] **Parsons, R.,** 1990. Electrical Double-Layer - Recent Experimental and Theoretical Developments, *Chemical Reviews,* **90,** 813-826.

[101] **Randles, J. E. B.,** 1948. A Cathode Ray Polarograph: Part II The Current Voltage Curves, *Transactions of the Faraday Society,* **44,** 327-338.

[102] **Singhal, P., Kawagoe, K. T., Christian, C. N. and Kuhr, W. G.,** 1997. Sinusoidal voltammetry for the analysis of carbohydrates at copper electrodes, *Analytical Chemistry,* **69,** 1662-1668.

[103] **Harrick, N. J.,** 1979. Internal Reflection Spectroscopy, Harrick Publications, New York.

[104] **Tamao, K., Sumitani, K. and Kumada, M.,** 1972. Selective Carbon-Carbon Bond Formation by Cross-Coupling of Grignard-Reagents with Organic Halides - Catalysis by Nickel-Phosphine Complexes, *Journal of the American Chemical Society,* **94,** 4374-4376.

[105] **Kumada, M.,** 1980. Nickel and Palladium Complex Catalyzed Cross-Coupling Reactions of Organometallic Reagents with Organic Halides, *Pure and Applied Chemistry,* **52,** 669-679.

[106] **Corriu, J. P. and Masse, J. P.,** 1972. Activation of Grignard-Reagents by Transition-Metal Complexes - New and Simple Synthesis of Trans-Stilbenes and Polyphenyls, *Journal of the Chemical Society-Chemical Communications,* 144-146.

[107] **Tamura, M. and Kochi, J.,** 1971. Mechanism of Silver-Catalyzed Reaction of Grignard Reagents with Alkyl Halides, *Journal of the American Chemical Society,* **93,** 1483-1485.

[108] **Tamura, M. and Kochi, J.,** 1971. Alkylcopper(I) in Coupling of Grignard Reagents with Alkyl Halides, *Journal of the American Chemical Society,* **93,** 1485-1487.

[109] **Kochi, J. K.,** 1974. Electron-Transfer Mechanisms for Organometallic Intermediates in Catalytic Reactions, *Accounts of Chemical Research,* **7,** 351-360.

[110] **Murahash.Si, Tanba, Y., Yamamura, M. and Moritani, I.,** 1974. Reactions of Ortho-Carbon Sigma-Bonded Aromatics-Palladium Complexes with Alkyllithium - Selective Syntheses of Ortho-Alkyl Substituted Aromatic-Compounds, *Tetrahedron Letters,* **15***,* 3749-3752.

[111] **Negishi, E.-i.,** 1980. Organometallics in organic synthesis, Wiley, New York.

[112] **Negishi, E.-i.,** 2002. Handbook of organopalladium chemistry for organic synthesis, Wiley Interscience, New York.

[113] **Murahashi, S. I., Yamamura, M., Yanagisawa, K., Mita, N. and Kondo, K.,** 1979. Stereoselective Synthesis of Alkenes and Alkenyl Sulfides from Alkenyl Halides Using Palladium and Ruthenium Catalysts, *Journal of Organic Chemistry,* **44,** 2408-2417.

[114] **Kosugi, M., Hagiwara, I. and Migita, T.,** 1983. 1-Alkenylation on Alpha-Position of Ketone - Palladium-Catalyzed Reaction of Tin Enolates and 1-Bromo-1-Alkenes, *Chemistry Letters,* **12,** 839-840.

[115] **Kosugi, M., Shimizu, Y. and Migita, T.,** 1977. Alkylation, Arylation, and Vinylation of Acyl Chlorides by Means of Organotin Compounds in Presence of Catalytic Amounts of Tetrakis(Triphenylphosphine)Palladium(O), *Chemistry Letters*, **6**, 1423-1424.

[116] **Milstein, D. and Stille, J. K.,** 1979. Palladium-Catalyzed Coupling of Tetraorganotin Compounds with Aryl and Benzyl Halides - Synthetic Utility and Mechanism, *Journal of the American Chemical Society,* **101,** 4992-4998.

[117] **Jabri, N., Alexakis, A. and Normant, J. F.,** 1981. Vinyl-Copper Derivatives .13. Synthesis of Conjugated Dienes of Very High Stereoisomeric Purity, *Tetrahedron Letters,* **22,** 959-962.

[118] **Hatanaka, Y. and Hiyama, T.,** 1988. Cross-Coupling of Organosilanes with Organic Halides Mediated by Palladium Catalyst and Tris(Diethylamino)Sulfonium Difluorotrimethylsilicate, *Journal of Organic Chemistry,* **53,** 918-920.

[119] **Hatanaka, Y. and Hiyama, T.,** 1990. Stereochemistry of the Cross-Coupling Reaction of Chiral Alkylsilanes with Aryl Triflates - a Novel-Approach to Optically-Active Compounds, *Journal of the American Chemical Society,* **112,** 7793-7794.

[120] **Hatanaka, Y., Matsui, K. and Hiyama, T.,** 1989. A One-Pot Synthesis of Conjugated Dienynes by Palladium-Mediated 3 Component Cross-Coupling Reaction, *Tetrahedron Letters,* **30,** 2403-2406.

[121] **Pereyre, M., Quintard, J.-P. and Rahm, A.,** 1987. Tin in organic synthesis, Butterworths, Boston.

[122] **Keck, G. E., Enholm, E. J., Yates, J. B. and Wiley, M. R.,** 1985. One Electron C-C Bond Forming Reactions Via Allylstannanes - Scope and Limitations, *Tetrahedron,* **41,** 4079-4094.

[123] **Echavarren, A. M. and Stille, J. K.,** 1987. Palladium-Catalyzed Coupling of Aryl Triflates with Organostannanes, *Journal of the American Chemical Society,* **109,** 5478-5486.

[124] **Negishi, E., King, A. O. and Okukado, N.,** 1977. Selective Carbon-Carbon Bond Formation Via Transition-Metal Catalysis .3. Highly Selective Synthesis of Unsymmetrical Biaryls and Diarylmethanes by Nickel-Catalyzed or Palladium-Catalyzed Reaction of Aryl Derivatives and

Benzylzinc Derivatives with Aryl Halides, *Journal of Organic Chemistry,* **42,** 1821-1823.

[125] **Negishi, E., Bagheri, V., Chatterjee, S., Luo, F. T., Miller, J. A. and Stoll, A. T.,** 1983. Selective Carbon-Carbon Bond Formation Via Transition-Metal Catalysis .36. Palladium-Catalyzed Acylation of Organozincs and Other Organometallics as a Convenient Route to Ketones, *Tetrahedron Letters,* **24,** 5181-5184.

[126] **Knochel, P. and Singer, R. D.,** 1993. Preparation and Reactions of Polyfunctional Organozinc Reagents in Organic-Synthesis, *Chemical Reviews,* **93,** 2117-2188.

[127] **Prasad, A. S. B., Stevenson, T. M., Citineni, J. R., Nyzam, V. and Knochel, P.,** 1997. Preparation and reactions of new zincated nitrogen-containing heterocycles, *Tetrahedron,* **53,** 7237-7254.

[128] **Miyaura, N. and Suzuki, A.,** 1995. Palladium-Catalyzed Cross-Coupling Reactions of Organoboron Compounds, *Chemical Reviews,* **95,** 2457-2483.

[129] **Suzuki, A.,** 1998. Organoboron Compounds, *Metal Catalyzed Cross-coupling Reactions,* **21**, 517 p., Diederich, F. and Stang, P. J., Wiley-VCH, Weinheim, New York.

[130] **Wright, S. W., Hageman, D. L. and Mcclure, L. D.,** 1994. Fluoride-Mediated Boronic Acid Coupling Reactions, *Journal of Organic Chemistry,* **59,** 6095-6097.

[131] **Tamao, K., Sumitani, K., Kiso, Y., Zembayashi, M., Fujioka, A., Kodama, S., Nakajima, I., Minato, A. and Kumada, M.,** 1976. Nickel-Phosphine Complex-Catalyzed Grignard Coupling .1. Cross-Coupling of Alkyl, Aryl, and Alkenyl Grignard-Reagents with Aryl and Alkenyl Halides - General Scope and Limitations, *Bulletin of the Chemical Society of Japan,* **49,** 1958-1969.

[132] **Amatore, C., Jutand, A., Negri, S. and Fauvarque, J. F.,** 1990. Efficient Palladium-Catalyzed Synthesis of Unsymmetrical Donor-Acceptor Biaryls and Polyaryls, *Journal of Organometallic Chemistry,* **390,** 389-398.

[133] **Hiyama, T. and Hatanaka, Y.,** 1994. Palladium-Catalyzed Cross-Coupling Reaction of Organometalloids through Activation with Fluoride-Ion, *Pure and Applied Chemistry,* **66,** 1471-1478.

[134] **Diederich, F. and Stang, P. J.,** 1998. Metal catalyzed cross-coupling reactions, Wiley-VCH, Weinheim, New York.

[135] **Smith, W. S.,** 1987. Engineered Materials Handbook, ASM International, Ohio.

[136] **Donnet, J.-B.,** 1998. Carbon Fibers, Marcel Dekker, New York.

[137] **Lubin, G. and Peters, S. T.,** 1998. Handbook of Composites, Chapman & Hall, London, New York.

[138] **Weitzsacker, C. L., Bellamy, M. and Sherwood, P. M. A.,** 1994. Studies of the Effect of Size on Carbon-Fiber Surfaces, *Journal of Vacuum Science & Technology a-Vacuum Surfaces and Films,* **12,** 2392-2397.

[139] **Weitzsacker, C. L. and Sherwood, P. M. A.,** 1995. X-Ray Photoelectron Spectroscopic Studies of Carbon-Fiber Surfaces .19. Surface Chemical-Changes during Electrochemical Oxidation in Base, *Surface and Interface Analysis,* **23,** 551-558.

[140] **Weitzsacker, C. L., Xie, M. and Drzal, L. T.,** 1997. Using XPS to investigate fiber matrix chemical interactions in carbon-fiber-reinforced composites, *Surface and Interface Analysis,* **25,** 53-63.

[141] **Ibarra, L., Macias, A. and Palma, E.,** 1996. Stress-strain and stress relaxation in oxidated short carbon fiber-thermoplastic elastomer composites, *Journal of Applied Polymer Science,* **61,** 2447-2454.

[142] **Delamar, M., Desarmot, G., Fagebaume, O., Hitmi, R., Pinson, J. and Saveant, J. M.,** 1997. Modification of carbon fiber surfaces by electrochemical reduction of aryl diazonium salts: Application to carbon epoxy composites, *Carbon,* **35,** 801-807.

[143] **Sarac, A. S., Serantoni, M., Tofail, S. A. M. and Cunnane, V. J.,** 2004. Morphological and spectroscopic analyses of poly [N-vinylcarbazole-co-vinylbenzenesulfonic acid] copolymer electrografted on carbon fiber: the effect of current density, *Applied Surface Science,* **229,** 13-18.

[144] **Sarac, A. S., Serantoni, M., Tofail, S. A. M., Henry, J., Cunnane, V. and McMonagle, J. B.,** 2005. Characterisation of nanosize thin films of electrografted N-vinylcarbazole copolymers (P[NVCz-co-VBSA] and P[NVCz-co-3-MeTh]) onto carbon fibre AFM, XPS, and Raman spectroscopy, *Applied Surface Science,* **243,** 183-198.

[145] **Sonmez, G. and Sarac, A. S.,** 2003. Structural study of pyrrole-EDOT copolymers on carbon fiber micro-electrodes, *Synthetic Metals,* **135,** 459-460.

[146] **Jamal, M., Sarac, A. S. and Magner, E.,** 2004. Conductive copolymer-modified carbon fibre microelectrodes: electrode characterisation and electrochemical detection of p-aminophenol, *Sensors and Actuators B-Chemical,* **97,** 59-66.

[147] **Serantoni, M., Sarac, A. S. and Sutton, D.,** 2005. FIB-SIMS investigation of carbazole-based polymer and copolymers electrocoated onto carbon fibers, and an AFM morphological study, *Surface & Coatings Technology,* **194,** 36-41.

[148] **Bismarck, A., Lee, A. F., Sarac, A. S., Schulz, E. and Wilson, K.,** 2005. Electrocoating of carbon fibres: A route for interface control in carbon fibre reinforced poly methylmethacrylate?, *Composites Science and Technology,* **65,** 1564-1573.

[149] **Dean, J. A.,** 1999. Lange's Handbook of Chemistry (15th Edition), McGraw-Hill, New York.

[150] **Lide, D. R.,** 2005. CRC Handbook of Chemistry and Physics., CRC Press, Boca Raton, FL.

[151] **Fiordiponti, P. and Pistoia, G.,** 1989. An Impedance Study of Polyaniline Films in Aqueous and Organic Solutions, *Electrochimica Acta,* **34,** 215-221.

[152] **Chen, W. C., Wen, T. C. and Teng, H. S.,** 2003. Polyaniline-deposited porous carbon electrode for supercapacitor, *Electrochimica Acta,* **48,** 641-649.

[153] **Weng, T. C. and Teng, H. S.,** 2001. Characterization of high porosity carbon electrodes derived from mesophase pitch for electric double-layer capacitors, *Journal of the Electrochemical Society,* **148,** A368-A373.

[154] **Lewandowski, A., Zajder, M., Frackowiak, E. and Beguin, F.,** 2001. Supercapacitor based on activated carbon and polyethylene oxide-KOH-H2O polymer electrolyte, *Electrochimica Acta,* **46,** 2777-2780.

[155] **Politis, J. K., Somoza, F. B., Kampf, J. W. and Curtis, M. D.,** 1999. A comparison of structures and optoelectronic properties of oxygen- and sulfur-containing heterocycles: Conjugated nonylbisoxazole and nonylbithiazole oligomers, *Chemistry of Materials,* **11,** 2274-2284.

[156] **Raimundo, J. M., Blanchard, P., Gallego-Planas, N., Mercier, N., Ledoux-Rak, I., Hierle, R. and Roncali, J.,** 2002. Design and synthesis of push-pull chromophores for second-order nonlinear optics derived from rigidified thiophene-based pi-conjugating spacers, *Journal of Organic Chemistry,* **67,** 205-218.

[157] **Cao, J. and Curtis, M. D.,** 2003. Polarons, bipolarons, and pi-dimers of bis(3,4-ethylene-dioxythiophene)-(4,4 '-dialkyl-2,2 '-bithiazole)-co-oligomers. Direct measure of the intermolecular exciton transfer interaction, *Chemistry of Materials,* **15,** 4424-4430.

[158] **Cebeci, F. C., Sezer, E. and Sarac, A. S.,** 2006. Synthesis and electrochemical characterization of bis(3,4-ethylene-dioxythiophene)-(4,4 -dinonyl-2,2'-bithiazole) comonomer, *Electrochimica Acta,* **doi:10.1016/j.electacta.2006.08.033,**

[159] **Marque, P., Roncali, J. and Garnier, F.,** 1987. Electrolyte Effect on the Electrochemical Properties of Poly(3-Methylthiophene) Thin-Films, *Journal of Electroanalytical Chemistry,* **218,** 107-118.

[160] **Roncali, J.,** 1992. Conjugated Poly(Thiophenes) - Synthesis, Functionalization, and Applications, *Chemical Reviews,* **92,** 711-738.

[161] **Ahonen, H. J., Lukkari, J. and Kankare, J.,** 2000. n- and p-doped poly(3,4-ethylenedioxythiophene): Two electronically conducting states of the polymer, *Macromolecules,* **33,** 6787-6793.

[162] **Belanger, D., Ren, X. M., Davey, J., Uribe, F. and Gottesfeld, S.,** 2000. Characterization and long-term performance of polyaniline-based electrochemical capacitors, *Journal of the Electrochemical Society,* **147,** 2923-2929.

[163] **Lota, K., Khomenko, V. and Frackowiak, E.,** 2004. Capacitance properties of poly(3,4-ethylenedioxythiophene)/carbon nanotubes composites, *Journal of Physics and Chemistry of Solids,* **65,** 295-301.

[164] **Ryu, K. S., Lee, Y. G., Hong, Y. S., Park, Y. J., Wu, X., Kim, K. M., Kang, M. G., Park, N. G. and Chang, S. H.,** 2004. Poly(ethylenedioxythiophene) (PEDOT) as polymer electrode in redox supercapacitor, *Electrochimica Acta,* **50,** 843-847.

[165] **Arbizzani, C., Mastragostino, M. and Meneghello, L.,** 1996. Polymer-based redox supercapacitors: A comparative study, *Electrochimica Acta,* **41,** 21-26.

[166] **Ryu, K. S., Lee, Y. G., Hong, Y. S., Park, Y. J., Wu, X. L., Kim, K. M., Kang, M. G., Park, N. G. and Chang, S. H.,** 2004. Poly(ethylenedioxythiophene) (PEDOT) as polymer electrode in redox supercapacitor, *Electrochimica Acta,* **50,** 843-847.

[167] **Tanguy, J., Mermilliod, N. and Hoclet, M.,** 1987. Capacitive Charge and Noncapacitive Charge in Conducting Polymer Electrodes, *Journal of the Electrochemical Society,* **134,** 795-802.

[168] **Otero, T. F., Cantero, I. and Grande, H.,** 1999. Solvent effects on the charge storage ability in polypyrrole, *Electrochimica Acta,* **44,** 2053-2059.

[169] **Chung, T. C., Kaufman, J. H., Heeger, A. J. and Wudl, F.,** 1984. Charge storage in doped poly(thiophene) optical an electrochemical studies, *Physical Review B,* **30,** 702-710.

APPENDICES

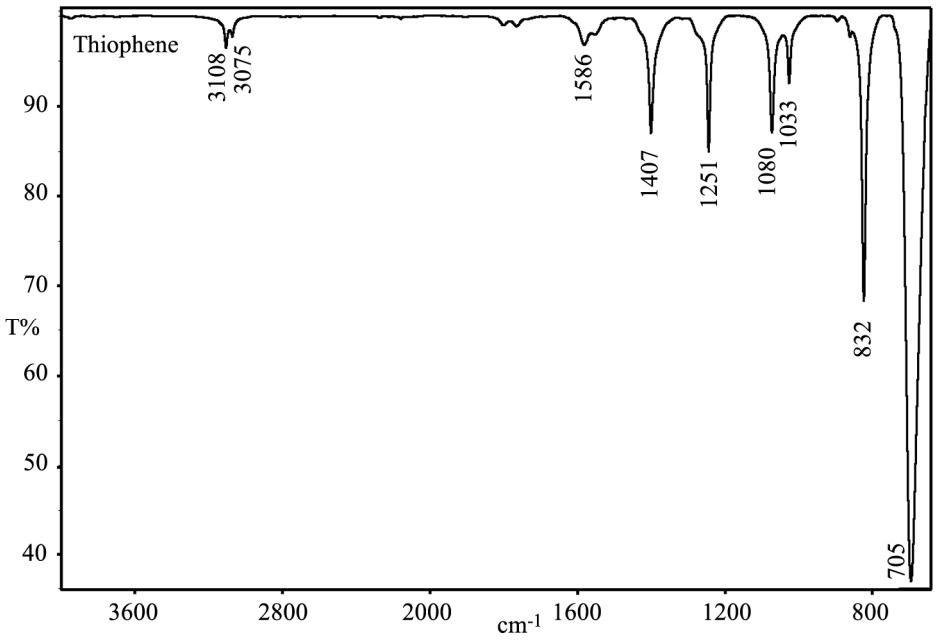

Figure A.1: ATR-FTIR spectrum of thiophene monomer.

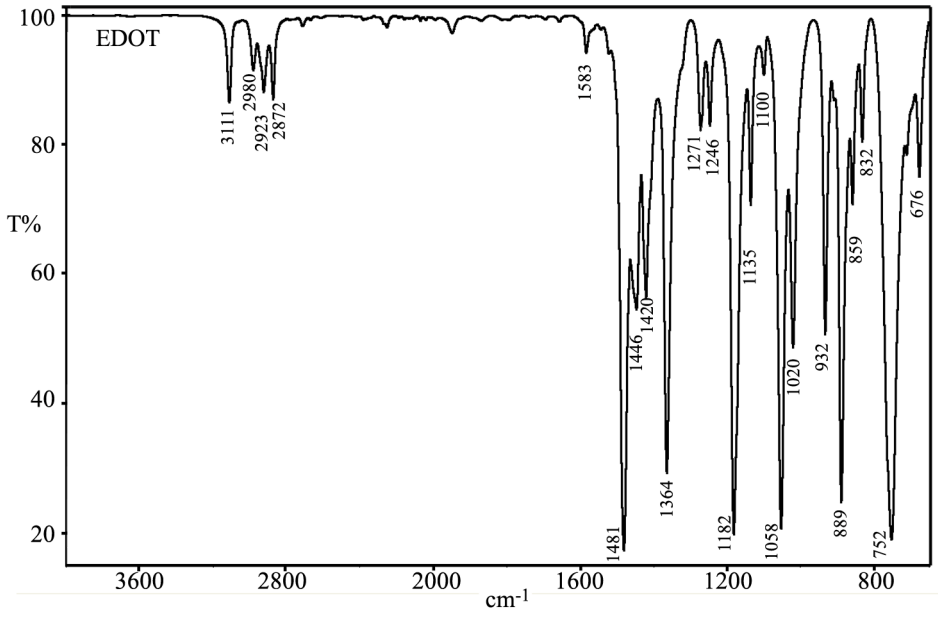

Figure A.2: ATR-FTIR spectrum of EDOT monomer.

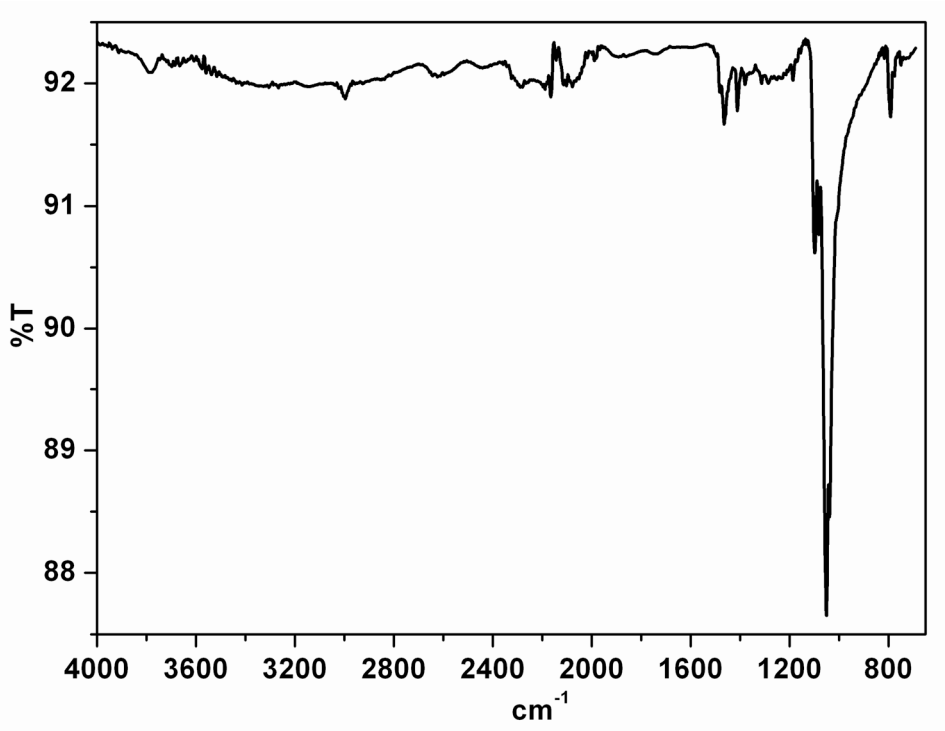

Figure A.3: ATR-FTIR spectrum of bare CFME.

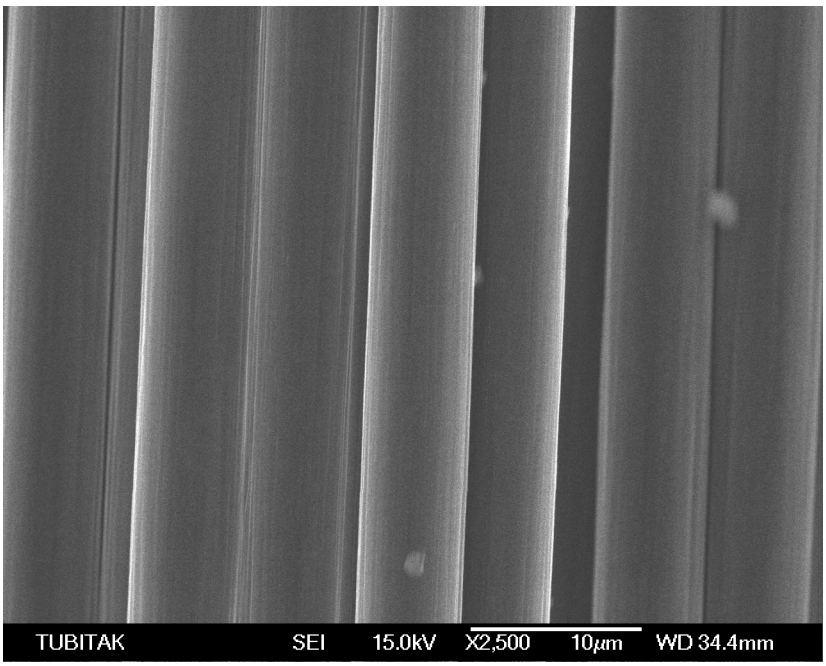

Figure B.1: FE-SEM image of bare CFME at x2500 magnifications.

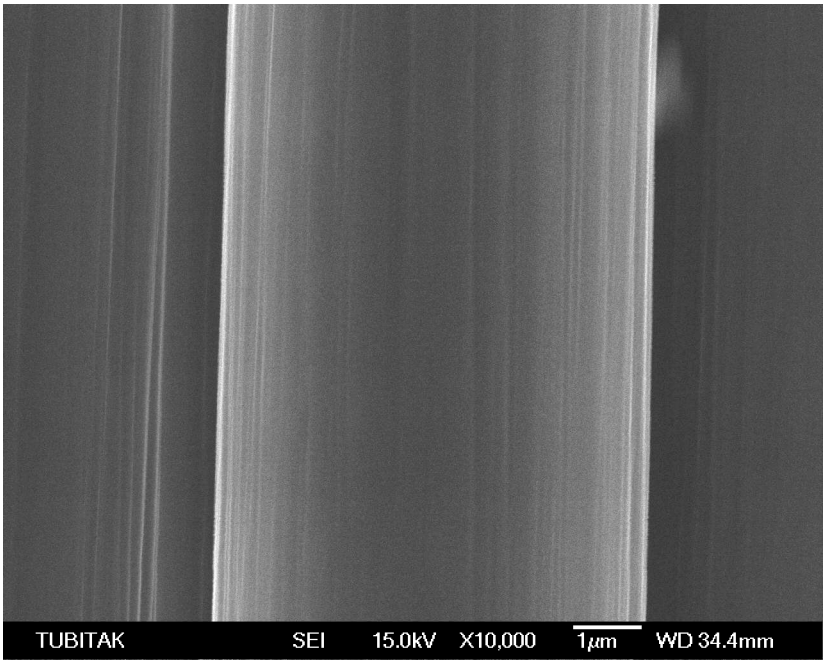

Figure B.2: FE-SEM image of bare CFME at x10000 magnifications.

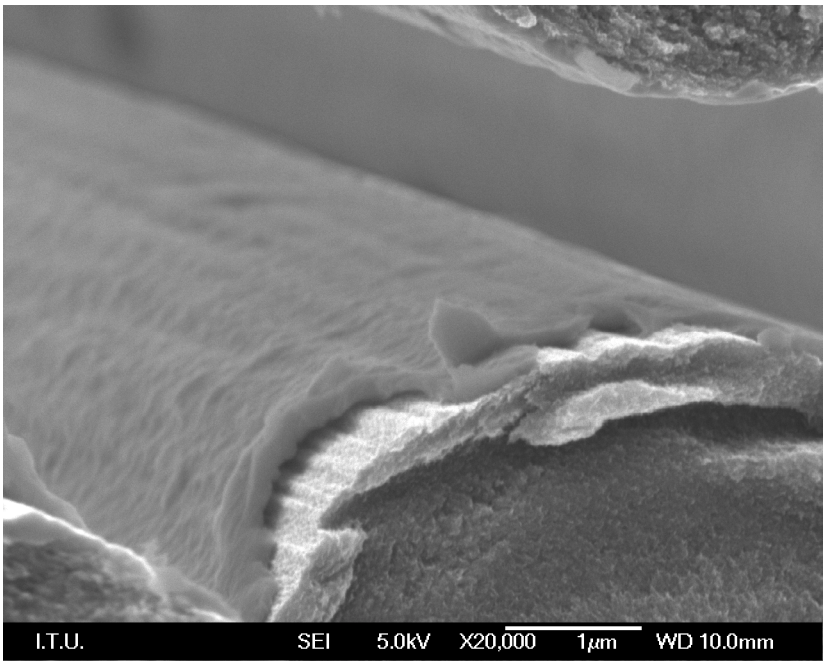

Figure B.3: FE-SEM image of PENBTE at low deposition charge.

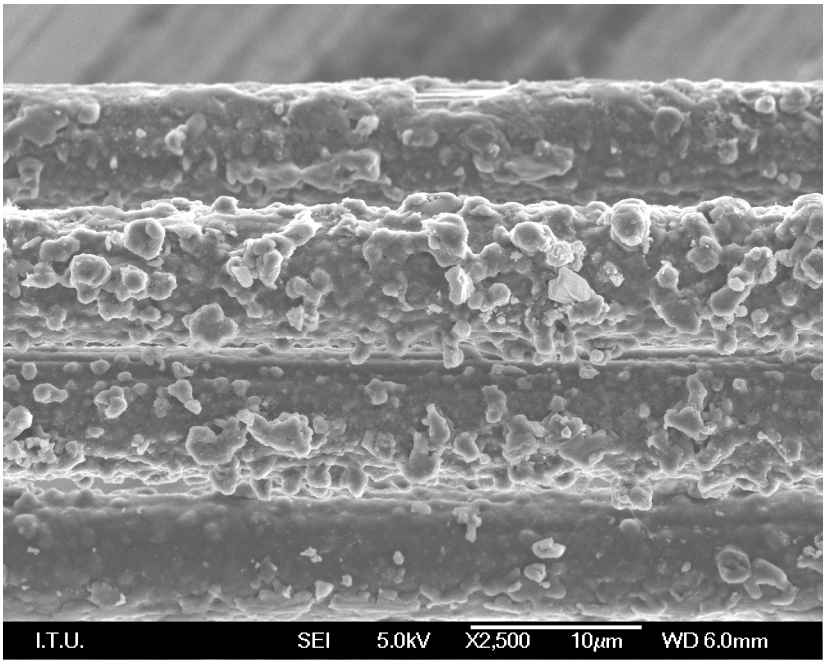

Figure B.4: FE-SEM image of PENBTE at high deposition charge.

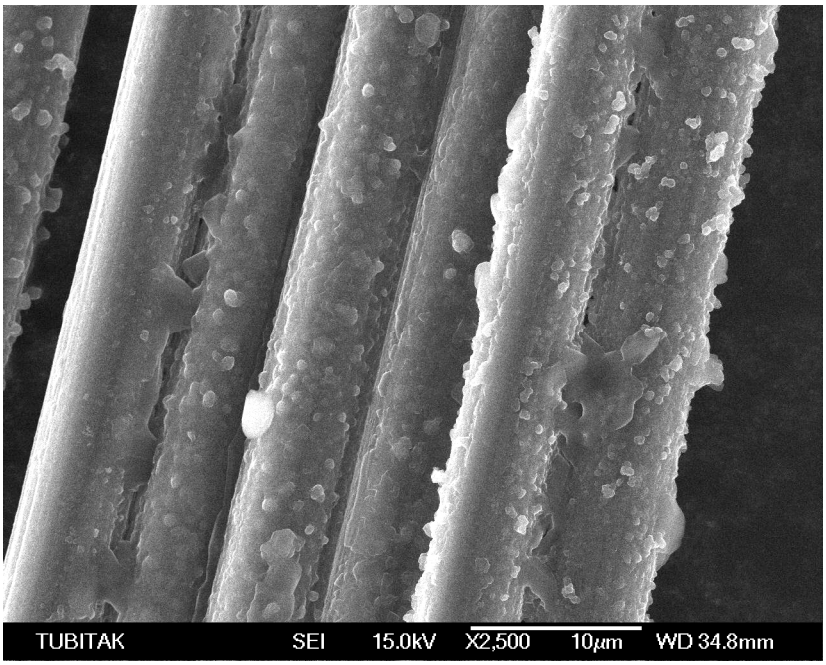

Figure B.5: FE-SEM images of a potentiodynamically deposited copolymer of EDOT and ENBTE charge 2.262 C cm^{-2} and mole ratio of 0.60 on CFME at 2500 magnifications.

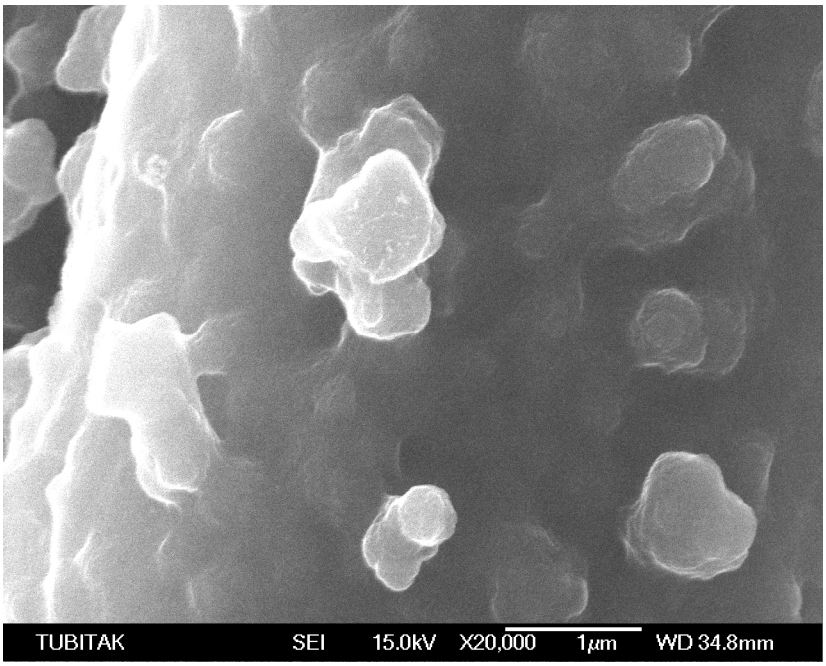

Figure B.6: FE-SEM images of a potentiodynamically deposited copolymer of EDOT and ENBTE charge 2.262 C cm^{-2} and mole ratio of 0.60 on CFME at 20000 magnifications.

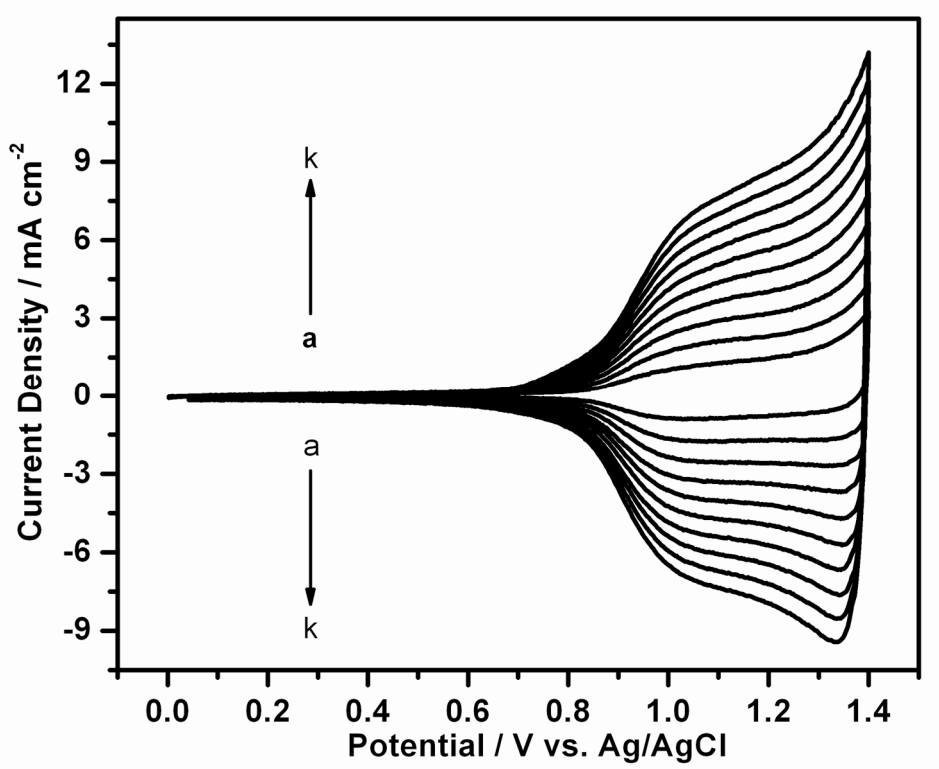

Figure C.1: Cyclic voltammogram of the electrochemically polymerized PTNBTT film (Qdep=5.5 C cm^{-2}) in a monomer free electrolyte solution scanned at (a) 20, (b) 40, (c) 60, (d) 80, (e) 100, (f) 120, (g) 140, (h) 160, (i) 180, and (k) 200 mV s^{-1}.

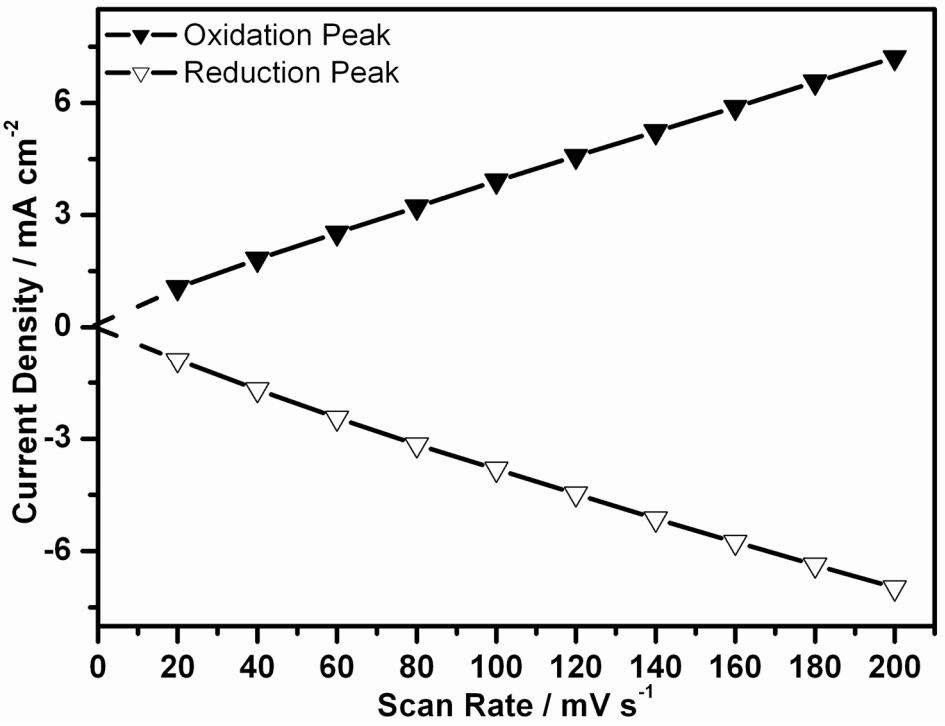

Figure C.2: Scan rate dependency of PTNBTT from Figure C.1.

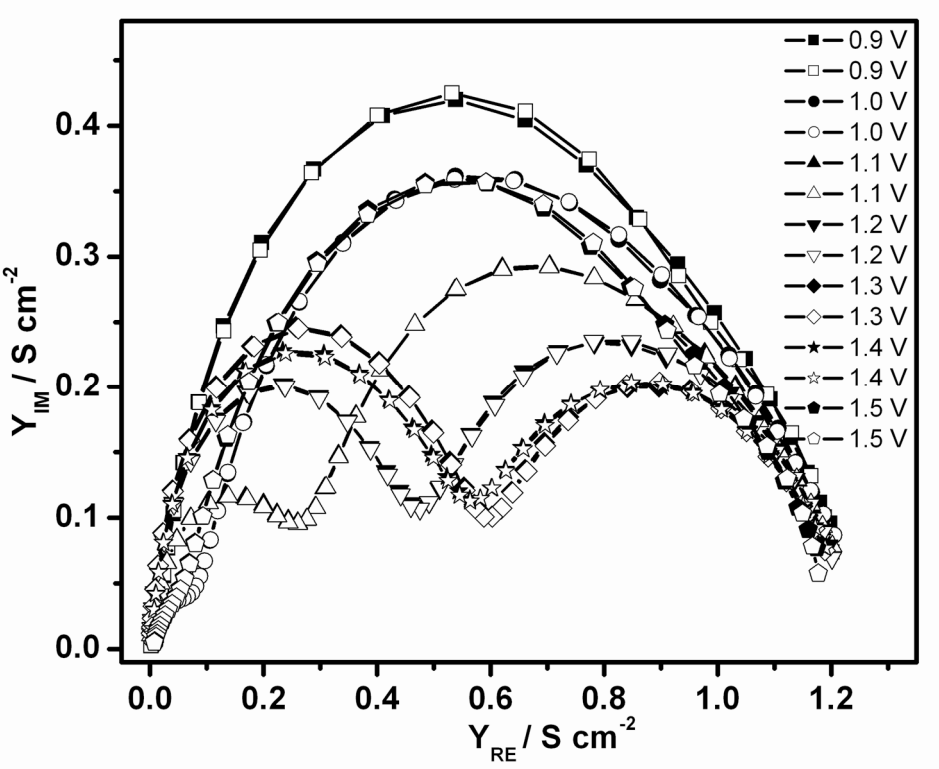

Figure D.1: Potential dependence of complex plane admittance plots of a PTNBTT film on CFME deposited with a charge of of Q_{dep}= 9.6 C cm^{-2}.

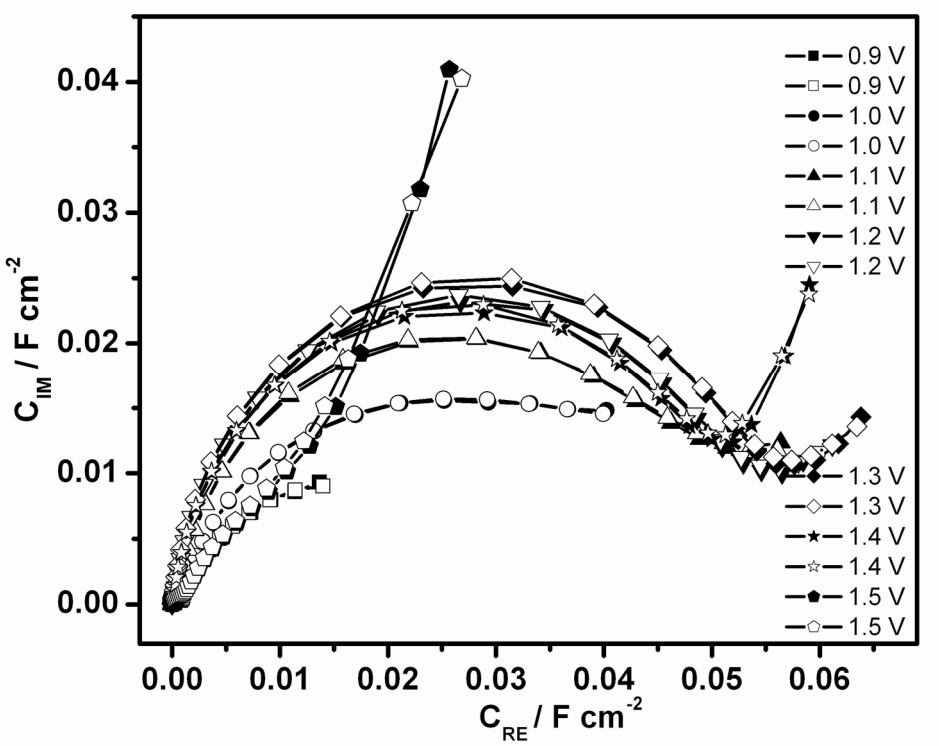

Figure D.2: Potential dependence of complex plane capacitance plots of a PTNBTT film on CFME deposited with a charge of of Q_{dep}= 9.6 C cm^{-2}.

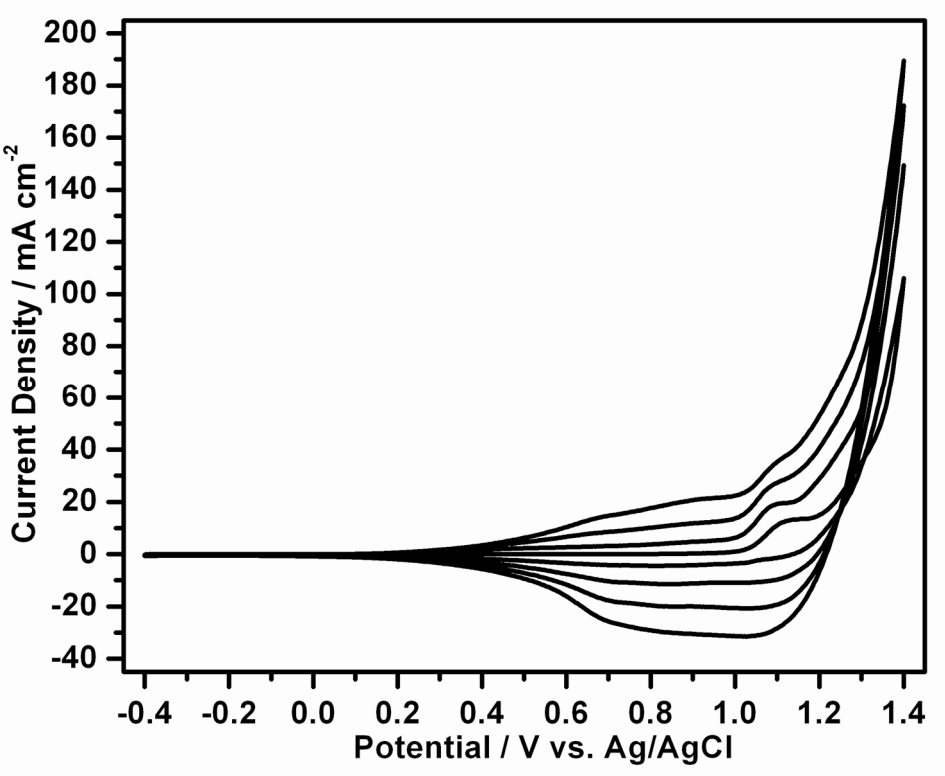

Figure E.1: Electrocopolymerization of 1mM BTh and 1mM ENBTE (x=0.85) onto CFME in 0.1M Et_4NBF_4 /DCM solution. Deposition charge of 4.952 C cm^{-2}.

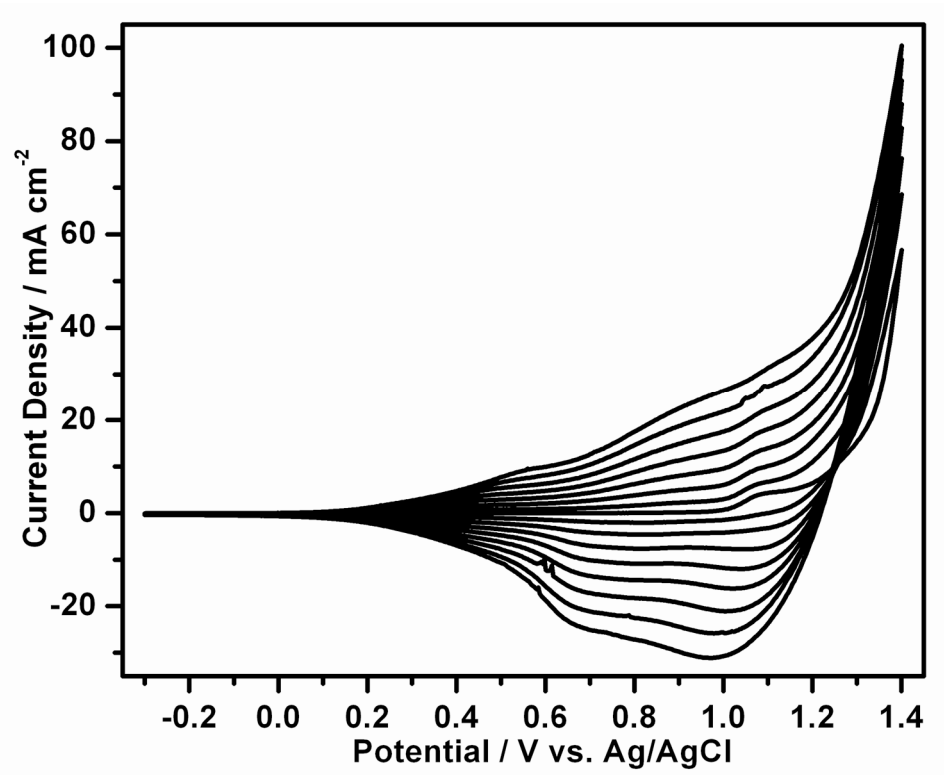

Figure E.2: Electrocopolymerization of 1mM BTh and 1mM ENBTE (x=0.875) onto CFME in 0.1M Et_4NBF_4 /DCM solution. Deposition charge of 2.161 C cm^{-2}.

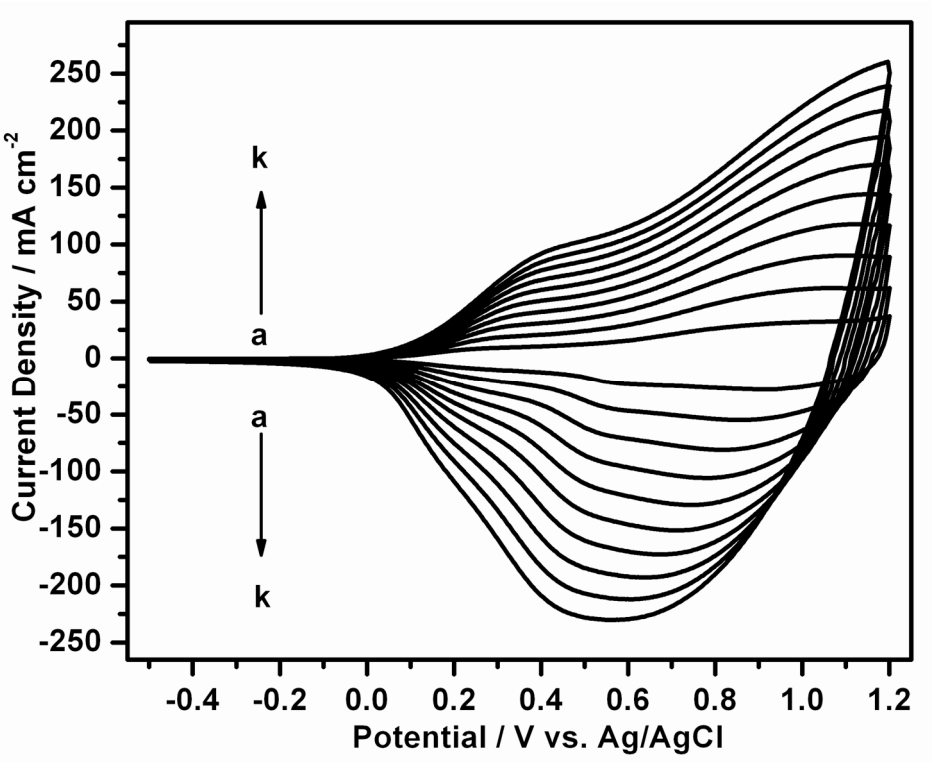

Figure F.1: CV of electrochemically copolymerized BTh and ENBTE (x=0.85) film (4.952 C cm^{-2}) in a monomer free electrolyte solution scanned at (a) 20, (b) 40, (c) 60, (d) 80, (e) 100, (f) 120, (g) 140, (h) 160, (i) 180, and (k) 200 mV s^{-1}.

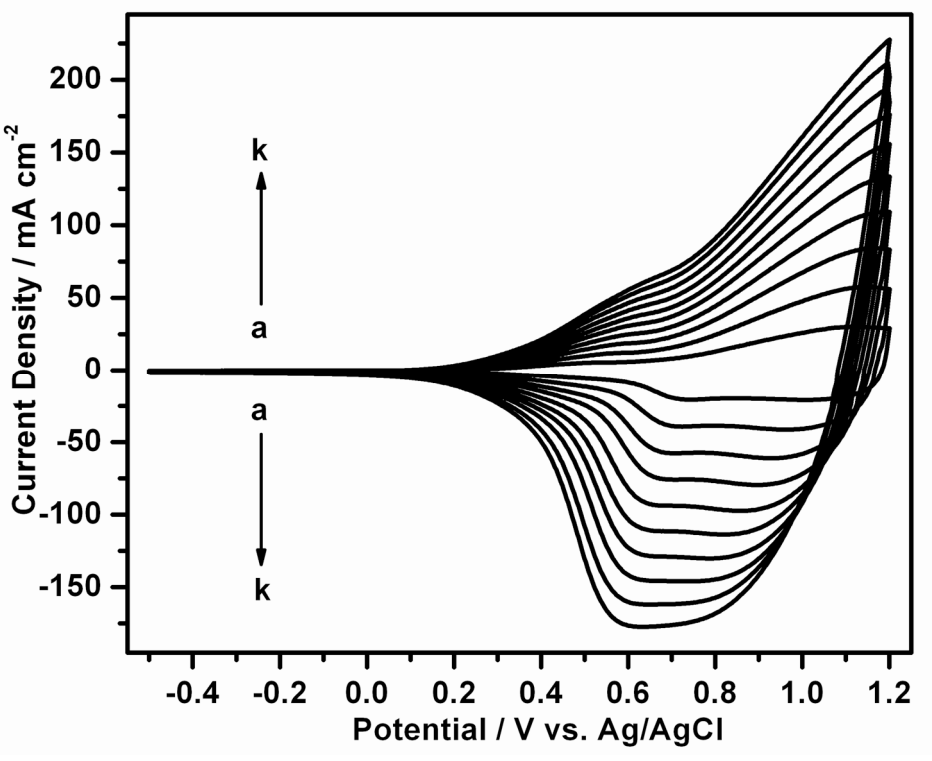

Figure F.2: CV of electrochemically copolymerized BTh and ENBTE (x=0.925) film (4.575 C cm^{-2}) in a monomer free electrolyte solution scanned at (a) 20, (b) 40, (c) 60, (d) 80, (e) 100, (f) 120, (g) 140, (h) 160, (i) 180, and (k) 200 mV s^{-1}.

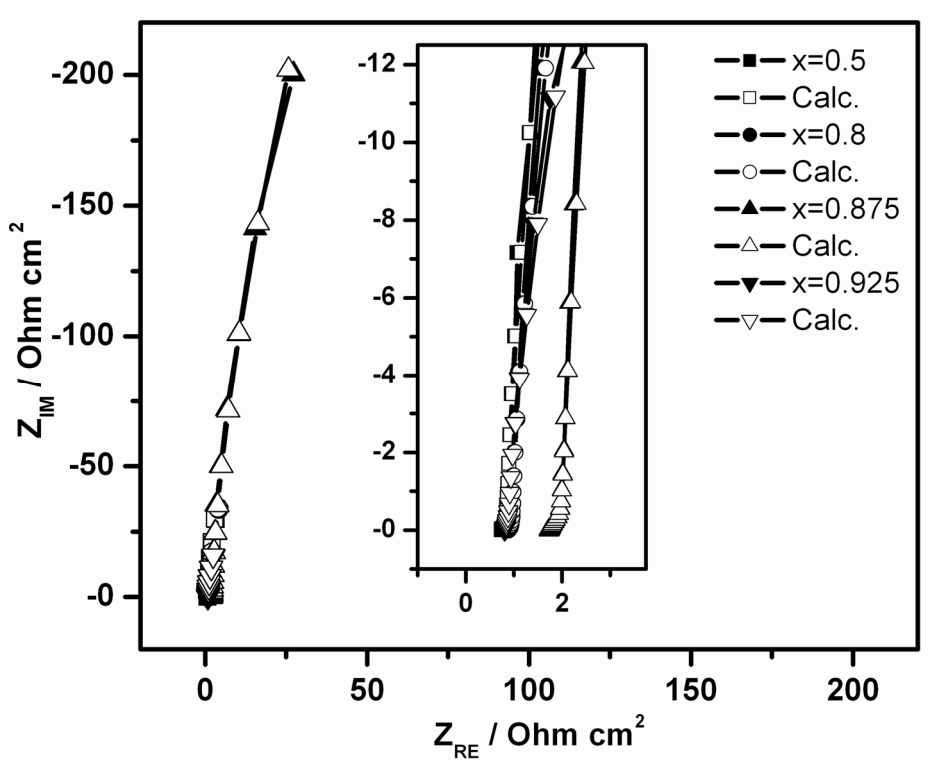

Figure G.1: Complex plane impedance plots of the BTh and ENBTE copolymers at different mole fractions at 0.8V DC potential. Inset 1: An expanded complex plane view of the high frequency region. Results are given with calculation fit in open interior symbols.

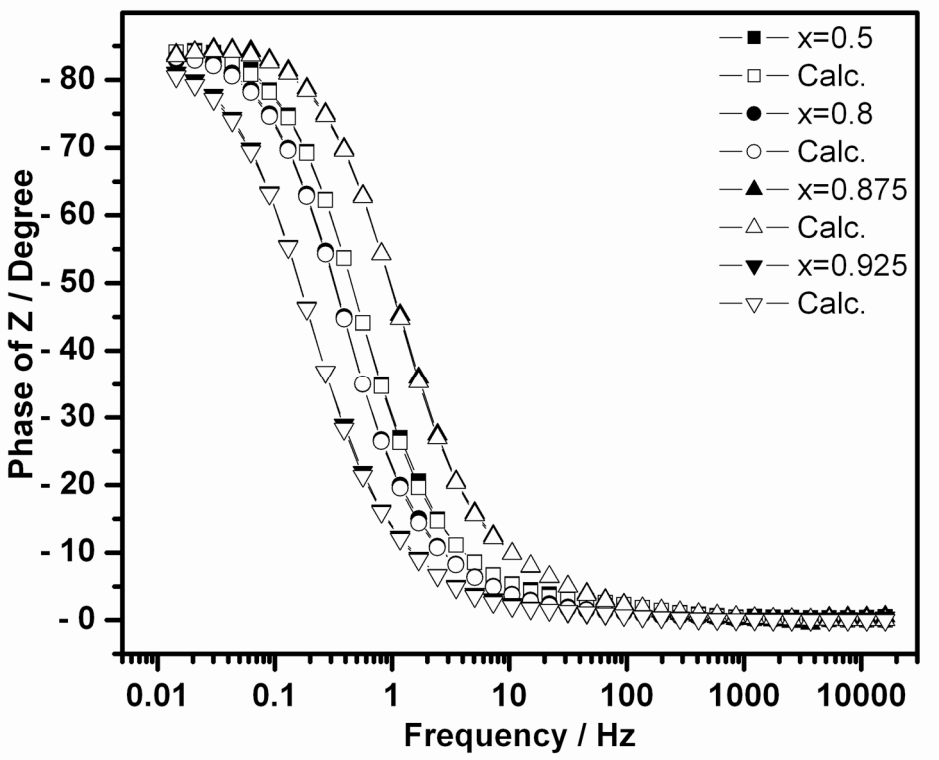

Figure G.2: Bode phase angle plots of the BTh and ENBTE copolymers at different mole fractions at 0.8V DC potential.

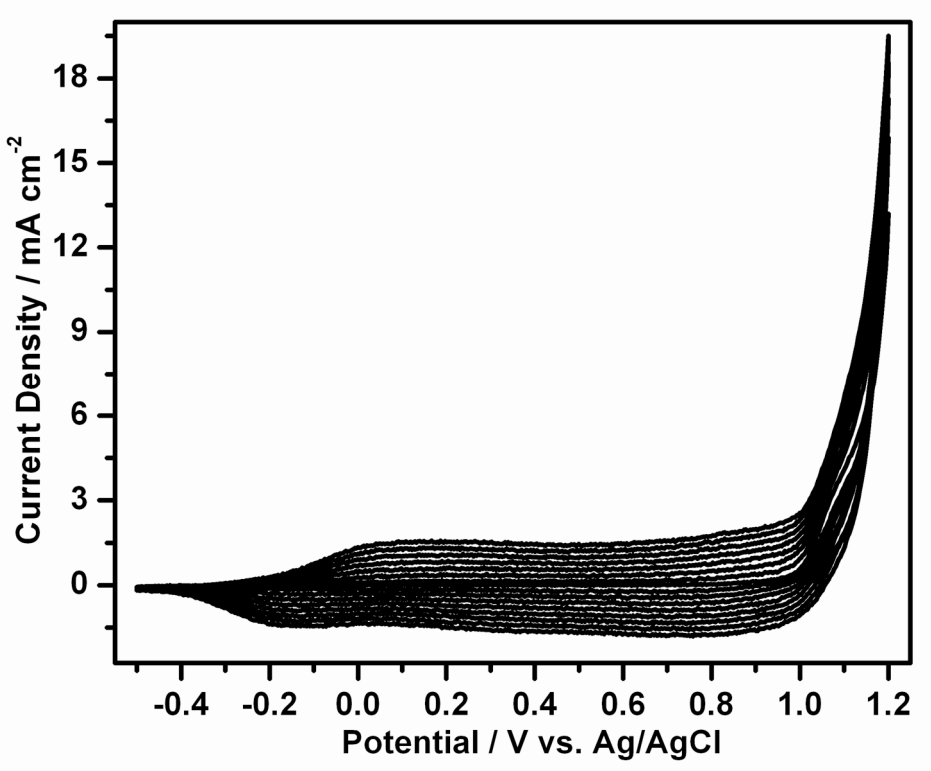

Figure H.1: Electrocopolymerization of EDOT and ENBTE (x=0.90) onto CFME in 0.1M Et_4NBF_4 /DCM solution. Deposition charge of 0.876 C cm^{-2}.

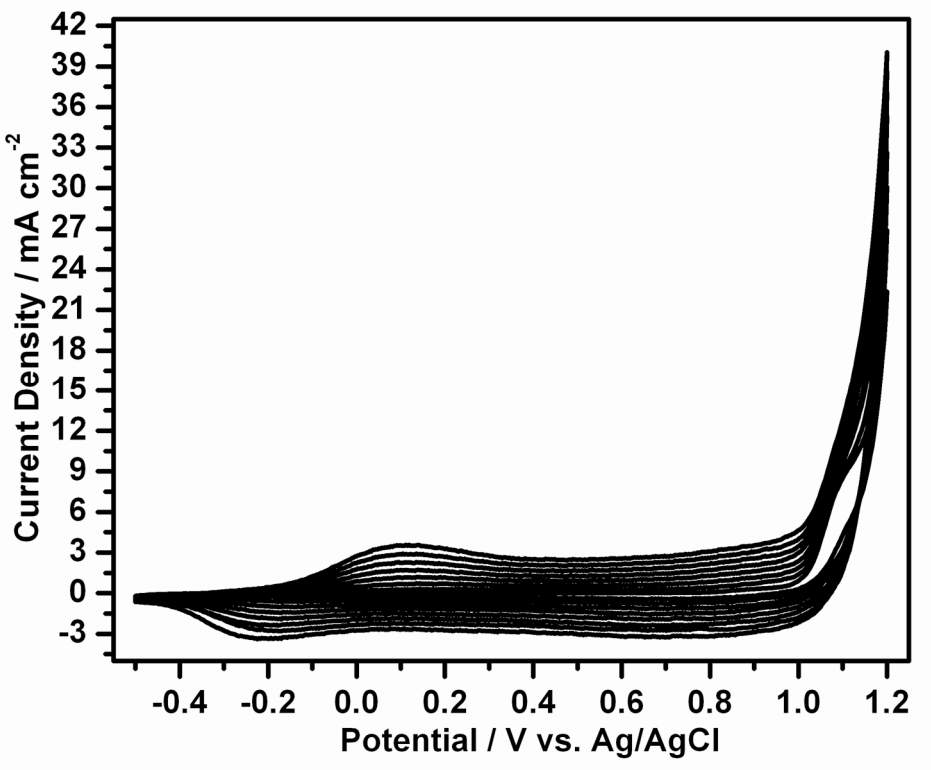

Figure H.2: Electrocopolymerization of EDOT and ENBTE (x=0.95) onto CFME in 0.1M Et_4NBF_4 /DCM solution. Deposition charge of 1.663 C cm^{-2}.

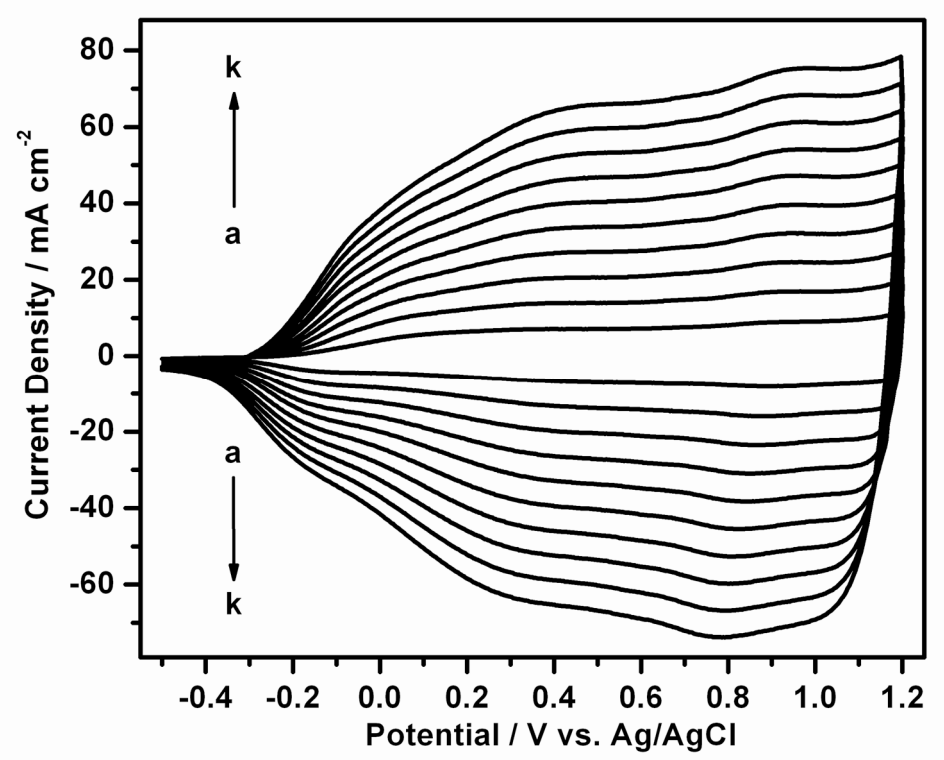

Figure I.1: CV of electrochemically copolymerized BTh and ENBTE (x=0.85) film (4.952 C cm^{-2}) in a monomer free electrolyte solution scanned at (a) 20, (b) 40, (c) 60, (d) 80, (e) 100, (f) 120, (g) 140, (h) 160, (i) 180, and (k) 200 mV s^{-1}.

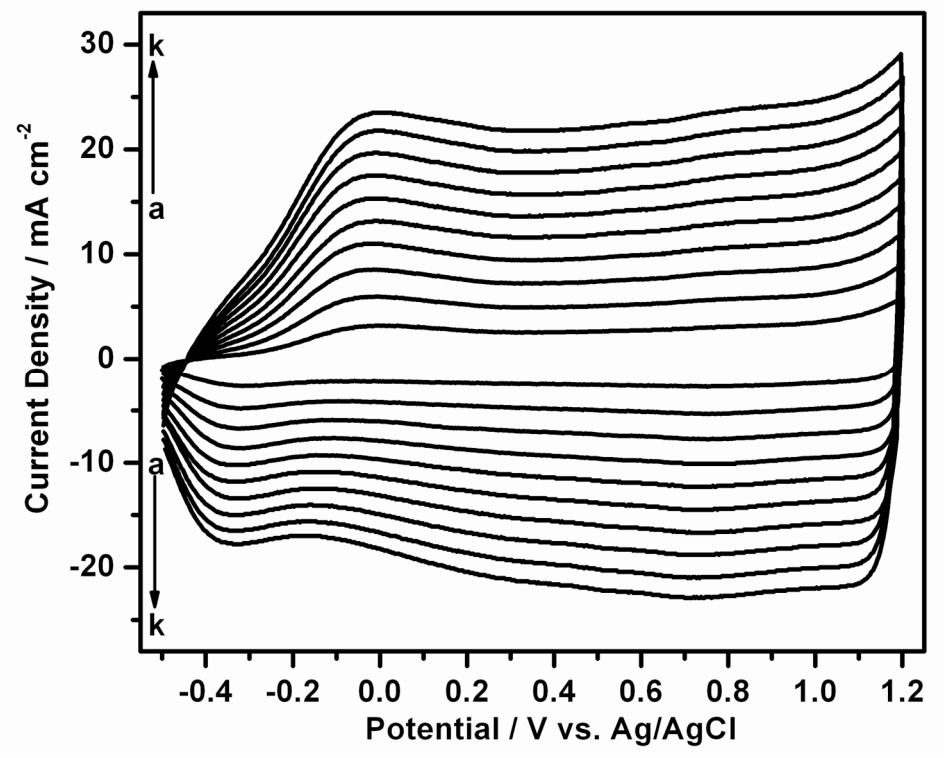

Figure I.2: CV of electrochemically copolymerized EDOT and ENBTE (x=0.95) film (1.663 C cm^{-2}) in a monomer free electrolyte solution scanned at (a) 20, (b) 40, (c) 60, (d) 80, (e) 100, (f) 120, (g) 140, (h) 160, (i) 180, and (k) 200 mV s^{-1}.

Table A.1: Potential dependence of the parameters calculated for PENBTE film deposited with a charge of 994 mC cm^{-2}.

	Potential / V vs. Ag/AgCl					
	E=0.0V	E=0.2V	E=0.4V	E=0.6V	E=0.8V	E=1.0V
R_S / Ohm cm^2	0.7932	0.7003	0.6897	0.6926	0.6998	0.7056
C_{dl} / F cm^{-2}	0.0051	0.0743	0.1005	0.1051	0.1355	0.1392
R_1 / Ohm cm^2	1.164	1.154	0.7853	1.33	0.01	0.01
CPE_1; Y_o/ S s^{-n} cm^{-2}	0.7798	0.0294	0.0034	0.2259	4.22E-06	1.22E-04
n	0.8801	0.9598	0.9761	0.9712	2.10E-07	1.01E-07
R_2 / Ohm cm^2	0.305	1.61	0.3079	38.36	0.0205	0.01
W; Y_o / S $s^{-0.5}$ cm^{-2}	1.77E-19	4.81E-20	1.00E-20	4.03E-15	0.0017	0.0015
C_{CF} / F cm^{-2}	7.41E-04	0.0173	0.0221	0.0497	0.323	0.4067
R_{CF} / Ohm cm^2	0.1055	0.0339	0.0247	0.0219	0.0434	0.0443
Chi-squared	1.28E-03	1.05E-04	5.44E-05	4.10E-05	1.09E-04	1.38E-04

Table A.2: Potential dependence of the parameters calculated for PENBTE film deposited with a charge of 666 mC cm^{-2}.

	Potential / V vs. Ag/AgCl					
	E=0.0V	E=0.2V	E=0.4V	E=0.6V	E=0.8V	E=1.0V
R_S / Ohm cm^2	5.259	2.95	2.833	2.871	0.0645	1.00E-07
C_{dl} / F cm^{-2}	9.76E-05	0.0226	0.0167	0.0158	0.0182	0.0229
R_1 / Ohm cm^2	24.68	3.375	0.1623	0.1593	0.1406	0.1763
CPE_1; Y_o/ S s^{-n} cm^{-2}	9.37E-04	0.0049	0.0291	0.0257	0.0238	0.0201
n	0.9055	0.8867	0.9817	0.9843	0.9832	0.9758
R_2 / Ohm cm^2	268600	0.0239	2.148	17110	4024	2906
W; Y_o / S $s^{-0.5}$ cm^{-2}	1.27E-04	1.00E-18	3.91E-18	7.67E-05	6.29E-04	0.009
C_{CF} / F cm^{-2}	1.91E-05	0.0141	7.28E-05	2.17E-04	2.57E-08	2.72E-08
R_{CF} / Ohm cm^2	7.792	0.04316	0.06913	0.04356	2.855	2.92
Chi-squared	2.00E-03	1.99E-04	5.83E-05	4.28E-05	4.05E-05	3.95E-05

Table A.3: Potential dependence of the parameters calculated for PENBTE film deposited with a charge of 553 mC cm^{-2}.

	Potential / V vs. Ag/AgCl					
	E=0.0V	E=0.2V	E=0.4V	E=0.6V	E=0.8V	E=1.0V
R_S / Ohm cm^2	4.533	2.496	2.296	2.326	2.371	2.389
C_{dl} / F cm^{-2}	4.50E-05	0.0145	0.03454	0.03135	0.01204	1.797
R_1 / Ohm cm^2	86.98	3.558	60.86	76.85	0.1316	0.04706
CPE_1; Y_o/ S s^{-n} cm^{-2}	0.0012	0.7684	0.0032	0.0026	0.0245	0.5468
n	0.8321	0.957	0.8911	0.8675	0.9835	0.8321
R_2 / Ohm cm^2	525100	0.1081	1.03E+08	3.89E+14	1.00E+19	106900
W; Y_o / S $s^{-0.5}$ cm^{-2}	2.72E-20	5.45E-10	1.25E-17	9.31E-15	2.92E-14	5.63E-11
C_{CF} / F cm^{-2}	1.37E-05	9.18E-05	0.01565	0.01394	0.3919	0.03715
R_{CF} / Ohm cm^2	36.47	0.2448	0.07328	0.07716	65.04	1708
Chi-squared	4.82E-03	2.59E-04	4.75E-05	5.10E-05	4.84E-05	4.61E-05

Table A.4: Potential dependence of the parameters calculated for PENBTE film deposited with a charge of 357 mC cm^{-2}.

	Potential / V vs. Ag/AgCl					
	E=0.0V	E=0.2V	E=0.4V	E=0.6V	E=0.8V	E=1.0V
R_S / Ohm cm^2	3.881	2.769	2.696	2.629	2.734	2.752
C_{dl} / F cm^{-2}	1.58E-04	0.0101	0.0086	0.0211	0.0103	0.0227
R_1 / Ohm cm^2	12.45	0.0841	0.1469	1217	0.1246	0.0738
CPE_1; Y_o/ S s^{-n} cm^{-2}	0.1419	0.00582	0.01619	9.14E-04	0.01448	3.31E-04
n	0.8822	0.9497	0.9832	0.7503	0.9796	1.68E-10
R_2 / Ohm cm^2	200	2327	7540	3.51E+06	1.85E+07	0.01
W; Y_o / S $s^{-0.5}$ cm^{-2}	2.18E-10	3.24E-18	5.44E-14	2.97E-13	4.71E-15	7.14E-04
C_{CF} / F cm^{-2}	2.22E-05	2.29E-04	0.8991	2.73E-04	0.2162	0.05465
R_{CF} / Ohm cm^2	5.319	0.05143	15.58	0.16	87.99	0.00599
Chi-squared	4.61E-03	1.03E-04	6.89E-05	4.28E-03	5.13E-05	8.38E-05

Table A.5: Potential dependence of the parameters calculated for PENBTE film deposited with a charge of 121 mC cm^{-2}.

	Potential / V vs. Ag/AgCl					
	E=0.0V	E=0.2V	E=0.4V	E=0.6V	E=0.8V	E=1.0V
R_S / Ohm cm^2	2.072	1.925	2.109	2.13	2.11	2.188
C_{dl} / F cm^{-2}	0.0010	0.0046	0.0073	0.0070	0.0087	0.0107
R_1 / Ohm cm^2	0.9509	0.3814	166.9	1.846	0.48	1.614
CPE_1; Y_o/ S s^{-n} cm^{-2}	0.0011	0.0029	0.0057	0.0047	0.0032	0.0023
n	0.964	0.977	0.9714	0.9717	0.969	1
R_2 / Ohm cm^2	19360	0.1345	0.2398	0.2162	623	2330
W; Y_o / S $s^{-0.5}$ cm^{-2}	1.72E-05	1.29E-19	6.38E-17	7.79E-10	3.43E-04	5.61E+13
C_{CF} / F cm^{-2}	1.16E-04	2.56E-04	0.2772	0.2909	7.59E-05	0.1792
R_{CF} / Ohm cm^2	0.2598	0.07817	34.65	23.24	0.0554	2.192
Chi-squared	4.22E-04	5.15E-05	7.05E-05	6.92E-05	6.87E-05	4.20E-04

Table A.6: Potential dependence of the parameters calculated for PENBTE film deposited with a charge of 97 mC cm^{-2}.

	Potential / V vs. Ag/AgCl					
	E=0.0V	E=0.2V	E=0.4V	E=0.6V	E=0.8V	E=1.0V
R_S / Ohm cm^2	2.548	2.304	2.277	2.335	2.359	2.39
C_{dl} / F cm^{-2}	5.81E-05	0.00405	0.00551	0.00497	0.00741	0.00805
R_1 / Ohm cm^2	0.4297	0.7961	0.9101	0.82	424	2859
CPE_1; Y_o/ S s^{-n} cm^{-2}	8.29E-04	0.00225	0.00267	0.00265	3.33E-04	1.59E-20
n	0.9702	0.9684	0.9725	0.9736	0.8964	0.6516
R_2 / Ohm cm^2	50980	4718	14060	295100	10170	3062
W; Y_o / S $s^{-0.5}$ cm^{-2}	9.32E-05	6.29E-13	4.73E-05	6.37E-19	4.89E-04	2.44E+13
C_{CF} / F cm^{-2}	7.48E-04	0.1791	1.46E-04	0.3451	0.01745	0.0298
R_{CF} / Ohm cm^2	0.3788	4.268	0.04295	21.88	0.0955	0.1556
Chi-squared	3.00E-04	1.26E-04	6.28E-05	6.43E-05	1.08E-04	1.50E-03

BIOGRAPHY

Fevzi Çakmak Cebeci was born in Eynesil/Giresun in 1974. After finishing primary, secondary and high school in Samsun, he obtained his B. Sc. in Chemistry from Istanbul Technical University in Istanbul (1996).

He studied in the Rubner Group at Massachusetts Institute of Technology as a visiting student for fifteen months between November 2003 and February 2005.

He got his M. Sc. in Chemistry from Istanbul Technical University (1999) and he started his Ph. D. studies in Polymer Science and Technology program.

His research interests are mainly focus on polyelectrolyte multilayers, surface chemistry, materials science, nanotechnology, electrochemistry; electrochemical impedance spectroscopy, conducting polymers, electrochromic materials and devices.

He has been working as a research assistant in Chemistry Department of Istanbul Technical University since January 1998.